UNIVERSITY OF INSUBRIA

Ph.D. Course in Experimental and Translational Medicine (XXXIII cycle)

Department of Medicine and Surgery

A Novel Role of CDKL5 in the Inhibitory Synapse and a Possible Therapeutic Strategy for CDKL5-Related Defects

Supervisor: Prof. Charlotte KILSTRUP-NIELSEN
Coordinator: Prof. Daniela NEGRINI

Ph.D. Thesis of:
Dr. Roberta DE ROSA
Candidate n° 734439

Academic year 2019/2020

To my lovely family

Table of Contents

Summary

Mutations in the cyclin-dependent kinase like 5 gene (*CDKL5*) have been found in individuals with a rare X-linked neurodevelopmental disorder, CDKL5 deficiency disorder (CDD), characterised by early-onset epileptic encephalopathy, severe intellectual disability, drug-resistant seizures and infantile spasms (Fehr et al., 2013). In accordance with the localisation of *CDKL5* on the X-chromosome (Xp22), this disorder affects mostly females who are heterozygous for CDKL5 deficiency and mosaic for the mutated allele because of the random X-chromosome inactivation (Guerrini & Parrini, 2012). At present, no cure exists for patients with CDD and the development of rationally designed drug-based therapies is still extremely challenging due to the limited knowledge of CDKL5 functions. Most studies in CDKL5 deficient neurons and mice converge on a crucial role of CDKL5 in regulating excitatory neurotransmission. Indeed, CDKL5 interacts with PSD95 and controls maturation of dendritic spines and miniature excitatory postsynaptic currents (Zhu & Xiong, 2018). *Cdkl5*-KO mice are useful for the study of the molecular basis of CDD and for preclinical drug-testing since they recapitulate most features of the human disorder such as autistic-like traits, impaired learning and memory and motor control (Zhou et al., 2017). Nevertheless, spontaneous epilepsy is not present but an altered susceptibility to pro-convulsant drugs has been observed (Amendola et al., 2014; Yennawar et al., 2019).

Although the role of CDKL5 at excitatory synapses is widely studied, a potential role of the protein in the specific regulation of the inhibitory neurotransmission has been rather neglected up until now. Therefore, this thesis aims at exploring a potential role of CDKL5 at the inhibitory synapse. Γ-aminobutyric acid type A receptors ($GABA_ARs$) are the main inhibitory receptors of the nervous system and their dysfunction is intrinsically linked to epilepsy and autism-spectrum disorders (Comenencia-Ortiz et al., 2014). Indeed, GABAergic transmission controls neuronal excitability and synchronises neuronal networks to generate oscillations that underlie cognitive processes (Tyagarajan & Fritschy, 2014).

The cell membrane distribution of $GABA_ARs$ is dynamically regulated via the interactions with the subsynaptic scaffolding protein gephyrin (Tyagarajan & Fritschy, 2014). Among other important postsynaptic proteins at the inhibitory synapse are collybistin (CB), a brain-specific GDP/GTP-exchange factor, which regulates gephyrin recruitment from

intracellular deposits to postsynaptic membranes and neuroligin2 (NL2) that interacts with presynaptic neurexins.

In this study, we demonstrated that CDKL5 resides in the postsynaptic inhibitory compartment where it interacts with both CB and gephyrin. Loss of CDKL5 led not only to a reduced surface exposure of γ_2 subunit-containing $GABA_ARs$ but also to a reduction in the number of gephyrin-positive puncta, suggesting that CDKL5 might directly control the stabilisation of synaptic $GABA_ARs$ through its interaction with the cytoplasmic CB-gephyrin complex. Interestingly, CDKL5 was found to interact with the CB SH3 domain, which acts as a regulatory switch in CB. Finally, a putative role of CDKL5 in modulating NL2 phosphorylation appeared altogether suggesting that CDKL5 may directly influence the functioning of the postsynaptic scaffolding complex.

The above defects were accompanied by a decrease in the frequency of miniature inhibitory postsynaptic currents (mIPSCs). A similar result was observed when CDKL5 expression was acutely silenced, indicating that the impact of CDKL5 on the inhibitory neurotransmission could be ascribed to its effect at the postsynaptic site, though we cannot exclude a direct role of CDKL5 also in the presynaptic compartment. In this last regard, CDKL5 was shown to diminish the punctate staining of the presynaptic marker bassoon indicating that CDKL5 loss might lead to a reduced number of inhibitory synapses. Furthermore, *ex vivo* findings corroborated the *in vitro* ones; indeed, a deranged surface expression of synaptic $GABA_ARs$ was also found both in hippocampal slices and in synaptosomal fractions of fully symptomatic *Cdkl5*-KO mice. Lastly, our *ex vivo* electrophysiological recordings indicate that *Cdkl5*-KO mice have a hyperexcitability phenotype.

CDKL5 regulates MT dynamics and functions in part through its association with the MT plus-end tracking protein CLIP170, which represents the intracellular target of the neuroactive steroid pregnenolone (PREG) (Barbiero et al., 2019). Our laboratory demonstrated that PREG and its synthetic derivative pregnenolone-methyl-ether (PME) can normalise CLIP170 functioning and restore cellular and neuronal CDKL5-dependent defects (Barbiero et al., 2017b, 2020). In the current study, we tested its effect on the defective phenotypes in the inhibitory counterpart. Intriguingly, we found a restoration of surface expressed $GABA_AR$ γ_2 both *in vitro* and *ex vivo*, of the number of gephyrin puncta and of the deranged frequency of mIPSCs in *Cdkl5*-KO neurons. Accordingly, we also found a rescue of the presynaptic defect.

To sum up, in this Ph.D. thesis, we focused on the key component of the inhibitory synapse to elucidate possible alterations in the absence of CDKL5. Based on our

findings, we hypothesise that CDKL5 exerts a dual control on synaptic $GABA_AR$ expression: a direct regulation through its interaction with the gephyrin-CB-NL2 complex and an indirect effect through its control on MT dynamics. Future studies will aim at investigating, in further details, the molecular composition of the inhibitory synapse and the role of CDKL5 in regulating the conformational switch of CB. Moreover, in agreement with the control of CDKL5 of MT dynamics, the beneficial effect of PME treatment reveals that the pharmacological targeting of such dynamics might stabilise postsynaptic sites and potentiate $GABA_AR$ functioning, constituting an important breakthrough in the CDD field.

1 Introduction

1.1 *CDKL5* and its transcript isoforms

The cyclin-dependent kinase-like 5 gene (*CDKL5*; OMIM #300203) is located on the short arm of the X-chromosome at position 22.13 (Xp22.13) and is subject to X-chromosome inactivation. When this gene was cloned and sequenced, it was formerly termed serine-threonine kinase 9 (*STK9*) (Montini et al., 1998). A number of studies have investigated *CDKL5* structure and its transcript expression in different tissues (Kalscheuer et al., 2003; Montini et al., 1998; Williamson et al., 2012), but the set of transcripts and resulting protein isoforms remained incompletely characterised until 2016. In 2016, Hector and colleagues analysed the mRNA products of human *CDKL5* and mouse *Cdkl5* through a combination of bioinformatic analyses and molecular methods, leading to a more complete picture. The human *CDKL5* occupies approximately 240 kb of the X-chromosome and it is composed of 27 exons. The first five exons, namely 1, 1a, 1b, 1c/d, and 1e, are all untranslated and utilise the same ATG start codon in exon 2.

CDKL5 is known to undergo alternative splicing events and five transcript isoforms with distinct coding regions, *hCDKL5_1* to *hCDKL5_5*, have been found (Figure 1.1). *hCDKL5_1* (*CDKL5*$_{107}$ reported by Williamson *et al.* in 2012; 107 kDa; 960 amino acids) is the most abundant isoform expressed within the central nervous system (CNS) but was detected at low levels in other adult tested tissues (Hector et al., 2016). *hCDKL5_2* is identical to *hCDKL5_1* but includes also the 123 nucleotides long exon 17. *hCDKL5_3* and *hCDKL5_4* are identical to *hCDKL5_1* and *hCDKL5_2*, respectively, but lack 51 bases of coding sequence from the 3' end of exon 11. In contrast to the first four isoforms, *hCDKL5_5* (*CDKL5*$_{115}$ reported by Williamson *et al.* in 2012; 115 kDa; 1,030 amino acids) was only detected in testes amongst the adult tissues tested. Finally, considering *hCDKL5_5*, it is interesting to note that the most extreme C-terminal region of the protein and the 3'-untranslated region (UTR) are utterly different from those of the other isoforms (Hector et al., 2016).

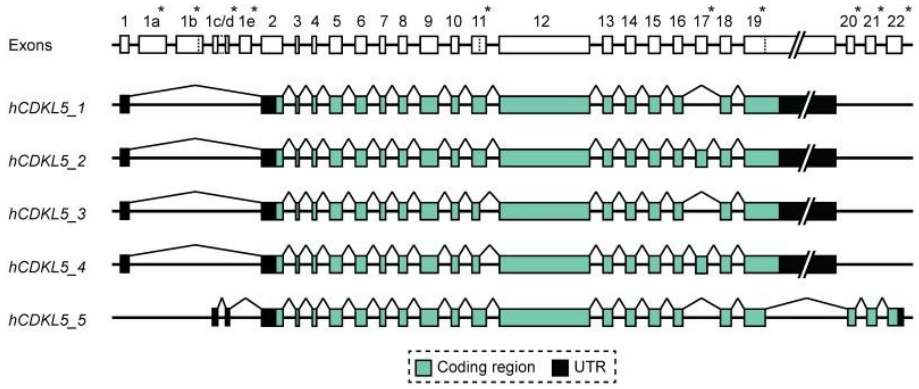

Figure 1.1 Schematic representation of human *CDKL5* and its transcript isoforms. The structure of human *CDKL5* and the exon composition of the five different coding isoforms (*hCDKL5_1* to *hCDKL5_5*) are shown. Splice events are indicated by lines between exons. Differences among the isoforms are indicated by asterisks. Alternative splice sites are indicated by dotted lines within exons (Hector et al., 2016).

The murine isoforms *mCdkl5_1* and *mCdkl5_2* are completely orthologous to their human counterparts. In contrast, the coding regions of the other three murine transcripts do not show full orthology to any human isoforms and are hence termed *mCdkl5_6*, *mCdkl5_7* and *mCdkl5_8* (Figure 1.2). *mCdkl5_1* represents the most abundant isoform expressed within the mouse brain, followed by *mCdkl5_2*. No mouse orthologues of *hCDKL5_3* and *hCDKL5_4* were identified, but it is intriguing that the expression of *mCdkl5_6* and *mCdkl5_7*, similarly to that of *hCDKL5_5*, is confined to the testes in the adult mouse, whereas *mCdkl5_8* is expressed in the spleen and at very low levels in other tissues (Hector et al., 2016).

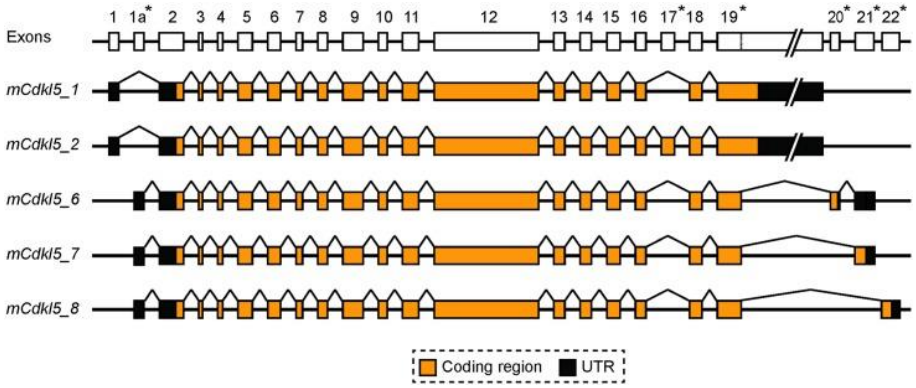

Figure 1.2 Schematic representation of murine *Cdkl5* and its transcript isoforms. Diagram illustrating the structure of murine *Cdkl5* and the exon composition of the different coding isoforms (*mCdkl5_1*, *_2*, *_6*, *_7*, *_8*). Splicing events are indicated by lines between exons. Differences among the isoforms are indicated by asterisks. Alternative splice sites are indicated by dotted lines within exons (Hector et al., 2016).

1.2 CDKL5 protein

CDKL5 belongs to the CMGC family of serine-threonine kinases, which includes cyclin-dependent kinases (CDKs), mitogen-activated protein kinases (MAPKs), glycogen synthase kinases (GSKs) and CDK-like kinases (CLKs) (Montini et al., 1998). Indeed, CDKL5 is characterised by a highly conserved NH_2-terminal catalytic domain (amino acids 13-297), homologous to that of the other CDKL-family members, and a large COOH-terminal extension of almost 700 amino acids (amino acids 297-960).

Drilling down into the details, the catalytic domain comprises an ATP-binding region (amino acids 19-43), a serine-threonine kinase active site (amino acids 131-143), and a conserved threonine-glutamate-tyrosine (TEY) motif within its activation loop (amino acids 169-171) (Bertani et al., 2006) the dual phosphorylation of which is required for activation of extracellular signal-regulated kinases (ERKs) (Pearson et al., 2001). In addition, it has been demonstrated that CDKL5 is able to both *cis*-phosphorylate (Lin et al., 2005) and *trans*-phosphorylate (Bertani et al., 2006), showing an autocatalytic activity directed against its TEY motif. The long C-terminal domain contains two distinct putative signals for nuclear import (NLS_1 and NLS_2; amino acids 312-315 and 784-789, respectively) and export (NES; amino acids 836-845). The C-terminal region, which is unique for CDKL5 and distinguishes it from other proteins, is highly conserved between different CDKL5 orthologs that differ only in the most extreme C-terminus, suggesting a potential crucial role. Accordingly, this region plays an important role in localising the kinase properly within the nuclear compartment, possibly by its interaction with other nuclear factors (Bertani et al., 2006; Lin et al., 2005) (Figure 1.3).

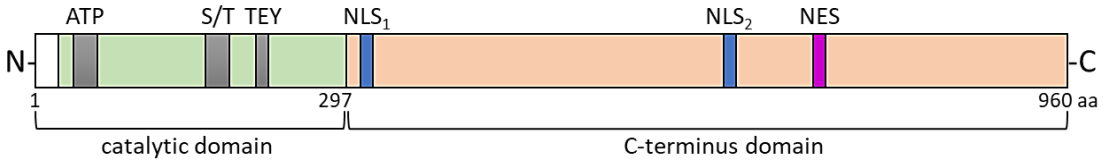

Figure 1.3 Schematic representation of the human isoform hCDKL5_1. Diagram depicting the CDKL5 isoform mainly expressed in the CNS with its principal functional domains. The catalytic domain is shown in green while the included ATP binding site (ATP; amino acids 19-43), the serine-threonine kinase active site (S/T; amino acids 131-143) and the TEY motif (amino acids 169-171) are highlighted in grey. The C-terminal domain is represented in red, the nuclear localisation signal 1 (NLS_1; amino acids 784-789) and 2 (NLS_2; amino acids 836-845) as well as the nuclear export signal (NES) are in blue and violet, respectively (adapted from Balestra et al., 2019).

The catalytic activity of CDKL5 must be tightly regulated. Post-translational modifications constitute a major regulatory mechanism of many proteins and CDKL5 is subjected to various phosphorylation events. For example, phosphorylation on Ser^{308} by dual-specificity tyrosine-phosphorylation-regulated kinase 1A (DYRK1A) interferes with the nuclear localisation of CDKL5, promoting its cytoplasmic location in Neuro2a cells (Oi et al., 2017). In cultured neurons, brain-derived neurotrophic factor (BDNF) induces transient phosphorylation of CDKL5 (Chen et al., 2010), which might be important for the activation of its downstream effectors. However, this is a reversible process and, accordingly, it has been reported that neuronal depolarisation induces the dephosphorylation of CDKL5 by protein phosphatase 1 (PP1), prompting its proteasome-dependent degradation (La Montanara et al., 2015). In particular, N-methyl-D-aspartate receptors (NMDARs) mediate this process, suggesting that CDKL5 may participate in activity-dependent neuronal development and function. In addition, CDKL5 undergoes active auto-phosphorylation and is present in cells in its phosphorylated form (Chen et al., 2010; La Montanara et al., 2015; Mari et al., 2005). Although the functional significance of this auto-phosphorylation has not been defined yet, it is possible that it is required for the activation of CDKL5.

1.3 CDKL5 localisation and expression patterns during development

Since the cloning of *CDKL5* in 1998, multiple studies converge on *CDKL5* mRNA being highly abundant in brain tissues but can also be detected in liver, kidney and testes; interestingly, the size of the mRNA appeared to be significantly shorter in the testes (Chen et al., 2010; Lin et al., 2005; Montini et al., 1998). Within the brain, *in situ* hybridisation studies indicated that *Cdkl5* is enriched throughout the brain with high levels in the cerebral cortex, hippocampus and cerebellum (Chen et al., 2010; Mari et al., 2005). A detailed analysis of *Cdkl5* expression in the adult mouse brain showed that transcript levels are particularly abundant in the most superficial cortical layers of the adult forebrain. Moreover, the hippocampus, a brain area that regulates learning and memory, shows a large amount of *Cdkl5* mRNA in all the *Cornu Ammonis* fields. Conversely, dopaminergic areas, including the *substantia nigra* or the ventral tegmental area, as well as noradrenergic areas, such as the *locus coeruleus*, express very low levels of *Cdkl5*. Interestingly, very high levels of *Cdkl5* transcripts are detected in several

thalamic nuclei, involved in sensory and motor signal relay and in the regulation of consciousness and sleep, whereas lower levels are detected in the cerebellum (Kilstrup-Nielsen et al., 2012).

At the protein level, CDKL5 is a ubiquitous protein that is mainly expressed in brain, testes and thymus (Lin et al., 2005; Rusconi et al., 2008). Moreover, CDKL5 is expressed at moderate levels in heart, lung, spleen and prostate and lower but detectable levels in liver, pancreas and skeletal muscle (Lin et al., 2005). Within the brain, in the adult mouse, CDKL5 is particularly expressed in hippocampus, cerebral cortex, thalamus and striatum, but its levels appear more reduced in the hypothalamus and cerebellum. In human adult brain tissues, numerous and diffused CDKL5-positive cells were found in both cerebral cortex and *corpus callosum*. Furthermore, in the human cerebellum, CDKL5 was detected in most cells corresponding to granular, molecular, and Purkinje cell layers (Rusconi et al., 2008).

At the cellular level, CDKL5 constitutively shuttles between the cytoplasm and the nucleus in mitotic cells, while the shuttling between these compartments is not constitutive in post-mitotic neurons. However, in both cases, the subcellular distribution of the protein appears to be modulated through a CRM1-dependent active nuclear export. The importance of this distribution is highlighted by pathogenic truncations of the C-terminus that lead to a constitutive nuclear accumulation of CDKL5 (Rusconi et al., 2008, 2011) . In the cytoplasm, CDKL5 is preferentially localised in structures that are highly dynamic and actin-enriched. At early developmental stages of cultured neurons, CDKL5 is localised in the growth cone, a dynamic structure at the tip of growing neurites (Chen et al., 2010; Nawaz et al., 2016), whereas in mature neurons CDKL5 is enriched in dendritic spines, where most excitatory synapses are present (Ricciardi et al., 2012). Recently, it has been shown that CDKL5 is also present at centrosomes of dividing cells and post-mitotic neurons (Barbiero et al., 2017a). Notably, immunostaining of primary neuronal cultures indicates that CDKL5 is expressed in both glutamatergic and GABAergic neurons, but not in glial cells (Rusconi et al., 2008). However, a separate study has found a distinct CDKL5 isoform expressed in the glia (Chen et al., 2010).

Intriguingly, CDKL5 levels vary during development in different districts. As previously mentioned, the CNS isoforms, *hCDKL5_1*, *_2*, *_3,* and *_4*, are all expressed at higher levels in the adult brain than in the foetal brain. Conversely, *hCDKL5_5* is expressed in the foetal brain even if, in the adult, it is found only in the testes. In mice, the most abundant *Cdkl5* isoforms, *mCdkl5_1* and *mCdkl5_2,* are expressed throughout embryonic and early postnatal development, increasing in levels and peaking within the

first few weeks after birth (Hector et al., 2016). Western blot analyses of CDKL5 protein levels in mice and rats have confirmed the transcript profile in adult brain even if the onset of CDKL5 expression is still debated (Lin et al., 2005; Rusconi et al., 2008; Chen et al., 2010). Several studies agree that CDKL5 protein levels reach the highest in conjunction with the development and differentiation of the brain, supporting a role of CDKL5 after the early stages of development. It is noteworthy that the detection of different transcript isoforms is suggestive of a complex developmental regulation of CDKL5 expression and levels during pre- and postnatal development. Despite this, the functional significance of different *CDKL5* transcript isoforms and their expression levels remains to be assessed. Furthermore, the patterns of CDKL5 expression need to be examined in post-mortem human tissues as well (Zhou et al., 2017).

1.4 Multiple roles of CDKL5 and its molecular functions

The expression pattern of CDKL5 suggests that it is involved in the regulation of neuronal development as well as in the maintenance of proper neuronal activity and morphology, and that it has a function in the adult brain. Its localisation to different subcellular compartments implies that it plays multiple roles and regulates distinct signalling pathways.

1.4.1 Substrates of CDKL5 and its kinase activity

Several laboratories have attempted to characterise the molecular functions of CDKL5 through protein pull-down studies, yeast *two-hybrid screening,* or chemical genetics in order to identify its interacting proteins and/or substrates.

To date, various CDKL5 interacting proteins have been identified of which some have been reported to be its substrates: in the nucleus, the kinase is able to interact with methyl-CpG binding-protein 2 (MeCP2), DNA methyltransferase 1 (DNMT1), serine/arginine-rich splicing factor SC35 (SC35) and histone deacetylase 4 (HDAC4), while in the cytoplasmic compartment its interactors are postsynaptic density protein 95 (PSD95), netrin-G1 ligand (NGL-1), amphiphysin 1 (Amph1), Shootin1, Rac Family Small GTPase 1 (Rac1), IQ Motif Containing GTPase Activating Protein 1 (IQGAP1) as well as the end-binding protein 2 (EB2) and the microtubule-associated protein 1S (MAP1S) (Figure 1.4).

The first CDKL5 interactor, MeCP2, was identified in 2005 by Mari and colleagues (Mari et al., 2005). The two proteins share a partial overlap in the spatial and temporal expression and were found to interact both *in vitro* and *in vivo.* CDKL5 mediates MeCP2 phosphorylation *in vitro* (Mari et al., 2005). Even though it is still unclear whether this happens also *in vivo*, it is known that specific events of MeCP2 phosphorylation regulate, among other functions, gene transcription, proper dendritic and synaptic development, and behavioural responses to experience (Cohen et al., 2012; Li et al., 2011) along with cell proliferation, division, migration, and differentiation (Bergo et al., 2015).

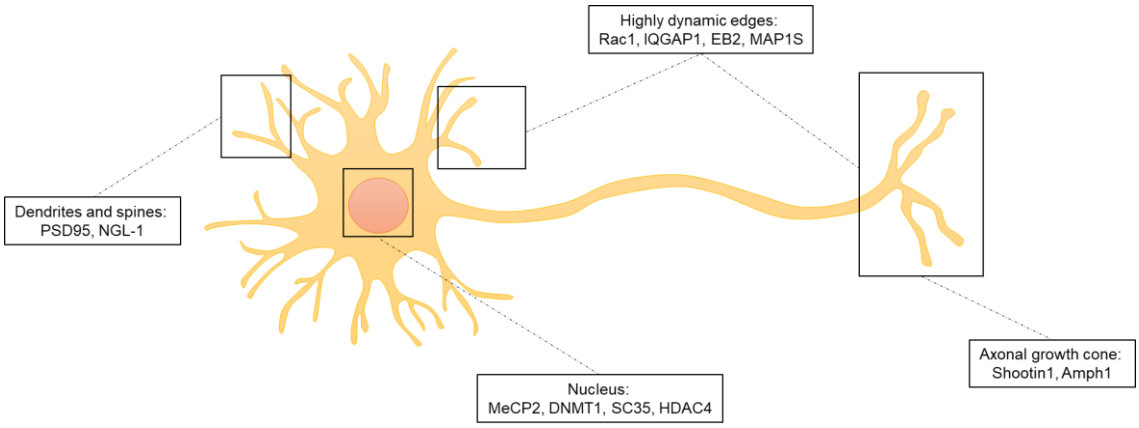

Figure 1.4 Schematic representation of the localisation of CDKL5 known interactors in neurons. CDKL5 functions occur both in the nucleus and in the cytoplasm. In the nucleus, CDKL5 interacts with and phosphorylates MeCP2 and DNMT1. Furthermore, the protein colocalises with SC35 in RNA speckles. In the cytoplasm, CDKL5 is involved in the regulation of actin cytoskeleton and dendritic arborisation. This function is mediated by the interaction with Rac1. Other interactors are PDS95, NGL-1, Shootin1, Amph1, IQGAP1, EB2 and MAP1S.

In an effort to identify kinases that phosphorylate DNMT1, the enzyme responsible for the maintenance of genomic DNA methylation, Kameshita and colleagues demonstrated that CDKL5 phosphorylates the DNMT1 N-terminus *in vitro* (Kameshita et al., 2008). Nonetheless, similarly to MeCP2, whether DNMT1 is phosphorylated by CDKL5 *in vivo* has not been determined. Through its interaction with two key epigenetic factors, CDKL5 may thus play a role in epigenetics and gene expression.

Subsequently, CDKL5 was found to localise and be associated with the splicing factor SC35, clustered in the so-called nuclear speckles where pre-mRNA splicing factors, ribonucleoprotein particles (snRNPs), spliceosome subunits and non-snRNP protein

splicing factors accumulate. These data suggest a role of CDKL5 in the regulation of the nuclear trafficking of splicing machinery (Ricciardi et al., 2009).

HDAC4 is a transcriptional repressor, which controls the expression of various genes of which some are important for synaptic function. In a phosphoproteomic-based study, HDAC4 was identified as a direct phosphorylation target of CDKL5. In line with its role in neuronal development and function, HDAC4 is highly abundant in neurons, where it is retained in the cytoplasm in a phosphorylation-dependent manner. CDKL5 phosphorylates HDAC4 at Ser^{632}, thereby regulating its cytoplasmic retention. CDKL5 loss leads to diminished HDAC4 phosphorylation increasing its nuclear translocation. This aberrant localisation promotes HDAC4 binding to DNA and the inhibition of gene transcription (Trazzi et al., 2016).

Synaptic targeting of CDKL5 is promoted by its interaction with the palmitoylated form of PSD95, a major scaffold protein in the postsynaptic density that regulates the organisation of synaptic proteins and synaptic strength. CDKL5 also forms a complex with PSD95 and NGL-1 of which the latter is a synaptic cell adhesion molecule that exerts a regulatory role in synapse formation and homeostasis. CDKL5 mediates NGL-1 phosphorylation at Ser^{631}, which is necessary to ensure stable binding to PSD95 (Ricciardi et al., 2012; Zhu et al., 2013).

Another cytoplasmic substrate of CDKL5 is Amph1, a multifunctional adaptor molecule involved in neurotransmission and synaptic vesicle recycling through clathrin-mediated endocytosis. CDKL5 phosphorylates Amph1 at Ser^{293}, negatively influencing its binding to endophilin, which is involved in synaptic vesicle endocytosis and receptor trafficking. These pieces of evidence underline once again that CDKL5 plays crucial roles in synaptic maintenance and function (Sekiguchi et al., 2013).

Nawaz and colleagues highlighted a role of CDKL5 in regulating axon specification and elongation in mouse primary hippocampal neurons through its interaction with Shootin1: CDKL5 silencing resulted in an increased number of neurons bearing no axon, while both silencing and overexpression of the kinase were associated with the formation of supernumerary axons and reduced axonal length (Nawaz et al., 2016). Shootin1 is a brain-specific protein acting as a determinant of axon formation during the process of neuronal polarisation. These data reinforced the evidence that CDKL5 is involved in the regulation of neuronal polarisation, at least in part, through its interaction with Shootin1.

Recently, in our laboratory, IQGAP1 has been identified as a novel CDKL5 interactor (Barbiero et al., 2017b). IQGAP1 is the most studied of the three members of the IQGAP family of proteins, which are responsible for the regulation of several processes based

on cytoskeletal remodelling, such as cell migration and polarity, proliferation, vesicle transport as well as intracellular signalling through the interaction with numerous proteins (Hedman et al., 2015). IQGAP1 regulates the interaction between microtubules (MTs) and actin networks, through the formation of a tripartite complex with activated Rac1 and CLIP170 (Fukata et al., 2002). CLIP170 is a plus-end MT binding protein that regulates MT stability acting as a rescue factor facilitating MT growth. Loss of CDKL5 was found to negatively impact the formation of the triple complex, resulting in an alteration of IQGAP1 localisation at the leading edge, a disruption of proper cell morphology and an impairment of the MT binding of CLIP170 (Barbiero et al., 2017b).

The two MT-binding proteins EB2 and MAP1S were recently found to interact with CDKL5 (Baltussen et al., 2018; Muñoz et al., 2018). EB2 was identified as a CDKL5 substrate through a chemical genetic approach and was found to be a *bona fide* substrate of CDKL5 *in vitro* and *in vivo*, although the functional consequences of this event are still unknown. Finally, MAP1S, the less characterised member of the MAP1 family proteins, was identified as a substrate of CDKL5 through two different approaches providing strong support for a functional role of this association (Baltussen et al., 2018; Muñoz et al., 2018).

A precise consensus sequence within CDKL5 substrates has been currently characterised. Despite this, some CDKL5 interactors have been crucial to outline the conserved consensus site(s) of CDKL5 phosphorylation. Indeed, Amph1 and its homologue Amph2, which is not phosphorylated by CDKL5, have been used to identify the RPXSX sequence as a putative consensus site (Katayama et al., 2015; Sekiguchi et al., 2013). Recently, the result of two distinct but highly complementary mass spectrometry-based phosphoproteomic approaches have revealed that CDKL5 prefers to phosphorylate serines that lie in the motif RPX[S/T][A/G/P], such as Ser^{900} (Muñoz et al., 2018) and Ser^{786} (Baltussen et al., 2018) of MAP1S and Ser^{222} of EB2 (Baltussen et al., 2018).

Considering the aforementioned data, it is pivotal to highlight that knowledge of the molecular targets of CDKL5 may help, firstly, to fully understand the signalling pathways that mediate the function of the kinase in neurons and, secondly, to identify substrates for pharmacological intervention.

1.4.2 CDKL5 in neuronal development and function

Among the above-mentioned interactors, MT-associated proteins such as IQGAP1, MAP1S, and EB2 are crucial because the interaction with the said proteins has allowed to demonstrate the participation of CDKL5 in the regulation of MT dynamics (Baltussen et al., 2018; Barbiero et al., 2017b; Muñoz et al., 2018). MT dynamics is the property exhibited by the MT plus-end to alternate periods of prolonged assembly to rapid disassembly and is fundamental for neurodevelopmental processes including formation, maintenance and remodelling of synaptic connections (Conde & Cáceres, 2009).

Defective MT dynamics associated with CDKL5 loss could explain why *Cdkl5*-KO neurons display altered migration (Barbiero et al., 2017b), different axonal defects, including axon specification, axon outgrowth along with altered growth cone morphology (Barbiero et al., 2020; Nawaz et al., 2016), and the impairment in both neurite growth and dendritic arborisation (Amendola et al., 2014; Chen et al., 2010; Fuchs et al., 2014; Wang et al., 2012). Moreover, the absence of CDKL5 impairs not only early neuronal development but also dendritic spine formation. Dendritic spines are specialised protrusions that characterise excitatory synapses; CDKL5 is highly enriched in the postsynaptic density, a dense protein complex composed of the key proteins for synaptic transmission, signal transduction, and cell adhesion (Ricciardi et al., 2012; Zhu et al., 2013).

Cdkl5-KO neurons show an increased number of immature spines such as filopodia-like and thin-headed spines (Ricciardi et al., 2012; Trazzi et al., 2016; Trovò et al., 2020) along with a reduced expression of synaptic markers and decreased frequency of miniature excitatory postsynaptic currents (mEPSCs) (Ricciardi et al., 2012; Zhu et al., 2013). In addition, several pieces of evidence suggest that CDKL5 regulates the targeting and trafficking of glutamate receptors to postsynaptic sites. For instance, the postsynaptic density fraction of *Cdkl5*-KO hippocampi presents an abnormal accumulation of GluN2B-containing NMDARs and SAP102, which regulates synaptic trafficking of GluN2B-containing glutamate receptors (Okuda et al., 2017). Recently, our laboratory demonstrated that CDKL5 deficiency in primary hippocampal neurons leads to deranged expression of the alpha-amino-3-hydroxy-5-methyl-4-iso-xazole propionic acid receptors (AMPARs). In particular, the GluA2 subunit was found dramatically reduced jointly with its hyper-phosphorylation on Ser^{880} and increased ubiquitination. These data also revealed that CDKL5 silencing alters the composition of membrane-

inserted AMPARs towards the GluA2-lacking calcium-permeable form, which may contribute, at least in part, to the altered synaptic functions and cognitive impairment linked to loss of CDKL5 (Tramarin et al., 2018).

1.5 Main components of the inhibitory synapse

Considering all the above studies, it is glaring that CDKL5 is localised at excitatory synapses and that CDKL5 loss perturbs excitatory synaptic structure and function. However, two types of synapses are distinguished in the CNS: excitatory synapses, mainly located at the postsynaptic spines, and inhibitory synapses, typically incorporated in the soma and dendritic shaft (Gray, 1959; Sheng & Kim, 2011). Although the role of CDKL5 has hitherto been studied mainly regarding excitatory synapses, very little is known about the influence of CDKL5 at the inhibitory counterpart of the synapse. This Ph.D. project aims at investigating the possible role of CDKL5 in inhibitory neurotransmission, which is pivotal to control neuronal excitability and to synchronise neuronal networks to generate oscillations that underlie cognitive processes.

The essential neurotransmitter receptors of inhibitory synapses are γ-aminobutyric acid type A receptors ($GABA_A$Rs) and glycine receptors. In this Ph.D. thesis, I have focused on $GABA_A$Rs, which are the main mediators of GABAergic transmission and represent the key source of inhibition in the adult brain. Such receptors are pentamers composed of two α, two β, and one γ or δ subunit (Comenencia-Ortiz et al., 2014).$GABA_A$Rs on the neuronal cell surface exist as diffuse receptor populations or as synaptic as well as extrasynaptic clusters. Synaptic and extrasynaptic $GABA_A$Rs mediate phasic and tonic inhibition, respectively. The first ones efficaciously respond to high concentrations of GABA during neurotransmitter release into the synaptic cleft and are activated transiently, while the latter respond to lower ambient GABA concentrations or to GABA spill over from synapses and are activated continuously (Tretter et al., 2012). Of note, tonic current causes a steady inhibition and reduces neuronal excitability.

Both $GABA_A$Rs and glycine receptors interact directly with gephyrin, a well-known postsynaptic scaffold protein of the inhibitory synapses. Gephyrin is composed of three functional domains, viz. G-, C-, and E-domains: G- and E-domains form a stable three-dimensional structure while the central C-domain is intrinsically unstructured and gives structural flexibility to the protein. Moreover, gephyrin is capable of self-aggregating into a complex lattice due to dual multimerisation domains on its E- and G-domains. Therefore, the combination of self-aggregation and direct binding to glycine receptor and

$GABA_AR$ subunits enable their clustering at inhibitory postsynaptic sites (Groeneweg et al., 2018).

A yeast *two-hybrid screening*, aiming at searching for gephyrin-interacting proteins, identified the guanine nucleotide exchange factor (GEF) collybistin (CB) that catalyses the GTP-GDP exchange on the Rho family GTPase Cdc42 and is involved in regulating the submembrane distribution of gephyrin (Kins et al., 2000). Gephyrin interacts with the actin cytoskeleton; this interaction is mediated by the actin binding proteins profilin I and II as well as by the microfilament adaptors of the Mena/VASP family that also interact with each other and regulate microfilament dynamics. Other gephyrin interactors are the dynein light chains -1 and -2 (Dlc1 and Dlc2), which mediate local transport of synaptic proteins and provide a link to MTs and microfilaments. Finally, some GABAergic synapses are associated with the dystrophin-glycoprotein complex (DGC) that links the extracellular matrix with the cytoskeleton and neuroligins (NLs) that bridge the synaptic cleft by interaction with presynaptic neurexins (Tretter et al., 2008) (Figure 1.5).

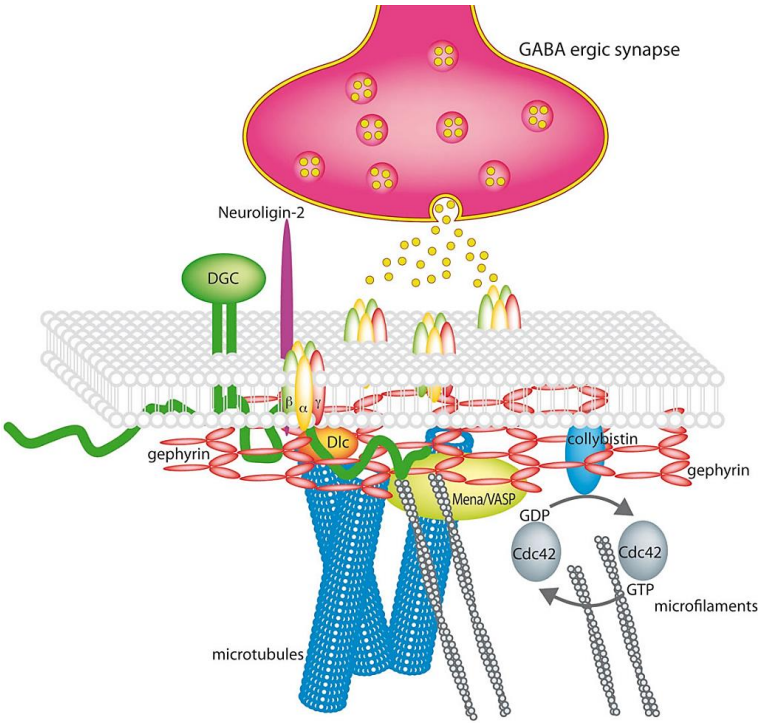

Figure 1.5 Schematic representation of the GABAergic synapse. Synaptic $GABA_AR$s are stabilised by a submembranous lattice of gephyrin through a direct interaction. The guanine nucleotide exchange factor (GEF) collybistin (CB) is associated with the cell membrane and interacts directly with gephyrin. Dlc1/2 and Mena/VASP are cytoskeleton associated proteins. The dystrophin-glycoprotein complex (DGC) stabilises the synapse and neuroligins bridge the synaptic cleft by interaction with presynaptic neurexins (Tretter et al., 2008).

1.6 CDKL5 Deficiency Disorder (CDD)

1.6.1 *CDKL5* pathological mutations

Since 2003, molecular genetics has allowed identifying mutations in *CDKL5* in patients affected by severe neurodevelopmental disorders. So far, in the vast majority of patients, the mutations are *de novo* as they are absent in the parents and only one familial case with three affected siblings has been described (Weaving et al., 2004). Most mutations are unique, but few recurrent mutations have been identified (Bahi-Buisson et al., 2012a).

To date, 317 *CDKL5* variants are listed in the RettBASE: RettSyndrome.org Variation Database (http://mecp2.chw.edu.au/cdkl5/cdkl5_home.php), consisting of 57.7% pathogenic mutations, 10.1% likely pathogenic mutations, 13.6% benign mutations, 5.4% likely benign mutations and 13.2% variants of unknown significance (VOUS) (Figure 1.6).

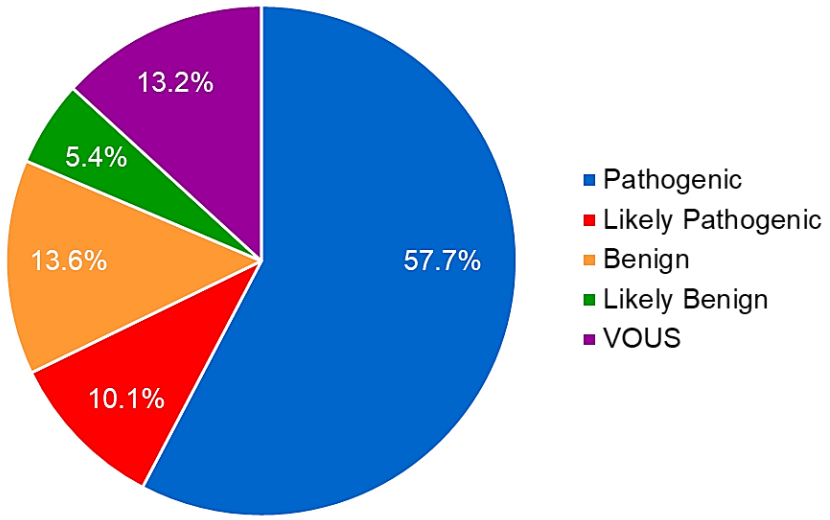

Figure 1.6 Schematic illustration of the distribution of pathogenicity in *CDKL5* variant database. The pie chart shows the distribution of *CDKL5* variants that are divided into pathogenic (183), likely pathogenic (32), benign (43), likely benign (17) and variants of unknown significance (VOUS; 42) (adapted by RettBASE: RettSyndrome.org Variation Database).

Pathogenic mutations are distributed throughout the entire coding sequence of *hCDKL5_1* and include missense and nonsense mutations, translocations, frameshift (small and large deletions as well as insertions), aberrant splicing and multiple mutations. Pathogenic missense mutations involve almost exclusively the catalytic domain (Figure 1.7), suggesting that the kinase activity of CDKL5 is particularly important for brain function (Bahi-Buisson et al., 2008a, 2012a; Fehr et al., 2015, 2016).

CDD mutations are mainly considered *loss of function* mutations as CDKL5 has less or no catalytic activity (Bertani et al., 2006; Rusconi et al., 2008). Furthermore, Szafranski and colleagues have highlighted the importance of CDKL5 dosage. Indeed, the authors reported seven females and four males from seven unrelated families with genomic duplications at Xp22, involving *CDKL5*. Increased dosage of *CDKL5* may affect the global output of the interactions with its substrates, leading to perturbation of synaptic plasticity and development (Szafranski et al., 2015).

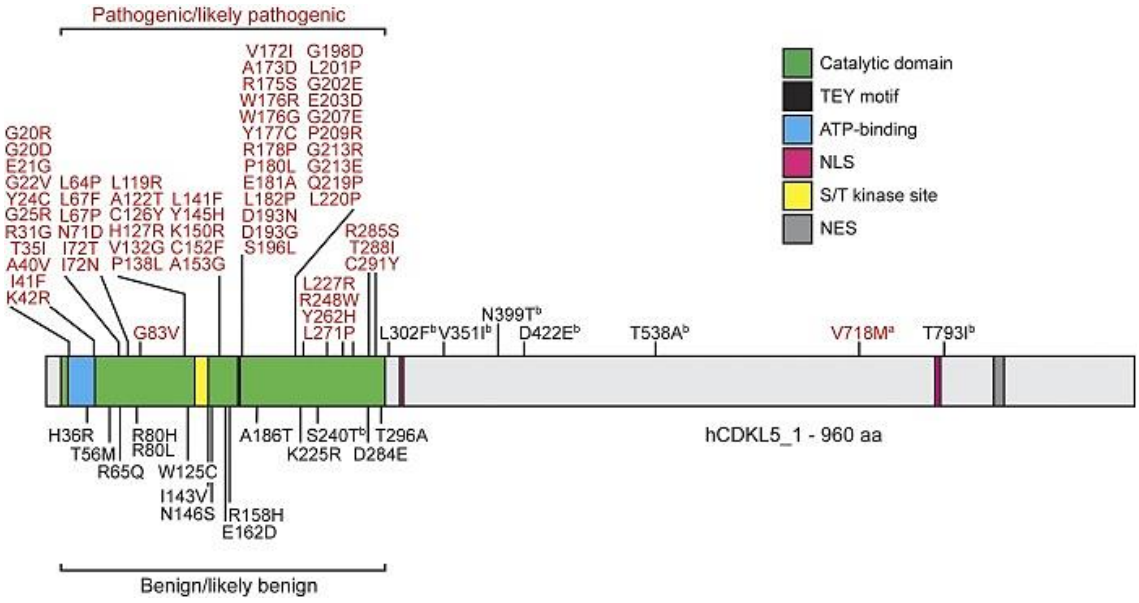

Figure 1.7 Pathogenic *CDKL5* missense variants in patients localise mainly in the catalytic domain. The image refers to hCDKL5_1, the predominant brain protein isoform. Numbers refer to the positions of amino acids. Variants in red (upper) are pathogenic or likely pathogenic. Variants in black (lower) are benign or likely benign. [a]Variant with a splicing consequence. [b]Variant of uncertain significance. NES = putative nuclear export signal; NLS = putative nuclear localization signal; ST = serine-threonine kinase active site; TEY = conserved threonine-glutamate-tyrosine motif (Hector et al., 2017).

1.6.2 The history of the disease: from Rett Syndrome to CDD

Pathologic variants in *CDKL5* cause CDKL5 deficiency disorder (CDD; OMIM #300203, #300672), which is a rare X-linked neurodevelopmental disorder, affecting one in 40,000 to 60,000 live births (Olson et al., 2019).

As previously described, *CDKL5* was first cloned in 1998 in a positional cloning effort to identify disease genes linked to Xp22 (Montini et al., 1998). A number of human genetic disorders were mapped to this region, including Nance-Horan syndrome (OMIM #302350), oral-facial-digital syndrome type 1 (OMIM #311200) and a novel locus for non-syndromic sensorineural deafness (OMIM #300066) (Montini et al., 1998). However, it was not until 2003 when a link between *CDKL5* mutations and disease was described in a case report of two female patients with X-linked infantile spasms and severe mental retardation (Kalscheuer et al., 2003). The triad of infantile spasms, hypsarrhythmia, and profound mental retardation is known as West syndrome or, when X-linked, infantile spasms syndrome (ISSX, OMIM #308350), mostly caused by mutations in the aristaless-related homeobox gene (*ARX*) at Xp21.3-p22.1 interval. The two severely affected girls were characterised by apparently *de novo* balanced X;autosome translocations disrupting *CDKL5* at Xp22.3 and, consequently, a second locus for ISSX was identified (Kalscheuer et al., 2003). Subsequently, some patients who had been diagnosed with atypical Rett Syndrome (RTT, OMIM #312750) were found to carry *CDKL5* mutations (Tao et al., 2004; Weaving et al., 2004).

Classical RTT is characterised by a period of normal development, followed by a regression, where patients lose their acquired skills such as hand use, speech, and social interaction. This typical regression is completely absent in CDD. Indeed, numerous works highlighted the correlation between *CDKL5* mutations and a clinical picture characterised by early onset of epilepsy within the first three months, severe encephalopathy, intractable neonatal seizures, severe X-linked infantile spasms, mental retardation, and autistic features with intellectual disability (Archer et al., 2006; Bahi-Buisson et al., 2008b, 2012b; Evans et al., 2005; Rosas-Vargas et al., 2008; Russo et al., 2009).

In 2013, the pathology associated with CDKL5 deficiency was established as an independent clinical entity referred to as CDKL5 disorder (Fehr et al., 2013b) or, lately, as CDKL5 deficiency disorder (CDD). In this thesis, I will use the acronym CDD.

1.6.3 Clinical features associated with CDD

A full clinical picture of CDD is still limited as a broader number of patients is needed to delineate more thoroughly the natural history of this disease and to identify its main features in order to better define the diagnostic criteria. As mentioned, the first mutations in *CDKL5* were initially identified in patients with the clinical diagnosis of the early-seizure variant of RTT and only later these patients were classified as a distinct clinical entity. Indeed, in a study from 2013, 77 females, aged from 6 months to 22.4 years, and 9 males, aged from 1.1 to 14.9 years, with a pathogenic or potentially pathogenic *CDKL5* mutation were enrolled to assess their clinical presentation and physical appearance (Fehr et al., 2013b). It was found that less than 25% of the cases fulfilled the clinical criteria of atypical RTT previously described by Neul and colleagues (Neul et al., 2010), especially because of the absence of regression in over two-thirds of patients. Importantly, this confirmed previous studies (Artuso et al., 2010; Bahi-Buisson et al., 2008b) and allowed to classify CDD as a separate disorder from RTT. CDD was described as being mainly characterised by early-onset seizures occurring within the first three months after birth, severe intellectual and gross motor impairment, while it is less frequent that CDD patients achieve independent walking as well as show microcephaly and major congenital malformations (Figure 1.8).

Recently, Olson and colleagues proposed the minimum CDD diagnostic criteria to include a pathogenic or likely pathogenic *CDKL5* variant along with motor and cognitive developmental delays and epilepsy with onset in the first year of life (Figure 1.9). However, some patients with CDD may be atypical and not meet these formal criteria (Olson et al., 2019).

Extremely likely[a]	Seizures within the first year of life (90% by 3 months) Global developmental delay Severely impaired gross motor function
Very likely[b]	Sleep disturbances Abnormal muscle tone Bruxism Gastrointestinal issues
Likely[c]	Subtle dysmorphic features including three or more of the following: broad/prominent forehead; large 'deep-set' eyes; full lips; tapered fingers; and anteverted nares in males Hand stereotypies Laughing and screaming spells Cold hands or feet Breathing disturbances Peripheral vasomotor disturbances
Unlikely[d]	Independent walking Microcephaly Major congenital malformations

Figure 1.8 Clinical features suggesting a diagnosis of CDD. The figure shows the most typical features of females and males with CDD. These features can be used as a guide to assist decision-making where targeted *CDKL5* mutation analysis is being considered. [a]Observed in >90% of cases in the current study; [b]Observed in 80–90% of cases in the current study; [c]Observed more variably in 40–80% of cases in the current study; [d]Observed in <10% of cases in the current study (Fehr et al., 2013b).

Common Clinical Characteristics	Proposed Minimal Diagnostic Criteria
• Epilepsy, early onset, and refractory • Severe global developmental delay • Intellectual disability • Hypotonia • Cortical visual impairment • Sleep disturbance • Dyskinetic movements • Autonomic and breathing disturbances • GI disturbances (reflux, constipation) • Dysphagia	• A pathogenic or likely pathogenic variant in the *CDKL5* gene • Motor and cognitive developmental delays • Epilepsy with onset in the first year of life

Figure 1.9 Common clinical characteristics and proposed minimal diagnostic criteria. The figure displays a list of common clinical features of CDD patients and what are the minimum diagnostic criteria of this disorder according to Olson and colleagues. GI = Gastrointestinal. (Olson et al., 2019).

Interestingly, some dysmorphic features were supposed to be useful for the diagnosis of CDD (Figure 1.10). Indeed, females affected by CDD are frequently characterised by prominent and/or broad forehead, deep-set but large appearing eyes, full lips, and tapered fingers while most affected males were more dysmorphic with distinctly anteverted nares, short philtrum and everted upper lip. (Fehr et al., 2013b).

Figure 1.10 Examples of facial, hand and feet features in females (from *a* to *g*) and males (*h*) with CDD. These photographs highlight frequently observed facial features including a prominent and/or broad forehead, high hairline, relative mid-face hypoplasia, deep-set but large-appearing eyes and infra-orbital shadowing. Moreover, some patients show well-defined philtrum, tapered fingers, broad hallux, hallux valgus and regular toes (Fehr et al., 2013b).

Over time, much effort has been made to outline the clinical aspects of CDD patients. All these studies are crucial because the selection of diagnostic criteria as well as the identification of specific somatic features are useful for clinical management and ensure a high degree of homogeneity in patients enrolled in treatment trials and other clinical studies.

1.6.4 CDD: genotype-phenotype relationship

Genotype-phenotype correlation studies of *CDKL5* mutations have been attempted over the years (Bahi-Buisson et al., 2008b, 2012a; Fehr et al., 2016; Kalscheuer et al., 2003; Russo et al., 2009). However, such prediction is still extremely difficult due to the limited number of patients and the small number of recurrent mutations. In addition, the clinical phenotypes among patients with recurrent mutations are heterogeneous. This is likely due to the X-linked status of *CDKL5* and to the fact that most patients are heterozygous females. As a result of random X-chromosome inactivation (XCI), female patients carrying the same genetic mutation can have different mosaic expression of *CDKL5*, thus resulting in a spectrum of phenotypes (Zhou et al., 2017). Lastly, these clinical studies should take into account the molecular aspects associated with *CDKL5* mutations.

A wider knowledge of the effect of pathogenic mutations on the expression and activity of CDKL5 might help to better outline phenotype-genotype correlations, which is pivotal from a therapeutic point of view.

1.6.5 CDD and mouse models

Animal models are instrumental to understand the molecular mechanisms underlying the onset of a disease and, although not summarising all aspects of a disorder, they generally represent an excellent tool to study gene functions. Thanks to the development of both *Cdkl5* constitutive and conditional KO mouse models, it has been possible to shed light on the roles of CDKL5.

The first *Cdkl5*-KO mouse model was generated by Wang and colleagues, reproducing a splice site mutation previously found in a CDD patient (Archer et al., 2006). Thanks to the deletion of mouse *Cdkl5* exon 6 by homologous recombination in embryonic stem cells, they created a mouse model in C57BL/6 genetic background with a truncation in the N-terminal domain of CDKL5, disrupting the kinase activity and resulting in *loss of function* of CDKL5. These animals recapitulate most symptoms associated with CDD, including impaired motor control on the rotarod, hyperactivity in locomotor assay, deficits in learning and memory in a fear conditioning assay, and hindlimb clasping, a phenotype believed to be related to impaired motor control. *Cdkl5*-KO animals also show aberrant auditory-evoked potentials and autistic-like deficits in social interactions in a three-chambered social approach assay and in home-cage social behaviour (Wang et al., 2012). Two years later, Amendola and collaborators (Amendola et al., 2014) produced a second mouse model, deleting *Cdkl5* exon 4 in mice with C57BL/6J genetic background, through standard gene targeting in embryonic stem cells. This new model confirmed most behavioural defects described by Wang and colleagues (Wang et al., 2012), such as abnormal hindlimb clasping, impaired motor coordination and defective working memory. In addition to the previous model, these mice showed a reduced number of head tracks along with altered visual-evoked potentials, which indicate deficient visual processing. Altogether, these features mimic the stereotypic hand movements, hypotonia, eye-tracking abnormalities, reduced social interaction and intellectual disability observed in CDD patients (Amendola et al., 2014). It is noteworthy that the discrepancy in motor activity between these two models could be due to the different genetic background of animals and/or the different experimental setting used to assess locomotor activity. Recently, a further characterisation of the model carrying the deletion

of *Cdkl5* exon 6 was carried out by Jhang and colleagues (Jhang et al., 2017). Several behavioural tests recapitulated the primary characteristics of autism spectrum disorders, including impaired social interaction and communication as well as repetitive grooming and digging behaviours. Moreover, features of attention deficit hyperactivity disorder (ADHD) were delineated, such as increased locomotor activity, impulsivity and aggressiveness, along with deficits in motor and spatial learning (Jhang et al., 2017). Finally, to obtain a more extensive knowledge on the behavioural consequences of the loss of CDKL5, a third KO mouse model was generated by the deletion of *Cdkl5* exon 2 through Cre-LoxP recombination, in the genetic background C57BL/6N. These mice exhibited enhanced anxiety- and fear-related behaviours, significant hypoactivity, impairments in acquisition and long-term retention of spatial reference memory as well as in working memory (Okuda et al., 2017, 2018).

In addition to constitutive *Cdkl5*-KO mice, conditional mouse models were used to relate the behavioural features described above to distinct populations of neurons. Amendola and colleagues generated two murine models, which carried a Cre-conditional KO allele of *Cdkl5* with the specific deletion in glutamatergic cortical neurons (*Emx1*::Cre-mediated) and in GABAergic forebrain neurons (*Dlx5/6*::Cre-mediated). Interestingly, these two models revealed a double dissociation of behavioural phenotypes as hindlimb clasping defects and reduced head tracking responses were only present in the *Emx1*-conditional *Cdkl5*-KO mice, while decreased locomotion was found in the *Dlx5/6*-conditional *Cdkl5*-KO mice (Amendola et al., 2014). Moreover, a mouse model carrying the ablation of CDKL5 expression specifically in glutamatergic forebrain neurons has recently been generated (Nex-cKO). These animals were comparable with WT mice regarding basic sensory and motor function as well as anxiety and social behaviours, whereas they displayed an impairment in spatial working memory, increased locomotor activity and hindlimb clasping (Tang et al., 2017). Lastly, mice lacking CDKL5 expression selectively in forebrain GABAergic neurons (Dlx-cKO) showed an autistic-like phenotype characterised by reduced social preference and increased stereotypic behaviours but revealed relative preservation of learning and memory, motor coordination, and anxiety-related behaviours. In addition, they exhibited an enhancement of excitatory synaptic transmission and circuit-level hyperexcitability, coupled with elevated levels of NMDA receptors (Tang et al., 2019).

Surprisingly, in video-electroencephalography monitoring, none of these models presented spontaneous epileptic seizures, a key phenotype in the human pathology. The causes of this divergence may be the contribution of the genetic background to seizure

susceptibility and differences in brain connectivity as well as in CDKL5 function/modification between humans and mice (Tang et al., 2017, 2019; Wang et al., 2012; Yennawar et al., 2019). Despite this, Amendola and colleagues observed an abnormal electroencephalogram response to a pro-convulsant treatment with kainic acid (Amendola et al., 2014). In contrast, the KO model produced by Okuda and collaborators showed normal sensitivity to kainic acid, but presented significant hyperexcitability in response to NMDA, pointing out that CDKL5 may regulate seizure susceptibility by controlling the postsynaptic localisation of GluN2B-containing NMDARs in the hippocampus (Okuda et al., 2017). Moreover, *Cdkl5*^{R59X} knock-in mice exhibited decreased latency to seizure upon pentylenetetrazol administration, suggesting an underlying hyperexcitability that may be contributing to their behavioural alterations (Yennawar et al., 2019).

Considering that most CDD patients are heterozygous females with mosaic expression of the mutated allele, a detailed characterisation of heterozygous female *Cdkl5*-KO (*Cdkl5*+/−) mice was fundamental to advance preclinical and translational studies. In this regard, Fuchs and collaborators (Fuchs et al., 2018a) have recently provided a behavioural and molecular analysis of heterozygous female mice, derived from the *Cdkl5*-KO strain (Amendola et al., 2014). These mice showed several aspects of CDD, including autistic-like behaviours, motor impairment, defects in learning and memory, and abnormal breathing patterns. CDKL5 levels were found lower in the hippocampus and cerebellum compared to the cortex possibly explaining the severe phenotypic outcome in hippocampus-dependent behaviour. Finally, the heterozygous female mice also exhibited neuroanatomical defects, such as dendritic hypotrophy, reduced spine density, and an increased number of immature dendritic spines. Taking together, these findings demonstrated that the heterozygous females represent a valuable animal model for preclinical studies on CDD (Fuchs et al., 2018a).

1.6.6 Therapeutic strategies for CDD

Since the discovery of the involvement of CDKL5 in neurological disorders there have been pivotal steps towards an increased knowledge of CDKL5; however, more studies are still needed to allow the development of therapeutic strategies for CDD patients. Unfortunately, there are currently no specific treatments that arrest or slow down the progression of the disease. Therefore, the management is mainly symptomatic and aimed at maximising the developmental and cognitive potential. As mentioned, one of

the major problems in CDD is epilepsy, which is mostly refractory to medication. Regarding this, the antiepileptic drugs valproate and vigabatrin are commonly used during stage I (early epilepsy, from 1 to 10 weeks of birth), but when patients develop myoclonic and multifocal epilepsy, seizure control is lost. Indeed, at this stage of the disease, levetiracetam can be useful to treat myoclonic seizures while topiramate can be effective against tonic seizures (Bahi-Buisson et al., 2012b). Very recently, 20 CDD patients with treatment-resistant epilepsy have been enrolled in an open-label drug trial to provide class III evidence for the long-term safety and efficacy of cannabidiol (CBD) administration. Intriguingly, this study revealed that adjuvant therapy with CBD significantly reduced seizure frequency in CDD patients and this improvement was stable during time (Devinsky et al., 2018).

In the last years, pharmaceutical targeting of deficient pathways in animal models of CDD has been proven efficient in restoring some neuroanatomical and behavioural deficits. Loss of CDKL5 has been found to strongly affect both AKT/mTOR and AKT/GSK-3β pathways. As regards the AKT/mTOR pathway, in 2015, Della Sala and collaborators demonstrated that treatment with IGF-1, an activator of this pathway, could rescue defective ribosomal protein S6 phosphorylation, spine density, and PSD95 levels in young *Cdkl5*-KO mice. Of note, these molecular alterations could not be linked to lower-than-normal levels of endogenous IGF-1, as cortical IGF-1 levels were normal. Moreover, IGF-1 administration was effective also in adult mice, whose synaptic deficit was already established, and seemed to induce the formation of long-lasting spines (Della Sala et al., 2016). On the other hand, Fuchs and colleagues tested a pharmacological intervention to modulate the AKT/GSK-3β pathway in order to correct hippocampal developmental defects due to the loss of CDKL5. More specifically, the authors found that treatment with the GSK-3β inhibitor SB216763 restored neuron survival, dendritic maturation as well as spine development, and recovered the performance of *Cdkl5*-KO mice in hippocampus-dependent memory tasks. Moreover, one month after treatment withdrawal, the positive effects were still present, suggesting a long-term impact of the drug on such phenotypes (Fuchs et al., 2015). However, SB216763 is not usable in humans as it competes with ATP in its binding to GSK-3β, leading to potential non-specific effects. Consequently, non-ATP competitive compounds are supposed to be more suitable for therapeutic use in humans. One of these molecules is Tideglusib, which is able to improve hippocampal development and hippocampus-dependent behaviours specifically in juvenile *Cdkl5*-KO mice. Indeed, although GSK-3β activity is impaired to the same extent in young and adult *Cdkl5*-KO mice, Tideglusib

treatment administered in adulthood has no positive effects (Fuchs et al., 2018b). These findings denote that the pharmacotherapy with GSK-3β inhibitors may be effective in CDD patients only if administered early in postnatal development.

Another pharmacological target is HDAC4. As previously described, the loss of CDKL5 impairs HDAC4 activity and induces its nuclear localisation. It is important to highlight that nuclear translocation of HDCA4 is accompanied by a decrease in histone acetylation and, in turn, may produce distinctive cellular effects through epigenetic and non-epigenetic mechanisms of gene regulation, which may contribute to the brain phenotype of CDD patients. For this reason, Trazzi and colleagues tested LMK235, a drug that inhibits HDAC4. This compound completely restored hippocampus-dependent memory in *Cdkl5*-KO mice, which is in line with the role of HDAC4 in memory formation. Besides, LMK235 was able to normalise defective survival and maturation of neuronal precursor cells of *Cdkl5*-KO mice (Trazzi et al., 2016).

Lately, in our laboratory pregnenolone (PREG) was found to have positive effects on CDKL5-related morphological defects both in cycling cells and in neurons (Barbiero et al., 2017b). PREG is an endogenous steroid generated from cholesterol by the action of CYP11A1 that is known to bind and activate CLIP170 by changing its conformation and potentiating its microtubule binding in this way promoting MT dynamics (Weng et al., 2013), which are altered in CDKL5-lacking cells (Baltussen et al., 2018; Barbiero et al., 2017b, 2020). Besides, the efficacy of the synthetic non-metabolisable derivative pregnenolone-methyl-ether (PME; also known as 3β-methoxy-pregnenolone) has been evaluated. Intriguingly, PME is capable of ameliorating the morphological alterations found in both young and mature *Cdkl5*-KO neurons (Barbiero et al., 2020). These results suggest that PME may represent an interesting alternative to PREG in a future clinical application as, while maintaining the same biological action, it is devoid of the undesired side effects due to the metabolism of PREG into downstream steroids (Bianchi & Baulieu, 2012; Duchossoy et al., 2011). In addition to these compounds, in our laboratory, it has been demonstrated that tianeptine, a cognitive enhancer and antidepressant drug, known to recruit and stabilise AMPARs at the synaptic sites, is capable of rescuing the expression and membrane insertion of AMPARs as well as the number of PSD95 clusters. Indeed, tianeptine treatment normalised GluA2 expression in *Cdkl5*-silenced neurons (Tramarin et al., 2018). Interestingly, in a previous study, tianeptine was able to improve the respiration phenotype in a mouse model of RTT (Pozzo-Miller et al., 2015), making this drug an interesting candidate for the treatment of CDD.

Although these data raise hope that pharmaceutical intervention is possible for CDD, the field still needs to further elucidate the networks regulated by CDKL5 to provide the basis for the rational design of disease-modifying therapeutic strategies.

1.6.7 Neuroactive steroids as a possible pharmacological approach for CDD

Neuroactive steroids are one of the drug classes, which have recently raised interest in the CDD field. The concept that steroids could be synthesised *de novo* in the brain was introduced by Baulieu and colleagues in the '80s (Baulieu, 1998; Melcangi et al., 2008). These steroids were named "neurosteroids" to refer to their atypical origin and to differentiate them from the steroids derived from classic steroidogenic tissues such as gonads, placenta and adrenal glands (Magnaghi, 2007). Subsequently, the term "neuroactive steroids" was used to indicate steroids that target neurons and glial cells, including hormonal steroids originated in the peripheral glands, steroids locally synthesised by the neurons and glial cells (neurosteroids) and synthetic steroids, some of them used in clinical practice (Giatti et al., 2019). Of note, since neurosteroidogenesis takes place not only in neurons but mainly in glial cells, which possess the enzymes capable of forming neurosteroids or convert hormonal steroids into neuroactive metabolites, the nervous system is considered a steroidogenic organ (Magnaghi, 2007; Tvrdeić & Poljak, 2016). The neurosteroid synthesis (Figure 1.11) starts inside the mitochondria, where lipophilic cholesterol is not able to freely pass through the aqueous environment in order to reach the inner mitochondrial membranes. Thus, it must be translocated through the hydrophilic media by a process that involves a multimolecular complex composed by several proteins such as the translocator protein of 18kDa (TSPO), the steroidogenic acute regulatory protein (StAR), the adenine nucleotide transporter protein (ANT) and the voltage-dependent anion channel protein (VDAC) (Giatti et al., 2019). Once cholesterol is transported from the outer to the inner mitochondrial membrane, it is converted into PREG by the cytochrome P450 enzyme 11A1 (CYP11A1), which is located close to the inner mitochondrial membrane. Interestingly, this specific hydroxylase involved in cholesterol side chain cleavage was found at the level of the white matter throughout the brain through immunocytochemical evidence (Baulieu, 1998). PREG represents the precursor of all other endogenous neurosteroids as it is further metabolised in the endoplasmic reticulum by multiple, subsequent enzymatic reactions. The latter are catalysed with a variety of enzymes

(CYP450 as well as non CYP450 types) and are able to produce functionally and structurally diverse neurosteroids (Tvrdeić & Poljak, 2016). In one of the above reactions, the enzyme 3β-hydroxysteroid dehydrogenase (3β-HSD) converts PREG into progesterone (PROG), which also serves as a precursor for the synthesis of important neurosteroids. Indeed, PROG is reduced by the 5α-reductase (5α-R) to 5α-dihydroprogesterone (5α-DHP), which, in turn, is reduced to 5α-pregnan-3α-ol-20-one, also known as allopregnanolone (ALLO), by the 3α-hydroxysteroid-dehydrogenase (3α-HSD).

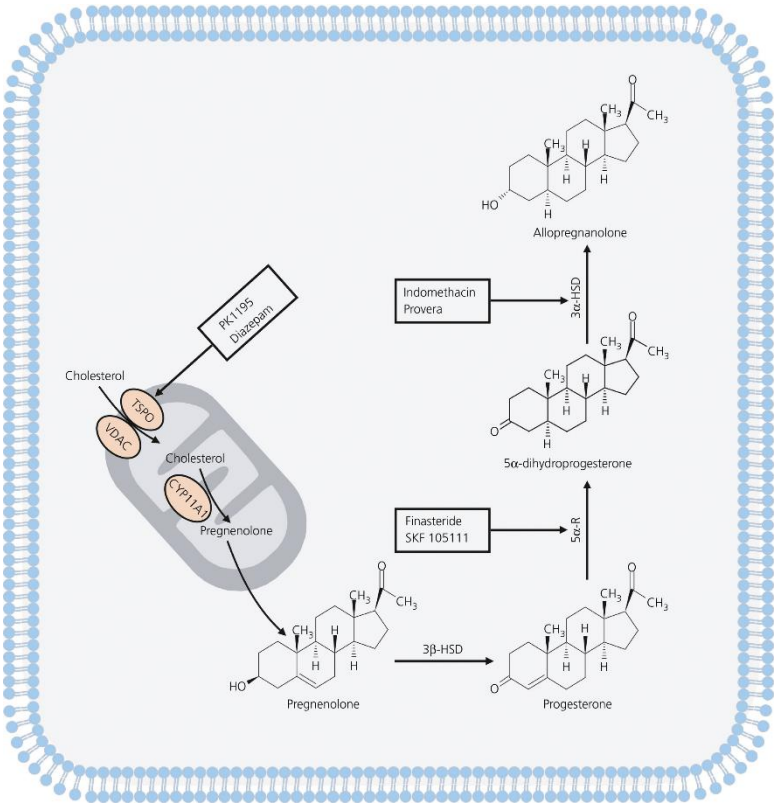

Figure 1.11 The *de novo* neurosteroid synthesis. A schematic diagram of neurosteroidogenesis with selected enzymes and drugs inhibiting enzyme. This process starts with cholesterol, which is translocated across the mitochondrial membrane by translocator protein (TSPO) and accessory proteins such as the 32-kDa voltage-dependent anion channel (VDAC). Then, the mitochondrial cytochrome P450 enzyme 11A1 (CYP11A1) converts cholesterol to pregnenolone, which diffuses into the cytosol. Cytosolic pregnenolone (PREG) is subsequently converted to progesterone (PROG) by 3β-hydroxysteroid dehydrogenase (3β-HSD). PROG, either newly synthesised locally, or of peripheral origin, is reduced to 5α-dihydroprogesterone (5α-DHP) and then to allopregnanolone (5α-pregnan-3α-ol-20-one; ALLO) by the enzymes 5α-reductase (5α-R) and 3αhydroxysteroid-dehydrogenase (3α-HSD) respectively. Pharmacological agents such as finasteride and indomethacin inhibit the enzymes 5α-R and 3α-HSD respectively (Belelli et al., 2017).

A variety of physiological (e.g. development, puberty, pregnancy, stress, ovarian cycle) and pathophysiological (e.g. stress, panic attacks, major depression, schizophrenia, pregnancy, neural development and ageing) are associated with changes in neurosteroid levels. Particularly, perturbations in the levels of progesterone-derived steroids could be partly attributable to postpartum depression and premenstrual tension, and certain neurological problems such as catamenial epilepsy (Belelli et al., 2017; Belelli & Lambert, 2005).

In accordance with the aim of this thesis, it is crucial to mention that neuronal inhibition could be enhanced by the above-mentioned physiological and pathophysiological as well as drug-induced changes in neurosteroid levels. Indeed, some progesterone metabolites, including ALLO, exert two different effects on $GABA_A$Rs: on one hand, a GABA-modulatory effect (at low concentrations), being selective positive allosteric modulators of such receptors, and, on the other hand, a GABA-mimetic effect (at high concentrations), being able to directly activate the $GABA_A$R-channel complex and to suppress the excitatory neurotransmission (Belelli & Lambert, 2005; Chuang & Reddy, 2018).

The functional role of $GABA_A$Rs in the regulation of network excitability and susceptibility to brain disorders could represent a novel target for CDD, paving the way to new therapeutic strategies. Eventually, the possibility of using synthetic neurosteroids to treat CDD patients might be of striking interest.

2 Aim of the Work

Most studies converge on a role of CDKL5 in regulating dendritic spine formation and functions; so far, CDKL5 appears to control excitatory neurotransmission by regulating the expression of PSD95 and specific subunits of NMDARs and AMPARs. Despite this, the possible role of CDKL5 in regulating inhibitory neurotransmission is still unknown. A further investigation of its function at inhibitory synapses would allow to characterise in more details the molecular aspects underlying the autistic-like and the epileptic phenotype of CDD patients. Indeed, seizures are the most disabling symptoms in CDD, and seizure management is particularly troublesome since most patients are refractory to conventional anti-epileptic drugs. For these reasons, the aim of my Ph.D. project was to explore the possible role of CDKL5 in neuronal inhibition, pursuing three independent approaches:

a) **Characterising the interaction between CDKL5 and the main actors of the inhibitory synapse from a molecular point of view.** In a recent publication, CDKL5 was identified as the direct interactor of CB but no functional role was elucidated. The first part of the project was aimed at analysing the interaction of CDKL5 with the key inhibitory components required for $GABA_AR$ clustering, such as CB and gephyrin. Moreover, CB alternates between a folded inactive conformation, in which it cannot interact with phosphoinositides of the plasma membrane, and an open extended conformation, which allows inhibitory receptor clustering and function (Papadopoulos & Soykan, 2011). Therefore, hypothesising that CDKL5 could have a potential role in regulating the conformation of collybistin, we found it relevant to map the CDKL5 interaction surface of CB.

b) **Clarifying CDKL5 role in the inhibitory synapse, through biochemical and electrophysiological analyses, in order to understand if the absence of CDKL5 could lead to basal defects in this compartment.** The second intent was to evaluate what CDKL5 deficiency in this compartment entailed, shedding light on its possible role. To this end we decided to study the postsynaptic compartment from a biochemical point of view, focusing on synaptic $GABA_AR$ subunits, gephyrin and neuroligin2 (NL2) analysing their membrane exposure

and possible phosphorylation events. To understand if CDKL5 loss leads to a functional impairment, we decided to integrate our results with electrophysiological recordings.

c) **Performing a pharmacological treatment to target and normalise basal defects in synaptic $GABA_AR$ expression and function.** We hypothesise that CDKL5 may regulate $GABA_AR$ expression through its control on MT dynamics. Indeed, our published and submitted results indicate that CDKL5 loss impacts the functionality of CLIP170 with negative consequences on MT dynamics that appear to contribute to defects in neuronal morphology and maturation of dendritic spines. The synthetic neuroactive steroid PME represents a fundamental tool that allows studying the involvement of MT dynamics in CDKL5-dependent defects. We therefore decided to test the effect of PME on CDKL5-dependent inhibitory defects. Treatment with PME was therefore scheduled both *in vitro*, on *Cdkl5*-KO primary hippocampal neurons, and *in vivo*, in fully symptomatic *Cdkl5*-KO mice.

In summary, the aim of this study is to understand the role played by CDKL5 in the inhibitory synapse and to investigate the possible beneficial effect of PME in restoring the inhibitory defects due to the absence of CDKL5.

3 Materials and Methods

3.1 Ethical statement

Protocols and use of animals were approved by the Animal Ethics Committee of the University of Insubria and in accordance with the guidelines released by the Italian Ministry of Health (D.L. 2014/26) and the European Community directives regulating animal research (2010/63/EU). Juvenile and adult mice were euthanised by cervical dislocation, while neonates were sacrificed by exposure to CO_2 followed by decapitation.

3.2 Mouse strains, husbandry and genotyping

All mice were handled according to protocols approved by the Italian Ministry of Health. *Cdkl5* wild-type (WT) and *Cdkl5* knock-out (KO) mice were obtained crossing heterozygous females (*Cdkl5*$^{-/+}$) with WT males. Littermate controls were used for all experiments. After weaning, mice were housed three to five per cage (activity enriched) on a 12 h light/dark cycle in a temperature-controlled environment with food and water provided *ad libitum*. All efforts were made to minimise suffering. Genotyping of pups and embryos was performed using the PCRBIO Rapid Extract PCR Kit (Resnova, PB10.24-40). Extracted DNA was amplified in a proprietary buffer system using PCRBIO HS Taq Mix Red (Resnova, PB10.23-02) with specific primers for *Cdkl5*: 5' ACGATAGAAATAGAGGATCAACCC 3' (#108 forward), 5' CCCAAGTATACCCCTTTCCA 3' (#109 reverse) and 5' CTGTGACTAGGGGCTAGAGA 3' (#125 reverse). Embryos of either sex were used to generate primary cultures of hippocampal neurons.

3.3 Primary neuronal cultures

Primary hippocampal cultures were prepared from embryonic day 17 (E17) mouse embryos considering the day of the vaginal plug as E0. *Cdkl5*-WT and *Cdkl5*-KO embryos were obtained from pregnant *Cdkl5*$^{-/+}$ females crossed with WT males, kept on a CD1 background. Pregnant *Cdkl5*$^{-/+}$ female mice were sacrificed by cervical dislocation and the embryos were recovered and hippocampi rapidly dissected. After washing in

Hank's balanced salt solution with calcium and magnesium (HBSS/Ca^{2+}/Mg^{2+}; Gibco, 14025100), the hippocampi were dissociated by incubation at 37°C for 10 min in 0.25% trypsin (Gibco, 25200-056) and further washed in HBSS/Ca^{2+}/Mg^{2+}. Neurons were suspended in dissecting medium [Dulbecco's modified Eagle's medium (DMEM; Euroclone, ECM0101L), 10% horse serum (Euroclone, ECS0090L), 2 mM L-glutamine (Euroclone, ECB3000D), 1 mM sodium pyruvate (Gibco, 11360-039)] to block the action of trypsin. Eventually, cells were mechanically dissociated by pipetting and plated on coverslips coated with 1 mg/mL poly-L-lysine (Sigma-Aldrich, P2636) in 24-well plates (densities: 60,000 neurons/well, 300 cells/mm^2 for both immunofluorescence and western blotting) or in 6-well plates (densities: 225,000 neurons/well, 234 cells/mm^2 for electrophysiological studies). Regarding *in vitro* biotinylation, neurons were directly plated on 6-well plates coated with 0.1 mg/mL poly-L-lysine (Sigma-Aldrich, P2636) (densities: 400,000 neurons/well, 416 cells/mm^2). Neurons were maintained in neurobasal medium (Life Technologies, 21103-049) supplemented with 1X GlutaMAX™ supplement (Gibco, 35050-038) and 2% B27 (Gibco, 17504044) in a humified incubator with 5% of CO_2 at 37°C. After 3 days *in vitro* (DIV), cytosine β-D-arabinofuranoside (Sigma-Aldrich, C1768) was added to cultured neurons at final concentration of 2 µM to prevent astroglial proliferation.

3.4 Pharmacological treatment

Pregnenolone-methyl-ether (PME) was kindly provided by Massimilliano Bianchi (Transpharmation Ltd, Ireland). Primary hippocampal neurons were treated at DIV11 with 0.3 and 1 µM PME or DMSO 0.1% (vehicle), one pulse, for 72 h. Male *Cdkl5*-WT and *Cdkl5*-KO mice were treated with PME (10 mg/kg) or sesame oil (vehicle) through subcutaneous injection for 7 days starting from postnatal day (PND) 60.

3.5 Plasmids

pEGFP-gephyrin, pRK5myc-CB2-$SH3^+$, pRK5myc-CB2-ΔSH3, pRK5myc-CB2-$SH3^+$-ΔPH, pRK5myc-CB2-ΔSH3-ΔPH have been kindly provided by Theophilos Papadopoulos's laboratory. All the above constructs were generated as described previously (Harvey et al., 2004). pFlag-CDKL5-FL encoding the 107 kDa splice variant was generated as described elsewhere (Williamson et al., 2012).

3.6 Cell cultures

Human embryonic kidney 293 (HEK293T) cells were maintained in DMEM (Euroclone, ECM0101L) supplemented with 10% fetal bovine serum (FBS; Euroclone, ECS0180L), 2 mM L-glutamine (Euroclone, ECB3000D), penicillin/streptomycin (100 units/mL and 100 µg/mL respectively, Euroclone, ECB3001D) at 37°C with 5% CO_2. Cells were cultured in 60 mm Petri dishes for 24 h and Lipofectamine™ 3000 (Life Technologies, L3000015) was used to co-transfect 2.5 µg of each construct (ratio of 1:1) for a total amount of 5 µg.

3.7 Antibodies

The following primary antibodies were used in immunofluorescence and western blotting experiments: rabbit anti-CDKL5 (Sigma, HPA002847), mouse anti-CDKL5 (Santa Cruz, sc-376314), mouse anti-Flag (Sigma, F4042), mouse anti-gephyrin (Santa Cruz, sc-25311), mouse anti-pSer^{270} gephyrin (SYSY, 147011), rabbit anti-collybistin (SYSY, 261003), mouse anti-Neuroligin2 (SYSY, 129511) , rabbit anti-$GABA_AR$ γ_2 (SYSY, 224003), rabbit anti-$GABA_AR$ β_3 (SYSY, 224403), rabbit anti-pERK 1/2 (Santa Cruz, sc-16982), mouse tERK 1/2 sc-514302), mouse anti-GluA2 (Millipore, MAB397), mouse anti-bassoon (Santa Cruz, sc-58509), chicken anti-MAP2 (SYSY, 188006), rabbit anti-GAPDH (Sigma, G9545), mouse anti-αTubulin (Sigma-Aldrich, T6074). Secondary antibodies Alexa Fluor anti-mouse 555nm (ab150114), anti-rabbit 488nm (ab150077), anti-chicken 488nm (A-11039) and anti-chicken 405nm (ab175674) for immunofluorescence experiments were purchased from Abcam or Invitrogen. HRP conjugated secondary anti-mouse (115-035-062) and anti-rabbit (111-035-144) antibodies for western blottings were obtained from Jackson Immunoresearch.

3.8 Immunofluorescence on primary hippocampal neurons

After fixation in 4% formaldehyde (Pierce™, 28908) with 4% sucrose (Sigma-Aldrich, 16104), neurons were blocked in 1X Phosphate Buffered Saline (PBS) with 5% goat serum (Euroclone, ECS0200D) and 0.2% Triton X-100. To analyse surface exposed γ_2 subunit-containing $GABA_AR$, the immunostaining was performed under non-permeabilising conditions, therefore neurons were blocked in 1X PBS with 5% goat

serum but without 0.2% Triton X-100. Then neurons were incubated with the appropriate primary antibody overnight at 4°C and subsequently with the secondary antibody for 1 h at room temperature. Slides were mounted with ProLong Gold antifade reagent (Life Technologies, P36930).

Gephyrin puncta, bassoon puncta and surface expression of $GABA_AR$ γ_2 clusters were analysed at DIV14 by staining with the specific antibodies using MAP2 staining to visualise neuronal dendrites. Images were captured using a 60x objective coupled to an Olympus BX51 fluorescence microscope equipped with Retiga R1 (QImaging) CCD camera. The number of gephyrin and bassoon puncta along with the fluorescence intensity of $GABA_AR$ γ_2 clusters were measured in 30 µm long segments of 10-30 dendrites per condition, using the software Fiji ImageJ (function: analyse particles or measure).

3.9 Immunofluorescent staining of hippocampal slices

Mice were deeply anesthetised with CO_2, brains were removed and cut along the midline and frozen in liquid nitrogen. Slices were then cut with cryostat (30 µm) and fixed by immersion in 2% formaldehyde plus 2% sucrose in 1X PBS for 90 seconds. Slides were blocked for 1 h in blocking solution (0.05% goat serum, 3% Triton X-100 in 1X PBS) incubated with anti-$GABA_AR$ γ_2 antibody (1:1000) in a humid chamber overnight at 4°C. After incubation with the secondary antibody (Alexa Fluor anti-rabbit 488 nm) for 1 h at room temperature the slices were mounted with ProLong Gold antifade reagent (Life Technologies, P36930) (Schneider Gasser et al., 2006). Images of the molecular layer of the dentate gyrus were acquired with a LEICA TCS SL confocal microscope (LEITZ; Leica Mycrosystems, Wetzlar, Germany) with objective 63X (NA 1.32; zoom factor = 8) and the pinhole set at 1 Airy unit. Four slices per animal were analysed and the number of $GABA_AR$ γ_2 clusters was quantified using the software Fiji ImageJ (function: analyse particles). Optimised threshold values and size filters (0.1 - 0.8 μm^2) were applied for all the images to identify $GABA_AR$ γ_2 clusters. The number of $GABA_AR$ γ_2 puncta was calculated in four identical sections for each slice (in order to have a mean of four separate zones of the dentate gyrus per single slide) and expressed per μm^2 (McLeod et al., 2017).

3.10 Western blotting

Samples were separated by 8-10% SDS-PAGE, transferred to nitrocellulose membranes, and blocked in 5% non-fat milk in TBS [20 mM Tris-HCl, pH 7.4, 150 mM NaCl (Sigma-Aldrich)] with 0.2% Tween-20 (TBS-T). Blots were incubated with primary antibodies overnight at 4°C, washed in TBS-T, and incubated with appropriate secondary antibodies for 1 h at room temperature. After extensive washes, blots were developed with protein detection system-ECL (Genespin, STS-E500) coupled to G:BOX Chemi Imaging System (Syngene). Densitometric expression analyses were performed using ImageJ software. Protein expression levels were normalised using GAPDH as internal standard. However, for the immunoprecipitation experiment *in vitro* as well as for the cell surface biotinylation assay, protein levels were quantified differently as described below. Primary hippocampal neurons were lysed directly in Laemmli buffer 3X and a volume corresponding to approximately 10 µg of proteins was separated by SDS-PAGE and western blotting.

3.11 Immunoprecipitation

For immunoprecipitation (IP) of CDKL5 *ex vivo,* we used 1 mg of a mouse brain extract (PND20) lysed in lysis buffer [50 mM Tris-HCl pH 7.4, 150 mM NaCl, 1% Triton X-100, 1 mM EDTA, 1 mM EGTA, 1X protease inhibitor cocktail (PIC; Sigma-Aldrich, P8340) and 1X PhosSTOP (Roche, 4906837001)]. The lysate was pre-cleared with 20 µL of slurry protein-G agarose (Life Technologies, 15920010) for 1 h at 4°C on a rotating wheel and, subsequently, incubated overnight at 4°C with 1 µg of anti-CDKL5 or unrelated IgGs as control (anti-Flag). The immunocomplexes were precipitated with 30 µL of slurry protein-G agarose for 2 h at 4°C on a rotating wheel, washed four times for 10 min with lysis buffer (50 mM Tris-HCl pH 7.4, 200 mM NaCl, 1% Triton X-100, 1 mM EDTA, 1 mM EGTA, 1X PIC and 1X PhosSTOP) and analysed by SDS-PAGE and western blotting.

For IP of CDKL5 *in vitro*, HEK293T cells were harvested in 1X PBS on ice, lysed in 300 µL of lysis buffer (50 mM Tris-HCl pH 7.4, 150 mM NaCl, 1% Triton X-100, 1 mM EDTA, 1 mM EGTA, 1X PIC and 1X PhosSTOP) for 30 min. Cell lysates were sonicated and clarified by centrifugation at 14,000 rpm for 10 min at 4°C, where after the supernatants were collected and quantified by Quick Start™ Bradford Kit (Bio-Rad, 5000205). 400 µg

of HEK293T extract was incubated overnight at 4°C, on a rotating wheel, with 1 µg of anti-CDKL5. Subsequently, the immunocomplexes were precipitated with 30 µL of slurry protein-G agarose (Life Technologies, 15920010) for 2 h at 4°C on rotating wheel, washed four times for 10 min with lysis buffer and analysed by SDS-PAGE and western blotting. Changes in the interaction between Flag-CDKL5 and each collybistin construct were evaluated as the ratio co-IP/IP, normalised on total cell lysate (input).

3.12 Dephosphorylation Assay

Hemi-hippocampi of *Cdkl5*-WT and *Cdkl5*-KO mouse brains (PND60) were homogenised with tissue grinder (30 strokes) in 450 µL of lysis buffer (50 mM Tris-HCl pH 7.4, 150 mM NaCl, 1% Triton X-100, 1 mM EDTA, 1 mM EGTA, 1X PIC). Each extract was then divided into two parts and lysed for 30 min with or without 1X PhosSTOP on ice. 100 µg of protein extract was incubated with or without 1200 U of lambda-phosphatase (λPP; NEB, P0753S) in 150 µL of lysis buffer supplemented with 1 mM $MnCl_2$ and 1X NEBuffer for protein metallophosphatase (PMP) for 3 h at 30°C. Subsequently, the reaction was stopped by incubation at 65°C for 15 min. The samples were analysed by SDS-PAGE on 8% gel with 150:1 acrylamide:bisacrylamide and western blotting.

3.13 Biotinylation and purification of plasma membrane-associated proteins

Biotinylation assays were performed according to a previously described protocol (Arancibia-Cárcamo et al., 2006; Ferreira et al., 2015) with slight modifications. Primary hippocampal neurons at DIV14 were washed twice with HBSS/Ca^{2+}/Mg^{2+}, followed by incubation with 0.5 mg/mL Sulfo-NHS-SS-Biotin (Cyanagen, B101N,0050) for 15 min at 4°C under mild shaking. Cells were then washed twice with HBSS/Ca^{2+}/Mg^{2+} supplemented with glycine (50 mM) and BSA (0.5%). After a 30 min incubation, cells were lysed with standard radio-immunoprecipitation assay buffer (RIPA) buffer (50 mM Tris-HCl pH 7.4, 150 mM NaCl, 1% NP40, 0.1% SDS, 0.5% SDC, 1 mM EDTA, 2 mM EGTA, 1X PhosSTOP, 1X PIC). Subsequently, the lysates were placed in microcentrifuge tubes and left to solubilise with rotation on a wheel at 4°C for 1 h. After solubilisation, the lysates were sonicated briefly, and cell and nuclear debris were

removed by centrifugation at 14,000 g for 15 min. The supernatants were quantified by BCA protein assay kit (Pierce™, 23227) and 500 µg of cell lysates were precipitated with 50 µL of StreptAvidin UltraLink Resin (Pierce™, 53114) overnight at 4°C on rotating wheel. The slurry was spun down from the supernatant (4000 g, 5 min) and washed three times for 5 min in RIPA containing 500 mM NaCl followed by a further wash in standard RIPA. Finally, the samples were eluted with Laemmli gel loading buffer and heated at 70°C for 10 min prior to SDS-PAGE and western blotting. Surface expression of postsynaptic proteins was evaluated as the ratio between biotinylated fraction (surface) and total cell lysate.

3.14 Synaptosomal fractionation

CD1 mouse hippocampi were homogenised using a tissue grinder in homogenization buffer [320 mM sucrose (Sigma-Aldrich, 16104), 5 mM sodium pyrophosphate (Sigma-Aldrich, 71516), 1 mM EDTA, 10 mM HEPES (Sigma-Aldrich, H4034) pH 7.4, and protease inhibitor mixture]. The homogenate was then centrifuged at 800 g for 10 min at 4°C to yield P1 (nuclear fraction) and S1 fractions. S1 fraction was further centrifuged at 17,000 g for 20 min at 4°C to yield P2 (membrane/crude synaptosome) and S2 (cytosol) fractions. P2 was resuspended in homogenisation buffer and layered onto nonlinear sucrose gradient cushion (1.2 M, 1.0 M, and 0.8 M sucrose from bottom to top), then centrifuged at 82,500 g for 2 h at 4°C. Synaptosomes were collected at the interface of 1.0 M and 1.2 M sucrose cushion. Collected synaptosomes were diluted with 10 mM HEPES pH 7.4, to reach a final concentration to 320 mM sucrose and then centrifuged at 150,000 g for 30 min at 4°C (Heo et al., 2018). In the end, the homogenate and the P1, S2 and synaptosomal fractions were incubated in RIPA buffer (50 mM Tris-HCl pH 7.5, 150 mM NaCl, 1% NP40, 0.1% SDS, 0.5% SDC, 1 mM EDTA, 1 mM EGTA, 1X PIC and 1X PhosSTOP) for 20 min on ice, quantified with BCA Protein Assay Kit and analysed by western blotting.

3.15 *In vitro* electrophysiological recordings

GABA-mediated inhibitory post synaptic currents in miniature (mIPSCs) were recorded by patch-clamp technique in whole-cell voltage clamp configuration in presence of 1 µM tetrodotoxin (TTX, Tocris), which is a reversible blocker of the sodium channel thus

blocking the generation of action potentials. The miniature postsynaptic currents occur spontaneously by the release of single synaptic vesicles, meaning that they are events generated from the quantal release of neurotransmitter molecules interacting with their postsynaptic receptors. These recordings were obtained from primary hippocampal neurons at DIV14 using the Axopatch 200B amplifier and the pClamp-10 software (Axon Instruments). Recordings were performed in Krebs'-Ringer's-HEPES (KRH) external solution (125 mM NaCl, 5 mM KCl, 1.2 mM $MgSO_4$, 1.2 mM KH_2PO_4, 2 mM $CaCl_2$, 6 mM glucose, 25 mM HEPES-NaOH pH 7.4). Recording pipettes were fabricated from glass capillary (World Precision Instrument) using a two-stage puller (Narishige); they were filled with the cesium-gluconate intracellular solution (130 mM: 8 mM CsCl, 2 mM NaCl, 10 mM HEPES, 4 mM EGTA, 4 mM MgATP, 0.3 mM GTP pH 7.3) and the tip resistance was 3-5 MΩ. In order to identify inhibitory miniature events, primary hippocampal neurons were held at +10 mV. The recorded traces have been analysed using Clapfit-pClamp 10 software, after choosing an appropriate threshold.

3.16 *Ex vivo* electrophysiological recordings

Coronal slices containing the hippocampus (400 µm) were obtained from *Cdkl5*-WT and *Cdkl5*-KO mice at PND60 using a standard method and maintained in an interface chamber (Lüthi et al., 1997). Briefly, after being anesthetised with CO_2, animals were decapitated, and brains were quickly removed from the skull and placed in ice-cold cutting solution (83 mM NaCl, 2.5 mM KCl, 1.25 mM NaH_2PO_4, 21 mM $NaHCO_3$, 72 mM sucrose, 25 mM glucose 25, 0.45 mM sodium ascorbate, 1 mM $CaCl_2$, 4 mM $MgCl_2$). Slice were kept at interface for 30 min at 35 °C; the pH was maintained at 7.4 by bubbling carbogen (5% CO_2, 95% O_2). During the field recording experiments, slices were submersed and perfused at 33°C with artificial cerebro-spinal fluid (ACSF; 125 mM NaCl, 2.5 mM KCl, 1.25 mM NaH_2PO_4, 26 mM $NaHCO_3$, 10 mM glucose, 1.5 mM $CaCl_2$, 1 mM $MgCl_2$) bubbled with 95% O_2/5% CO_2, pH 7.4. Schaffer collateral in stratum CA3 was stimulated by a concentric electrode (WPI, TM33CCINS; 2-3 µm in diameter) and multiple population spikes (polyspikes) were recorded from the CA1 pyramidal layer by a borosilicate glass microelectrode (1-2 mΩ) filled with ACSF. A stimulating intensity that elicited 50-60% of maximal polyspikes amplitude (0.05 Hz, 1 ms pulse duration) was used. In order to increase the excitability in CA1, Schaffer collateral was stimulated using 30 sweeps at 1 Hz (intensity and duration as above).

3.17 Statistical Analysis

All experiments and analyses were performed knowing the respective genotypes of the animals. Data quantification were analysed with Prism software (GraphPad) and all values were expressed as the mean±SEM. The significance of western blotting and immunofluorescence results was evaluated by unpaired Student's t-test, One-way ANOVA followed by Tukey's multiple comparisons test and Two-way ANOVA followed by Tukey's multiple comparisons test or Fischer's LSD test. The significance of *in vitro* electrophysiological studies was evaluated by Mann Whitney U test, Kruskal-Wallis test, followed by Dunn's multiple comparisons test, One-way ANOVA followed by Tukey's multiple comparisons test and unpaired Student's t-test. Statistical evaluations of *ex vivo* electrophysiological recordings were performed by unpaired Student's t-test.

3.18 Nomenclature

CDKL5 written in upper case letters refers to the human and mouse protein. *CDKL5* and *Cdkl5* reported in *italics* indicate, respectively, the human and the murine genes and transcripts.

4 Results

4.1 CDKL5 interacts with the molecular complex of collybistin and gephyrin

In a recent study, Uezu and colleagues used an *in vivo* chemico-genetic proximity-labelling approach to discover novel inhibitory postsynaptic proteins (Uezu et al., 2016). In a clustergram of this work, the authors identified CDKL5 as a direct interactor of CB. CB, which is encoded by *Arhgef9*, is a brain-specific GEF selectively localised at the GABAergic postsynapses (Kins et al., 2000). It interacts with gephyrin (Kins et al., 2000), a scaffold protein that forms postsynaptic lattices at these synapses (Tretter et al., 2012; Tyagarajan & Fritschy, 2014).

To evaluate a possible role of CDKL5 at the inhibitory synapses, we investigated its interaction with proteins that play a fundamental role in the organisation of the inhibitory sites. In particular, gathering the evidence provided by Uezu and colleagues, we performed immunoprecipitation (IP) experiments allowing us to detect both CB and gephyrin among the CDKL5-interacting proteins. In detail, lysates from PND20 mouse brains were used to immunoprecipitate CDKL5 and, through the subsequent western blotting (WB), we could appreciate both CB and gephyrin in the immunoprecipitate (Figure 4.1).

This result confirms the interaction between CDKL5 and CB as reported by Uezu *et al.* (Uezu et al., 2016), further including also gephyrin as part of the complex. Altogether, this might suggest a novel role of CDKL5 in regulating inhibitory receptor clustering and function.

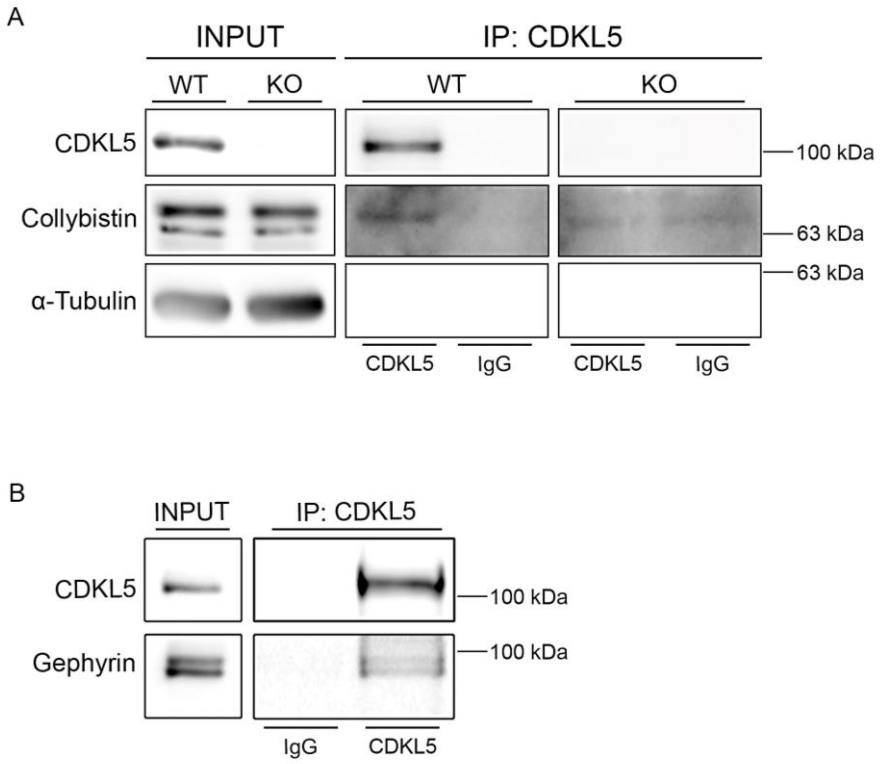

Figure 4.1 CDKL5 belongs to the molecular complex of collybistin (CB) and gephyrin *ex vivo*. A-B) Representative IP experiment of PND20 mouse brain lysates with an anti-CDKL5 antibody or unrelated IgGs. Whole brain lysate (input; 2.5%) and immunocomplexes were analysed through WB with antibodies against CDKL5, CB **(A)** and gephyrin **(B)**. In **(A)**, CDKL5 was precipitated from *Cdkl5*-WT and -KO lysates while only WT lysates were used in **(B)**. n=3.

CB harbours three major functional domains (Figure 4.2): a Src homology 3 (SH3), a nucleotide exchange factor (DH) that selectively activates the small GTPase Cdc42 and a pleckstrin-homology (PH) domain (Kins et al., 2000). Considering the direct interaction between CDKL5 and CB, we proceeded mapping the CB domains involved in this interaction. In rodents, three splice variants of CB have been reported (CB 1-3; Figure 4.2), differing in their C-termini. CB2 and CB3 isoforms are expressed in adult neurons and are present with or without the SH3 domain (Harvey et al., 2004; Kins et al., 2000). Expression vectors of myc-tagged CB2 (kindly provided by Papadopoulos, University of Göttingen) with or without the SH3 domain, myc-CB2-SH3$^+$ and myc-CB2-ΔSH3, as well as with or without the PH domain, myc-CB2-SH3$^+$-ΔPH and myc-CB2-ΔSH3-ΔPH, were transfected into HEK293T cells together with Flag-tagged CDKL5 and the lysates used for IP experiments.

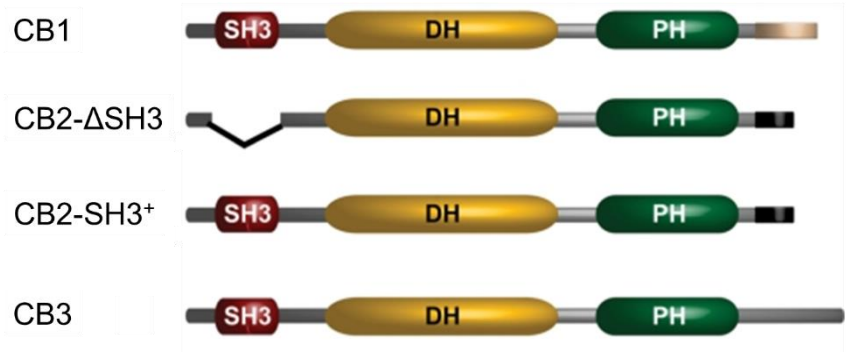

Figure 4.2 Schematic representation of the domain structures of known CB isoforms. CB splice variants (CB 1-3) carry a dbl-homology (DH) and a pleckstrin-homology (PH) domain connected by a short linker sequence. The DH-domain mediates the GDP/GTP-exchange activity. The PH region is thought to regulate the membrane attachment of GEFs by binding to phosphatidylinositol-3-phosphate. The N-terminal region contains a Src homology 3 (SH3) domain, although two splice variants of CB2 and CB3 were detected, one containing ($SH3^+$) and one lacking (ΔSH3) the SH3-domain. Importantly, this domain acts as an autoinhibitory domain maintaining CB in an inactive conformation (adapted from Papadopoulos & Soykan, 2011).

Upon IP of CDKL5 with an anti-CDKL5 antibody, we analysed the presence of the CB derivatives through WB (Figure 4.3A). It appeared that only CB derivatives containing the SH3 domain interact significantly with CDKL5 since the CB-ΔSH3 and CB-ΔSH3-ΔPH were barely detectable in the WB. The quantification of the interaction in three separate experiments confirmed this: the ratio co-IP/IP, normalised with the respective input, is significantly lower in lysates from cells expressing pFLAG-CDKL5 with myc-CB2-ΔSH3 or myc-CB2-ΔSH3-ΔPH (Figure 4.3B; myc-CB2-$SH3^+$: 1.00±0.00; myc-CB2-ΔSH3: 0.04±0.02; myc-CB2-$SH3^+$-ΔPH: 0.51±0.15; myc-CB2-ΔSH3-ΔPH: 0.12±0.05). Moreover, in accordance with the *ex vivo* IP, we also detected gephyrin in the co-immunoprecipitate of cells expressing CDKL5. Interestingly, this interaction appears to be independent of exogenously expressed CB but whether the lowly expressed endogenous CB mediates this interaction remains presently unclear.

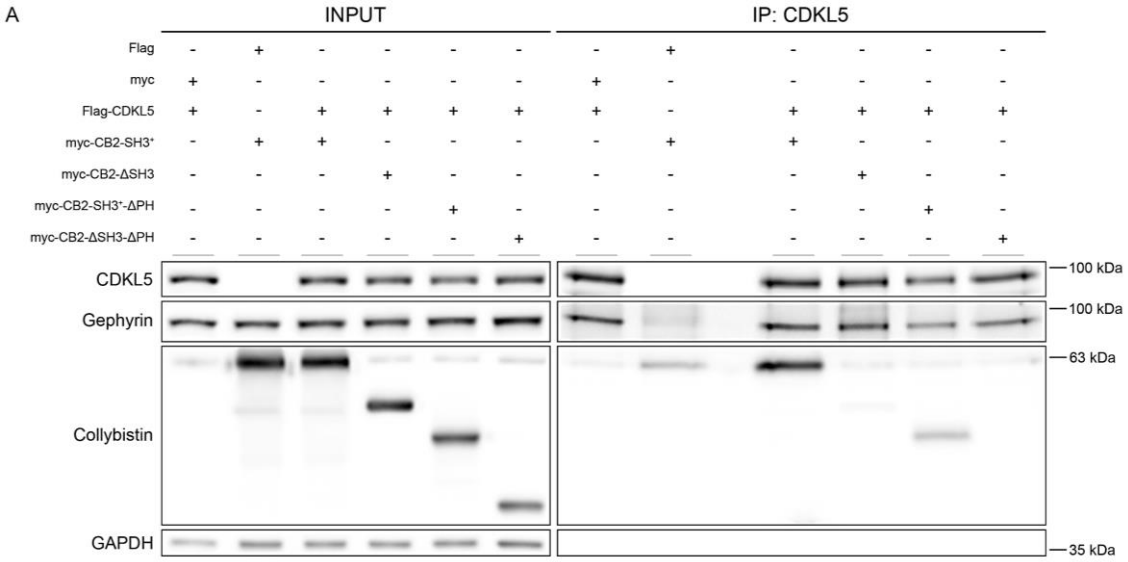

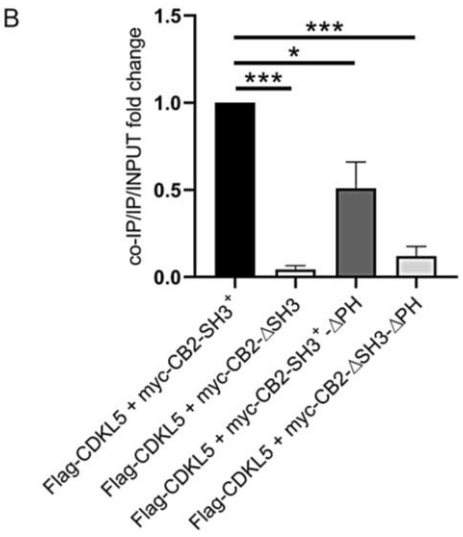

Figure 4.3 The SH3 domain of CB is required for the interaction with CDKL5. A) Flag-CDKL5 was expressed in HEK293T cells with the indicated myc-CB2 derivatives and immunoprecipitated with a monoclonal anti-CDKL5 antibody. Whole cell lysates (input; 3%) and immunoprecipitated proteins were analysed through WB using antibodies against CDKL5, CB, gephyrin and, as loading control, GAPDH. **B)** The graph shows the quantification of the interaction between CDKL5 and the distinct CB derivatives: the ratio co-IP/IP was normalised with the respective input and then reported as fold change over CB2-SH3$^+$. Values are presented as mean±SEM. n=3. Statistical analysis: One-way ANOVA, followed by Tukey's post-hoc; *p<0.05; ***p<0.001.

4.2 Neuroligin2 seems to be more phosphorylated in the absence of CDKL5

Being CDKL5 a kinase and considering that the phosphorylation status of various postsynaptic proteins has frequently been associated with neuronal activation and synaptic plasticity, we proceeded investigating whether phosphorylation of gephyrin, CB and neuroligin2 (NL2) might change in the absence of CDKL5.

As mentioned, gephyrin anchors, clusters and stabilises $GABA_ARs$ at inhibitory synapses of the mammalian brain. It self-aggregates into a hexagonal lattice and interacts with various inhibitory synaptic proteins, among which CB and NL2 (Groeneweg et al., 2018; Ko et al., 2015). The latter is a neuronal transmembrane protein that was identified as the first adhesion molecule being constitutively and selectively present in inhibitory postsynaptic sites. Moreover, NL2 is involved in the differentiation and maturation events at nascent inhibitory postsynapses (Poulopoulos et al., 2009).

Since phosphospecific antibodies against these proteins are not commercially available, we exploited the fact that the migration of some proteins in SDS-PAGE is influenced by their phosphorylation status. To assess protein phosphorylation, we incubated mouse hippocampal extracts with lambda-phosphatase (λPP) and separated the proteins through SDS-PAGE (8%, 150:1 acrylamide:bis-acrylamide) followed by WB. The efficient dephosphorylation was confirmed by the disappearance of $pSer^{270}$-Gephyrin and pERK 1/2 signals in the λPP-treated lysates (Figure 4.4). We also confirmed previous data showing that CDKL5 acquired a higher mobility upon dephosphorylation (La Montanara et al., 2015).

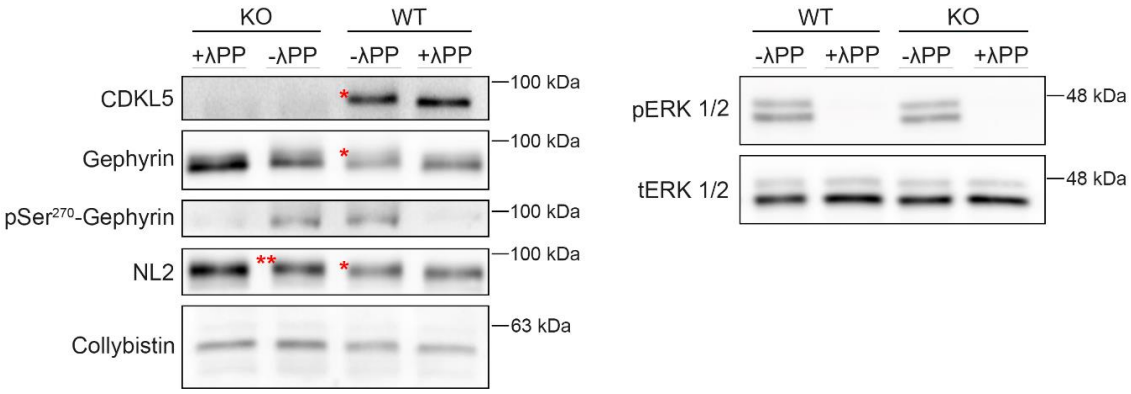

Figure 4.4 Dephosphorylation assay on hippocampal lysates of *Cdkl5*-WT and *Cdkl5*-KO mice. WB showing the mobility of CDKL5, gephyrin, NL2 and CB after 3 h incubation of *Cdkl5*-WT and -KO hippocampal lysates (PND60) with or without lambda-phosphatase (λPP). $pSer^{270}$-Gephyrin and pERK 1/2 were used as index of the successful treatment. Asterisks illustrate retarded electrophoretic mobility of the analysed proteins. (*) indicates the difference between -λPP and +λPP in WT samples; (**) indicates a slight difference in migration of NL2 in -λPP *Cdkl5*-KO lysate. The extracts were separated under appropriate electrophoretic conditions on 8% SDS-PAGE with 150:1 acrylamide:bis-acrylamide. n=1 mice/group.

In agreement with the high number of phosphorylation sites of gephyrin (Zacchi et al., 2014), its electrophoretic mobility appeared faster upon λPP treatment in both *Cdkl5*-WT and *Cdkl5*-KO lysates, as shown in figure 4.4. However, as there is no difference in basal conditions (-λPP) between WT and KO samples, CDKL5 does not seem to be involved in this phosphorylation. Regarding CB, we did not appreciate any change in its electrophoretic mobility in either -λPP or +λPP samples. However, comparing the migration of NL2 in untreated *Cdkl5*-WT and -KO lysates the protein appeared to migrate more slowly in the KO sample, though this difference was very slight. The reduced mobility of NL2 in *Cdkl5*-KO samples would be compatible with its increased phosphorylation in the absence of CDKL5, thus indicating that CDKL5 influences NL2 phosphorylation indirectly. Future experiments will be performed to address this aspect in further details.

4.3 Total expression levels of inhibitory synaptic proteins are not affected by CDKL5 deficiency

The above results show that CDKL5 interacts with proteins that are involved in the synaptic clustering of $GABA_A$Rs. We therefore decided first to evaluate the total expression levels of the main inhibitory synaptic proteins, among which γ_2 and β_3 subunit-containing $GABA_A$Rs, gephyrin, CB and NL2. $GABA_A$Rs are the main receptors supporting inhibition in the CNS (Bogdanov, 2019). Synaptic $GABA_A$Rs generate phasic inhibition and are predominantly characterised by the presence of the γ_2 subunit in combination with two α_1, α_2 or α_3 subunits together with two β_2 or β_3 subunits (Luscher et al., 2011). Among the β subunits, the most abundant and widespread subunit is β_2, while the distribution of the β_3 subunit is more discrete although highly expressed (Olsen & Sieghart, 2008).

Protein abundance was analysed in total lysates of primary hippocampal neurons obtained from *Cdkl5*-WT and -KO embryos and cultured until DIV14, a time point when neurons under our culture conditions can be considered mature (La Montanara et al., 2015). As shown in figure 4.5, we did not find any variation in the analysed proteins between *Cdkl5*-WT and -KO primary hippocampal neuronal lysates (WT gephyrin: 1.00±0.06; KO gephyrin: 1.08±0.11; WT $GABA_A$R γ_2: 1.00±0.07; KO $GABA_A$R γ_2: 0.98±0.15; WT $GABA_A$R β_3: 1.00±0.04; KO $GABA_A$R β_3: 1.09±0.09; WT NL2: 1.00±0.10; KO NL2: 1.26±0.14; WT CB: 1.00±0.05 vs KO CB: 0.97±0.08).

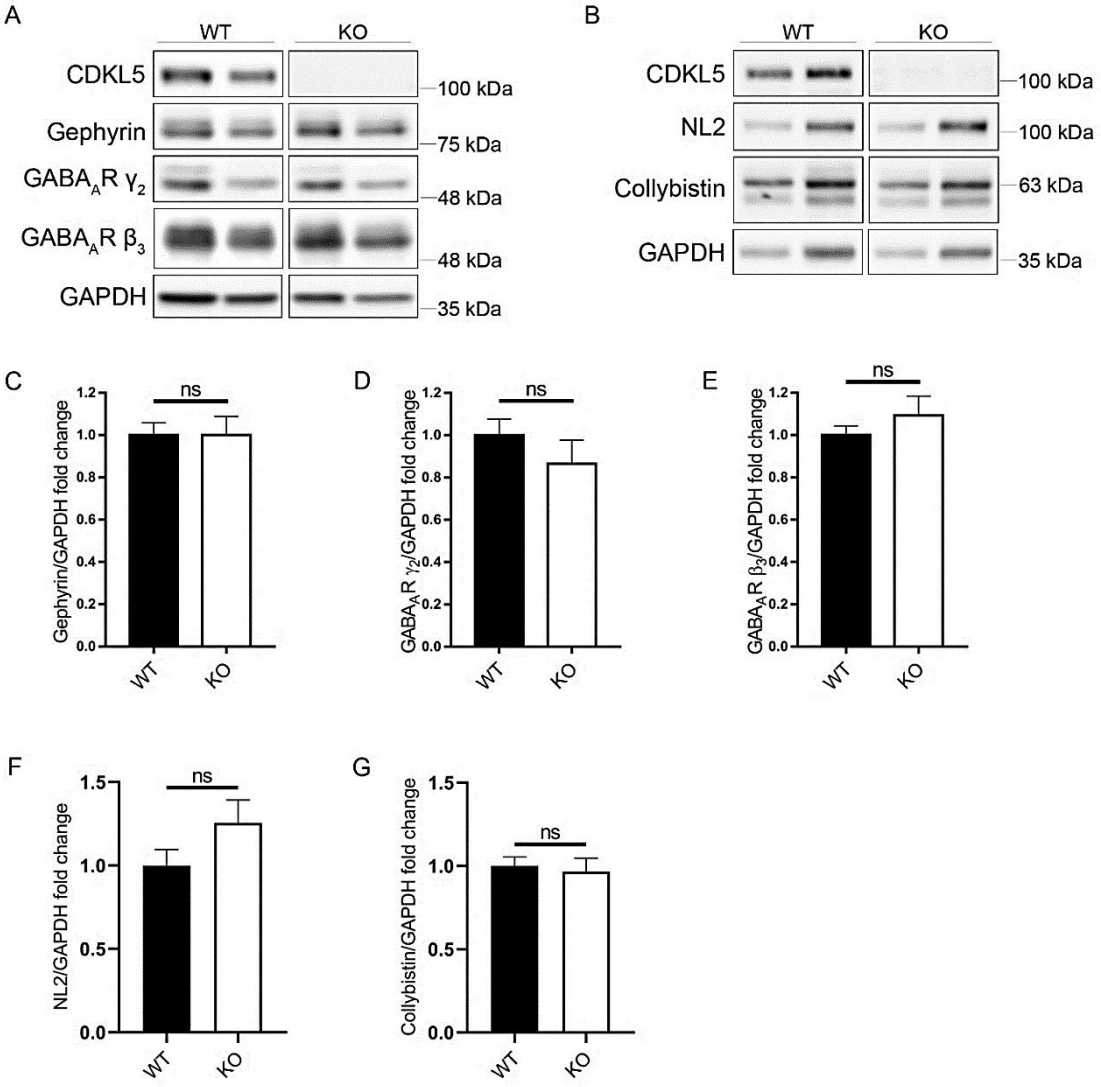

Figure 4.5 Evaluation of total expression levels of the main inhibitory proteins in the absence of CDKL5. A-B) Representative WB analysis of whole cell lysates of *Cdkl5*-WT and *Cdkl5*-KO primary hippocampal neurons at DIV14. GAPDH was used as loading control. **C-G)** The graphs show the quantification of gephyrin **(C)**, $GABA_AR\ \gamma_2$ **(D),** $GABA_AR\ \beta_3$ **(E)**, NL2 **(F)** and CB **(G)** expression levels. Values are presented as mean±SEM. n=6-8/group from at least three independent preparations. Statistical analysis: unpaired Student's t-test; ns, p>0.05.

4.4 CDKL5 deficiency alters the surface expression levels of $GABA_AR$ subunits

We proceeded performing the highly sensitive cell surface biotinylation assay to investigate if the absence of CDKL5 might influence the surface expression of $GABA_ARs$. The biotinylation approach allows to covalently link cell surface receptors with biotin, which can then be affinity purified. In particular, sulfo-NHS-biotin (N-hydroxysulfosuccinimidobiotin) is a biotin derivative that is commonly used in neuronal receptor trafficking experiments. It contains a negatively charged sulphate group, which confers membrane impermeability thus minimising labelling of intracellular proteins (Arancibia-Cárcamo et al., 2006).

Upon biotinylation of primary hippocampal *Cdkl5*-WT and -KO neurons, the biotinylated proteins were affinity purified and the whole lysate and purified proteins analysed by WB (Figure 4.6A). To determine the proportion of the total receptor pool that resides at the cell surface, we quantified the ratio of the biotinylated fraction (surface) over the receptor pool in the total lysate. As control of the biotinylation of surface exposed proteins, we verified that the cytoplasmic protein GAPDH was barely present in the pool of affinity purified proteins (Figure 4.6B-C). In line with previous reports, we observed reduced levels of surface exposed AMPAR subunit GluA2 in *Cdkl5*-KO neurons compared with the WT controls (Figure 4.6B) (Tramarin et al., 2018; Yennawar et al., 2019). Besides, we found that *Cdkl5*-KO neurons displayed reduced surface levels of both γ_2 and β_3 subunit-containing $GABA_ARs$, even if only β_3 reaches statistical significance (Figure 4.6B-C). Intriguingly, surface levels of the transmembrane protein NL2 resulted to be affected by the absence of CDKL5 (Figure 4.6C). As discussed below, this is in line with the increased NL2 phosphorylation in *Cdkl5*-KO neurons. Although preliminary and not yet utterly significant, these data showed an intriguing difference between the two experimental groups indicating that membrane levels of postsynaptic inhibitory proteins are reduced in *Cdkl5*-KO neurons (WT GluA2: 1.00±0.00; KO GluA2: 0.59±0.00; WT $GABA_ARs$ γ_2: 1.00±0.00; KO $GABA_ARs$ γ_2: 0.80±0.23; WT NL2: 1.00±0.00; KO NL2: 0.56±0.07; WT $GABA_ARs$ β_3: 1.00±0.00; KO $GABA_ARs$ β_3: 0.74±0.00).

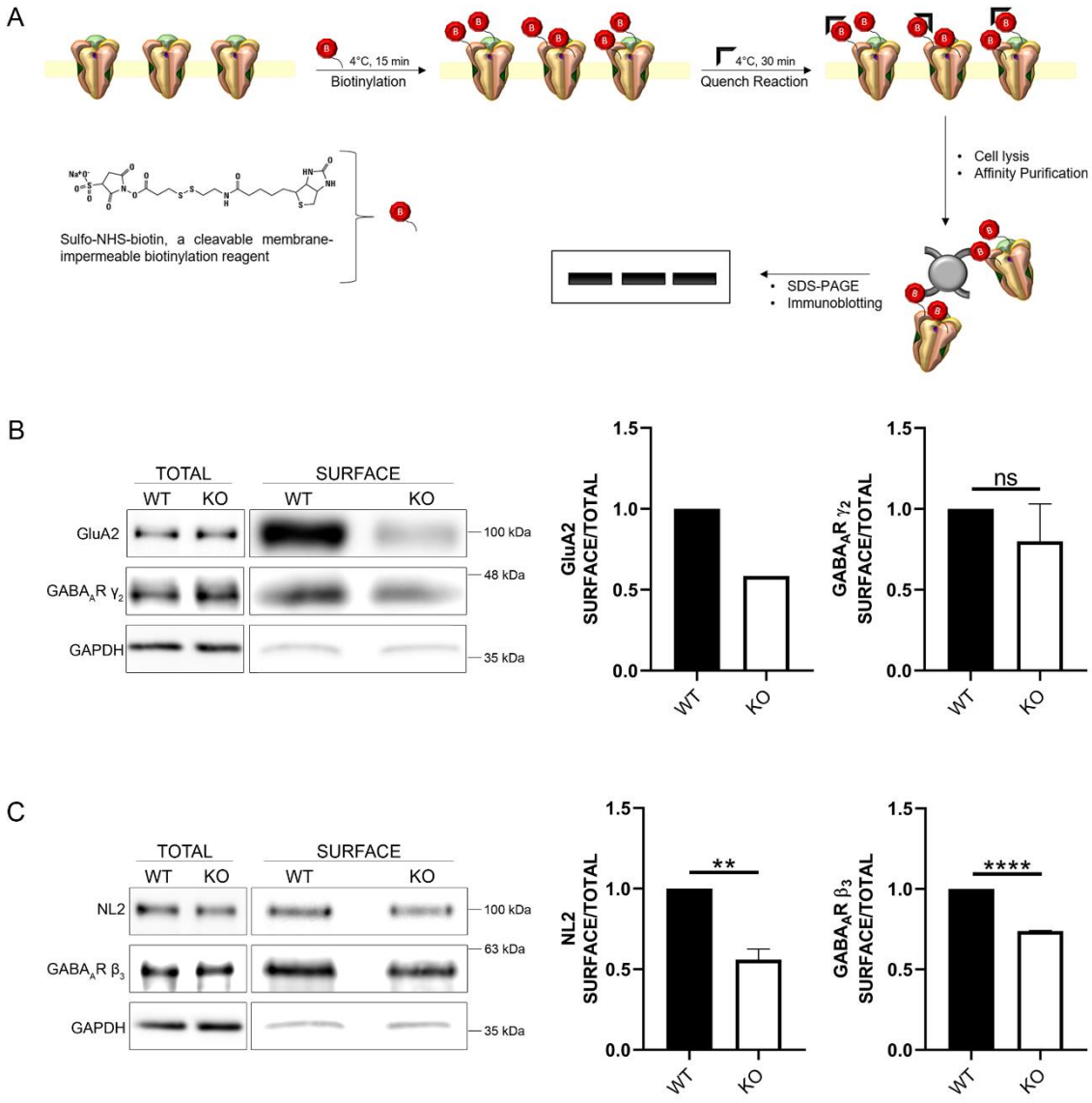

Figure 4.6 Cell surface biotinylation assay to determine surface expression of GABA$_A$Rs and NL2 in *Cdkl5*-KO primary neurons. A) Schematic diagram of cell surface biotinylation protocol. Sulfo-NHS-biotin is allowed to bind surface proteins in conditions that block endocytosis. Upon quenching of unreacted biotin, cells are solubilised in RIPA buffer and biotinylated proteins are precipitated using streptavidin beads. The precipitated complexes are analysed through WB together with the whole cell lysate. **B-C)** Representative WB of a biotinylation experiment of *Cdkl5*-WT and *Cdkl5*-KO primary hippocampal neurons at DIV14. The surface fraction was obtained from 500 µg of lysate, while 30 µg of whole cell lysate was used as total. Levels of GluA2, γ$_2$ and β$_3$ GABA$_A$R subunits, and NL2 were analysed and GAPDH was used as loading control in the total lysate and to verify that intracellular proteins were not biotinylated (surface). The graphs show the ratio of surface/total levels of GluA2, GABA$_A$R γ$_2$, GABA$_A$R β$_3$ and NL2. GluA2: n=1/group from one experiment; NL2, GABA$_A$R γ$_2$ and GABA$_A$R β$_3$: n=3/group from three independent preparations. Values are presented as mean±SEM. Statistical analysis: unpaired Student's t-test; **p<0.01; ****p<0.0001; ns, p>0.05.

4.5 CDKL5 deficiency impairs the expression of synaptic $GABA_ARs$ and gephyrin clusters

The above experiment suggests that the loss of CDKL5 leads to an impaired surface expression of synaptic $GABA_ARs$. To get further evidence of this, we examined the surface expression of the γ_2 subunit of $GABA_ARs$ through immunofluorescent staining of primary *Cdkl5*-WT and -KO neurons.

According to the *in vitro* biotinylation experiment, decreased membrane expression of synaptic $GABA_AR$ subunit γ_2 could be observed also through the immunofluorescence analysis that was performed under non-permeabilising conditions to detect only the surface exposed receptors (Figure 4.7; WT: 1.00±0.03; KO: 0.84±0.02).

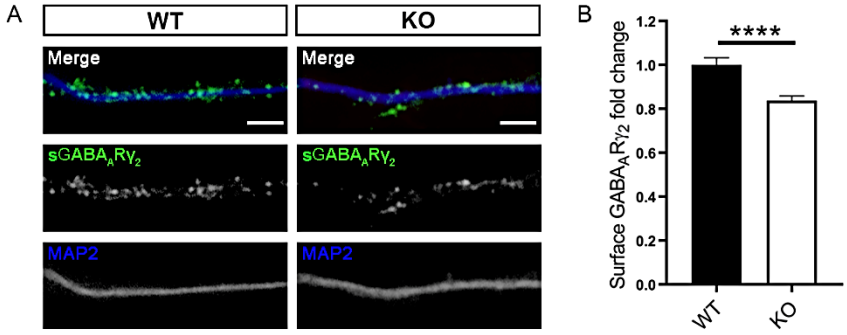

Figure 4.7 CDKL5 deficiency impairs the expression of synaptic $GABA_ARs$. A) Surface exposed $GABA_AR$ γ_2 (green, $sGABA_AR$ γ_2) was detected through immunostaining of *Cdkl5*-WT and *Cdkl5*-KO primary hippocampal neurons at DIV14 under non-permeabilising conditions. MAP2 (blue) was used as dendritic marker. Scale bar, 5 µm. **B)** The graph shows the quantification of the fluorescence intensity of $sGABA_AR$ γ_2 staining of 30 µm long dendritic MAP2-positive segments. Values are presented as mean±SEM. n=6-8/group from four independent preparations. Statistical analysis: unpaired Student's t-test; ****p<0.0001.

As previously reported, the stabilisation of $GABA_ARs$ at inhibitory synapses depends on their post-translational modifications and on their interaction with the scaffold protein gephyrin. Since gephyrin plays an important role in $GABA_AR$ clustering and having demonstrated that surface levels of synaptic $GABA_ARs$ are reduced in *Cdkl5*-KO neurons, we found it relevant to analyse whether CDKL5 deficiency impacted the number of gephyrin-positive puncta.

Despite the fact that CDKL5 deficiency did not impact gephyrin expression levels, immunofluorescence analyses of *Cdkl5*-KO primary hippocampal neurons revealed a significant reduction in the number of gephyrin-positive puncta (Figure 4.8; WT: 23.77±0.60; KO: 16.88±0.65).

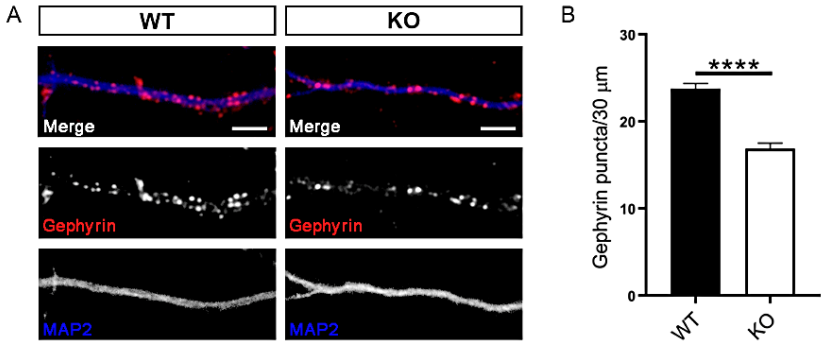

Figure 4.8 CDKL5 loss causes a reduced number of gephyrin-positive puncta. A) Gephyrin clusters (red) in dendritic MAP2-positive segments (blue) of DIV14 *Cdkl5*-WT and -KO primary hippocampal neurons. Scale bar, 5 µm. **B)** The graph shows the quantification of gephyrin puncta along 30 µm long segments. Values are presented as mean±SEM. n=8-10/group from five independent experiments. Statistical analysis: unpaired Student's t test; ****p<0.0001.

Although we did not manage to evaluate collybistin-positive puncta because of the poor quality of the antibody in immunofluorescence experiments, the above-mentioned results point out that CDKL5, probably through its interaction with gephyrin and collybistin, regulates membrane levels of synaptic $GABA_A$Rs.

4.6 CDKL5 deficiency leads to impaired inhibitory neurotransmission

We proceeded addressing the functional consequences associated with the loss of CDKL5 in the inhibitory postsynaptic compartment in collaboration with Dr. Flavia Antonucci (Department of Medical Biotechnology and Translational Medicine, University of Milan). In particular, inhibitory postsynaptic currents in miniature (mIPSCs) of primary hippocampal cultures at DIV14 were recorded by patch-clamp technique in whole-cell voltage clamp configuration.

The patch clamp technique allows observing the currents in single ionic channels. It requires the formation of a tight seal between the cell membrane and the glass tip of a recording electrode, which is characterised by a very high resistance. This resistance ensures that most of the currents, originating in a small patch of membrane, flow into the pipette and further into the current-measurement circuitry. The patching electrode is obtained from a pointed glass capillary, filled with a saline solution, on which a chlorinated silver wire has been added (Hamill et al., 1981). In this technique, the capillary tip is placed on the cell membrane and the tight seal between the tip of glass and the membrane is generated by a gentle suction (cell-attached configuration). However, applying a stronger and rapid suction, the membrane fraction surrounded by the tip of the capillary is broken, thus allowing to record all the currents flowing through the entire active membrane (whole-cell configuration).

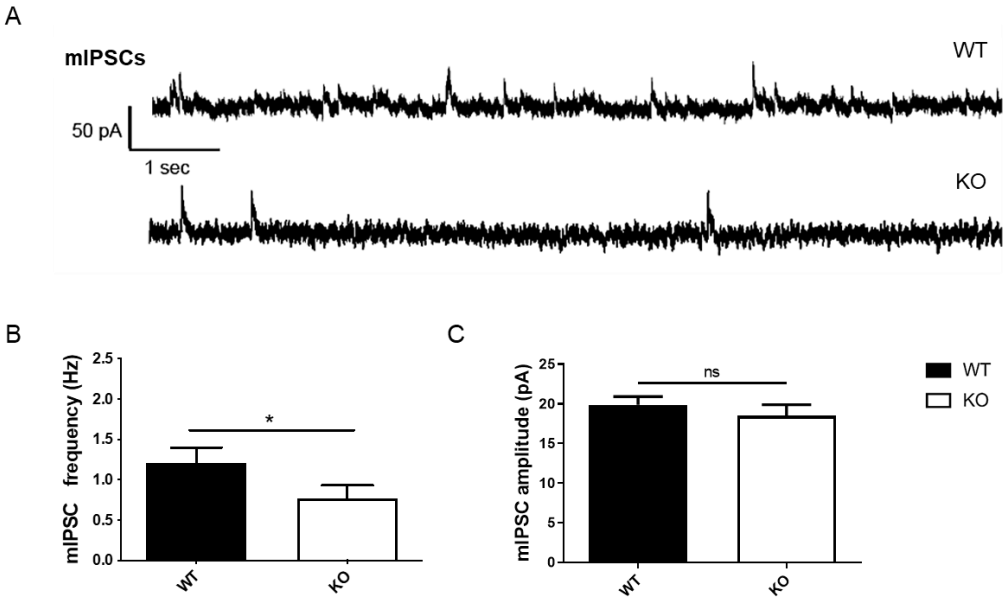

Figure 4.9 The loss of CDKL5 leads to a reduction in the frequency of mIPSCs. A) Representative traces of mIPSCs recorded from primary hippocampal neurons from *Cdkl5*-WT and *Cdkl5*-KO at DIV14 patching at +10 mV. **B-C)** Graph showing mIPSC frequency **(B)** and amplitude **(C)** in *Cdkl5*-WT and -KO cultures. Values are presented as mean±SEM. *Cdkl5*-WT cultures: n=16, *Cdkl5*-KO cultures: n=11 from three different experiments. Statistical analysis of mIPSC frequency: Mann Whitney U test; *p<0.05. Statistical analysis of mIPSC amplitude: unpaired Student's t-test; *p<0.05; ns, p>0.05.

While CDKL5 loss did not affect the amplitude of mIPSCs (Figure 4.9; WT: 19.88±1.01; KO: 18.49±1.39), electrophysiological recordings showed a significant reduction in the frequency (Figure 4.9; WT: 1.21±0.19; KO: 0.77±0.16).

Interestingly, the same result was obtained in primary hippocampal neurons silenced for CDKL5 expression and innervated by non-silenced CDKL5-positive cells (Figure 4.10). In this experiment, CDKL5 expression was abruptly silenced through the transfection of a CDKL5-silencing construct (shCDKL5) using as negative control shLacZ. Both vectors expressed the shRNA from a bicistronic cassette expressing also GFP allowing visualising the silenced neurons. In addition, non-transfected neurons (NT) were used as negative control. Transfections were performed at DIV11 and mIPSCs were recorded at DIV14 (mIPSC frequency = NT: 1.56±0.14; shLacZ: 1.61±0.25; shCDKL5: 0.89±0.15; mIPSC amplitude = NT: 14.36±0.53; shLacZ: 15.82±1.33; shCDKL5: 14.65±0.71).

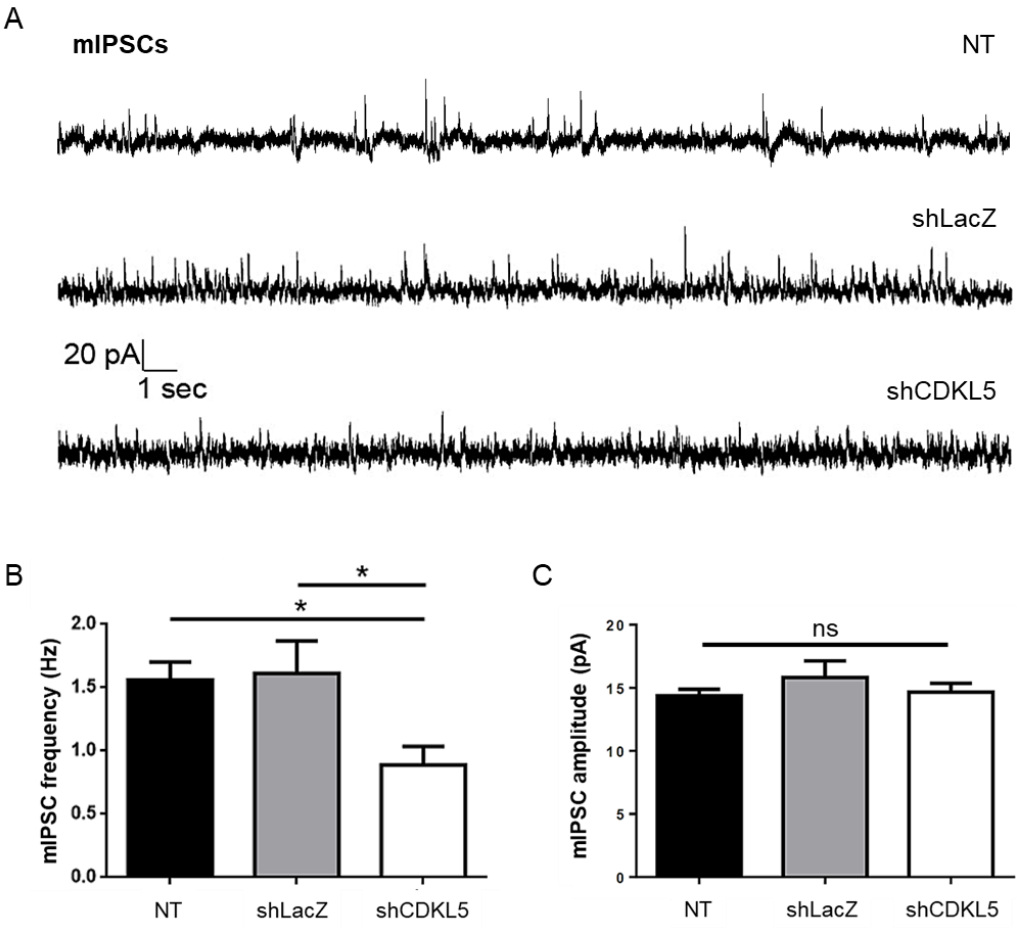

Figure 4.10 CDKL5 deficiency leads to impaired inhibitory transmission. A) Representative traces of mIPSCs recorded from primary hippocampal neurons silenced for CDKL5 expression (shCDKL5) and in control neurons (shLacZ). Neurons were transfected with shRNA vectors expressing also GFP at DIV11 and mIPSCs were recorded at DIV14 patching at +10 mV. **B, C)** Graphs showing mIPSC frequency **(B)** and amplitude **(C)** upon acute CDKL5-silencing. Values are presented as mean±SEM. NT n=10, shLacZ n=5, shCDKL5 n=13 from three different experiments. Statistical analysis: One-way ANOVA, followed by Tukey's post-hoc; *p<0.05; ns, p>0.05.

Altogether, these electrophysiological studies indicate that CDKL5 deficiency leads to an altered inhibitory neurotransmission. Even though a direct effect of CDKL5 loss at the presynaptic site cannot be excluded, the silencing studies imply that the absence of CDKL5 at the postsynaptic site is sufficient to cause the impaired mIPSCs.

4.7 The loss of CDKL5 impacts the presynaptic compartment

Considering our electrophysiological data showing a reduction in the frequency of mIPSCs, we decided to explore if CDKL5 loss influenced the presynaptic compartment. To this aim, we analysed one of the most common presynaptic markers, bassoon. Bassoon is a 420-kDa protein specifically localised at the active zone of presynaptic nerve terminals, where it is involved in the structural organisation of the neurotransmitter release site (Richter et al., 1999).

We evaluated the number of bassoon-positive puncta in *Cdkl5*-WT and -KO neurons at DIV14 through immunofluorescent staining. As reported in figure 4.11, we found that the number of bassoon-positive puncta was significantly reduced in *Cdkl5*-KO primary hippocampal cultures (WT: 29.98±0.86; KO: 20.32±0.69). This result suggests that the loss of CDKL5 leads to a presynaptic defect; however, since bassoon is present at the presynaptic site of both excitatory and inhibitory synapses (Richter et al., 1999), we are currently evaluating whether CDKL5 loss affects the inhibitory presynaptic site analysing the number of vesicular GABA transporter (VGAT)-positive puncta.

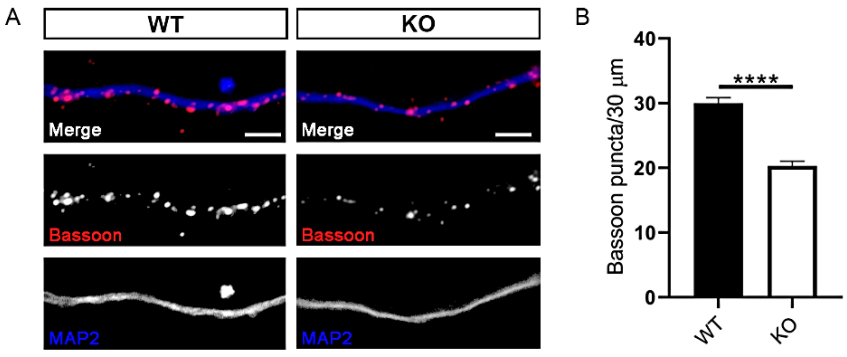

Figure 4.11 Bassoon puncta are reduced in *Cdkl5*-KO hippocampal neurons. A) Bassoon puncta (red) in dendritic MAP2-positive segments (blue) of DIV14 *Cdkl5*-WT and -KO primary hippocampal neurons. Scale bar, 5 µm. **B)** The graph shows the quantification of bassoon puncta along 30 µm long segments. Values are presented as mean±SEM. n=7/group from four independent experiments. Statistical analysis: unpaired Student's t test; ****p<0.0001.

To sum up, our data indicate that CDKL5 loss leads not only to a postsynaptic but also to a presynaptic defect. These alterations are supported by the electrophysiological findings and, considering the recordings obtained in CDKL5-silenced neurons, alterations in the postsynaptic site might represent the primary defect that has repercussions on the presynaptic counterpart.

4.8 CDKL5-related defects are ameliorated by PME treatment

As previously described, recent findings converge on a role of CDKL5 in regulating MT dynamics through the interaction with various MT-binding proteins (Baltussen et al., 2018; Barbiero et al., 2017b, 2020). Among them, the MT plus-end tracking protein CLIP170 regulates MT dynamics acting as a rescue factor, thus facilitating MT growth (Komarova et al., 2002). It has been shown that CDKL5 deficiency interferes with the formation of the IQGAP1/CLIP170/Rac1 ternary complex and negatively influences the MT-binding of CLIP170. According to our data, CDKL5 loss impacts neuronal MT dynamics, which is likely to underlie some of the morphologic and molecular defects in neurons (Barbiero et al., 2017b, 2020, 2021 *under revision*). From a pharmacological point of view, PREG, through its activating function on CLIP170, was demonstrated to be capable of ameliorating CDKL5-related defects both in cycling cells and in neurons (Barbiero et al., 2017b). Recently, in our laboratory it has been demonstrated that the non-metabolisable synthetic analogue of PREG, PME, is capable of rescuing not only axonal phenotypes in young neurons, but also the dendritic spine defects associated with CDKL5 loss *in vitro* and *in vivo* (Barbiero et al., 2017b, 2020, 2021 *under revision*). PME maintains the same biological action of PREG but is devoid of the downstream effects linked to the further metabolism of PREG.

Considering the pivotal role of MTs in the membrane stabilisation of gephyrin and $GABA_A$Rs through their interaction with various proteins at the postsynaptic site (Bogdanov, 2019; Kittler et al., 2004; Luscher et al., 2011), we decided to evaluate if PME might have any effect on the CDKL5-dependent defects in $GABA_A$R expression and function that we found in *Cdkl5*-KO primary hippocampal neurons.

4.8.1 Effect of PME on reduced surface expression of synaptic $GABA_AR$s and gephyrin clusters in *Cdkl5*-KO neurons

We first examined if PME could promote the membrane stabilisation of $GABA_AR$s through its effect on MT dynamics. Thus, primary hippocampal neurons were treated with 0.3 and 1 µM PME for 72 hours starting from DIV11 and surface levels of $GABA_AR$ γ_2 were examined at DIV14 through immunofluorescence. Our data (Figure 4.12) showed that treatment with PME could rescue the decreased surface expression of synaptic $GABA_AR$s in *Cdkl5*-KO primary hippocampal cultures without affecting the expression in WT neurons (WT 0.1% DMSO: 1.00±0.03; WT 0.3 µM PME: 0.99±0.02; WT 1 µM PME: 0.98±0.03; KO 0.1% DMSO: 0.89±0.02; KO 0.3 µM PME: 1.08±0.03; KO 1 µM PME: 1.03±0.04).

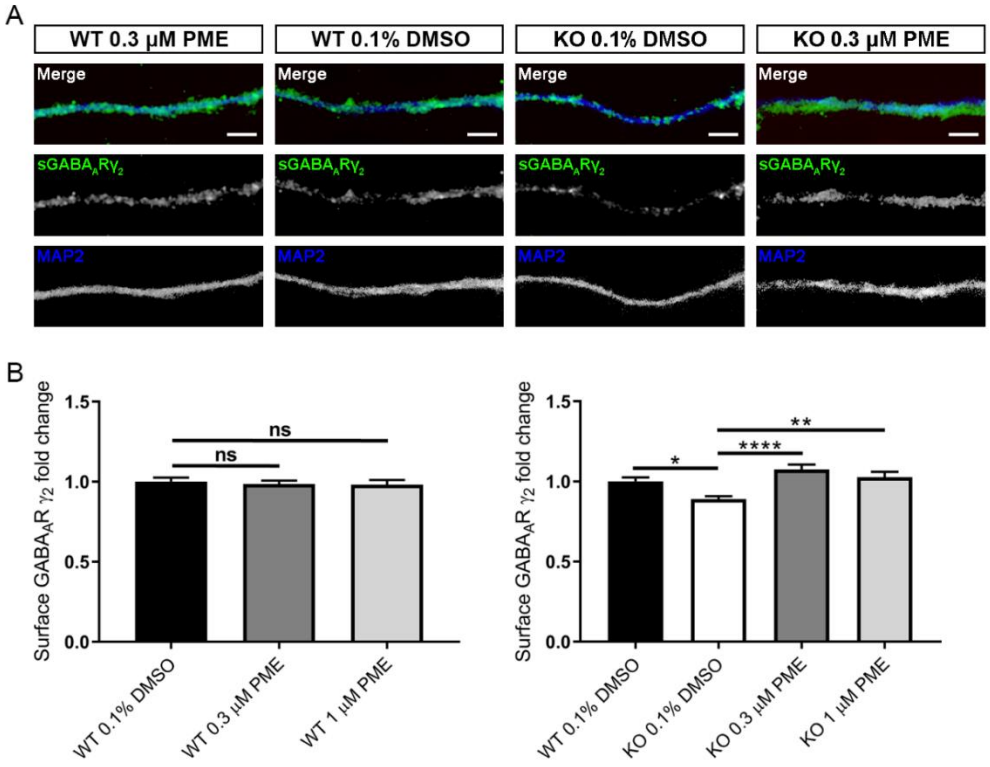

Figure 4.12 PME treatment rescues the decreased surface expression of synaptic $GABA_AR$s in *Cdkl5*-KO primary hippocampal neurons. A) Surface exposed $GABA_AR$ γ_2 (s$GABA_AR$ γ_2, green) was detected through immunostaining under non-permeabilising conditions of *Cdkl5*-WT and -KO neurons treated with 0.3-1 µM PME or vehicle (0.1% DMSO) at DIV11 for 72 hours. MAP2 (blue) staining, performed under permeabilising conditions, was used as dendritic marker. Scale bar, 5 µm. **B)** The graph shows the fluorescence intensity of s$GABA_AR$ γ_2 per 30 µm long dendritic segments. Values are presented as mean±SEM. n=5-6/group from four independent preparations. Statistical analysis: One-way ANOVA, followed by Tukey's post-hoc; *p<0.05; **p<0.01; ****p<0.0001; ns, p>0.05.

In parallel, we analysed the number of gephyrin puncta. As reported in figure 4.13, treatment with PME at both concentrations had a beneficial effect on the reduced number of gephyrin-positive puncta in *Cdkl5*-KO primary hippocampal neurons (WT 0.1% DMSO: 29.33±1.02; WT 0.3 µM PME: 28.47±1.06; WT 1 µM PME: 27.41±0.76; KO 0.1% DMSO: 17.67±0.76; KO 0.3 µM PME: 26.83±1.19; KO 1 µM PME: 26.55±0.91).

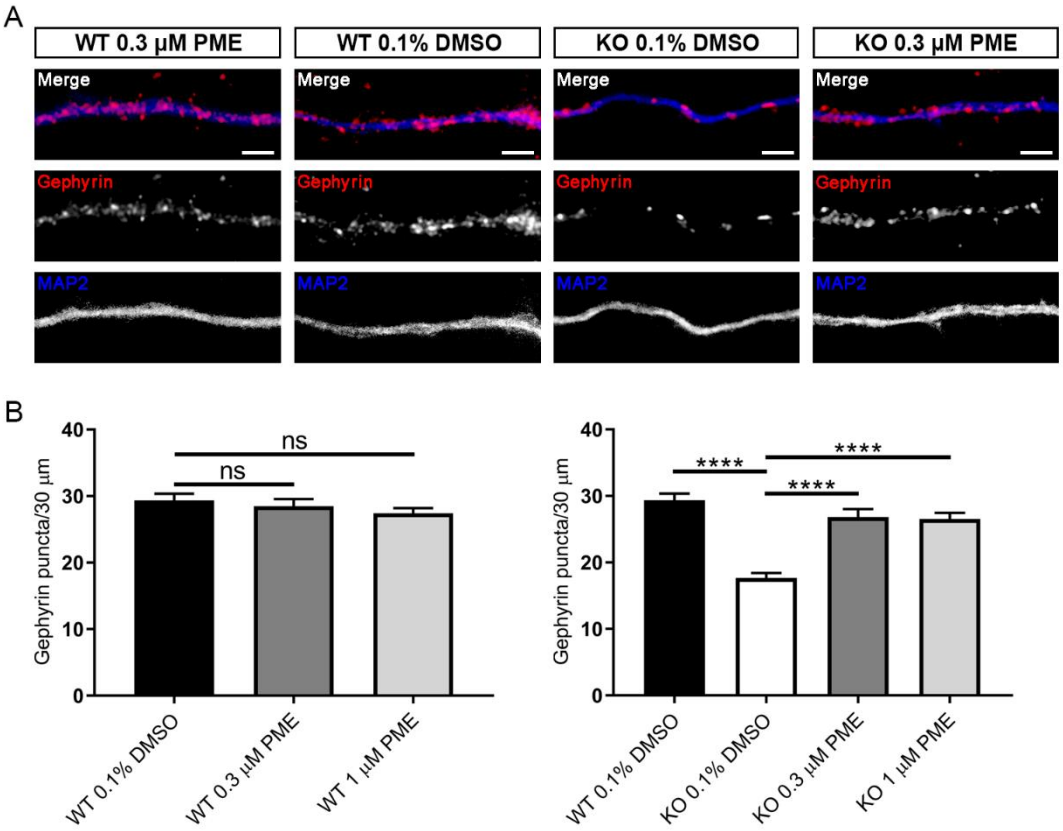

Figure 4.13 PME treatment normalises the reduced number of gephyrin puncta in *Cdkl5*-KO neurons. A) *Cdkl5*-WT and *Cdkl5*-KO primary hippocampal neurons were treated with 0.3-1 µM PME or vehicle (0.1% DMSO) at DIV11 for 72 hours. Neurons were stained for gephyrin (red) and MAP2 (blue). Scale bar, 5 µm. **B)** The graph shows the number of gephyrin puncta per 30 µm long dendritic segments. Values are presented as mean±SEM. n=6/group from four independent preparations. Statistical analysis: One-way ANOVA, followed by Tukey's post-hoc; ****p<0.0001; ns, p>0.05.

4.8.2 Effect of PME on the reduced frequency of mIPSCs in *Cdkl5*-KO neurons

Since CDKL5-related defects were accompanied by an altered inhibitory neurotransmission, we proceeded analysing the effect of PME on mIPSCs in *Cdkl5*-KO neurons. As above, neurons were treated for 72 hours with 0.3 µM PME prior to electrophysiological recordings. Interestingly, PME treatment rescued the decreased mIPSC frequency of primary hippocampal cultures at DIV14 (Figure 4.14; mIPSC frequency = WT 0.1% DMSO: 1.48±0.16; KO 0.1% DMSO: 0.66±0.07; KO 0.3 µM PME: 1.33±0.13; mIPSC amplitude = WT 0.1% DMSO: 18.61±1.13; KO 0.1% DMSO: 18.44±0.95; KO 0.3 µM PME: 19.98±1.66).

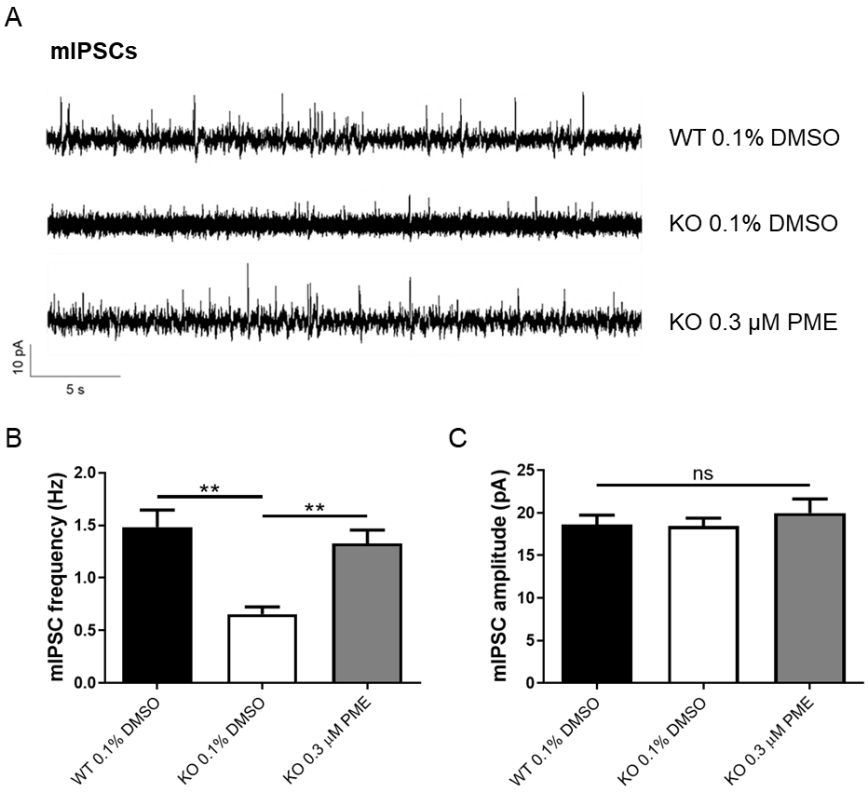

Figure 4.14 Positive effect of PME on the diminished frequency of mIPSCs in *Cdkl5*-KO neurons. A) Representative traces of mIPSCs in *Cdkl5*-WT and -KO primary hippocampal neurons treated as indicated with either vehicle (0.1% DMSO) or 0.3 µM PME for 72 h starting at DIV11. **B-C)** Graphs showing mIPSC frequency **(B)** and amplitude **(C)** of *Cdkl5*-WT and -KO neurons treated as indicated. Values are presented as mean±SEM. *Cdkl5*-WT vehicle n=24, *Cdkl5*-KO vehicle n=27, *Cdkl5*-KO PME 0.3 µM n=22 from three different experiments. Statistical analysis mIPSC frequency: Kruskal-Wallis test, followed by Dunn's multiple comparisons test; **p<0.01. Statistical analysis mIPSC amplitude: One-way ANOVA, followed by Tukey's post-hoc; ns, p>0.05.

4.8.3 Effect of PME on the decreased number of bassoon-positive puncta in *Cdkl5*-KO neurons

Confident of the positive effect of PME on the above postsynaptic defects, we proceeded evaluating the number of bassoon puncta. According to the electrophysiological rescue, PME treatment was capable of normalising the presynaptic defect found in *Cdkl5*-KO primary hippocampal cultures. Indeed, as a result of the pharmacological treatment, the number of bassoon-positive puncta was increased (Figure 4.15; WT 0.1% DMSO: 29.88±0.94; WT 0.3 µM PME: 28.85±0.65; WT 1 µM PME: 28.95±0.93; KO 0.1% DMSO: 21.84±0.66; KO 0.3 µM PME: 25.96±0.62; KO 1 µM PME: 28.16±0.62).

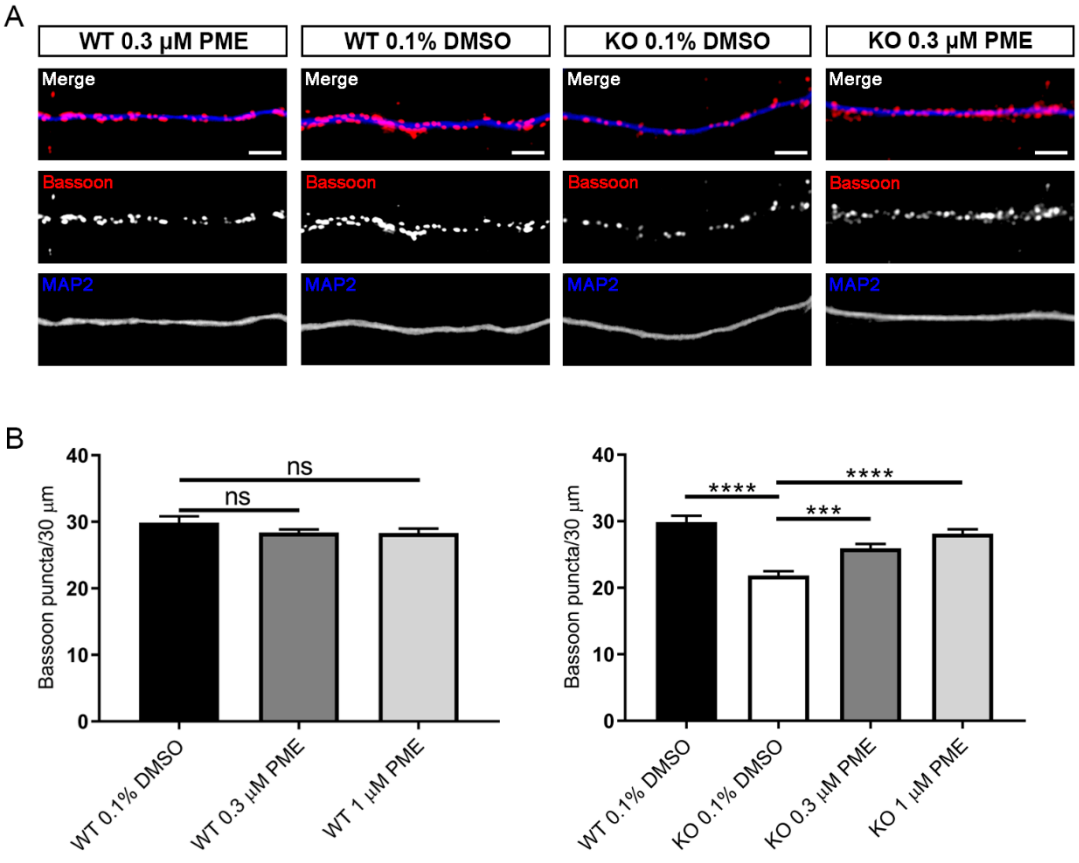

Figure 4.15 PME treatment has a beneficial effect on the decreased number of bassoon puncta in *Cdkl5*-KO neurons. A) Immunofluorescent staining with bassoon (red) and MAP2 (blue) of *Cdkl5*-WT and *Cdkl5*-KO primary hippocampal neurons treated with 0.3-1 µM PME or vehicle (0.1% DMSO) at DIV11 for 72 hours. Scale bar, 5 µm. **B)** The graph shows the number of bassoon puncta in 30 µm long dendritic segments. Values are presented as mean±SEM. n=3/group from three independent preparations. Statistical analysis: One-way ANOVA, followed by Tukey's post-hoc; ***p<0.001; ****p<0.0001; ns, p>0.05.

4.8.4 Treatment with PME restores synaptic $GABA_AR$ defects *in vivo*

Encouraged by the beneficial effect of PME *in vitro*, we found it challenging to analyse the effect of this compound also *in vivo.* We thus performed a pilot experiment on male *Cdkl5*-KO mice at PND60, when they are fully symptomatic. *Cdkl5*-WT and -KO mice were treated for seven consecutive days with PME (10 mg/kg) or sesame oil as vehicle through a subcutaneous injection (s.c.). Subsequently, hippocampal sections were subjected to immunofluorescent staining against $GABA_AR$ γ_2 subunit and observed through confocal imaging (Figure 4.16A).

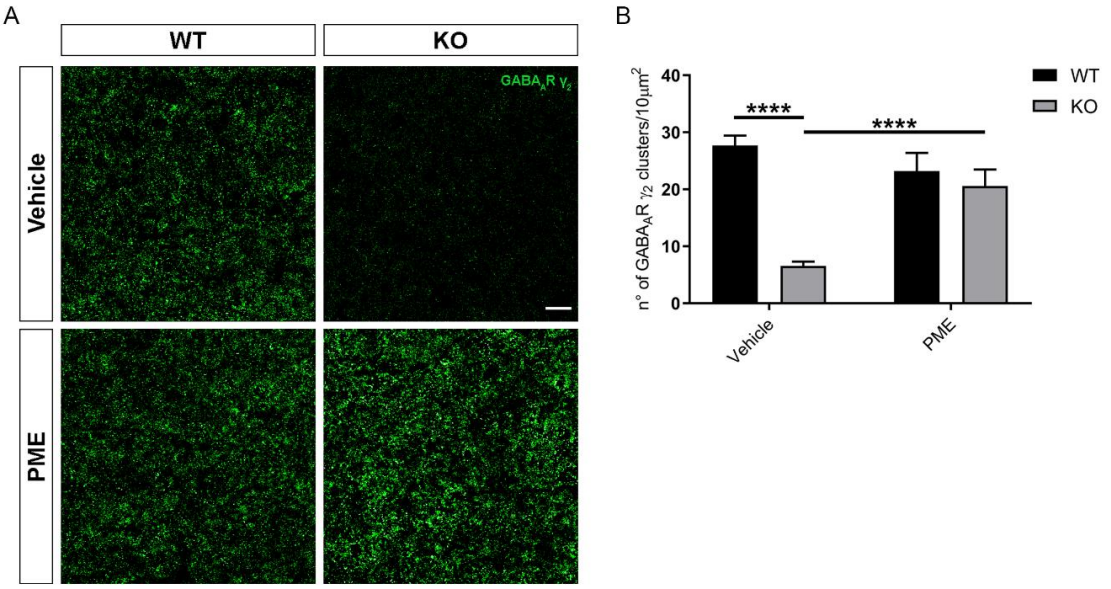

Figure 4.16 Rescue of reduced levels of hippocampal $GABA_AR$ γ_2 clusters in *Cdkl5*-KO mice treated *in vivo* with PME. A) Hippocampal slices (dentate gyrus) from *Cdkl5*-WT and *Cdkl5*-KO male mice treated with PME (10 mg/kg, s.c. for seven days starting from PND60) or sesame oil (vehicle) were stained for $GABA_AR$ γ_2. Scale bar, 5 µm. **B)** The graph shows the quantified levels of $GABA_AR$ γ_2 clusters/100 µm^2. Values are presented as mean±SEM. *Cdkl5*-WT vehicle n=5 mice, *Cdkl5*-WT PME n=4 mice, *Cdkl5*-KO vehicle n=5 mice, *Cdkl5*-KO PME n=5 mice. Statistical analysis: Two-way ANOVA followed by Tukey's post-hoc; ****p<0.0001.

This result was in line with our *in vitro* data; indeed, as disclosed in figure 4.16B, the number of $GABA_AR$ γ_2 clusters was dramatically and significantly reduced in the dentate gyrus of vehicle-treated *Cdkl5*-KO hippocampi compared to WT animals (WT vehicle: 27.73±1.67; KO vehicle: 6.55±0.78). Interestingly, the pharmacological treatment with PME could visibly rescue the synaptic defect in *Cdkl5*-KO mice (WT PME: 23.21±3.19; KO PME: 20.59±2.90).

4.8.5 Reduced levels of $GABA_AR$ γ_2 in the postsynaptic compartment of *Cdkl5*-KO hippocampi are restored upon treatment with PME

The above data demonstrate that CDKL5 loss alters the surface expression of synaptic $GABA_ARs$ both *in vitro* and *ex vivo* as well as the number of gephyrin clusters, defects that were restored upon PME treatment. Therefore, we found it crucial to analyse through a complementary biochemical approach the content of gephyrin together with $GABA_AR$ γ_2 subunit in *Cdkl5*-WT and *Cdkl5*-KO hippocampi. We thus isolated the synaptosomal fraction, highly enriched in synaptic proteins, from hippocampi of *Cdkl5*-WT and -KO mice treated with either vehicle or PME and analysed the expression of $GABA_AR$ γ_2 and gephyrin through WB. Of note, the same amount of lysate was loaded to evaluate synaptic protein composition in a comparable number of synaptosomes and GAPDH was used as internal control. The quality of the synaptosomal fractionation was confirmed through WB showing the expected enrichment of PSD95, the AMPA-receptor subunit GluA2, and CDKL5 in the synaptosomal fraction while nuclear histone H1 was totally absent (Figure 4.17A).

Interestingly, a significant decrease in the expression of γ_2 subunit-containing $GABA_ARs$ was observed in synaptosomes of vehicle-treated *Cdkl5*-KO mice compared to the control group. Consistent with the effect of PME described above, a strong tendency in the raise of defective $GABA_AR$ γ_2 levels upon PME treatment was observed in synaptosomes of *Cdkl5*-KO mice (Figure 4.17B; WT vehicle: 1.00±0.05; WT PME: 0.96±0.12; KO vehicle: 0.75±0.07; KO PME: 0.95±0.07). As shown in figure 4.17C, gephyrin levels in the synaptosomal fraction did not vary amongst the experimental groups (WT vehicle: 1.00±0.07; WT PME: 0.89±0.08; KO vehicle: 1.00±0.09; KO PME: 1.11±0.12). This result can be explained with the bias that the protocol introduces for the enrichment of coupled pre- and postsynaptic structures containing comparable amounts of the postsynaptic density scaffolds. Lastly, total expression levels of both γ_2 subunit-containing $GABA_ARs$ (WT vehicle: 1.00±0.05; WT PME: 0.96±0.07; KO vehicle: 1.01±0.09; KO PME: 0.86±0.05) and gephyrin (WT vehicle: 1.00±0.05; WT PME: 1.19±0.08; KO vehicle: 1.20±0.13; KO PME: 1.14±0.11) did not change between *Cdkl5*-WT and *Cdkl5*-KO hippocampal lysates (Figure 4.17D). Since we did not observe any difference in total protein levels amongst the four analysed groups, the reduction of γ_2 subunit-containing $GABA_ARs$ in the synaptosomes may be explained by impaired localisation events, possibly caused by defective MT dynamics due to CDKL5 loss.

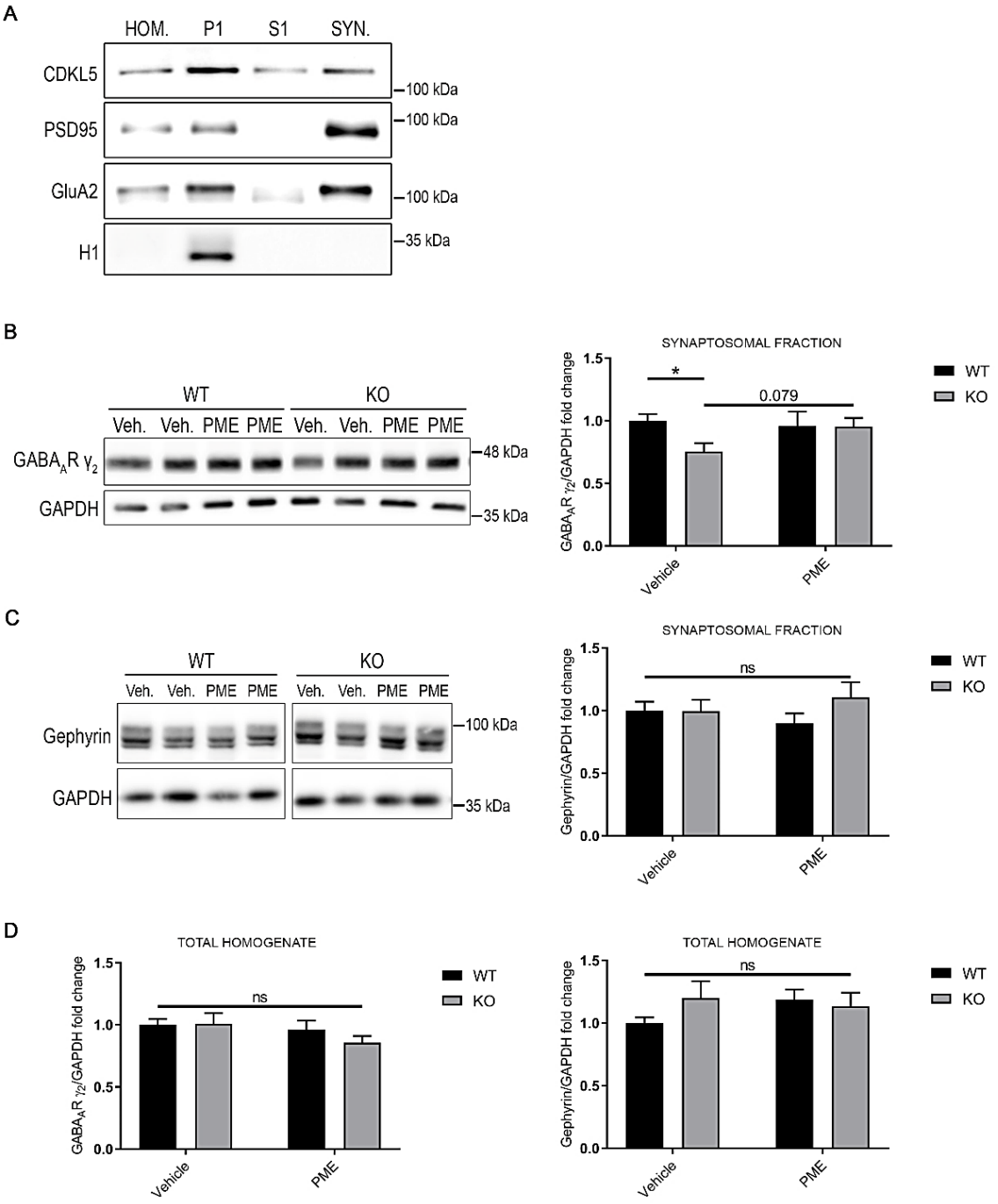

Figure 4.17 Decreased levels of GABA$_A$R γ$_2$ in the postsynaptic compartment of *Cdkl5*-KO hippocampi are restored upon treatment with PME. A) Subcellular fractionation of mouse hippocampi was monitored by WB analyses of synaptic and non-synaptic proteins. Total homogenate (HOM; whole lysate), nuclei/debris (P1), cytosol (S1), and synaptosomal fractions (SYN) were analysed. **B-C)** Representative WB of synaptosomal fractions from hippocampi of *Cdkl5*-WT and -KO mice showing γ$_2$ subunit-containing GABA$_A$Rs and gephyrin. Graphs show GABA$_A$R γ$_2$ subunit and gephyrin levels normalised to GAPDH. **D)** Graphs show the total expression levels (total homogenate) of γ$_2$ subunit-containing GABA$_A$Rs and gephyrin normalised to GAPDH. n>8 mice/group. Values are presented as mean±SEM. Statistical analysis: Two-way ANOVA, followed by Fischer's LSD test; *p<0.05; ns, p>0.05.

4.9 *Cdkl5*-KO mice develop polyspikes in response to repetitive stimulation

Early-onset epilepsy is known as one of the main hallmark features of CDD. Given this aspect and considering our *ex vivo* data showing a reduction in synaptic $GABA_A$Rs, we explored whether this inhibitory defect mirrored a hyperexcitability phenotype *ex vivo*, despite the absence of spontaneous seizures in *Cdkl5*-KO mice.

Extracellular field potentials are electrical signals measured in the extracellular space. They are typically generated by the electrical activity of a population of neurons that cause changes in the extracellular potential (Johnston & Wu, 1994).

In collaboration with Dr. Lia Chiara Forti (Department of Biotechnology and Life Sciences, University of Insubria), we performed an experiment in which extracellular field potentials from the CA1 region of the hippocampus were recorded after stimulating the Schaffer collaterals in the CA3 region. In response to electrical stimulation of the Schaffer collaterals, it is therefore possible to record a negative deflection of the extracellular potential, called signal from population spikes. In particular, it is generated by the firing of action potentials in a population of neurons, the cell bodies of which are in the *stratum pyramidale* of CA1 (Figure 4.18A-B). This downward deflection represents the first peak of the electrophysiological trace and it is indicated as P_1 (Figure 4.18C). Using pharmacological agents such as 100 µM picrotoxin to block inhibition, or an electrophysiological protocol to decrease inhibition (Thompson & Gahwiler, 1989) or in pathologic conditions such as epilepsy (Lüthi et al., 1997), further negative deflections of the potential appear in the signal. These are called multiple population spikes or polyspikes (P_n; Figure 4.18D) and are generated by burst discharges from neurons.

In our experimental procedure, we chose a stimulating intensity (0.05 Hz, 1 ms pulse duration) that elicited 50-60% of maximal signal amplitude. In order to verify if the number of polyspikes, generated after P_1, were different between *Cdkl5*-WT and *Cdkl5*-KO hippocampal slices, the protocol provided by Lüthi and colleagues (Lüthi et al., 1997) was adopted. According to this study, the repetitive stimulation of Schaffer collateral with 30 sweeps at 1 Hz (intensity and duration as above) could increase the excitability in CA1 stratum because it provoked an activity dependent disinhibition.

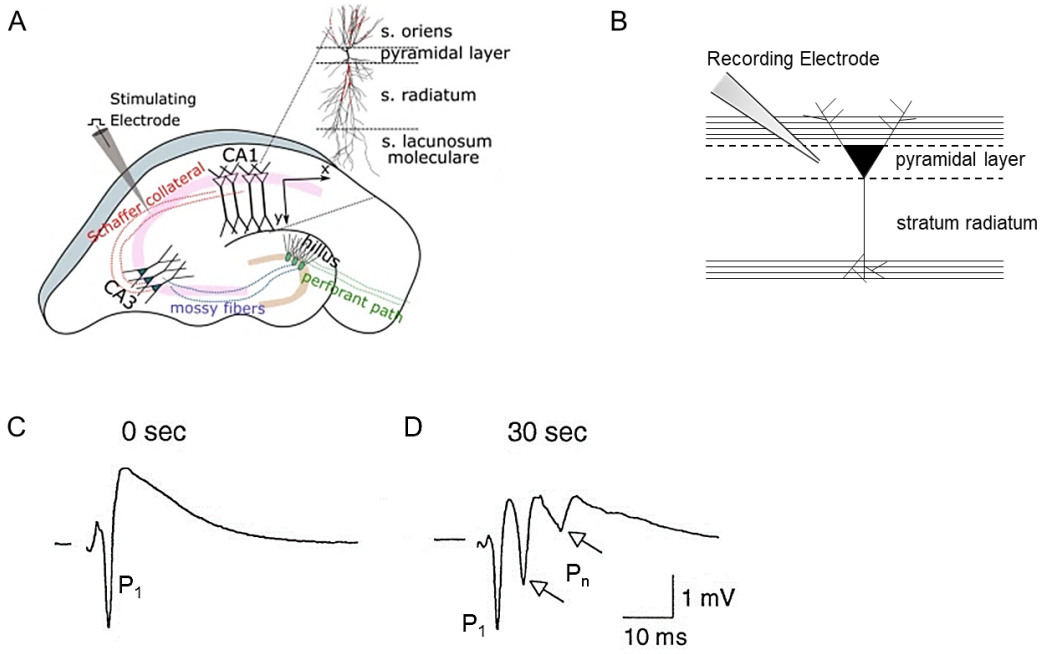

Figure 4.18 Extracellular recording of polyspikes in CA1 pyramidal layer. A) Diagram of a hippocampal slice where CA1 and CA3 subfields as well as Schaffer collaterals of the synaptic pathway are labelled. The recording of neural activity from the CA1 area is evoked by the electrical stimulation of the Schaffer collaterals in the CA3 region. **B)** Illustration of pyramidal layer where the recording electrode is placed extracellularly in the CA1 field. **C)** Example of field potentials evoked by a stimulating intensity (0.05 Hz, 1 ms pulse duration) that elicit 50-60% of maximal signal amplitude represented by the first peak (P_1). P_1 is the negative deflection generated by the summation of action potentials of different neurons belonging to the *stratum pyramidale*. **D)** Representative traces where polyspikes (P_n), indicated by arrows, are evoked by repetitive stimulation (1 Hz for 30 seconds) of the Schaffer collaterals (adapted from Karadas et al., 2018; Lüthi et al., 1997).

Our results demonstrated that hippocampal slices from *Cdkl5*-KO mice exhibited an increased polyspiking activity in the CA1 field upon 1 Hz of stimulation, as compared with *Cdkl5*-WT mice (Figure 4.19A). After field potential recordings, averages of the number of the first 5, of the last 10, and of all 30 consecutive sweeps were measured and compared between *Cdkl5*-WT and *Cdkl5*-KO slices. The latter showed a significant rise in the number of polyspikes during repetitive stimulations (Figure 4.19B). Since a significant difference was found in all of the three above-mentioned conditions, we proceeded conducting a more detailed analysis on the traces generated by the average of the 30 sweeps. The mean areas of P_1 and the sum of the areas of P_n (ΣP_n) were calculated for a time length of 15 ms. While the average of P_1 areas of *Cdkl5*-KO slices was identical to *Cdkl5*-WT slices, the average of ΣP_n areas was bigger in *Cdkl5*-KO mice (Figure 4.19C). Of note, since no polyspikes were observed in either of the experimental groups after 15 ms, we evaluated traces during the first 15 ms.

To sum up, this raise in epileptiform activity suggests that *Cdkl5*-KO mice may have an altered inhibition or excitation and a greater seizure susceptibility than the WT counterpart.

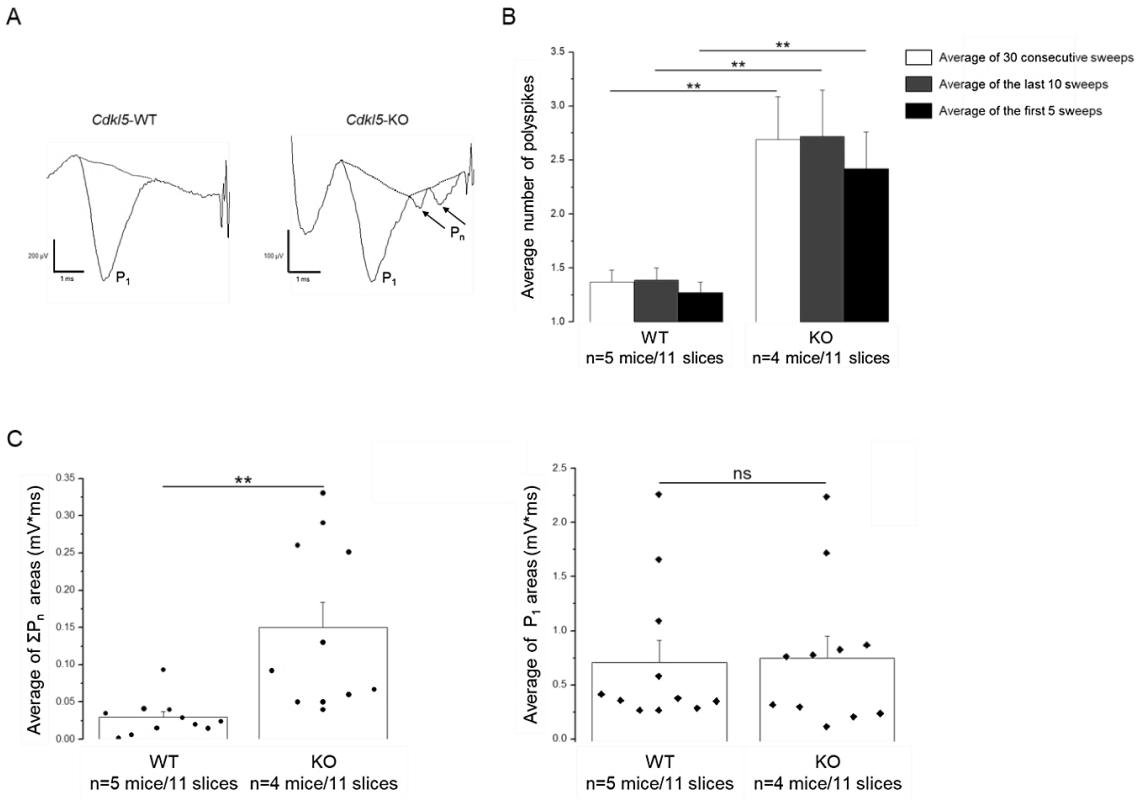

D

		WT (n=11)		KO (n=11)			
		Mean	SEM	Mean	SEM	t-test	p value
	Average number of polyspikes in 30 consecutive sweeps	1.37	0.11	2.68	0.40	**	0.005
	Average number of polyspikes in the first 5 sweeps	1.27	0.10	2.42	0.34	**	0.003
	Average number of polyspikes in the last 10 sweeps	1.39	0.11	2.72	0.43	**	0.007
Polyspikes in 30 consecutive sweeps	Average of P_1 areas (mV*ms)	0.71	0.20	0.75	0.20	ns	0.880
	Average of ΣP_n areas (mV*ms)	0.03	0.01	0.15	0.03	**	0.003

Figure 4.19 *Cdkl5*-KO hippocampal slices exhibit an epileptiform activity. A) Example of field potentials evoked by stimulation of the Schaffer collaterals and recorded in the *stratum pyramidale* of the CA1 area. P_1: first peak; P_n: polyspikes. **B-C)** After repetitive stimulation (1 Hz for 30 seconds), slices from *Cdkl5*-KO mice exhibited an increase in the number of polyspikes **(B)** and in the average of ΣP_n areas, but the average of P_1 area was the same as *Cdkl5*-WT slices **(C)**. **D)** The table illustrates mean values obtained from the analysis and the related statistic. n=5 *Cdkl5*-WT mice/11 hippocampal slices; n=4 *Cdkl5*-KO mice/11 hippocampal slices. Statistical analysis: unpaired Student's t-test; **p<0.01; ns, p>0.05.

5 Discussion

In the mammalian brain, synapses link neurons to other nerve cells thereby forming the specific neural circuits central to all brain functions. Two types of synapses are distinguished in the CNS: type I (asymmetric, also known as excitatory synapses) mainly located in dendritic spines and type II (symmetric, also defined as inhibitory synapses) typically incorporated in the soma and dendritic shafts (Ko et al., 2015). Type I synapses use glutamate to mediate excitatory synaptic transmission, while type II synapses use GABA and glycine to mediate inhibitory synaptic transmission. CDKL5 is a serine-threonine kinase, highly expressed in the brain, mainly in neuronal nuclei and dendrites (Olson et al., 2019). So far, the role of CDKL5 has been studied predominantly in excitatory synapses (Zhu & Xiong, 2018); on the contrary, up to now very little is known about the influence of CDKL5 at inhibitory synapses. Indeed, CDKL5 was reported in the past to be almost exclusively localised at excitatory synapses as it marginally colocalised with inhibitory synaptic markers (Ricciardi et al., 2012); nevertheless, CDKL5 is expressed in both glutamatergic and GABAergic neurons (Rusconi et al., 2008; Tang et al., 2017, 2019), suggesting that it may have distinctive functional roles in both neuronal populations (Schroeder et al., 2019).

Beyond the well-established role of CDKL5 at glutamatergic synapses, the results of this thesis shed light on a hitherto undescribed function of CDKL5 in the inhibitory compartment, possibly helping explaining the seizure phenotype observed in CDD patients. By applying biochemical and electrophysiological approaches on *in vitro* and *in vivo* models of CDD we have demonstrated, for the first time, that CDKL5 controls $GABA_AR$ expression and that its loss leads to an altered inhibitory neurotransmission that may generate an altered excitation-inhibition balance causing the seizure phenotype. Furthermore, we obtained important proof-of-principle data demonstrating that the pharmacological stimulation of MT dynamics with the synthetic neurosteroid PME can rescue the defective phenotypes associated with CDKL5 deficiency.

5.1 CDKL5 deficiency leads to dysfunctions in the inhibitory synapse

$GABA_A$Rs are ion channels permeable to chlorine and bicarbonate ions and are members of the family of channels with cysteine loops at the extracellular N-terminal (Bogdanov, 2019). In the mammalian CNS, these receptors can be localised to postsynaptic inhibitory specialisations or at extrasynaptic sites, where they mediate inhibitory neurotransmission. Indeed, while synaptic $GABA_A$Rs are activated transiently following the release of GABA from presynaptic vesicles, extrasynaptic $GABA_A$Rs are typically activated continuously by ambient GABA concentrations and thus mediate tonic inhibition. The difference in proprieties is reflected by a different subunit composition of the two receptor subtypes (Comenencia-Ortiz et al., 2014).

Herein, we analysed synaptic $GABA_A$Rs focusing our attention on γ_2 subunit-containing $GABA_A$Rs as *in situ* hybridisation has disclosed that this is the most abundant subunit in rat brain (Olsen & Sieghart, 2008). We first showed, through immunofluorescence analyses, a significant reduction of $GABA_A$R γ_2 surface expression in both hippocampal neurons and slices of *Cdkl5*-KO mice. This defect was corroborated through biochemical approaches. Since CDKL5 loss did not impact the total expression levels of synaptic $GABA_A$R subunits, we performed the highly sensitive cell surface biotinylation assay to investigate if the absence of CDKL5 influenced their surface expression levels. This technique is particularly useful if antibodies to the protein in question are either unsuitable for microscopy or are raised to intracellular and hence inaccessible domains (Arancibia-Cárcamo et al., 2006). With this approach, we found that *Cdkl5*-KO hippocampal cultures exhibited a reduced expression of membrane-inserted γ_2 containing $GABA_A$Rs. While the above-mentioned results are still preliminary, they corroborated the immunofluorescence analyses, indicating that CDKL5 loss may affect the membrane insertion and/or stabilisation of synaptic $GABA_A$Rs.

$GABA_A$Rs are assembled within the endoplasmic reticulum, transported to the Golgi, and then to the plasma membrane (Mele et al., 2019). Surface-exposed $GABA_A$Rs continuously undergo recycling between the plasma membrane and the intracellular compartments (Mele et al., 2019). In the future, we will address through a modified version of the biotinylation assay if $GABA_A$R turnover is altered in *Cdkl5*-KO neurons.

Lastly, the surface exposure of β_3 subunit-containing $GABA_A$Rs, which represent a higher proportion of diffuse and/or extrasynaptic receptors (Jacob et al., 2008), was diminished. Considering that phosphorylation levels of β_3 are involved in stabilising

$GABA_AR$s in the plasma membrane (Mele et al., 2019), we will further evaluate through the same approach the role of CDKL5 role in receptor trafficking.

The clinical features commonly associated with *CDKL5* mutations include early onset of epilepsy, intellectual disability, autistic features, motor impairment, hypotonia, and sleep disturbances (Fehr et al., 2013b). It is interesting to note that mutations in genes encoding the proteins that we found to be impaired in the absence of CDKL5 are associated with symptoms similar to those that characterise CDD patients. In particular, the gene encoding $GABA_AR$ γ_2 subunit, *GABRG2*, is the most common epilepsy-associated $GABA_AR$ gene. This feature is in agreement with the fact that the γ_2 subunit plays a central role in postsynaptic $GABA_AR$ assemblies and is required for synaptic trafficking, clustering, and maintenance of such receptors. *In vitro* studies demonstrated that *de novo* $GABA_AR$ γ_2 mutations, associated with epileptic encephalopathies, led to a reduction in cell surface expression of such receptor subunit (Shen et al., 2017). Accordingly, the same phenotype was also found in $GABA_AR$ γ_2 variants associated with childhood epilepsy (Reinthaler et al., 2015). Intriguingly, pathogenic variants in *GABRG2* have recently been described in a patient affected by atypical RTT (Cogliati et al., 2019). Lastly, variants in *GABRB3,* encoding the $GABA_AR$ β_3 subunit, are also involved in developmental neurological disorders, including epilepsy and autism (Fatemi et al., 2009). An interesting point that we will take into account for our future experiments is that a mouse model of status epilepticus has shown reduced surface expression of $GABA_AR$ β_3 in hippocampal slices due to a deficit in phosphorylation of this subunit at $Ser^{408/409}$ (Terunuma et al., 2008).

The cell membrane distribution of synaptic $GABA_AR$s is dynamically regulated via the interactions with the subsynaptic scaffold molecule gephyrin, which binds and clusters synaptic $GABA_AR$s at sites directly opposite to GABA releasing axon terminals (Tyagarajan & Fritschy, 2014). In particular, gephyrin takes part in the aggregation but not in the surface insertion or stabilisation of α_2 and γ_2 containing $GABA_AR$s (Groeneweg et al., 2018). Accordingly, the reduction of surface expressed synaptic $GABA_AR$ was accompanied by a reduction in the number of gephyrin-positive puncta in *Cdkl5*-KO primary cultures. We are currently addressing whether the number of gephyrin puncta is altered in hippocampal slices of *Cdkl5*-KO brains. Of note, Pizzo and colleagues did not observe any decrease in gephyrin puncta in the primary visual cortex of *Cdkl5*-KO mice (Pizzo et al., 2016) but we envisage that defective gephyrin clustering *in vivo* might be limited to specific brain areas. Indeed, in an animal model of temporal lobe epilepsy,

gephyrin expression gradually decreased in the hippocampus during the acute and latent period of epileptogenesis (Fang et al., 2011).

Based on the above, we hypothesise that defective localisation of gephyrin and synaptic $GABA_ARs$ may help explaining, at least in part, the clinical manifestation of CDD patients' mutations. Therefore, the knowledge of the molecular mechanisms underlying defective $GABA_AR$ surface expression represents an important step in the CDKL5 field. The key to understand this mechanism is likely to be provided by the molecular interaction between CDKL5 and the cytoplasmic CB-gephyrin complex. CB is a brain-specific GDP/GTP-exchange factor, which interacts with gephyrin, thus regulating its recruitment from intracellular deposits to postsynaptic membranes (Papadopoulos & Soykan, 2011). The loss of CB leads to a strong reduction in gephyrin and synaptic $GABA_AR$ clusters in several regions of the forebrain, including hippocampus, amygdala and cerebellum (Papadopoulos et al., 2007, 2008).

In our study, we found that CDKL5 is capable of forming a complex with CB and gephyrin as demonstrated through IP experiment both *in vitro* and *ex vivo*. As a consequence, CDKL5 *de facto* resides in the inhibitory synapse and, in line with our result, the study of Uezu *et al.* disclosed that CDKL5 is one of the few proteins shared by both the excitatory and the inhibitory postsynaptic density (Uezu et al., 2016). We did not manage to evaluate the impact of CDKL5 loss on collybistin-positive puncta because of the poor quality of the antibody when used in immunofluorescence experiments. Despite this, since CB is required for inhibitory receptor clustering and function, via the recruitment of gephyrin (Körber et al., 2012), we speculate that CDKL5 plays a direct role in the stabilisation of the key components of the inhibitory synapse by the above interaction. Another important aspect to be considered is the fact that gephyrin self-aggregates into a hexagonal lattice, interacting not only with CB but also with NL2 (Groeneweg et al., 2018; Ko et al., 2015). The latter is a neuronal transmembrane protein that, through the interaction with presynaptic neurexins, controls the concentration of $GABA_ARs$ at the synaptic site (Poulopoulos et al., 2009). Moreover, it is involved in the differentiation and maturation of GABAergic but not glutamatergic or glycinergic synapses *in vivo* (Poulopoulos et al., 2009).

In parallel to the IPs, we analysed the phosphorylation status of gephyrin, CB and NL2, envisaging that CDKL5, being a kinase, might regulate the above molecular complex in a phosphorylation dependent manner. While the phosphorylation of gephyrin at several sites is crucial for its functions at the inhibitory postsynaptic density (Tyagarajan & Fritschy, 2014), we did not find evidence of CDKL5 being involved in this regulation

through our λPP assays. Further, the electrophoretic mobility of CB in λPP-untreated lysates did not reveal detectable phosphorylation changes in the absence of CDKL5. On the contrary, a possible role of CDKL5 in controlling indirectly NL2 phosphorylation emerged, possibly through a hitherto unknown phosphatase that removes phosphate groups from NL2. This result is particularly intriguing as phosphorylation regulates the membrane stability of NL2. Indeed, the cAMP-dependent protein kinase (PKA) has recently been shown to phosphorylate NL2 at Ser^{714}, causing its rapid dispersal from inhibitory synaptic clusters and reducing its surface levels, consequently diminishing the concentration of synaptic $GABA_A$Rs (Halff et al., 2020). This finding is compatible with the reduced surface levels of NL2 that we have observed in the biotinylation experiments. Therefore, according to our hypothesis, CDKL5 loss might thus increase NL2 phosphorylation, impacting on its surface exposure and thus reducing synaptic $GABA_A$R membrane expression.

To sum up, CDKL5 might be involved in the regulation of the stability of γ_2 containing $GABA_A$Rs at the inhibitory synaptic sites, controlling directly the cytoplasmic CB-gephyrin complex and indirectly the NL2 phosphorylation. To address this last point, we are currently performing two-dimensional gel electrophoresis on hippocampal lysates from *Cdkl5*-WT and -KO mice at PND60.

To dig further into the molecular mechanism through which CDKL5 regulates the CB-gephyrin complex, we mapped the CB domains to investigate whether their interaction was phosphorylation-independent. As mentioned, CB has three major functional domains, namely SH3, DH and PH (Kins et al., 2000). In particular, the SH3 domain plays a crucial role in regulating CB functions. Indeed, at postsynaptic sites, CB can adopt a closed auto-inhibited conformation due to the presence of the SH3 domain but, upon binding to NL2 or the Rho-like GTPase TC10, it switches it to the open form and drives inhibitory synaptic differentiation. This change towards the open state allows its PH-domain to bind phosphatidylinositol-3-phosphate (PI3P) of the plasma membrane (Papadopoulos & Soykan, 2011).
Herein, through the expression of CB derivatives with or without the SH3 domain in a heterologous cell system, we demonstrated that the SH3 domain of CB is required for the interaction with CDKL5. Accordingly, the large C-terminal region of CDKL5 is proline-rich with different PXXP sequences, which are required for the binding to proteins with SH3 domains. In the past, Lin *et al.* speculated that CDKL5 might regulate SH3 domain

containing proteins (Lin et al., 2005) but CB is the first SH3 domain-containing protein interacting with CDKL5. Therefore, we hypothesise that CDKL5 might modulate the conformational switch of CB and, *ergo*, its activity through the interaction with its SH3 domain.

Further studies will be performed to address if CDKL5 regulates the switch of CB from its closed-to-open state. These analyses will be crucial to elucidate further the molecular functions of CDKL5 at the inhibitory synapse and to better understand how CDKL5 controls the formation of the cytoplasmic CB-gephyrin complex. Besides CB, we detected gephyrin in the immunocomplexes precipitated together with CDKL5 suggesting that gephyrin is another CDKL5 interactor. Whether this interaction is direct or indirect has yet to be determined. In our *in vitro* IP experiments, gephyrin coprecipitated with CDKL5 regardless the presence of overexpressed CB. Whether the low levels of endogenous CB in HEK293T cells mediate the interaction will be established through future experiments.

5.2 CDKL5 deficiency impairs the functional GABAergic synapse

The above-mentioned defects were accompanied by a reduction in the frequency of mIPSCs in *Cdkl5*-KO neurons. A similar result was observed when CDKL5 expression is acutely silenced through the transfection of a CDKL5-silencing construct expressing also GFP. Our experimental settings allowed recording the mIPSCs of CDKL5 silenced neuron (GFP-positive) that was innervated by untransfected cells. Therefore, the altered inhibitory neurotransmission could be ascribed to a direct role of CDKL5 at the postsynaptic site, being the presynaptic compartment normal. The major phenotype of CDKL5 deficiency in both *Cdkl5*-KO and silenced neurons was a remarkable decrease in mIPSC frequency, hence reflecting a strong reduction in the number of functional GABAergic synapses. We speculate that loss of CDKL5 at the postsynaptic site influences GABAergic innervation in *Cdkl5*-KO cultures similar to what has been reported in cortical neurons for $GABA_AR$ γ_2 clusters upon silencing of GODZ, which is implicated in trafficking and postsynaptic accumulation of γ_2 subunit-containing $GABA_ARs$ (Fang et al., 2006). GODZ is the key enzyme that interacts with and palmitoylates this receptor subunit, thus controlling presynaptic GABAergic innervation. In support of our hypothesis, we observed a significantly reduced number of bassoon-positive puncta in

primary cultures of *Cdkl5*-KO neurons. Bassoon is involved in the structural organisation of the neurotransmitter release site and in synaptic vesicle recycling (Richter et al., 1999). Interestingly, it was demonstrated that the loss of bassoon in mice caused spontaneous epileptic seizures (Altrock et al., 2003). However, since bassoon is present in presynaptic terminals of both asymmetric and symmetric synapses (Richter et al., 1999), we are currently evaluating the impact of CDKL5 deficiency on VGAT, which is specifically expressed in inhibitory neurons. Finally, examining the colocalisation of post- and presynaptic markers, we will evaluate the density of inhibitory synapses to verify if CDKL5 loss leads to synaptic drop-out.

Of note, Ricciardi and colleagues did not find any reduction in the frequency of mIPSCs CDKL5-silenced neurons at DIV15 (Ricciardi et al., 2009). The discrepancy between these results could be due to the different experimental conditions.

5.3 PME treatment ameliorates CDKL5-related defects

The strong impact of CDKL5 on neuronal morphology suggests that the kinase may be involved in regulating cytoskeletal dynamics. Indeed, molecular mechanisms linking CDKL5 to such processes have recently been clarified with data from various laboratories linking CDKL5 to MT dynamics (Baltussen et al., 2018; Barbiero et al., 2017b, 2020; Muñoz et al., 2018). In our laboratory, CDKL5 was demonstrated to regulate the functioning of the MT plus-end tracking protein CLIP170 that is implicated in MT-dynamics (Barbiero et al., 2017b). CLIP170 has recently been identified as the intracellular receptor for the neuroactive steroid PREG. The latter potentiates CLIP170 interaction with MTs and the MT-associated proteins (Weng et al., 2013). As an endogenous neurosteroid, PREG can be further metabolised into other steroids that can accomplish different functions: among the metabolites of PREG, pregnenolone-sulfate and ALLO can target $GABA_AR$s and calcium channels, hence modulating neurotransmission (Weng & Chung, 2016). The possible off-target effects of PREG limit its potential from a pharmacological point of view. Therefore, we decided to evaluate the efficacy of its non-metabolisable derivative PME, which maintains the biological activity of PREG on MT dynamics (Fontaine-Lenoir et al., 2006) but is devoid of the effects caused by the metabolism of PREG. Our published and submitted studies indicate that the pharmacological targeting of CLIP170 with PME has a remarkable capacity of ameliorating not only axonal phenotypes in young neurons but also the dendritic spine defects associated with CDKL5 loss (Barbiero et al., 2017b, 2020). Our studies have

demonstrated that PME induces the open conformation of CLIP170 and its binding to MTs (Barbiero et al., 2020, 2021 *under revision*). It is pivotal to underline that, in *in vitro* studies, this compound did not show affinity for any neurotransmitter receptor of the CNS, while it was demonstrated to enhance tubulin assembly by binding to the MT-associated protein MAP2 (Bianchi & Baulieu, 2012; Weng & Chung, 2016). Based on these results it appears that altered MT dynamics contribute significantly to CDKL5-dependent phenotypes.

In this thesis, we showed that PME can rescue the decreased frequency of mIPSCs in *Cdkl5*-KO primary cultures. This functional normalisation corresponded well with the rise in surface exposure of synaptic $GABA_AR$s as well as the increased number of both gephyrin and bassoon puncta. Therefore, the molecular rescue was accompanied by the functional restoration of GABAergic synapses upon PME treatment. Consistent with our *in vitro* results, we demonstrated that the number of γ_2 subunit-containing $GABA_AR$ clusters was restored in hippocampal slices of *Cdkl5*-KO mice treated with subcutaneous injections of PME (10 mg/kg) for seven consecutive days starting from PND60, when they are fully symptomatic. The biochemical analysis of synaptosomal preparations further corroborated the immunofluorescence data. Indeed, PME treatment also restored $GABA_AR$ γ_2 levels in hippocampal synaptosomes. Since the absence of CDKL5 did not affect the total levels of $GABA_AR$ γ_2 subunit, their reduction in the synaptosomal fraction might be a consequence of altered transport or recycling. Furthermore, we have recently demonstrated that the treatment with PME *in vivo* completely restored hippocampal-dependent spatial memory defects in *Cdkl5*-KO mice (Barbiero et al., 2021 *under revision*).

At the molecular level, it is possible that the beneficial effect of PME on CDKL5-related defects that we found in the inhibitory compartment is due to its ability to regulate the conformation of CLIP170, thus promoting MT dynamics. Our recent studies demonstrate that the loss of CDKL5 negatively impacts the invasion of MTs into dendritic spines and that PME restores such defect (Barbiero et al., 2021 *under revision*).

Regarding the inhibitory synapse, it is important to highlight that gephyrin was first identified as a tubulin-associated protein with the ability to form a bridge between glycine receptors and the polymerised tubulin (Kirsch et al., 1991). In addition, it binds to the dynein light chains (Dlc1/2) and kinesin 1 (KIF5), which are two types of motor proteins (Groeneweg et al., 2018). As described, gephyrin is organised into a MT- and microfilament-associated hexagonal protein lattice which facilitates the spatial distribution of $GABA_AR$s at the postsynaptic membrane (Mele et al., 2016). However,

during MT-based transport, $GABA_A$Rs require $GABA_A$R-associated protein (GABARAP) and the glutamate receptor-interacting protein (GRIP1) as adaptor proteins (Mele et al., 2019).

We thus hypothesise that CDKL5 exerts a dual control on synaptic $GABA_A$R expression: a direct regulation through its interaction with the gephyrin-CB complex and an indirect effect through its control on MT dynamics. Based on our results, the latter appears as an important target for disease modifying therapies worth of future studies.

Our findings may have interesting implications for patients with *CDKL5* mutations. In this last regard, many classical anti-epileptic drugs target $GABA_A$Rs but the response to these drugs depends on the abundance and composition of such receptors; reduced surface exposure or altered receptor composition has been linked to drug resistance (Deeb et al., 2012). As mentioned, most CDD patients are refractory to conventional anti-epileptic drugs (Bahi-Buisson et al., 2008a). As a consequence, our previous studies (Barbiero et al., 2017b, 2020, 2021 *under revision*) along with all pieces of evidence reported in this thesis pave the way for studies on novel compounds which, similarly to PME, could bypass the need of CDKL5. Currently, there are no approved therapies for CDD and any pharmacological strategies that reduce the frequency, duration or severity of seizures may positively impact the quality of life for CDD patients. In this regard, Marinus Pharmaceuticals has completed the Marigold Study, which is a phase 3 (double-blind, randomised, placebo-controlled) clinical trial evaluating the use of oral ganaxolone in children and young adults with CDD (https://www.themarigoldstudy.com/en-uk/). Ganaxolone, which is an analogue to the neurosteroid ALLO, is not believed to have nuclear hormone activity and cannot be converted into metabolites. This compound was used in clinical trials for the treatment of catamenial epilepsy disorder and was shown to be an effective anticonvulsant in different rodent seizures models (Bialer et al., 2013). By and large, neurosteroids, acting at both synaptic and extrasynaptic $GABA_A$Rs, are powerful modulators of such receptors and can rapidly alter neuronal excitability by potentiating phasic and tonic inhibitory neurotransmission (Chuang & Reddy, 2018). The Marigold Study disclosed that patients receiving ganaxolone showed a significant 32.2 percent median reduction in 28-day major motor seizure frequency, compared to a 4.0 percent reduction for placebo-treated patients.

In this thesis, we focused our attention on synaptic $GABA_A$Rs; however, the extrasynaptic counterpart is extremely important from a pharmacological point of view. Indeed, neurosteroids are more efficacious on extrasynaptic δ subunit-containing $GABA_A$Rs that mediate tonic inhibition. In detail, at low concentrations neurosteroids

allosterically potentiate $GABA_AR$ currents, while at high concentrations they can directly activate the receptor by binding directly at the orthosteric site (Chuang & Reddy, 2018). Intriguingly, dysregulation of neuronal activity and changes in the composition and function of $GABA_ARs$ contribute to the development of epilepsy. Hence, since the extrasynaptic counterpart is highly enriched in the hippocampus, future studies will aim at investigating the principal subunits of this receptor subtype, such as α_4, α_5 and δ.

5.4 *Cdkl5*-KO mice exhibit an altered epileptiform activity

Constitutive *Cdkl5*-KO mice exhibited enhanced synaptic transmission and long-term potentiation in the hippocampal CA1 region (Okuda et al., 2017). Nonetheless, these changes were not fully recapitulated in the glutamatergic conditional KO mice (Nex-cKO) (Tang et al., 2017), suggesting that CDKL5 function in GABAergic neurons may contribute to synaptic hyperexcitability as shown in Dlx-cKO mice (Tang et al., 2019). Considering the synergic contribution of different neuronal populations, we decided to assess extracellular field potentials of both *Cdkl5*-WT and -KO hippocampal slices. In particular, based on the protocol provided by Lüthi *et al.* (Lüthi et al., 1997), we analysed the potential of hippocampal slices to develop polyspikes, most likely due to the generation of neuronal burst discharges, in response to repetitive stimulation of the Schaffer collateral. Indeed, repetitive stimulation at relatively low frequencies results in a gradual increase in the excitability of hippocampal CA1 pyramidal cells and represent an important endogenous process underlying some aspects of epilepsy (Thompson & Gahwiler, 1989). In our CDD model, repetitive stimulation of the Schaffer collateral provoked an increased polyspiking of the CA1 pyramidal neurons in *Cdkl5*-KO slices. Indeed, both the average number of polyspikes and the mean of ΣP_n areas resulted to be greater than *Cdkl5*-WT slices, while the average of P_1 areas of *Cdkl5*-KO slices was identical to the WT counterpart, suggesting that this defect was due to an activity dependent disinhibition. Therefore, *Cdkl5*-KO mice are supposed to have a hyperexcitability phenotype, which may explain the autistic-like features reported in this animal model (Jhang et al., 2017; Wang et al., 2012). Indeed, hyperexcitability at the circuit and network levels has been found to be associated with mouse models of autism-spectrum disorders (Rubenstein & Merzenich, 2003). Interestingly, hyperexcitability has been also observed in animal models of early infantile epileptic encephalopathy (Lopez-Santiago et al., 2017). Our recordings disclosed that CDKL5 loss raised the epileptiform activity of *Cdkl5*-KO mice. In line with our results, previous studies demonstrated that

both constitutive (Okuda et al., 2017) and conditional (Yennawar et al., 2019) CDD mouse models displayed drug-induced seizure susceptibility. Nevertheless, the exact mechanisms underlying this higher seizure susceptibility in *Cdkl5*-KO mice remain to be established. The above-mentioned burst discharges might be based on the activity-dependent disinhibition of excitatory synaptic transmission and/or on the activation of NMDARs which strengthen the excitation (Thompson & Gahwiler, 1989). In this last regard, it has been recently demonstrated that an enhancement of NMDAR signalling can contribute to circuit hyperexcitability, indicating that enhanced excitatory synaptic transmission may be a homeostatic response to a transient alteration of GABAergic signalling during development (Okuda et al., 2017; Tang et al., 2019). Intriguingly, activity-dependent disinhibition results from naturally occurring mechanisms which are capable of producing transient or chronic increases in hippocampal excitability and constitute a determinant for the genesis of epilepsy (Thompson & Gahwiler, 1989). Consequently, our electrophysiological findings provide a significant insight into the CDD field as, to the best of our knowledge, *Cdkl5*-KO animal models do not exhibit hyperexcitability, suggesting seizures-like behaviours, without pharmacological manipulation.

5.5 Conclusion

In this study, we have demonstrated for the first time that CDKL5 resides and plays a direct role in inhibitory synapses. Indeed, our results indicate that CDKL5 controls the expression of functional $GABA_A$Rs at synaptic sites, in part through its interaction with the cytoplasmic CB-gephyrin complex but also through its control of MT dynamics (Figure 5.1A). Besides, we have investigated the effect of the synthetic neuroactive steroid PME on CDKL5-related defects, both *in vitro* and *in vivo*. This compound is able to bypass the need of CDKL5, promoting MT dynamics in *Cdkl5*-KO neurons, and thereby stabilises postsynaptic sites, potentiating $GABA_A$R functioning (Figure 5.1B). As a consequence, it might represent an important breakthrough in CDD field. Indeed, since the pharmacological targeting of $GABA_A$Rs is fundamental for seizure management, we believe that the restoration of $GABA_A$R expression would also be beneficial for the cognitive defects and autistic-like features linked to CDD.

To conclude, although there have been important steps towards an increased knowledge of CDKL5 functions since the discovery of its involvement in neurological disorders (Kalscheuer et al., 2003), more is still needed in order to allow the development of therapeutic strategies for CDD. Elucidating the networks regulated by CDKL5 can undeniably provide the basis for the rational design of therapeutic strategies.

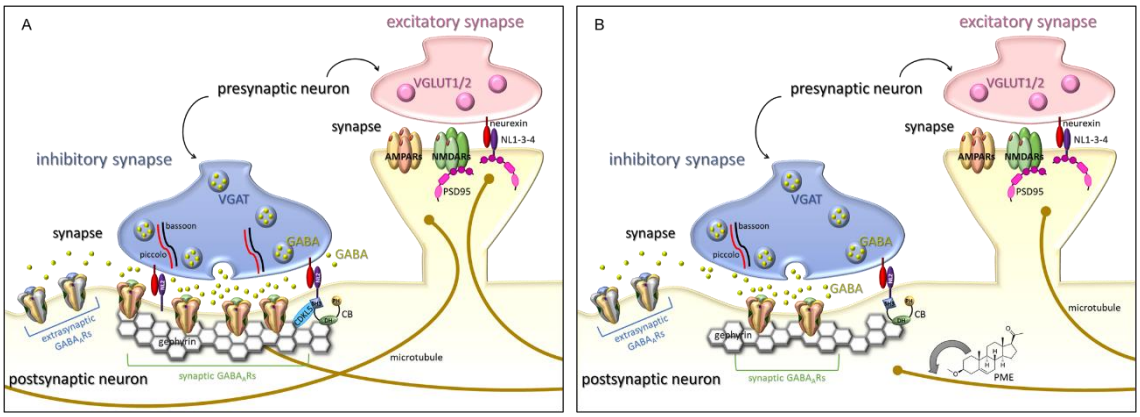

Figure 5.1 Diagram representing our working hypothesis. A) Model depicting that CDKL5 controls the formation and stability of both excitatory and inhibitory postsynaptic sites through its interaction with specific proteins such as PSD95 and the molecular complex of CB and gephyrin, thus placing CDKL5 as a key kinase for neuronal functions. Moreover, CDKL5 regulates MT dynamics, reinforcing the organisation of the postsynaptic sites. **B)** In the inhibitory synapse, the absence of CDKL5 leads to a reduction in gephyrin, synaptic $GABA_ARs$ and bassoon. Interestingly, by interacting with MT binding proteins, PME promotes MT dynamics, thus restoring CDKL5-dependent defects. CDKL5: cyclin-dependent kinase-like 5; PSD95: postsynaptic density protein 95; VGLUT1/2: vesicular glutamate transporter 1; AMPARs: α-amino-3-hydroxy-5-methyl-4-isoxazolepropionic acid receptors; NMDARs: N-methyl-D-aspartate receptors; CB: collybistin; NL1-2-3-4: neuroligin1-2-3-4; $GABA_ARs$: γ-aminobutyric acid type A receptors; vesicular GABA transporter: VGAT; PME: pregnenolone-methyl-ether.

6 Bibliography

Altrock, W. D., Tom Dieck, S., Sokolov, M., *et al.* (2003). Functional inactivation of a fraction of excitatory synapses in mice deficient for the active zone protein bassoon. *Neuron*, 37(5), 787–800.

Amendola, E., Zhan, Y., Mattucci, C., *et al.* (2014). Mapping pathological phenotypes in a mouse model of CDKL5 disorder. *PLoS ONE*, 9(5), 1–12.

Arancibia-Cárcamo, I. L., Fairfax, B. P., Moss, S. J., *et al.* (2006). Studying the localization, surface stability and endocytosis of neurotransmitter receptors by antibody labeling and biotinylation approaches (chapter 6). *CRC Press*, The Dynamic Synapse: Molecular Methods in Ionotropic Receptor Biology (Josef T. Kittler, Stephen J. Moss), 1st ed., 336 pp.

Archer, H. L., Evans, J., Edwards, S., *et al.* (2006). CDKL5 mutations cause infantile spasms, early onset seizures, and severe mental retardation in female patients. *Journal of Medical Genetics*, 43(9), 729–734.

Artuso, R., Mencarelli, M. A., Polli, R., *et al.* (2010). Early-onset seizure variant of Rett syndrome: Definition of the clinical diagnostic criteria. *Brain and Development*, 32(1), 17–24.

Bahi-Buisson, N., & Bienvenu, T. (2012b). CDKL5-related disorders: From clinical description to molecular genetics. *Molecular Syndromology*, 2(3–5), 137–152.

Bahi-Buisson, N., Kaminska, A., Boddaert, N., et al. (2008b). The three stages of epilepsy in patients with CDKL5 mutations. Epilepsia, 49(6), 1027–1037.

Bahi-Buisson, N., Nectoux, J., Rosas-Vargas, H., *et al.* (2008a). Key clinical features to identify girls with CDKL5 mutations. *Brain*, 131(10), 2647–2661.

Bahi-Buisson, N., Villeneuve, N., Caietta, E., *et al.* (2012a). Recurrent mutations in the CDKL5 gene: Genotype-phenotype relationships. *American Journal of Medical Genetics*, 158 A(7), 1612–1619.

Balestra, D., Giorgio, D., Bizzotto, M., *et al.* (2019). Splicing Mutations Impairing CDKL5 Expression and Activity Can be Efficiently Rescued by U1snRNA-Based Therapy. *Int J Mol Sci.*, 20(17), 4130–4146.

Baltussen, L. L., Negraes, P. D., Silvestre, M., *et al.* (2018). Chemical genetic identification of CDKL 5 substrates reveals its role in neuronal microtubule dynamics. *The EMBO Journal*, 37(24), e99763 (1–18).

Barbiero, I., De Rosa, R., & Kilstrup-Nielsen, C. (2019). Microtubules: A key to understand and correct neuronal defects in CDKL5 deficiency disorder? *International Journal of Molecular Sciences*, 20(17), 4075 (1–18). **[Appendix I]**

Barbiero, I., Peroni, D., Siniscalchi, P., *et al.* (2020). Pregnenolone and pregnenolone-methyl-ether rescue neuronal defects caused by dysfunctional CLIP170 in a neuronal model of CDKL5 Deficiency Disorder. *Neuropharmacology*, 164, 107897. **[Appendix II]**

Barbiero, I., Peroni, D., Tramarin, M., *et al.* (2017b). The neurosteroid pregnenolone reverts microtubule derangement induced by the loss of a functional CDKL5-IQGAP1 complex. *Human Molecular Genetics*, 26(18), 3520–3530.

Barbiero, I., Valente, D., Chandola, C., *et al.* (2017a). CDKL5 localizes at the centrosome and midbody and is required for faithful cell division. *Scientific Reports*, 7(1), 6228 (1–12).

Barbiero, I., Zamberletti, E., Tramarin, M., *et al.* (2021). Pregnenolone-methyl-ether (PME) activates CLIP170 and improves hippocampal-dependent deficits and spine maturation in a mouse model of CDKL5 deficiency disorder. *Neuropsychopharmacology*. **[under revision; Appendix III]**

Baulieu, E. E. (1998). Neurosteroids: A novel function of the brain. *Psychoneuroendocrinology*, 23(8), 963–987.

Belelli, D., Brown, A. R., Mitchell, S. J., *et al.* (2017). Endogenous neurosteroids influence synaptic GABAA receptors during post- natal development. *Journal of Neuroendocrinology*, 30(2), 1–38.

Belelli, D., & Lambert, J. J. (2005). Neurosteroids: Endogenous regulators of the GABAAreceptor. *Nature Reviews Neuroscience*, 6(7), 565–575.

Bergo, A., Strollo, M., Gai, M., *et al.* (2015). Methyl-CpG binding protein 2 (MeCP2) localizes at the centrosome and is required for proper mitotic spindle organization. *Journal of Biological Chemistry*, 290(6), 3223–3237.

Bertani, I., Rusconi, L., Bolognese, F., *et al.* (2006). Functional consequences of mutations in CDKL5, an X-linked gene involved in infantile spasms and mental retardation. *Journal of Biological Chemistry*, 281(42), 32048–32056.

Bialer, M., Johannessen, S. I., Levy, R. H., *et al.* (2013). Progress report on new antiepileptic drugs: A summary of the Thirteenth Eilat Conference on New Antiepileptic Drugs and Devices (EILAT XIII). *Epilepsy Research*, 103(1), 2–30.

Bianchi, M., & Baulieu, E. E. (2012). 3β-Methoxy-pregnenolone (MAP4343) as an innovative therapeutic approach for depressive disorders. *PNAS*, 109(5), 1713–1718.

Bogdanov, Y. D. (2019). Dynamic Regulation of GABAA Receptor Biosynthesis and Transport. *Neuroscience and Behavioral Physiology*, 49(7), 838–846.

Chen, Q., Zhu, Y. C., Yu, J., *et al.* (2010). CDKL5, a protein associated with Rett syndrome, regulates neuronal morphogenesis via Rac1 signaling. *Journal of Neuroscience*, 30(38), 12777–12786.

Chuang, S. H., & Reddy, D. S. (2018). Genetic and molecular regulation of extrasynaptic GABA-A receptors in the brain: Therapeutic insights for epilepsy. *Journal of Pharmacology and Experimental Therapeutics*, 364(2), 180–197.

Cogliati, F., Giorgini, V., Masciadri, M., *et al.* (2019). Pathogenic variants in STXBP1 and in genes for GABAa receptor subunities cause atypical rett/rett-like phenotypes. *International Journal of Molecular Sciences*, 20(15), 3621 (1–18).

Cohen, S., Gabel, H. W., Hemberg, M., *et al.* (2012). Regulates Nervous System Development and Function. *Neuron*, 72(1), 72–85.

Comenencia-Ortiz, E., Moss, S. J., & Davies, P. A. (2014). Phosphorylation of GABA A receptors influences receptor trafficking and neurosteroid actions. *Psychopharmacology*, 231(17), 3453-3465.

Conde, C., & Cáceres, A. (2009). Microtubule assembly, organization and dynamics in axons and dendrites. *Nature Reviews Neuroscience*, 10(5), 319–332.

Deeb, T. Z., Maguire, J., Moss, S. J. (2012). Possible alterations in GABAA receptor signaling that underlie benzodiazepine-resistant seizures. *Epilepsia*, 53(s9), 79–88.

Della Sala, G., Putignano, E., Chelini, G., *et al.* (2016). Dendritic Spine Instability in a Mouse Model of CDKL5 Disorder Is Rescued by Insulin-like Growth Factor 1. *Biological Psychiatry*, 80(4), 302–311.

Devinsky, O., Verducci, C., Thiele, E. A., *et al.* (2018). Open-label use of highly purified CBD (Epidiolex®) in patients with CDKL5 deficiency disorder and Aicardi, Dup15q, and Doose syndromes. *Epilepsy and Behavior*, 86, 131–137.

Duchossoy, Y., David, S., Baulieu, E. E., *et al.* (2011). Treatment of experimental spinal cord injury with 3β-methoxy- pregnenolone. *Brain Research*, 1403, 57–66.

Evans, J. C., Archer, H. L., Colley, J. P., *et al.* (2005). Early onset seizures and Rett-like features associated with mutations in CDKL5. *European Journal of Human Genetics*, 13(10), 1113–1120.

Fang, C., Deng, L., Keller, C. A., *et al.* (2006). GODZ-mediated palmitoylation of GABA(A) receptors is required for normal assembly and function of GABAergic inhibitory synapses. *Journal of Neuroscience*, 26(49), 12758–12768.

Fang, M., Shen, L., Yin, H., *et al.* (2011). Downregulation of gephyrin in temporal lobe epilepsy neurons in humans and a rat model. *Synapse*, 65(10), 1006–1014.

Fatemi, S. H., Reutiman, T. J., Folsom, T. D., *et al.* (2009). GABAA receptor downregulation in brains of subjects with autism. *J Autism Dev Disord*, 39(2), 223–230.

Fehr, S., Downs, J., Ho, G., *et al.* (2016). Functional abilities in children and adults with the CDKL5 disorder. *American Journal of Medical Genetics*, 170(11), 2860–2869.

Fehr, S., Leonard, H., Ho, G., *et al.* (2015). There is variability in the attainment of developmental milestones in the CDKL5 disorder. *Journal of Neurodevelopmental Disorders*, 7(1), 1–13.

Fehr, S., Wilson, M., Downs, J., *et al.* (2013). The CDKL5 disorder is an independent clinical entity associated with early-onset encephalopathy. *European Journal of Human Genetics*, 21(3), 266–273.

Ferreira, J. S., Schmidt, J., Rio, P., *et al.* (2015). GluN2B-containing NMDA receptors regulate AMPA receptor traffic through anchoring of the synaptic proteasome. *Journal of Neuroscience*, 35(22), 8462–8479.

Fontaine-Lenoir, V., Fellous, A., Duchossoy, Y., *et al.* (2006). Microtubule-associated protein 2 (MAP2) is a neurosteroid receptor. *PNAS*, 103(12), 4711–4716.

Fuchs, C., Fustini, N., Trazzi, S., *et al.* (2018b). Treatment with the GSK3-beta inhibitor Tideglusib improves hippocampal development and memory performance in juvenile, but not adult, Cdkl5 knockout mice. *European Journal of Neuroscience*, 47(9), 1054–1066.

Fuchs, C., Gennaccaro, L., Trazzi, S., *et al.* (2018a). Heterozygous CDKL5 Knockout Female Mice Are a Valuable Animal Model for CDKL5 Disorder. *Neural Plasticity*, 2018, 1–18.

Fuchs, C., Rimondini, R., Viggiano, R., *et al.* (2015). Inhibition of GSK3β rescues hippocampal development and learning in a mouse model of CDKL5 disorder. *Neurobiology of Disease*, 82(2015), 298–310.

Fuchs, C., Trazzi, S., Torricella, R., *et al.* (2014). Loss of CDKL5 impairs survival and dendritic growth of newborn neurons by altering AKT/GSK-3β signaling. *Neurobiology of Disease*, 70, 53–68.

Fukata, M., Watanabe, T., Noritake, J., *et al.* (2002). Rac1 and Cdc42 capture microtubules through IQGAP1 and CLIP-170. *Cell*, 109(7), 873–885.

Giatti, S., Garcia-Segura, L. M., Barreto, G. E., *et al.* (2019). Neuroactive steroids, neurosteroidogenesis and sex. *Progress in Neurobiology*, 176, 1–17.

Gray, E. G. (1959). Axo-somatic and axo-dendritic synapses of the cerebral cortex: an electron microscope study. *Journal of Anatomy*, 93(4), 420–433.

Groeneweg, F. L., Trattnig, C., Kuhse, J., *et al.* (2018). Gephyrin: a key regulatory protein of inhibitory synapses and beyond. *Histochemistry and Cell Biology*, 150(5), 489–508.

Guerrini, R., & Parrini, E. (2012). Epilepsy in Rett syndrome, and CDKL5- and FOXG1-gene-related encephalopathies. *Epilepsia*, 53(12), 2067–2078.

Halff, E., Hannan, S., Smart, T., *et al.* (2020). PKA-mediated phosphorylation of Neuroligin-2 regulates its cell surface expression and synaptic stabilisation. *BioRXiv*, 1–28.

Hamill, O. P., Marty, A., Neher, E., *et al.* (1981). Improved patch-clamp techniques for high-resolution current recording from cells and cell-free membrane patches. *Pflügers Archiv - European Journal of Physiology*, 391(2), 85–100.

Harvey, K., Duguid, I. C., Alldred, M. J., *et al.* (2004). The GDP-GTP exchange factor collybistin: An essential determinant of neuronal gephyrin clustering. *Journal of Neuroscience*, 24(25), 5816–5826.

Hector, R. D., Dando, O., Ritakari, T. E., *et al.* (2016). Characterisation of CDKL5 Transcript Isoforms in Human and Mouse. *PLoS ONE*, 11(6), e0157758 (1–22).

Hector, R. D., Kalscheuer, V. M., Hennig, F., *et al.* (2017). CDKL5 variants. *Neurology Genetics*, 3(6), e200 (1–11).

Hedman, A. C., Smith, J. M., & Sacks, D. B. (2015). The biology of IQGAP proteins: beyond the cytoskeleton. *EMBO Reports*, 16(4), 427–446.

Heo, S., Diering, G. H., Na, C. H., *et al.* (2018). Identification of long-lived synaptic proteins by proteomic analysis of synaptosome protein turnover. *PNAS*, 115(16), E3827–E3836.

Jacob, T. C., Moss, S. J., & Jurd, R. (2008). GABAA receptor trafficking and its role in the dynamic modulation of neuronal inhibition. *Nat Rev Neurosci.*, 9(5), 331–343.

Jhang, C. L., Huang, T. N., Hsueh, Y. P., *et al.* (2017). Mice lacking cyclin-dependent kinase-like 5 manifest autistic and ADHD-like behaviors. *Human Molecular Genetics*, 26(20), 3922–3934.

Johnston & Wu. (1994). Foundations of Cellular Neurophysiology. *The MIT Press.*, 710 pp., ISBN: 9780262100533.

Kalscheuer, V. M., Tao, J., Donnelly, A., *et al.* (2003). Disruption of the serine/threonine kinase 9 gene causes severe X-linked infantile spasms and mental retardation. *American Journal of Human Genetics*, 72(6), 1401–1411.

Kameshita, I., Sekiguchi, M., Hamasaki, D., *et al.* (2008). Biochemical and Biophysical Research Communications Cyclin-dependent kinase-like 5 binds and phosphorylates DNA methyltransferase 1. *Biochemical and Biophysical Research Communications*, 377(4), 1162–1167.

Karadas, M., Wojciechowski, A. M., Huck, A., *et al.* (2018). Feasibility and resolution limits of opto-magnetic imaging of neural network activity in brain slices using color centers in diamond. *Scientific Reports*, 8(1), 4503 (1–14).

Katayama, S., Sueyoshi, N., & Kameshita, I. (2015). Critical determinants of substrate recognition by cyclin-dependent kinase-like 5 (CDKL5). *Biochemistry*, 54(19), 2975–2987.

Kilstrup-Nielsen, C., Rusconi, L., La Montanara, P., *et al.* (2012). What we know and would like to know about CDKL5 and its involvement in epileptic encephalopathy. *Neural Plasticity*, 1–11.

Kins, S., Betz, H., & Kirsch, J. (2000). Collybistin, a newly identified brain-specific GEF, induces submembrane clustering of gephyrin. *Nature Neuroscience*, 3(1), 22–29.

Kirsch, J., Langosch, D., Prior, P., *et al.* (1991). The 93-kDa glycine receptor-associated protein binds to tubulin. *Journal of Biological Chemistry*, 266(33), 22242–22245.

Kittler, J. T., Thomas, P., Tretter, V., *et al.* (2004). Huntingtin-associated protein 1 regulates inhibitory synaptic transmission by modulating γ-aminobutyric acid type A receptor membrane trafficking. *PNAS*, 101(34), 12736–12741.

Ko, J., Choii, G., & Um, J. W. (2015). The balancing act of GABAergic synapse organizers. *Trends in Molecular Medicine*, 21(4), 256–268.

Komarova, Y. A., Akhmanova, A. S., Kojima, S. I., *et al.* (2002). Cytoplasmic linker proteins promote microtubule rescue in vivo. *Journal of Cell Biology*, 159(4), 589–599.

Körber, C., Richter, A., Kaiser, M., *et al.* (2012). Effects of distinct collybistin isoforms on the formation of GABAergic synapses in hippocampal neurons. *Molecular and Cellular Neuroscience*, 50(3–4), 250–259.

La Montanara, P., Rusconi, L., Locarno, A., *et al.* (2015). Synaptic synthesis, dephosphorylation, and degradation: A novel paradigm for an activity-dependent neuronal control of CDKL5. *Journal of Biological Chemistry*, 290(7), 4512–4527.

Lin, C., Franco, B., & Rosner, M. R. (2005). CDKL5/Stk9 kinase inactivation is associated with neuronal developmental disorders. *Human Molecular Genetics*, 14(24), 3775–3786.

Li, H., Zhong, X., Chau, K. F., *et al.* (2011). Loss of Activity-Induced Phosphorylation of MeCP2 Enhances Synaptogenesis, LTP, and Spatial Memory. *Nature Neuroscience*, 14(8), 1001–1008.

Lopez-Santiago, L. F., Yuan, Y., Wagnon, J. L., *et al.* (2017). Neuronal hyperexcitability in a mouse model of SCN8A epileptic encephalopathy. *PNAS*, 114(9), 2383–2388.

Luscher, B., Fuchs, T., & Kilpatrick, C. L. (2011). GABA(A) Receptor Trafficking-Mediated Plasticity of Inhibitory Synapses. *Neuron*, 70(3), 385–409.

Lüthi, A., Van Der Putten, H., Botteri, F. M., *et al.* (1997). Endogenous serine protease inhibitor modulates epileptic activity and hippocampal long-term potentiation. *Journal of Neuroscience*, 17(12), 4688–4699.

Magnaghi, V. (2007). GABA and Neuroactive Steroid Interactions in Glia: New Roles for Old Players? *Curr Neuropharmacol*, 5(1), 47–64.

Mari, F., Azimonti, S., Bertani, I., *et al.* (2005). CDKL5 belongs to the same molecular pathway of MeCP2 and it is responsible for the early-onset seizure variant of Rett syndrome. *Human Molecular Genetics*, 14(14), 1935–1946.

McLeod, F., Marzo, A., Podpolny, M., *et al.* (2017). Evaluation of synapse density in hippocampal rodent brain slices. *Journal of Visualized Experiments*, 2017(128), 56153 (1–8).

Melcangi, R. C., Garcia-Segura, L. M., & Mensah-Nyagan, A. G. (2008). Neuroactive steroids: State of the art and new perspectives. *Cellular and Molecular Life Sciences*, 65(5), 777–797.

Mele, M., Costa, R. O., & Duarte, C. B. (2019). Alterations in GABAA-receptor trafficking and synaptic dysfunction in brain disorders. *Frontiers in Cellular Neuroscience*, 13, 77 (1–16).

Mele, M., Leal, G., & Duarte, C. B. (2016). Role of GABAAR trafficking in the plasticity of inhibitory synapses. *Journal of Neurochemistry*, 139(6), 997–1018.

Montini, E., Andolfi, G., Caruso, A., *et al.* (1998). Identification and characterization of a novel serine-threonine kinase gene from the Xp22 region. *Genomics*, 51(3), 427–433.

Muñoz, I. M., Morgan, M. E., Peltier, J., *et al.* (2018). Phosphoproteomic screening identifies physiological substrates of the CDKL 5 kinase. *The EMBO Journal*, 37(24), e99559 (1–19).

Nawaz, M. S., Giarda, E., Bedogni, F., *et al.* (2016). CDKL5 and shootin1 interact and concur in regulating neuronal polarization. *PLoS ONE*, 11(2), e0148634 (1–18).

Neul, J. L., Kaufmann, W. E., Glaze, D. G., *et al.* (2010). Rett syndrome: Revised diagnostic criteria and nomenclature. *Annals of Neurology*, 68(6), 944–950.

Oi, A., Katayama, S., Hatano, N., *et al.* (2017). Subcellular distribution of cyclin-dependent kinase-like 5 (CDKL5) is regulated through phosphorylation by dual specificity tyrosine-phosphorylation-regulated kinase 1A (DYRK1A). *Biochemical and Biophysical Research Communications*, 482(2), 239–245.

Okuda, K., Kobayashi, S., Fukaya, M., *et al.* (2017). CDKL5 controls postsynaptic localization of GluN2B-containing NMDA receptors in the hippocampus and regulates seizure susceptibility. *Neurobiol. Dis.*, 106, 158–170.

Okuda, K., Takao, K., Watanabe, A., *et al.* (2018). Comprehensive behavioral analysis of the Cdkl5 knockout mice revealed significant enhancement in anxiety- and fear-related behaviors and impairment in both acquisition and long-term retention of spatial reference memory. *PLoS ONE*, 13(4),1–34.

Olsen, R. W., & Sieghart, W. (2008). International Union of Pharmacology. LXX. Subtypes of γ-aminobutyric acid A receptors: Classification on the basis of subunit composition, pharmacology, and function. Update. *Pharmacological Reviews*, 60(3), 243–260.

Olson, H. E., Demarest, S. T., Pestana-Knight, E. M., *et al.* (2019). Cyclin-Dependent Kinase-Like 5 Deficiency Disorder: Clinical Review. *Pediatric Neurology*, 97, 18–25.

Papadopoulos, T., Eulenburg, V., Reddy-Alla, S., *et al.* (2008). Collybistin is required for both the formation and maintenance of GABAergic postsynapses in the hippocampus. *Molecular and Cellular Neuroscience*, 39(2), 161–169.

Papadopoulos, T., Korte, M., Eulenburg, V., *et al.* (2007). Impaired GABAergic transmission and altered hippocampal synaptic plasticity in collybistin-deficient mice. *The EMBO Journal*, 26(17), 3888–3899.

Papadopoulos, T., & Soykan, T. (2011). The Role of Collybistin in Gephyrin Clustering at Inhibitory Synapses: Facts and Open Questions. *Frontiers in Cellular Neuroscience*, 5, 11 (1–10).

Pearson, G., Robinson, F., Gibson, T. B., *et al.* (2001). Mitogen-activated protein (MAP) kinase pathways: Regulation and physiological functions. *Endocrine Reviews*, 22(2), 153–183.

Pizzo, R., Gurgone, A., Castroflorio, E., *et al.* (2016). Lack of Cdkl5 Disrupts the Organization of Excitatory and Inhibitory Synapses and Parvalbumin Interneurons in the Primary Visual Cortex. *Frontiers in Cellular Neuroscience*, 10, 261 (1–16).

Poulopoulos, A., Aramuni, G., Meyer, G., *et al.* (2009). Neuroligin 2 Drives Postsynaptic Assembly at Perisomatic Inhibitory Synapses through Gephyrin and Collybistin. *Neuron*, 63(5), 628–642.

Pozzo-Miller, L., Pati, S., & Percy, A. K. (2015). Rett Syndrome: Reaching for Clinical Trials. *Neurotherapeutics*, 12(3), 631–640.

Reinthaler, E. M., Dejanovic, B., Lal, D., *et al.* (2015). Rare variants in γ-aminobutyric acid type A receptor genes in rolandic epilepsy and related syndromes. *Annals of Neurology*, 77(6), 972–986.

Ricciardi, S., Kilstrup-nielsen, C., Bienvenu, T., *et al.* (2009). CDKL5 influences RNA splicing activity by its association to the nuclear speckle molecular machinery. *Human Molecular Genetics*, 18(23), 4590–4602.

Ricciardi, S., Ungaro, F., Hambrock, M., *et al.* (2012). CDKL5 ensures excitatory synapse stability by reinforcing NGL-1-PSD95 interaction in the postsynaptic compartment and is impaired in patient iPSC-derived neurons. *Nature Cell Biology*, 14(9), 911–923.

Richter, K., Langnaese, K., Kreutz, M. R., *et al.* (1999). Presynaptic Cytomatrix Protein Bassoon Is Localized at Both Excitatory and Inhibitory Synapses of Rat Brain. *The Journal of Comparative Neurology*, 408(3), 437–448.

Rosas-Vargas, H., Bahi-Buisson, N., Philippe, C., *et al.* (2008). Impairment of CDKL5 nuclear localisation as a cause for severe infantile encephalopathy. *Journal of Medical Genetics*, 45(3), 172–178.

Rubenstein, J. L. R., & Merzenich, M. M. (2003). Model of autism: increased ratio of excitation/inhibition in key neural systems. *Genes Brain Behav.*, 2(5), 255–267.

Rusconi, L., Kilstrup-Nielsen, C., & Landsberger, N. (2011). Extrasynaptic N-Methyl-D-aspartate (NMDA) receptor stimulation induces cytoplasmic translocation of the

CDKL5 kinase and its proteasomal degradation. *Journal of Biological Chemistry*, 286(42), 36550–36558.

Rusconi, L., Salvatoni, L., Giudici, L., *et al.* (2008). CDKL5 expression is modulated during neuronal development and its subcellular distribution is tightly regulated by the C-terminal tail. *Journal of Biological Chemistry*, 283(44), 30101–30111.

Russo, S., Marchi, M., Cogliati, F., *et al.* (2009). Novel mutations in the CDKL5 gene, predicted effects and associated phenotypes. *Neurogenetics*, 10(3), 241–250.

Schneider Gasser, E. M., Straub, C. J., Panzanelli, P., *et al.* (2006). Immunofluorescence in brain sections: Simultaneous detection of presynaptic and postsynaptic proteins in identified neurons. *Nature Protocols*, 1(4), 1887–1897.

Schroeder, E., Yuan, L., Seong, E., *et al.* (2019). Neuron-Type Specific Loss of CDKL5 Leads to Alterations in mTOR Signaling and Synaptic Markers. *Molecular Neurobiology*, 56(6), 4151–4162.

Sekiguchi, M., Katayama, S., Hatano, N., *et al.* (2013). Identification of amphiphysin 1 as an endogenous substrate for CDKL5, a protein kinase associated with X-linked neurodevelopmental disorder. *Archives of Biochemistry and Biophysics*, 535(2), 257–267.

Shen, D., Hernandez, C. C., Shen, W., *et al.* (2017). De novo GABRG2 mutations associated with epileptic encephalopathies. *Brain*, 140(1), 49–67.

Sheng, M., & Kim, E. (2011). The postsynaptic organization of synapses. Cold Spring Harbor Perspectives in Biology, 3(12), a005678 (1–20).

Szafranski, P., Golla, S., Jin, W., *et al.* (2015). Neurodevelopmental and neurobehavioral characteristics in males and females with CDKL5 duplications. *Eur. J. Hum. Genet.* 23, 915–921.

Tang, S., Terzic, B., Wang, I. J., *et al.* (2019). Altered NMDAR signaling underlies autistic-like features in mouse models of CDKL5 deficiency disorder. *Nature Communications*, 10(1), 2655 (1–14).

Tang, S., Wang, I. T. J., Yue, C., *et al.* (2017). Loss of CDKL5 in glutamatergic neurons disrupts hippocampal microcircuitry and leads to memory impairment in mice. *The Journal of Neuroscience*, 37(31), 7420–7437.

Tao, J., Van Esch, H., Hagedorn-Greiwe, M., *et al.* (2004). Mutations in the X-Linked Cyclin-Dependent Kinase-like 5 (CDKL5/STK9) Gene Are Associated with Severe Neurodevelopmental Retardation. *American Journal of Human Genetics*, 75(6), 1149–1154.

Terunuma, M., Xu, J., Vithlani, M., *et al.* (2008). Deficits in phosphorylation of GABAA receptors by intimately associated protein kinase C activity underlie compromised synaptic inhibition during status epilepticus. *The Journal of Neuroscience*, 28(2), 376–384.

Thompson, S. M., & Gahwiler, B. H. (1989). Activity-dependent disinhibition. I. Repetitive stimulation reduces IPSP driving force and conductance in the hippocampus in vitro. *Journal of Neurophysiology*, 61(3), 501–511.

Tramarin, M., Rusconi, L., Pizzamiglio, L., *et al.* (2018). The antidepressant tianeptine reverts synaptic AMPA receptor defects caused by deficiency of CDKL5. *Human Molecular Genetics*, 27(12), 2052–2063.

Trazzi, S., Fuchs, C., Viggiano, R., *et al.* (2016). HDAC4: A key factor underlying brain developmental alterations in CDKL5 disorder. *Human Molecular Genetics*, 25(18), 3887–3907.

Trovò, L., Fuchs, C., De Rosa, R., *et al.* (2020). The green tea polyphenol epigallocatechin-3-gallate (EGCG) restores CDKL5-dependent synaptic defects in vitro and in vivo. *Neurobiology of Disease*, 138, 104791 (1–13).

Tretter, V., & Moss, S. J., (2008). GABA(A) receptor dynamics and constructing GABAergic synapses. *Frontiers in Molecular Neuroscience*, 1(7), 1–13.

Tretter, V., Mukherjee, J., Maric, H. M., *et al.* (2012). Gephyrin, the enigmatic organizer at GABAergic synapses. *Frontiers in Cellular Neuroscience*, 6(23), 1–16.

Tvrdeić, A., & Poljak, L. (2016). Neurosteroids, GABAA receptors and neurosteroid based drugs: are we witnessing the dawn of the new psychiatric drugs? *Endocrine Oncology and Metabolism*, 2(1), 60–71.

Tyagarajan, S. K., & Fritschy, J. M. (2014). Gephyrin: A master regulator of neuronal function? *Nature Reviews Neuroscience*, 15(3), 141–156.

Uezu, A., Kanac J., Bradshaw, T. W. A. (2016). Identification of an Elaborate Complex Mediating Postsynaptic Inhibition. *Science*, 353(6304), 1123–1129.

Wang, I. T. J., Allen, M., Goffin, D., *et al.* (2012). Loss of CDKL5 disrupts kinome profile and event-related potentials leading to autistic-like phenotypes in mice. *PNAS*, 109(52), 21516–21521.

Weaving, L. S., Christodoulou, J., Williamson, S. L., *et al.* (2004). Mutations of CDKL5 Cause a Severe Neurodevelopmental Disorder with Infantile Spasms and Mental Retardation. *Am. J. Hum. Genet.* 75(6), 1079–1093.

Weng, J. H., & Chung, B. C. (2016). Nongenomic actions of neurosteroid pregnenolone and its metabolites. *Steroids*, 111, 54–59.

Weng, J. H., Liang, M. R., Chen, C. H., *et al.* (2013). Pregnenolone activates CLIP-170 to promote microtubule growth and cell migration. *Nature Chemical Biology*, 9(10), 636–642.

Williamson, S. L., Giudici, L., Kilstrup-Nielsen, C., *et al.* (2012). A novel transcript of cyclin-dependent kinase-like 5 (CDKL5) has an alternative C-terminus and is the predominant transcript in brain. *Human Genetics*, 131(2), 187–200.

Yennawar, M., White, R. S., & Jensen, F. E. (2019). AMPA receptor dysregulation and therapeutic interventions in a mouse model of CDKL5 deficiency disorder. *Journal of Neuroscience*, 39(24), 4814–4828.

Zacchi, P., Antonelli, R., & Cherubini, E. (2014). Gephyrin phosphorylation in the functional organization and plasticity of GABAergic synapses. *Frontiers in Cellular Neuroscience*, 8, 103 (1–9).

Zhou, A., Han, S., & Zhou, Z. J. (2017). Molecular and genetic insights into an infantile epileptic encephalopathy – CDKL5 disorder. *Front Biol.* 12(1), 1–6.

Zhu, Y. C., Li, D., Wang, L., *et al.* (2013). Palmitoylation-dependent CDKL5-PSD-95 interaction regulates synaptic targeting of CDKL5 and dendritic spine development. *PNAS*, 110(22), 9118–9123.

Zhu, Y. C., & Xiong, Z.-Q. (2018). Molecular and Synaptic Bases of CDKL5 Disorder. *Developmental Neurobiology*, 79(1), 8–19.

Appendix I

International Journal of
Molecular Sciences

MDPI

Review

Microtubules: A Key to Understand and Correct Neuronal Defects in CDKL5 Deficiency Disorder?

Isabella Barbiero, Roberta De Rosa and Charlotte Kilstrup-Nielsen *

Department of Biotechnology and Life Sciences, (DBSV), University of Insubria, Via Manara 7, 21052 Busto Arsizio (VA), Italy
* Correspondence: c.kilstrup-nielsen@uninsubria.it; Tel.: +39-033-133-9430

Received: 25 July 2019; Accepted: 19 August 2019; Published: 21 August 2019

Abstract: CDKL5 deficiency disorder (CDD) is a severe neurodevelopmental encephalopathy caused by mutations in the X-linked *CDKL5* gene that encodes a serine/threonine kinase. CDD is characterised by the early onset of seizures and impaired cognitive and motor skills. Loss of CDKL5 in vitro and in vivo affects neuronal morphology at early and late stages of maturation, suggesting a link between CDKL5 and the neuronal cytoskeleton. Recently, various microtubule (MT)-binding proteins have been identified as interactors of CDKL5, indicating that its roles converge on regulating MT functioning. MTs are dynamic structures that are important for neuronal morphology, migration and polarity. The delicate control of MT dynamics is fundamental for proper neuronal functions, as evidenced by the fact that aberrant MT dynamics are involved in various neurological disorders. In this review, we highlight the link between CDKL5 and MTs, discussing how CDKL5 deficiency may lead to deranged neuronal functions through aberrant MT dynamics. Finally, we discuss whether the regulation of MT dynamics through microtubule-targeting agents may represent a novel strategy for future pharmacological approaches in the CDD field.

Keywords: CDKL5; microtubules; neuronal morphology; +TIP; CLIP170; EB1–3; MAP1S; microtubule-targeting agents; pregnenolone

1. Introduction

The cyclin-dependent kinase-like 5 (*CDKL5*) gene is known since 1998, when it was identified in a transcriptional mapping approach to identify disease-causing genes in the Xp22 region [1]. However, the gene caught significant attention only in 2003, when translocations interrupting *CDKL5* were identified in two female patients with severe X-linked infantile spasms and intellectual disability [2]. Rapidly afterwards, in 2004, more reports described missense and frame-shift mutations in various positions of *CDKL5* in individuals with clinical manifestations, ranging from atypical Rett syndrome (RTT) to autism [3–5]. In the following reports, mutations in *CDKL5* were commonly identified in patients clinically diagnosed with the early seizure variant of RTT and it was only in 2013 that the pathology associated with *CDKL5* deficiency was established as an independent clinical entity referred to as CDKL5 disorder [6] or, lately, as CDKL5 deficiency disorder (CDD). The first clinical manifestation of CDD is normally treatment-resistant seizures that appear within the first three months after birth [7]. Moreover, CDD patients are characterised by developmental delay, intellectual disability, gross motor impairment, strong hypotonia, sleep disturbances, gastrointestinal problems, breathing problems and hand stereotypies. Some of these symptoms overlap with those of RTT, and the main distinction between the two pathologies is the absence of a period of regression, which is among the diagnostic criteria for RTT [8], in patients with *CDKL5* mutations.

The clinical manifestations linked to *CDKL5* mutations underscore the importance of the encoded serine/threonine kinase for brain functions. Studies aimed at understanding the molecular pathways

controlled by CDKL5 and the neuronal and neuroanatomic consequences associated with its deficiency have in the last years provided crucial information of CDKL5 functions. Importantly, very recently, reports from more laboratories converge on a functional link between CDKL5 and microtubules (MTs) [9–12]. MTs, together with actin and intermediate filaments, constitute a highly dynamic architectural element of neurons and are fundamental for intracellular cargo transport and for the accommodation of structural neuronal changes that underlie synaptic plasticity [13]. Various brain disorders have been linked to mutations in genes that control MT-related processes, and the pharmacological targeting of MTs or the associated proteins are currently being tested in preclinical and clinical studies [14,15].

We will here review the recent findings regarding CDKL5 functions with particular focus on its MT-related functions and the possible translational value of these findings for CDKL5-related disorders.

2. Microtubules

Microtubules are constituted by dimers of α- and β-tubulin, polymerising in a head-to-tail fashion into proto-filaments that assemble laterally to form polarised tubular structures with so-called plus- and minus-ends exposing β- and α-tubulin, respectively [13] (Figure 1A). Assembly requires β-tubulin to be in its guanosine triphosphate (GTP)-bound form; the rapid hydrolysis into guanosine diphosphate (GDP) upon incorporation into the MT lattice generates a GTP-cap at the plus-end, favouring further polymerisation. In most cells, MTs are nucleated from the MT-organising centre (MTOC) with the minus-end of the MTs being embedded and stabilised in the γ-tubulin ring and the plus-ends radiating into the cytoplasm. Neuronal MTs, however, are rapidly released by MT-severing proteins and then transported into the neurites as short polymers. Further, in neurons, MT nucleation can also occur independently of the MTOC [16], with the minus-ends being capped and stabilised by specific proteins. The highly-polarised nature of neurons is mirrored in the organisation of the MT array: in the axon, MTs are uniformly oriented with the plus-ends facing the tip of the axon, while in dendrites they are of mixed polarity with both minus- and plus-ends pointing distally.

MTs are highly dynamic structures that undergo cycles of rapid growth and disassembly in a process defined as dynamic instability [13] (Figure 1B). The switch from growth to disassembly (or shrinkage) is called “catastrophe”, while the reverse is termed “rescue”. This dynamic instability, which occurs mainly at the MT plus-ends, provides a rapid reorganisation of the cytoskeleton that is necessary for many cellular functions, such as cell division and migration and formation of cell polarity. Various factors participate in the control of dynamic instability such as the fine regulation of MT-associated proteins, among which the plus-end tracking proteins (+TIPs) play a fundamental role [17], and the post-translational modifications (PTMs) of α- and β-tubulin that constitute the so-called “tubulin code” [18].

Tubulin PTMs present different allocations on the α/β-tubulin heterodimer with respect to their position on the MT lattice: detyrosination and deglutamylation take place on the C-terminal tail of tubulin that projects away from the MT lattice and provides interaction sites for the MT-associated proteins. Conversely, acetylation of α-tubulin on lysine 40 is found on the inside of the MT lumen (Figure 1C) [18]. Newly-synthesised α-tubulin generally contains a C-terminal tyrosine residue that undergoes enzymatic cyclic removal and re-addition. Detyrosinated MTs are normally considered stable and long-lived, even if the modification per se does not influence MT stability but rather alters the anchorage point for specific proteins. The irreversible removal of the penultimate glutamate from the primary sequence of α-tubulin, generating Δ2-tubulin, prevents α-tubulin re-tyrosination and represents a hallmark of stable MTs. Acetylation of α-tubulin on lysine 40 that, as mentioned, is located within the lumen of the MT lattice is synonymous of stable MTs. Although the causal link between tubulin PTMs and MT stability remains largely enigmatic, the consequences of their disruption can be fatal, as illustrated by animal models carrying inactivating mutations in genes encoding the modifying enzymes [19].

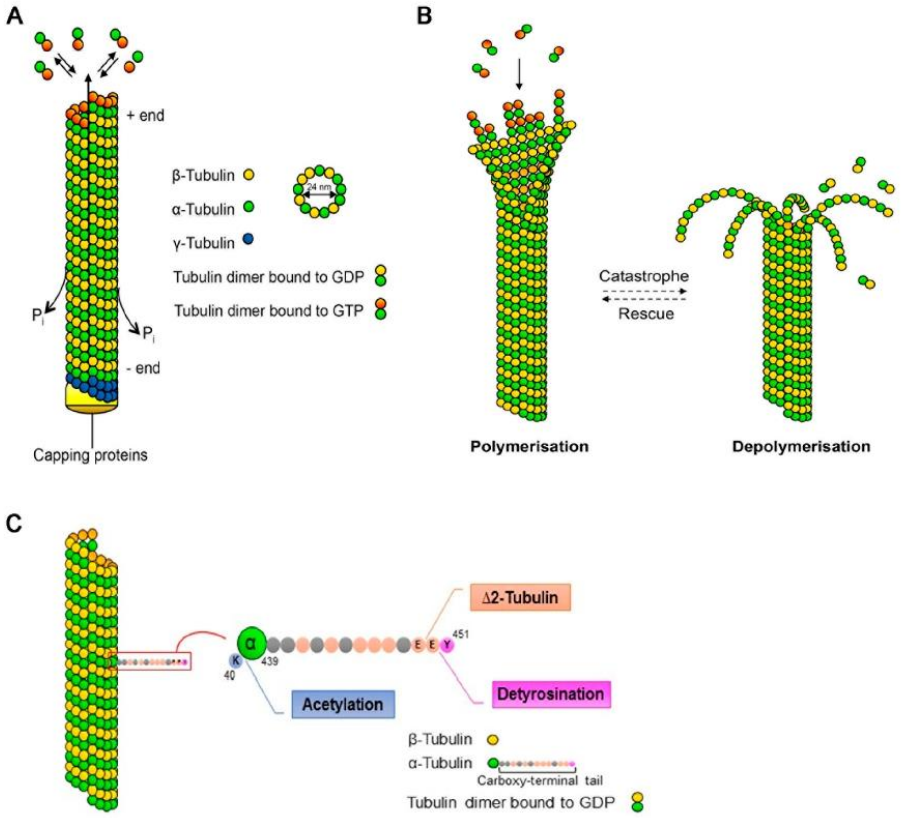

Figure 1. Microtubule dynamics and post-translational modifications. (**A**) Microtubules (MTs) are composed of α- and β-tubulin heterodimers that assemble to linear proto-filaments that associate laterally, forming the hollow MT cylinder. Assembly, which is nucleated from the γ-tubulin ring, occurs in a polarised fashion with the β-tubulin subunit oriented towards the growing plus-end. Newly-incorporated tubulin is bound to guanosine triphosphate (GTP) that gets rapidly hydrolysed upon polymerisation, generating guanosine diphosphate (GDP)-bound tubulin along the MT lattice. (**B**) MTs are dynamic structures undergoing cycles of growth (polymerisation) and shrinkage (depolymerisation). The switch from growth to shrinkage is termed catastrophe, whereas rescue indicates the switch from shrinkage to growth. (**C**) The α-tubulin subunit can be acetylated on lysine (K) 40, which is located on the inner side of the MT. The C-terminal tail of α-tubulin projects away from the MT lattice and undergoes various post-translational modifications. The extreme tyrosine residue (Y) can be enzymatically removed, generating detyrosinated α-tubulin, which normally correlates with long-lived MTs. Further removal of the penultimate glutamate (E) generates Δ2-tubulin.

As mentioned, dynamic instability is largely influenced by a plethora of proteins that bind MTs. Classical MT-associated proteins (MAPs) constitute an important group of proteins that bind along the MT lattice, influencing its polymerisation, stability and bundling. MAP1 family proteins, such as MAP1A, MAP1B and MAP1S, are high molecular weight complexes formed of heavy and light chains (LC) [20]. The capacity of these proteins to bind both MTs and actin suggests that they might simultaneously bind and cross-link these two cytoskeletal components. The MAP2 family includes MAP2 and Tau that accumulate in neuronal dendrites and axons, respectively, where they promote MT stability [21].

The +TIP family comprises another large group of diverse proteins that share the common feature of associating with the growing MT plus-end, where they control MT dynamics and functioning [22]. The plus-end tracking behaviour of these proteins can be visualised in live-imaging studies where the binding of the fluorescently tagged proteins to the growing MTs appears as comet-like dashes [23]. The end-binding proteins (EBs) form the central hub of the +TIPs; indeed, they provide the attachment site for other +TIPs thanks to their autonomous binding to MT plus-ends [24]. The EB family comprises EB1–3 that bind MTs through their calponin homology (CH) domain in the N-terminus, while they engage in specific protein interactions through C-terminal regions. The cytoskeleton-associated protein Gly-rich (CAP-Gly) domain proteins, including the cytoplasmic linker proteins (CLIP) CLIP170, CLIP115, and p150-Glued, constitute another important group of +TIPs that bind MT plus-ends indirectly via EBs but also by directly recognising the C-terminal EEY/F (glutamate-glutamate-tyrosine/phenylalanine) motif of α-tubulin [19,25,26]. Consistently, detyrosinated α-tubulin is deprived of the binding site for the CAP-Gly proteins. Another large group of +TIPs, including proteins like the CLIP-associated proteins (CLASP), the tumour suppressor adenomatousis polyposis coli protein (APC), p140Cap, and some kinesins (KIF), is characterised by an SxIP (serine-any amino acid-isoleucine-proline) motif through which they bind the EBs [17].

Functionally, the +TIPs can affect MT dynamics in opposing ways with the EBs suppressing the frequency of MT catastrophes and the CLIPs promoting MT rescue [22]. The +TIPs play an essential role in MT-related functions by mediating reciprocal interactions between the MT plus-ends and the cell cortex, where several of these proteins interact directly or indirectly with the actin cytoskeleton. This allows a subset of MTs to be selectively stabilised at specific sites under the cell membrane creating tracks for the delivery of proteins to the cell periphery and pulling forces on the MT network. In this way, the +TIPs are involved in various cellular processes including mitosis, cell migration and morphology [27]. Regarding neurons, various stages of neuronal development such as neuronal migration, axonal growth and dendritic spine maturation are strictly controlled by the +TIPs.

The importance of the proper regulation of the MT network for neuronal functions has been demonstrated through the pharmacological manipulation of MT dynamics. Indeed, axon formation can be artificially induced treating unpolarised neurons with the MT-stabilising drug, taxol [28]. On the other hand, both dendritic outgrowth and the maintenance of mushroom-headed spines were reduced through the inhibition of MT assembly [29,30]. Further, mutations in various genes encoding proteins that regulate MT dynamics can cause defects in neuronal migration and connectivity and have been linked to neurodevelopmental disorders characterised by intellectual disability and autistic features [31].

As mentioned, several links have recently been established between CDKL5 and MTs. Indeed, CDKL5 has recently been found to interact with the two +TIPs, CLIP170 and EB2 [9–11]. The latter was identified through a chemical genetic approach as a CDKL5 substrate and was thoroughly characterised as a bona fide phosphorylation target of CDKL5 in vitro and in vivo; the functional consequences of this event are still unknown, however [11], and neuronal functions of EB2 have not been described so far. CLIP170 was related functionally to CDKL5 through the identification of IQ motif containing GTPase activating protein 1 (IQGAP1) as a novel CDKL5 interactor [9]. IQGAP1 is an actin-binding protein that binds CLIP170 in a Rac1-dependent manner, facilitating the transient capture of MTs at specific cortical sites under the cell membrane [32,33]. Further, MAP1S, the less characterised member of the MAP1 family proteins, was identified as a substrate of CDKL5 through two different approaches providing strong support of a functional role of this association [11,12].

Since the discovery of the first patients with *CDKL5* mutations, CDKL5 functions have been studied in vitro and in vivo in proliferating cells, primary neurons, in mouse models carrying inactivating deletions of the *Cdkl5*-gene and in human induced pluripotent stem cells (iPSC)-derived neurons [34]. The overall picture emerging from these studies indicates that CDKL5 deficiency impacts cell proliferation, neuronal migration, and various aspects of neuronal morphology that are all processes that are strictly influenced by MT dynamics. These findings, demonstrating that CDKL5 functions converge on MT dynamics, may, therefore, provide a key to understand the mechanisms underlying CDD in more details.

3. Neuronal CDKL5 Related Defects

3.1. Axon Formation

In primary low-density cultures of hippocampal neurons, CDKL5 controls axon specification and outgrowth [35,36]. Axon elongation relies on the formation of stable MTs in the axonal shaft. These MTs form bundles covered with the axon specific MAP, Tau, and are organised in a polarised fashion, with the plus-ends oriented towards the peripheral tip. Such MT organisation generates tracks that facilitate the transport of proteins and organelles, thus providing the building blocks for new axonal segments. The axonal tip is characterised by a fan-shaped, motile structure, the growth cone, that probes the extracellular environment. In this way axon elongation and steering is directed in a process that depends on the complex remodelling and reorganisation of MTs and actin (Figure 2). The growth cone comprises the central region, enriched in MTs, and the peripheral domain, which is mainly composed of filamentous actin (F-actin); the two regions are separated by the transition zone in which actin arcs form a barrier against the extension of MTs into the peripheral zone [37]. Few MTs are capable of escaping the central domain and reach the growth cone periphery where they, thanks to the +TIPs, can couple to F-actin and associate with specific sites at the growth cone cortex. In particular, the +TIP CLIP170 accumulates in the axonal growth cone by binding to tyrosinated tubulin [19,38]. Interfering with CLIP170 expression impairs axon formation in primary neurons. This is accompanied by a reduced capacity of MTs to penetrate the actin arcs and protrude into the peripheral domain [39]. CDKL5 deficiency reduces the association of CLIP170 to MTs in proliferating cells and in the axonal growth cone of *Cdkl5*-KO neurons, which in both cases is accompanied by altered MT dynamics [9,40]. The binding of CLIP170 to MTs occurs when the protein is in its open active conformation whereas the intramolecular interaction between its terminal CAP-Gly domain and zinc-knuckle motifs causes a closed inactive conformation [41]. Interestingly, the neurosteroid pregnenolone (PREG), which induces the open conformation of CLIP170 through its direct binding to the protein [42], is capable of normalising the MT-binding of CLIP170 and restore axon specification and elongation in CDKL5 deficient neurons [9]. It thus seems likely that CDKL5 is involved in maintaining CLIP170 in its active conformation. The switching between the open and closed conformation of CLIP170 is known to depend on specific phosphorylation events. Whether CDKL5 regulates CLIP170 in a phosphorylation-dependent manner is still not known.

In the past, CDKL5 was proposed to affect axon formation through its interaction with Shootin1 [35]. Shootin1 is a key determinant for axon specification [43]; it was found to act as a clutch molecule that produces the traction force for axon outgrowth by coupling the retrograde flow of F-actin and cell adhesions [44]. Considering the novel link with CLIP170 it, thus, appears that CDKL5 may influence axon formation in different ways.

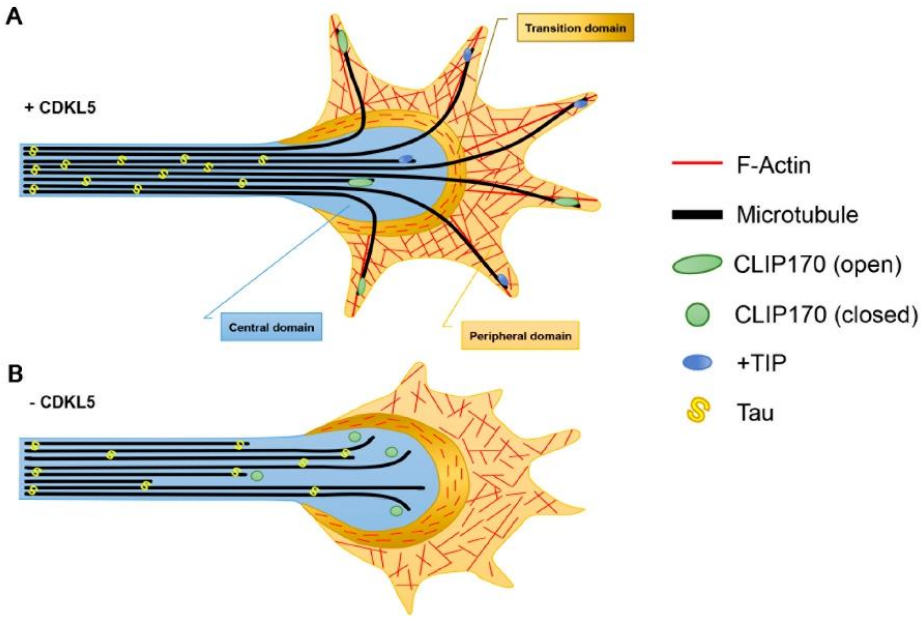

Figure 2. The effect of CDKL5 deficiency on microtubule dynamics in axonal growth cones. (**A**) In the axon, microtubules (MTs) are organised in a polar fashion with the plus-ends oriented distally. The central domain, which is contiguous with the axonal shaft, is rich in MTs that are bound by plus-end tracking proteins (+TIPS) including CLIP170. The peripheral domain is rich in actin that extends into the filopodia. The transition zone, lying in between these two domains, contains antiparallel actin arcs that form a barrier against the invasion of MTs into the peripheral domain. (**B**) In the absence of CDKL5, CLIP170 is in its closed conformation and is less associated with the MT plus-ends impacting their capacity to engorge into the actin rich area and leading to cessation of axonal outgrowth.

3.2. Dendritic Arborisation

CDKL5 deficiency was first shown, through silencing studies, to influence dendritic arborisation in vitro in primary cultures of rat cortical neurons and in vivo in migrating neurons derived from silenced neural progenitor cells [45]. Such defect has later been confirmed in cortical and hippocampal pyramidal neurons in *Cdkl5*-KO brains [46–48] and reproduced in vitro in *Cdkl5*-KO primary hippocampal neurons [36,40]. The penetrance of the phenotype in vitro may depend on the experimental conditions since contrasting data have been reported [11].

The control of CDKL5 on dendrite morphology was found to occur through Rac1, which is a critical regulator of actin remodelling. Recombinant CDKL5 was capable of pulling out Rac1 from neuronal lysates, an interaction that was further stimulated upon prior neuronal stimulation with brain-derived neurotrophic factor (Bdnf). Further, Bdnf activation of Rac1 was impaired in CDKL5 silenced cells, thus placing Rac1 downstream the kinase [45]. The exact mechanism through which CDKL5 activates Rac1 is unknown; however, it may be relevant to consider that CDKL5 controls the stability of the ternary IQGAP1/CLIP170/Rac1 complex [9]. IQGAP1 is widely implicated in Rac1/cdc42 signalling [49]. Indeed, IQGAP1 maintains the two small GTPases in their active GTP-bound state and acts as a scaffolding platform for Rac1/cdc42 signalling by recruiting their downstream effector proteins. Further, CLIP170 and IQGAP1 were reported to cooperate in controlling dendrite morphology, apparently by bridging MTs and the actin cytoskeleton [50]. Reduced CLIP170 or IQGAP1 levels led to the formation of a less complex dendritic arbor, a phenotype that resembles the one linked to CDKL5 deficiency and that could be prevented through the pharmacological stabilisation of F-actin.

CDKL5 may, thus, control the cytoskeleton dynamics involved in dendrite morphology by allowing the formation of the protein complex mediating Rac1 activation and bridging the MT and actin networks.

Another possible way in which CDKL5 regulates MT dynamics during dendritic arborisation may be represented by the phosphorylation on MAP1S, recently identified as a bona fide substrate of CDKL5 [11,12] (Figure 3). When phosphorylated on two serines (Ser786 and Ser812), located within the LC, MAP1S LCs have reduced affinity for MTs and appear to be more soluble. Interestingly, overexpression of phospho-defective MAP1S LCs in neurons forced the dendritic tips to settle in an aberrant looped conformation. In line with the capacity of MAP1 family members to increase MT stability [51], functional studies suggested that the increased binding of MAP1S to MTs in the absence of CDKL5 leads to less dynamic MT plus-ends. Indeed, EB3-GFP (green fluorescent protein) comets, the fluorescence of which over time is a measure of MT dynamicity, are longer lived in *Cdkl5*-KO neurons, but are restored to normal life-times upon MAP1S silencing [11].

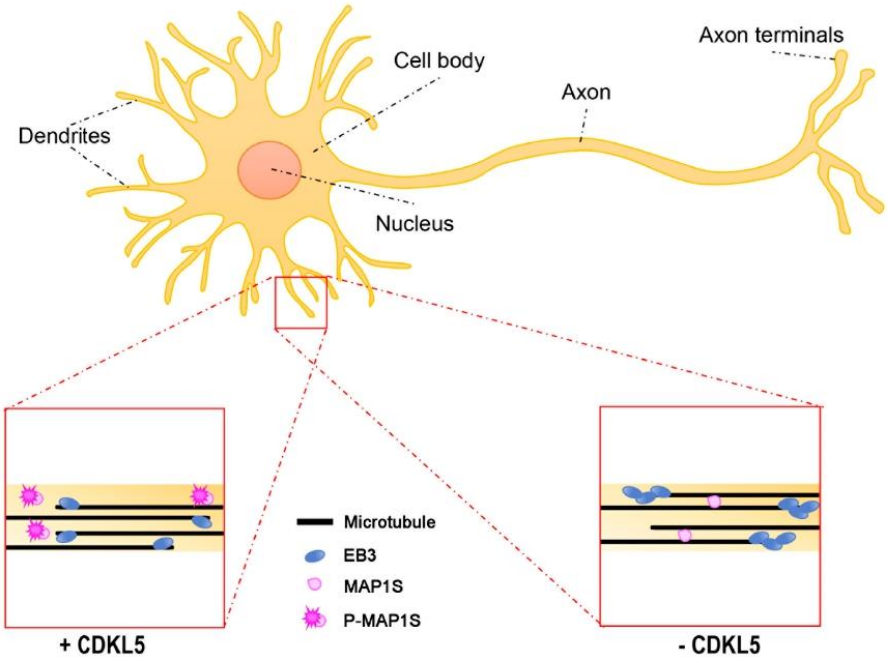

Figure 3. The effect of CDKL5 deficiency on dendritic microtubule dynamics. In dendrites, microtubules (MTs) have mixed orientations with the plus-ends oriented both proximally and distally. CDKL5 phosphorylates MAP1S inhibiting its binding to MTs (lower left). In the absence of CDKL5 (lower right), the binding of MAP1S to MTs is accompanied by increased life-time of EB3 binding to the plus-ends.

3.3. Dendritic Spines

Various studies in vitro and in vivo converge on a role of CDKL5 in controlling dendritic spine morphology and excitatory functions. Neurons devoid of CDKL5 are characterised by an increased number of filopodia-like protrusions and a reduced number of mushroom-shaped spines [52,53]. The enlarged spine heads, which distinguish mushroom-shaped spines, correlate with increased synaptic strength. Various neurologic conditions characterised by cognitive dysfunctions and autistic features have been linked to altered density and shape of dendritic spines [54]. CDKL5 is readily detectable in dendritic spines, where its synaptic accumulation is regulated both by the dendritic targeting of its mRNA, which undergoes local activity-dependent translation, and

through its interaction with post-synaptic density protein 95 (PSD95) [52,55,56]. CDKL5 is, thus, likely to influence directly various proteins involved in excitatory neurotransmission. Accordingly, CDKL5 affects the expression or phosphorylation of the post-synaptic markers PSD95, Homer, the α-amino-3-hydroxy-5-methylisozasole-4-propionic acid (AMPA)-receptor subunit GluA2, and NGL1 [52,56–58]. So far, we have very little information whether the neuroanatomical and molecular alterations in CDD mouse models are present also in the patients. However, reduced membrane levels of GluA2, which have been observed in vitro in neurons silenced for CDKL5 expression and in vivo in the hippocampus and perirhinal cortex of two mouse models of CDD, were recently confirmed in post-mortem brains from two CDD patients [58–60], suggesting the relevance of at least some CDKL5-related defects for the human pathology.

Plasticity-related changes in spine morphology are widely known to rely on remodelling of the actin cytoskeleton, which is highly enriched in dendritic protrusions [61]. MTs were for many years ignored as an integral part of dendritic spines; however, live imaging studies of fluorescently-tagged EB3, marking dynamic MTs, combined with other techniques, have allowed demonstrating that MTs do actually polymerise into dendritic spines in a rapid and transient manner [30,62,63] (Figure 4). The incursion of MTs into the spines is activity-dependent and contributes to the formation of mature dendritic spines. Actually, nocodazole-mediated inhibition of dynamic MTs impedes the Bdnf-induced structural changes that leads to the maturation of filopodia-like protrusions into mushroom-shaped spines [63]. The +TIP EB3 plays an active role in MT-dependent structural plasticity; actually, its silencing leads to a reduced number of mushroom-shaped spines. Paralleling the importance of a cross-talk between MTs and the actin cytoskeleton in the axonal growth cone, EB3 was found to provide a link to the actin cytoskeleton in the spines. Indeed, interactions between MT-bound EB3 with p140Cap and the actin stabilising factor cortactin is likely to create local signalling events that allow MT-actin communication in "activated" spines [30]. Interestingly, the actin–MT cooperation seems, in turn, to be enhanced by neuronal network activation; indeed, very recent data suggest that MT invasion occurs in specific spines through N-methyl-D-aspartate (NMDA)-receptor-mediated calcium influx that leads to actin remodelling at the base of the spine, thus allowing the targeting of the MTs [64].

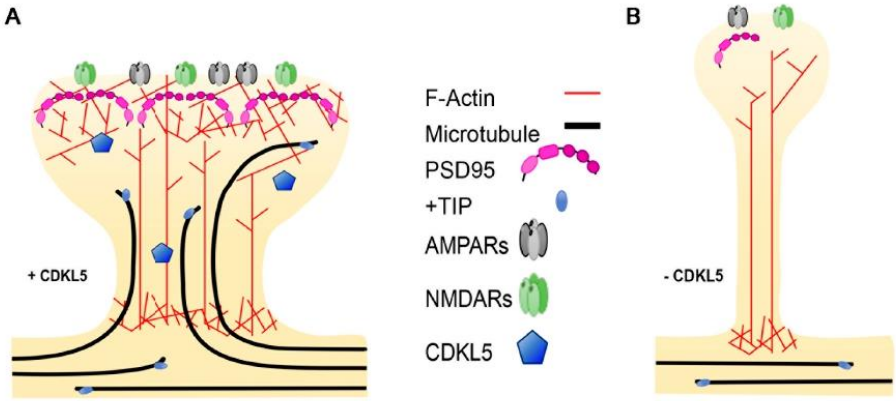

Figure 4. The effect of CDKL5 deficiency on dendritic spine morphology. (**A**) Dendritic spines, which are enriched in actin, are invaded by microtubules (MTs) upon neuronal activation. The plus-end tracking proteins (+TIP), bound to the MT plus-ends, interact with actin-binding proteins facilitating the invasion. (**B**) In the absence of CDKL5, MTs are less dynamic and fail to invade the spines, impacting the activity-dependent structural changes that lead to the formation of mushroom-shaped spines.

Regarding a possible role of CDKL5 in regulating spine morphogenesis through MT-related events, it is tempting to speculate that more +TIPs may be involved in regulating spine morphogenesis and functions creating other distinct links between MTs and the actin cytoskeleton. This would allow an expansion in the repertoire of possible signalling events underlying structural plasticity. While EB2 is broadly expressed in the neuronal soma, its levels are very low in the post-synaptic compartment [65]. Accordingly, CDKL5-dependent phosphorylation of EB2 on serine 223 can readily be detected in the proximal dendrites of patient iPSC-derived neurons [11]. The presence of CLIP170 in dendritic spines has so far not been reported. However, IQGAP1, which interacts with both CDKL5 and CLIP170, is present in spines [66], where it regulates spine morphogenesis [67], and *Iqgap1*-KO mice display cognitive defects and impaired long-term potentiation (LTP) [68]. IQGAP1 interacts with various post-synaptic proteins such as the AMPA-receptor GluA4, PSD95 and the NMDA-receptor complex [68,69]; it is, thus, intriguing to speculate that its interaction with CLIP170 might serve a role in regulating spine formation and functioning. Of further interest, disks large homolog 5 (DLG5), which was identified as a cellular substrate of CDKL5 [12], is an important regulator of dendritic spine formation [70]. DLG5 is member of the membrane-associated guanylate kinase (MAGUK) proteins and appears to control spine formation by facilitating the localisation of N-cadherin to the cell membrane. A possible link between DLG5 and MTs can be hypothesised based on its interaction with MARK3 (MT affinity regulating kinase 3), a kinase that controls cell polarity through the phosphorylation of specific MAPs, thus regulating their affinity for MTs [71].

Considering that MTs constitute fundamental tracks for the motor-based transport of cargoes, their invasion into dendritic spines is likely to provide a way of transporting cargoes into and out of these structures. The nature of which cargoes enter spines through MTs is still not clear. However, synaptotagmin has been found to be transported in a kinesin-dependent manner into dendritic spines [72]. Further studies will be relevant to analyse the contribution of altered MT dynamics to CDKL5-related spine defects and which cargoes might be influenced by CDKL5 deficiency.

4. Non-Neuronal CDKL5-Related Defects

The role of CDKL5 in regulating MT dynamics is consistent with our previous report that described CDKL5 as a centrosomal protein [10]. The centrosome is a central component of the cytoskeletal structure and consists of a scaffold core containing a large number of proteins, including γ-tubulin and the γ-tubulin ring complex (γ-TuRC) that typically surrounds a pair of cylindrical centrioles enclosed in the amorphous pericentriolar material (PCM) [73]. The centrosome is the primary MT-organising centre of the cells and, therefore, participates in fundamental cellular functions, such as cell motility, migration, polarity [74,75] and in the assembly and organisation of the mitotic spindle [76,77]. CDKL5 silencing causes an increase in the number of defective multipolar spindles, which is associated with polyploidisation and centrosome accumulation [10]. It is interesting to note that CDKL5 was recently found to interact with and phosphorylate the centrosomal protein CEP131 on serine 35 [12]. The functional role of this phosphorylation event was not further explored; however, silencing of CEP131 has been reported to cause centriole amplification and chromosomal instability [78], a phenotype that overlaps the one caused by CDKL5 deficiency [10]. Furthermore, CDKL5 and CEP131 share a common role in ciliogenesis [79,80]. The primary cilium is a eukaryotic organelle that is present on most quiescent and differentiated cells; it originates from a centrosome-derived structure, the basal body, and is composed by a central MT structure, the axoneme. The primary cilium acts as a cellular antenna that transmits signals from the extracellular environment to the inner site of the cell, thereby contributing to the regulation of numerous cellular processes such as proliferation, differentiation, migration and cell polarity [81]. Interestingly, defects in cilia morphogenesis and functioning have been associated with a large list of heterogeneous genetic disorders, known as ciliopathies [82]. Among the various clinical manifestations linked to ciliary dysfunctions, some share an overlap with those of CDD such as developmental delay, epilepsy, cognitive dysfunction and aberrant respiration. Cilium length appears to be influenced by CDKL5 levels [79,83]; a further understanding of how CDKL5

dysfunction impacts ciliary functions and the contribution of CEP131 and MT dynamics may pave the way for new perspectives in the CDKL5 field.

5. Possible Functional Outcome of Specific Pathogenic CDKL5 Mutations

The above studies linking CDKL5 to MT-related functions have been addressed in cells or tissues silenced for CDKL5 or with no expression of the protein. This reflects well the current view that CDD is caused by the absence of functional CDKL5 or by the expression of hypomorphic derivatives. Indeed, CDD-causing mutations in *CDKL5* include missense mutations, nonsense, frame-shift and splicing variants, and large genomic deletions [84]. The pathogenic missense mutations, which have been identified so far, fall almost exclusively within the catalytic domain of the protein. Functional studies based on the exogenous expression of mutated CDKL5 derivatives suggest that amino acid substitutions within the kinase domain impact negatively its catalytic activity [79,85–87]. Although these studies have highlighted the impact of missense mutations on CDKL5 functioning, it needs to be underlined that only very few of these mutations have been studied; we therefore cannot exclude that other missense mutations may generate hypermorphic CDKL5 derivatives. Regarding the nonsense and frame-shift variants, nonsense-mediated decay of the mutated mRNA is likely to impede the expression of the encoded protein, thus acting as hypomorphic or null mutations [84,88,89].

The existing animal models of CDD have addressed the consequences of the absence of CDKL5 either in the whole body or in distinct brain areas [46–48,90]. Recently, studies were performed in a mouse line expressing the pathogenic R59X allele, but since this causes the absence of CDKL5, it can be considered a functional null [60,91]. Although the generation of CDD mouse models has been extremely useful to deeply understand the roles of CDKL5, an important aspect that still remains to be addressed is how the expression of pathogenic hypomorphic CDKL5 derivatives affects neuronal functions. Hypothetically, such derivatives could behave as dominant negatives and interfere with the normal function of CDKL5 interactors, such as the MT-interacting proteins. Of relevance, CDKL5 localisation and cilium length is influenced by the expression of CDKL5 derivatives containing CDD-causing missense mutations that have not yet been characterised for the catalytic activity [79]. While the field is awaiting such animal models, primary fibroblasts and iPSC-derived neurons obtained from CDD patients will be very informative. Finally, it must be remembered that large genomic duplications, including *CDKL5*, have been identified in individuals with varying degrees of macrocephaly and learning disabilities [92], suggesting the relevance of analysing the effect of increased CDKL5 levels on MT-related functions.

6. Therapeutic Relevance of CDKL5-Dependent MT Defects

Alterations of the MT cytoskeleton have been linked to neurodegenerative and neurodevelopmental disorders such as schizophrenia and autism and major depression disorder [15,93]. Efforts have, therefore, been put into the development of therapeutic strategies targeting the neuronal cytoskeleton for these disorders [14,94]. The pharmacological stabilisation of MTs with the consequent block of mitosis has for decades been used for cancer treatment; the possibility of repositioning these drugs has been considered for brain disorders. MT-stabilising drugs were initially considered for neurodegenerative disorders that are characterised by compromised tau functions and altered MT structure and axonal transport [94]. Taxol (paclitaxel) promotes MT stability by binding within the MT lumen and increasing the lateral interactions between adjacent proto-filaments [95]. When considering the use of MT-stabilising drugs for brain disorders, it is fundamental to consider their capacity to pass the blood–brain barrier and their possible neuropathy side effects. While proof-of-principle studies supported the beneficial effect of taxol-mediated MT stabilisation on a mouse model presenting tau pathology in spinal motor neurons [96], this drug has a limited bioavailability in brain since it does not cross the blood–brain barrier. As taxol, Epothilone D (EpoD) binds and stabilises MTs, but it has the advantage of being brain penetrant, thus holding a stronger therapeutic potential for brain disorders [97]. EpoD has been tested in animal models of tauopathies where doses much lower (1/30) than those used in

cancer trials were found to be effective in stabilising MTs and to be capable of reducing cognitive deficits present in these models [98,99]. While EpoD and other drugs with similar MT-stabilising activities may possess interesting therapeutic potentials for patients with neurodegenerative diseases, their clinical application for young patient groups, as for example CDD, is more difficult to imagine. Drugs that bind MTs directly will impact MT stability in a non-specific manner and may, thus, have broad and non-advantageous effects on neurodevelopmental processes that are still ongoing in young patients. The use of drugs that target MT-binding proteins may act more specifically and, therefore, represent valid therapeutic options. An interesting molecule is represented by NAP/davunetide, an eight amino acid peptide that is derived from the activity-dependent neuroprotective protein (ADNP) [100]. ADNP is a versatile protein interacting with SWI/SNF chromatin remodelling complexes and with the +TIPs EB1 and EB3 [101,102]. Mutations in *ADNP* have been linked to autism and intellectual disability, and *Adnp* haploinsufficiency in mice is linked to altered axonal transport and dendritic spine alterations [103]. The NAP peptide interacts with the EB-proteins and promotes axonal transport and MT stability [104]. In pre-clinical studies in mouse models of various neurodegenerative diseases NAP shows neuroprotection and improves cognitive defects [105]. In clinical studies, intra-nasal administration of NAP led to improved cognitive skills in Alzheimer's disease patients [106] and daily activities in schizophrenic patients [107].

The possibility of targeting of proteins that have been functionally linked to CDKL5 might hold an even higher therapeutic potential for CDD. Interestingly, the neuroactive steroid PREG was found to directly bind CLIP170, inducing its open active conformation, as well as MAP2 [108]. Notably, the treatment of CDKL5-silenced cells with PREG was capable of restoring the MT association of GFP-CLIP170 comets and neuronal defects linked to CDKL5 deficiency [9]. Treatment with PREG is known to enhance memory and cognition in rodents [109]. Further, clinical testing in humans indicated potential anti-depressive and anti-psychotic effects and a positive safety profile [110,111]. However, the clinical application of PREG is limited due to its short half-life and its conversion into other neuroactive steroids that altogether possess a broad range of activities acting at the genomic level and with numerous membrane-bound receptors [108]. The development and testing of synthetic derivatives with improved stability and that cannot be metabolised into the downstream steroids might represent a possibility for CDD. Of note, MAPREG is a synthetic PREG derivative that has anti-depressant activities in rat models of depression [112] and in the primate-like tree-shrew [113]. Like PREG, MAPREG/MAP4343 promotes MT dynamics apparently through its binding to MAP2. Through further studies it might be relevant to analyse the therapeutic potential of this or similar PREG derivatives on CDKL5-deficient neurons.

To conclude, the last findings of CDKL5 functions converging on MT dynamics are likely to be of great relevance not only for a deeper understanding of the neuronal dysfunctions linked to CDKL5 deficiency but also for the development of disease-modifying pharmacological approaches. Importantly, they may also lead to the identification of clinical diagnostic biomarkers. However, before considering MT-targeting drugs for clinical applications for CDD, we still need to understand in more detail how precisely CDKL5 deficiency affects MT dynamics.

Author Contributions: C.K.N. and I.B., writing—original draft preparation; R.D.R., reviewing, editing, figure preparation.

Funding: This work was supported by funding from the Telethon Foundation grant (GGP15098) to CKN.

Acknowledgments: We thank the Italian parents' association l'Albero di Greta for the financial support of the laboratory.

Conflicts of Interest: The authors declare no conflicts of interest.

Abbreviations

+TIP	plus-end tracking protein
ADNP	activity-dependent neuroprotective protein
AMPA	α-amino-3-hydroxy-5-methylisozasole-4-propionic acid
APC	adenomatousis polyposis coli
Bdnf	brain-derived neurotrophic factor
CAP-Gly	cytoskeleton-associtated protein Gly-rich
CDD	CDKL5 deficiency disorder
CDKL5	cyclin-dependent kinase-like 5
CH	calponin homology
CLASP	CLIP-associated protein
CLIP	cytoplasmic linker protein
DLG5	disks large homolog 5
E	glutamate
EB	end-binding protein
EEY/F	glutamate-glutamate-tyrosine/phenylalanine
EpoD	Epothilone D
F-actin	filamentous actin
γ-TuRC	γ-tubulin ring complex
GFP	green fluorescent protein
GTP	guanine triphospate
GDP	guanine diphosphate
IQGAP1	IQ motif containing GTPase activating protein 1
iPSC	induced pluripotent stem cell
K	lysine
KIF	kinesin
LC	light chain
LTP	long-term potentiation
MAGUK	membrane-associated guanylate kinase
MAP	microtubule associated protein
MARK3	MT affinity regulating kinase 3
MT	microtubule
MTOC	microtubule organising centre
NMDA	N-methyl-D-aspartate
PCM	pericentriolar material
PREG	pregnenolone
PSD95	post-synaptic density protein 95
PTM	post-translational modification
RTT	Rett syndrome
SxIP	serine-any protein-isoleucine-proline
Y	tyrosine

References

1. Montini, E.; Andolfi, G.; Caruso, A.; Buchner, G.; Walpole, S.M.; Mariani, M.; Consalez, G.; Trump, D.; Ballabio, A.; Franco, B. Identification and characterization of a novel serine-threonine kinase gene from the Xp22 region. *Genomics* **1998**, *51*, 427–433. [CrossRef] [PubMed]
2. Kalscheuer, V.M.; Tao, J.; Donnelly, A.; Hollway, G.; Schwinger, E.; Kübart, S.; Menzel, C.; Hoeltzenbein, M.; Tommerup, N.; Eyre, H.; et al. Disruption of the serine/threonine kinase 9 gene causes severe X-linked infantile spasms and mental retardation. *Am. J. Hum. Genet.* **2003**, *72*, 1401–1411. [CrossRef] [PubMed]
3. Tao, J.; Van Esch, H.; Hagedorn-Greiwe, M.; Hoffmann, K.; Moser, B.; Raynaud, M.; Sperner, J.; Fryns, J.-P.; Schwinger, E.; Gécz, J.; et al. Mutations in the X-linked cyclin-dependent kinase-like 5 (CDKL5/STK9) gene are associated with severe neurodevelopmental retardation. *Am. J. Hum. Genet.* **2004**, *75*, 1149–1154. [CrossRef]

4. Weaving, L.S.; Christodoulou, J.; Williamson, S.L.; Friend, K.L.; McKenzie, O.L.D.; Archer, H.; Evans, J.; Clarke, A.; Pelka, G.J.; Tam, P.P.L.; et al. Mutations of CDKL5 cause a severe neurodevelopmental disorder with infantile spasms and mental retardation. *Am. J. Hum. Genet.* **2004**, *75*, 1079–1093. [CrossRef]
5. Scala, E.; Ariani, F.; Mari, F.; Caselli, R.; Pescucci, C.; Longo, I.; Meloni, I.; Giachino, D.; Bruttini, M.; Hayek, G.; et al. CDKL5/STK9 is mutated in Rett syndrome variant with infantile spasms. *J. Med. Genet.* **2005**, *42*, 103–107. [CrossRef] [PubMed]
6. Fehr, S.; Wilson, M.; Downs, J.; Williams, S.; Murgia, A.; Sartori, S.; Vecchi, M.; Ho, G.; Polli, R.; Psoni, S.; et al. The CDKL5 disorder is an independent clinical entity associated with early-onset encephalopathy. *Eur. J. Hum. Genet.* **2013**, *21*, 266–273. [CrossRef]
7. Olson, H.E.; Demarest, S.T.; Pestana-Knight, E.M.; Swanson, L.C.; Iqbal, S.; Lal, D.; Leonard, H.; Cross, J.H.; Devinsky, O.; Benke, T.A. Cyclin-Dependent Kinase-Like 5 Deficiency Disorder: Clinical Review. *Pediatr. Neurol.* **2019**, *97*, 18–25. [CrossRef] [PubMed]
8. Neul, J.L.; Kaufmann, W.E.; Glaze, D.G.; Christodoulou, J.; Clarke, A.J.; Bahi-Buisson, N.; Leonard, H.; Bailey, M.E.S.; Schanen, N.C.; Zappella, M.; et al. Rett syndrome: Revised diagnostic criteria and nomenclature. *Ann. Neurol.* **2010**, *68*, 944–950. [CrossRef]
9. Barbiero, I.; Peroni, D.; Tramarin, M.; Chandola, C.; Rusconi, L.; Landsberger, N.; Kilstrup-Nielsen, C. The neurosteroid pregnenolone reverts microtubule derangement induced by the loss of a functional CDKL5-IQGAP1 complex. *Hum. Mol. Genet.* **2017**, *26*, 3520–3530. [CrossRef] [PubMed]
10. Barbiero, I.; Valente, D.; Chandola, C.; Magi, F.; Bergo, A.; Monteonofrio, L.; Tramarin, M.; Fazzari, M.; Soddu, S.; Landsberger, N.; et al. CDKL5 localizes at the centrosome and midbody and is required for faithful cell division. *Sci. Rep.* **2017**, *7*, 6228. [CrossRef]
11. Baltussen, L.L.; Negraes, P.D.; Silvestre, M.; Claxton, S.; Moeskops, M.; Christodoulou, E.; Flynn, H.R.; Snijders, A.P.; Muotri, A.R.; Ultanir, S.K. Chemical genetic identification of CDKL5 substrates reveals its role in neuronal microtubule dynamics. *EMBO J.* **2018**, *37*, e99763. [CrossRef] [PubMed]
12. Muñoz, I.M.; Morgan, M.E.; Peltier, J.; Weiland, F.; Gregorczyk, M.; Brown, F.C.; Macartney, T.; Toth, R.; Trost, M.; Rouse, J. Phosphoproteomic screening identifies physiological substrates of the CDKL5 kinase. *EMBO J.* **2018**, *37*, e99559. [CrossRef] [PubMed]
13. Kapitein, L.C.; Hoogenraad, C.C. Building the Neuronal Microtubule Cytoskeleton. *Neuron* **2015**, *87*, 492–506. [PubMed]
14. Varidaki, A.; Hong, Y.; Coffey, E.T. Repositioning Microtubule Stabilizing Drugs for Brain Disorders. *Front. Cell. Neurosci.* **2018**, *12*, 226. [CrossRef] [PubMed]
15. Bonini, S.A.; Mastinu, A.; Ferrari-Toninelli, G.; Memo, M. Potential Role of Microtubule Stabilizing Agents in Neurodevelopmental Disorders. *Int. J. Mol. Sci.* **2017**, *18*, 1627.
16. Stiess, M.; Maghelli, N.; Kapitein, L.C.; Gomis-Rüth, S.; Wilsch-Bräuninger, M.; Hoogenraad, C.C.; Tolić-Nørrelykke, I.M.; Bradke, F. Axon extension occurs independently of centrosomal microtubule nucleation. *Science* **2010**, *327*, 704–707. [CrossRef]
17. van de Willige, D.; Hoogenraad, C.C.; Akhmanova, A. Microtubule plus-end tracking proteins in neuronal development. *Cell. Mol. Life Sci.* **2016**, *73*, 2053–2077.
18. Yu, I.; Garnham, C.P.; Roll-Mecak, A. Writing and Reading the Tubulin Code. *J. Biol. Chem.* **2015**, *290*, 17163–17172. [CrossRef]
19. Erck, C.; Peris, L.; Andrieux, A.; Meissirel, C.; Gruber, A.D.; Vernet, M.; Schweitzer, A.; Saoudi, Y.; Pointu, H.; Bosc, C.; et al. A vital role of tubulin-tyrosine-ligase for neuronal organization. *Proc. Natl. Acad. Sci. USA* **2005**, *102*, 7853–7858.
20. Halpain, S.; Dehmelt, L. The MAP1 family of microtubule-associated proteins. *Genome Biol.* **2006**, *7*, 224. [CrossRef]
21. Dehmelt, L.; Halpain, S. Actin and microtubules in neurite initiation: Are MAPs the missing link? *J. Neurobiol.* **2004**, *58*, 18–33. [CrossRef]
22. Akhmanova, A.; Steinmetz, M.O. Tracking the ends: A dynamic protein network controls the fate of microtubule tips. *Nat. Rev. Mol. Cell Biol.* **2008**, *9*, 309–322. [CrossRef] [PubMed]
23. Perez, F.; Diamantopoulos, G.S.; Stalder, R.; Kreis, T.E. CLIP-170 highlights growing microtubule ends in vivo. *Cell* **1999**, *96*, 517–527. [CrossRef]
24. Mustyatsa, V.V.; Boyakhchyan, A.V.; Ataullakhanov, F.I.; Gudimchuk, N.B. EB-Family Proteins: Functions and Microtubule Interaction Mechanisms. *Biochem. Mosc.* **2017**, *82*, 791–802. [CrossRef] [PubMed]

25. Peris, L.; Thery, M.; Fauré, J.; Saoudi, Y.; Lafanechère, L.; Chilton, J.K.; Gordon-Weeks, P.; Galjart, N.; Bornens, M.; Wordeman, L.; et al. Tubulin tyrosination is a major factor affecting the recruitment of CAP-Gly proteins at microtubule plus ends. *J. Cell Biol.* **2006**, *174*, 839–849. [CrossRef] [PubMed]
26. Bieling, P.; Kandels-Lewis, S.; Telley, I.A.; van Dijk, J.; Janke, C.; Surrey, T. CLIP-170 tracks growing microtubule ends by dynamically recognizing composite EB1/tubulin-binding sites. *J. Cell Biol.* **2008**, *183*, 1223–1233. [CrossRef] [PubMed]
27. Tamura, N.; Draviam, V.M. Microtubule plus-ends within a mitotic cell are "moving platforms" with anchoring, signalling and force-coupling roles. *Open Biol.* **2012**, *2*, 120132. [CrossRef]
28. Witte, H.; Neukirchen, D.; Bradke, F. Microtubule stabilization specifies initial neuronal polarization. *J. Cell Biol.* **2008**, *180*, 619–632. [CrossRef] [PubMed]
29. Sharp, D.J.; Yu, W.; Baas, P.W. Transport of dendritic microtubules establishes their nonuniform polarity orientation. *J. Cell Biol.* **1995**, *130*, 93–103. [CrossRef] [PubMed]
30. Jaworski, J.; Kapitein, L.C.; Gouveia, S.M.; Dortland, B.R.; Wulf, P.S.; Grigoriev, I.; Camera, P.; Spangler, S.A.; Di Stefano, P.; Demmers, J.; et al. Dynamic microtubules regulate dendritic spine morphology and synaptic plasticity. *Neuron* **2009**, *61*, 85–100. [CrossRef] [PubMed]
31. Lasser, M.; Tiber, J.; Lowery, L.A. The Role of the Microtubule Cytoskeleton in Neurodevelopmental Disorders. *Front. Cell. Neurosci.* **2018**, *12*, 165. [CrossRef] [PubMed]
32. Fukata, M.; Watanabe, T.; Noritake, J.; Nakagawa, M.; Yamaga, M.; Kuroda, S.; Matsuura, Y.; Iwamatsu, A.; Perez, F.; Kaibuchi, K. Rac1 and Cdc42 capture microtubules through IQGAP1 and CLIP-170. *Cell* **2002**, *109*, 873–885. [CrossRef]
33. Hedman, D.; Reza Barzegar, H.; Rosén, A.; Wågberg, T.; Andreas Larsson, J. On the Stability and Abundance of Single Walled Carbon Nanotubes. *Sci. Rep.* **2015**, *5*, 16850. [CrossRef] [PubMed]
34. Zhu, Y.-C.; Xiong, Z.-Q. Molecular and Synaptic Bases of CDKL5 Disorder. *Dev Neurobiol* **2019**, *79*, 8–19. [CrossRef] [PubMed]
35. Nawaz, M.S.; Giarda, E.; Bedogni, F.; La Montanara, P.; Ricciardi, S.; Ciceri, D.; Alberio, T.; Landsberger, N.; Rusconi, L.; Kilstrup-Nielsen, C. CDKL5 and Shootin1 Interact and Concur in Regulating Neuronal Polarization. *PLoS ONE* **2016**, *11*, e0148634. [CrossRef] [PubMed]
36. Fuchs, C.; Medici, G.; Trazzi, S.; Gennaccaro, L.; Galvani, G.; Berteotti, C.; Ren, E.; Loi, M.; Ciani, E. CDKL5 deficiency predisposes neurons to cell death through the deregulation of SMAD3 signaling. *Brain Pathol.* **2019**. [CrossRef]
37. Conde, C.; Cáceres, A. Microtubule assembly, organization and dynamics in axons and dendrites. *Nat. Rev. Neurosci.* **2009**, *10*, 319–332. [CrossRef] [PubMed]
38. Nirschl, J.J.; Magiera, M.M.; Lazarus, J.E.; Janke, C.; Holzbaur, E.L.F. α-Tubulin Tyrosination and CLIP-170 Phosphorylation Regulate the Initiation of Dynein-Driven Transport in Neurons. *Cell Rep.* **2016**, *14*, 2637–2652. [CrossRef] [PubMed]
39. Neukirchen, D.; Bradke, F. Cytoplasmic linker proteins regulate neuronal polarization through microtubule and growth cone dynamics. *J. Neurosci.* **2011**, *31*, 1528–1538. [CrossRef] [PubMed]
40. Barbiero, I.; Peroni, D.; Siniscalchi, P.; Rusconi, L.; Tramarin, M.; De Rosa, R.; Motta, P.; Bianchi, M.; Kilstrup-Nielsen, C. Pregnenolone and pregnenolone-methyl-ether rescue neuronal defects caused by dysfunctional CLIP170 in a neuronal model of CDKL5 Deficiency Disorder. *Neuropharmacology*. under review.
41. Lansbergen, G.; Komarova, Y.; Modesti, M.; Wyman, C.; Hoogenraad, C.C.; Goodson, H.V.; Lemaitre, R.P.; Drechsel, D.N.; van Munster, E.; Gadella, T.W.J.; et al. Conformational changes in CLIP-170 regulate its binding to microtubules and dynactin localization. *J. Cell Biol.* **2004**, *166*, 1003–1014. [CrossRef] [PubMed]
42. Weng, J.-H.; Liang, M.-R.; Chen, C.-H.; Tong, S.-K.; Huang, T.-C.; Lee, S.-P.; Chen, Y.-R.; Chen, C.-T.; Chung, B.-C. Pregnenolone activates CLIP-170 to promote microtubule growth and cell migration. *Nat. Chem. Biol.* **2013**, *9*, 636–642. [CrossRef]
43. Toriyama, M.; Shimada, T.; Kim, K.B.; Mitsuba, M.; Nomura, E.; Katsuta, K.; Sakumura, Y.; Roepstorff, P.; Inagaki, N. Shootin1: A protein involved in the organization of an asymmetric signal for neuronal polarization. *J. Cell Biol.* **2006**, *175*, 147–157. [CrossRef] [PubMed]
44. Kubo, Y.; Baba, K.; Toriyama, M.; Minegishi, T.; Sugiura, T.; Kozawa, S.; Ikeda, K.; Inagaki, N. Shootin1-cortactin interaction mediates signal-force transduction for axon outgrowth. *J. Cell Biol.* **2015**, *210*, 663–676. [CrossRef]

45. Chen, Q.; Zhu, Y.-C.; Yu, J.; Miao, S.; Zheng, J.; Xu, L.; Zhou, Y.; Li, D.; Zhang, C.; Tao, J.; et al. CDKL5, a protein associated with rett syndrome, regulates neuronal morphogenesis via Rac1 signaling. *J. Neurosci.* **2010**, *30*, 12777–12786. [CrossRef] [PubMed]
46. Amendola, E.; Zhan, Y.; Mattucci, C.; Castroflorio, E.; Calcagno, E.; Fuchs, C.; Lonetti, G.; Silingardi, D.; Vyssotski, A.L.; Farley, D.; et al. Mapping pathological phenotypes in a mouse model of CDKL5 disorder. *PLoS ONE* **2014**, *9*, e91613. [CrossRef]
47. Tang, S.; Wang, I.-T.J.; Yue, C.; Takano, H.; Terzic, B.; Pance, K.; Lee, J.Y.; Cui, Y.; Coulter, D.A.; Zhou, Z. Loss of CDKL5 in Glutamatergic Neurons Disrupts Hippocampal Microcircuitry and Leads to Memory Impairment in Mice. *J. Neurosci.* **2017**, *37*, 7420–7437. [CrossRef]
48. Okuda, K.; Takao, K.; Watanabe, A.; Miyakawa, T.; Mizuguchi, M.; Tanaka, T. Comprehensive behavioral analysis of the Cdkl5 knockout mice revealed significant enhancement in anxiety- and fear-related behaviors and impairment in both acquisition and long-term retention of spatial reference memory. *PLoS ONE* **2018**, *13*, e0196587. [CrossRef]
49. Jacquemet, G.; Humphries, M.J. IQGAP1 is a key node within the small GTPase network. *Small GTPases* **2013**, *4*, 199–207. [CrossRef]
50. Swiech, L.; Blazejczyk, M.; Urbanska, M.; Pietruszka, P.; Dortland, B.R.; Malik, A.R.; Wulf, P.S.; Hoogenraad, C.C.; Jaworski, J. CLIP-170 and IQGAP1 cooperatively regulate dendrite morphology. *J. Neurosci.* **2011**, *31*, 4555–4568. [CrossRef]
51. Ramkumar, A.; Jong, B.Y.; Ori-McKenney, K.M. ReMAPping the microtubule landscape: How phosphorylation dictates the activities of microtubule-associated proteins. *Dev. Dyn.* **2018**, *247*, 138–155. [PubMed]
52. Ricciardi, S.; Ungaro, F.; Hambrock, M.; Rademacher, N.; Stefanelli, G.; Brambilla, D.; Sessa, A.; Magagnotti, C.; Bachi, A.; Giarda, E.; et al. CDKL5 ensures excitatory synapse stability by reinforcing NGL-1-PSD95 interaction in the postsynaptic compartment and is impaired in patient iPSC-derived neurons. *Nat. Cell Biol.* **2012**, *14*, 911–923. [CrossRef] [PubMed]
53. Della Sala, G.; Putignano, E.; Chelini, G.; Melani, R.; Calcagno, E.; Michele Ratto, G.; Amendola, E.; Gross, C.T.; Giustetto, M.; Pizzorusso, T. Dendritic Spine Instability in a Mouse Model of CDKL5 Disorder Is Rescued by Insulin-like Growth Factor 1. *Biol. Psychiatry* **2016**, *80*, 302–311. [CrossRef] [PubMed]
54. Lamprecht, R.; LeDoux, J. Structural plasticity and memory. *Nat. Rev. Neurosci.* **2004**, *5*, 45–54. [CrossRef] [PubMed]
55. La Montanara, P.; Rusconi, L.; Locarno, A.; Forti, L.; Barbiero, I.; Tramarin, M.; Chandola, C.; Kilstrup-Nielsen, C.; Landsberger, N. Synaptic synthesis, dephosphorylation, and degradation: A novel paradigm for an activity-dependent neuronal control of CDKL5. *J. Biol. Chem.* **2015**, *290*, 4512–4527. [CrossRef] [PubMed]
56. Zhu, Y.-C.; Li, D.; Wang, L.; Lu, B.; Zheng, J.; Zhao, S.-L.; Zeng, R.; Xiong, Z.-Q. Palmitoylation-dependent CDKL5-PSD-95 interaction regulates synaptic targeting of CDKL5 and dendritic spine development. *Proc. Natl. Acad. Sci. USA* **2013**, *110*, 9118–9123. [CrossRef] [PubMed]
57. Pizzo, R.; Gurgone, A.; Castroflorio, E.; Amendola, E.; Gross, C.; Sassoè-Pognetto, M.; Giustetto, M. Lack of Cdkl5 Disrupts the Organization of Excitatory and Inhibitory Synapses and Parvalbumin Interneurons in the Primary Visual Cortex. *Front. Cell. Neurosci.* **2016**, *10*, 261. [CrossRef]
58. Tramarin, M.; Rusconi, L.; Pizzamiglio, L.; Barbiero, I.; Peroni, D.; Scaramuzza, L.; Guilliams, T.; Cavalla, D.; Antonucci, F.; Kilstrup-Nielsen, C. The antidepressant tianeptine reverts synaptic AMPA receptor defects caused by deficiency of CDKL5. *Hum. Mol. Genet.* **2018**, *27*, 2052–2063. [CrossRef] [PubMed]
59. Ren, E.; Roncacé, V.; Trazzi, S.; Fuchs, C.; Medici, G.; Gennaccaro, L.; Loi, M.; Galvani, G.; Ye, K.; Rimondini, R.; et al. Functional and Structural Impairments in the Perirhinal Cortex of a Mouse Model of CDKL5 Deficiency Disorder Are Rescued by a TrkB Agonist. *Front. Cell. Neurosci.* **2019**, *13*, 169. [CrossRef] [PubMed]
60. Yennawar, M.; White, R.S.; Jensen, F.E. AMPA Receptor Dysregulation and Therapeutic Interventions in a Mouse Model of CDKL5 Deficiency Disorder. *J. Neurosci.* **2019**, *39*, 4814–4828. [CrossRef]
61. Ethell, I.M.; Pasquale, E.B. Molecular mechanisms of dendritic spine development and remodeling. *Prog. Neurobiol.* **2005**, *75*, 161–205. [CrossRef] [PubMed]
62. Hu, X.; Viesselmann, C.; Nam, S.; Merriam, E.; Dent, E.W. Activity-dependent dynamic microtubule invasion of dendritic spines. *J. Neurosci.* **2008**, *28*, 13094–13105. [CrossRef] [PubMed]

63. Gu, J.; Firestein, B.L.; Zheng, J.Q. Microtubules in dendritic spine development. *J. Neurosci.* **2008**, *28*, 12120–12124. [CrossRef] [PubMed]
64. Schätzle, P.; Esteves da Silva, M.; Tas, R.P.; Katrukha, E.A.; Hu, H.Y.; Wierenga, C.J.; Kapitein, L.C.; Hoogenraad, C.C. Activity-Dependent Actin Remodeling at the Base of Dendritic Spines Promotes Microtubule Entry. *Curr. Biol.* **2018**, *28*, 2081–2093. [CrossRef] [PubMed]
65. Pchitskaya, E.; Kraskovskaya, N.; Chernyuk, D.; Popugaeva, E.; Zhang, H.; Vlasova, O.; Bezprozvanny, I. Stim2-Eb3 Association and Morphology of Dendritic Spines in Hippocampal Neurons. *Sci. Rep.* **2017**, *7*, 17625. [CrossRef] [PubMed]
66. Schrick, C.; Fischer, A.; Srivastava, D.P.; Tronson, N.C.; Penzes, P.; Radulovic, J. N-cadherin regulates cytoskeletally associated IQGAP1/ERK signaling and memory formation. *Neuron* **2007**, *55*, 786–798. [CrossRef] [PubMed]
67. Jausoro, I.; Mestres, I.; Quassollo, G.; Masseroni, L.; Heredia, F.; Caceres, A. Regulation of spine density and morphology by IQGAP1 protein domains. *PLoS ONE* **2013**, *8*, e56574. [CrossRef]
68. Gao, C.; Frausto, S.F.; Guedea, A.L.; Tronson, N.C.; Jovasevic, V.; Leaderbrand, K.; Corcoran, K.A.; Guzmán, Y.F.; Swanson, G.T.; Radulovic, J. IQGAP1 regulates NR2A signaling, spine density, and cognitive processes. *J. Neurosci.* **2011**, *31*, 8533–8542. [CrossRef]
69. Nuriya, M.; Oh, S.; Huganir, R.L. Phosphorylation-dependent interactions of alpha-Actinin-1/IQGAP1 with the AMPA receptor subunit GluR4. *J. Neurochem.* **2005**, *95*, 544–552. [CrossRef]
70. Wang, S.-H.J.; Celic, I.; Choi, S.-Y.; Riccomagno, M.; Wang, Q.; Sun, L.O.; Mitchell, S.P.; Vasioukhin, V.; Huganir, R.L.; Kolodkin, A.L. Dlg5 regulates dendritic spine formation and synaptogenesis by controlling subcellular N-cadherin localization. *J. Neurosci.* **2014**, *34*, 12745–12761. [CrossRef]
71. Sandí, M.-J.; Marshall, C.B.; Balan, M.; Coyaud, É.; Zhou, M.; Monson, D.M.; Ishiyama, N.; Chandrakumar, A.A.; La Rose, J.; Couzens, A.L.; et al. MARK3-mediated phosphorylation of ARHGEF2 couples microtubules to the actin cytoskeleton to establish cell polarity. *Sci. Signal.* **2017**, *10*, eaan3286. [CrossRef] [PubMed]
72. McVicker, D.P.; Awe, A.M.; Richters, K.E.; Wilson, R.L.; Cowdrey, D.A.; Hu, X.; Chapman, E.R.; Dent, E.W. Transport of a kinesin-cargo pair along microtubules into dendritic spines undergoing synaptic plasticity. *Nat. Commun.* **2016**, *7*, 12741. [CrossRef] [PubMed]
73. Schatten, H. The mammalian centrosome and its functional significance. *Histochem. Cell Biol.* **2008**, *129*, 667–686. [PubMed]
74. Bettencourt-Dias, M.; Glover, D.M. Centrosome biogenesis and function: Centrosomics brings new understanding. *Nat. Rev. Mol. Cell Biol.* **2007**, *8*, 451–463. [CrossRef] [PubMed]
75. Nigg, E.A.; Raff, J.W. Centrioles, centrosomes, and cilia in health and disease. *Cell* **2009**, *139*, 663–678. [CrossRef]
76. Glotzer, M. Cytokinesis: GAP gap. *Curr. Biol.* **2009**, *19*, R162–R165. [CrossRef]
77. Lim, H.H.; Zhang, T.; Surana, U. Regulation of centrosome separation in yeast and vertebrates: Common threads. *Trends Cell Biol.* **2009**, *19*, 325–333. [CrossRef]
78. Staples, C.J.; Myers, K.N.; Beveridge, R.D.D.; Patil, A.A.; Lee, A.J.X.; Swanton, C.; Howell, M.; Boulton, S.J.; Collis, S.J. The centriolar satellite protein Cep131 is important for genome stability. *J. Cell. Sci.* **2012**, *125*, 4770–4779. [CrossRef]
79. Canning, P.; Park, K.; Gonçalves, J.; Li, C.; Howard, C.J.; Sharpe, T.D.; Holt, L.J.; Pelletier, L.; Bullock, A.N.; Leroux, M.R. CDKL Family Kinases Have Evolved Distinct Structural Features and Ciliary Function. *Cell Rep.* **2018**, *22*, 885–894. [CrossRef] [PubMed]
80. Graser, S.; Stierhof, Y.-D.; Lavoie, S.B.; Gassner, O.S.; Lamla, S.; Le Clech, M.; Nigg, E.A. Cep164, a novel centriole appendage protein required for primary cilium formation. *J. Cell Biol.* **2007**, *179*, 321–330. [CrossRef] [PubMed]
81. Malicki, J.J.; Johnson, C.A. The Cilium: Cellular Antenna and Central Processing Unit. *Trends Cell Biol.* **2017**, *27*, 126–140. [CrossRef] [PubMed]
82. Valente, E.M.; Rosti, R.O.; Gibbs, E.; Gleeson, J.G. Primary cilia in neurodevelopmental disorders. *Nat. Rev. Neurol.* **2014**, *10*, 27–36. [CrossRef]
83. Tam, L.-W.; Ranum, P.T.; Lefebvre, P.A. CDKL5 regulates flagellar length and localizes to the base of the flagella in Chlamydomonas. *Mol. Biol. Cell.* **2013**, *24*, 588–600. [CrossRef] [PubMed]

84. Hector, R.D.; Kalscheuer, V.M.; Hennig, F.; Leonard, H.; Downs, J.; Clarke, A.; Benke, T.A.; Armstrong, J.; Pineda, M.; Bailey, M.E.S.; et al. CDKL5 variants: Improving our understanding of a rare neurologic disorder. *Neurol. Genet.* **2017**, *3*, e200. [CrossRef] [PubMed]
85. Bertani, I.; Rusconi, L.; Bolognese, F.; Forlani, G.; Conca, B.; De Monte, L.; Badaracco, G.; Landsberger, N.; Kilstrup-Nielsen, C. Functional consequences of mutations in CDKL5, an X-linked gene involved in infantile spasms and mental retardation. *J. Biol. Chem.* **2006**, *281*, 32048–32056. [CrossRef]
86. Rusconi, L.; Salvatoni, L.; Giudici, L.; Bertani, I.; Kilstrup-Nielsen, C.; Broccoli, V.; Landsberger, N. CDKL5 expression is modulated during neuronal development and its subcellular distribution is tightly regulated by the C-terminal tail. *J. Biol. Chem.* **2008**, *283*, 30101–30111. [CrossRef] [PubMed]
87. Rosas-Vargas, H.; Bahi-Buisson, N.; Philippe, C.; Nectoux, J.; Girard, B.; N'Guyen Morel, M.A.; Gitiaux, C.; Lazaro, L.; Odent, S.; Jonveaux, P.; et al. Impairment of CDKL5 nuclear localisation as a cause for severe infantile encephalopathy. *J. Med. Genet.* **2008**, *45*, 172–178. [CrossRef]
88. Nectoux, J.; Heron, D.; Tallot, M.; Chelly, J.; Bienvenu, T. Maternal origin of a novel C-terminal truncation mutation in CDKL5 causing a severe atypical form of Rett syndrome. *Clin. Genet.* **2006**, *70*, 29–33. [CrossRef] [PubMed]
89. Russo, S.; Marchi, M.; Cogliati, F.; Bonati, M.T.; Pintaudi, M.; Veneselli, E.; Saletti, V.; Balestrini, M.; Ben-Zeev, B.; Larizza, L. Novel mutations in the CDKL5 gene, predicted effects and associated phenotypes. *Neurogenetics* **2009**, *10*, 241–250. [CrossRef] [PubMed]
90. Wang, I.-T.J.; Allen, M.; Goffin, D.; Zhu, X.; Fairless, A.H.; Brodkin, E.S.; Siegel, S.J.; Marsh, E.D.; Blendy, J.A.; Zhou, Z. Loss of CDKL5 disrupts kinome profile and event-related potentials leading to autistic-like phenotypes in mice. *Proc. Natl. Acad. Sci. USA* **2012**, *109*, 21516–21521. [CrossRef]
91. Tang, S.; Terzic, B.; Wang, I.-T.J.; Sarmiento, N.; Sizov, K.; Cui, Y.; Takano, H.; Marsh, E.D.; Zhou, Z.; Coulter, D.A. Altered NMDAR signaling underlies autistic-like features in mouse models of CDKL5 deficiency disorder. *Nat. Commun.* **2019**, *10*, 2655. [CrossRef] [PubMed]
92. Szafranski, P.; Golla, S.; Jin, W.; Fang, P.; Hixson, P.; Matalon, R.; Kinney, D.; Bock, H.-G.; Craigen, W.; Smith, J.L.; et al. Neurodevelopmental and neurobehavioral characteristics in males and females with CDKL5 duplications. *Eur. J. Hum. Genet.* **2015**, *23*, 915–921. [CrossRef] [PubMed]
93. Marchisella, F.; Coffey, E.T.; Hollos, P. Microtubule and microtubule associated protein anomalies in psychiatric disease. *Cytoskeleton (Hoboken)* **2016**, *73*, 596–611. [CrossRef] [PubMed]
94. Brunden, K.R.; Lee, V.M.-Y.; Smith, A.B.; Trojanowski, J.Q.; Ballatore, C. Altered microtubule dynamics in neurodegenerative disease: Therapeutic potential of microtubule-stabilizing drugs. *Neurobiol. Dis.* **2017**, *105*, 328–335. [CrossRef] [PubMed]
95. Amos, L.A. Microtubule structure and its stabilisation. *Org. Biomol. Chem.* **2004**, *2*, 2153–2160. [CrossRef] [PubMed]
96. Zhang, B.; Maiti, A.; Shively, S.; Lakhani, F.; McDonald-Jones, G.; Bruce, J.; Lee, E.B.; Xie, S.X.; Joyce, S.; Li, C.; et al. Microtubule-binding drugs offset tau sequestration by stabilizing microtubules and reversing fast axonal transport deficits in a tauopathy model. *Proc. Natl. Acad. Sci. USA* **2005**, *102*, 227–231. [CrossRef] [PubMed]
97. Brunden, K.R.; Ballatore, C.; Lee, V.M.-Y.; Smith, A.B.; Trojanowski, J.Q. Brain-penetrant microtubule-stabilizing compounds as potential therapeutic agents for tauopathies. *Biochem. Soc. Trans.* **2012**, *40*, 661–666. [CrossRef] [PubMed]
98. Zhang, B.; Carroll, J.; Trojanowski, J.Q.; Yao, Y.; Iba, M.; Potuzak, J.S.; Hogan, A.-M.L.; Xie, S.X.; Ballatore, C.; Smith, A.B.; et al. The microtubule-stabilizing agent, epothilone D, reduces axonal dysfunction, neurotoxicity, cognitive deficits, and Alzheimer-like pathology in an interventional study with aged tau transgenic mice. *J. Neurosci.* **2012**, *32*, 3601–3611. [CrossRef] [PubMed]
99. Brunden, K.R.; Zhang, B.; Carroll, J.; Yao, Y.; Potuzak, J.S.; Hogan, A.-M.L.; Iba, M.; James, M.J.; Xie, S.X.; Ballatore, C.; et al. Epothilone D improves microtubule density, axonal integrity, and cognition in a transgenic mouse model of tauopathy. *J. Neurosci.* **2010**, *30*, 13861–13866. [CrossRef] [PubMed]
100. Gozes, I. NAP (davunetide) provides functional and structural neuroprotection. *Curr. Pharm. Des.* **2011**, *17*, 1040–1044. [CrossRef] [PubMed]
101. Helsmoortel, C.; Vulto-van Silfhout, A.T.; Coe, B.P.; Vandeweyer, G.; Rooms, L.; van den Ende, J.; Schuurs-Hoeijmakers, J.H.M.; Marcelis, C.L.; Willemsen, M.H.; Vissers, L.E.L.M.; et al. A SWI/SNF-related autism syndrome caused by de novo mutations in ADNP. *Nat. Genet.* **2014**, *46*, 380–384. [CrossRef]

102. Oz, S.; Kapitansky, O.; Ivashco-Pachima, Y.; Malishkevich, A.; Giladi, E.; Skalka, N.; Rosin-Arbesfeld, R.; Mittelman, L.; Segev, O.; Hirsch, J.A.; et al. The NAP motif of activity-dependent neuroprotective protein (ADNP) regulates dendritic spines through microtubule end binding proteins. *Mol. Psychiatry* **2014**, *19*, 1115–1124. [CrossRef]
103. Gozes, I. ADNP Regulates Cognition: A Multitasking Protein. *Front. Neurosci.* **2018**, *12*, 873. [CrossRef]
104. Oz, S.; Ivashko-Pachima, Y.; Gozes, I. The ADNP derived peptide, NAP modulates the tubulin pool: Implication for neurotrophic and neuroprotective activities. *PLoS ONE* **2012**, *7*, e51458.
105. Gozes, I. The cytoskeleton as a drug target for neuroprotection: The case of the autism- mutated ADNP. *Biol. Chem.* **2016**, *397*, 177–184. [CrossRef] [PubMed]
106. Available online: https://www.alzforum.org/ (accessed on 21 July 2019).
107. Javitt, D.C.; Buchanan, R.W.; Keefe, R.S.E.; Kern, R.; McMahon, R.P.; Green, M.F.; Lieberman, J.; Goff, D.C.; Csernansky, J.G.; McEvoy, J.P.; et al. Effect of the neuroprotective peptide davunetide (AL-108) on cognition and functional capacity in schizophrenia. *Schizophr. Res.* **2012**, *136*, 25–31. [CrossRef]
108. Weng, J.-H.; Chung, B.-C. Nongenomic actions of neurosteroid pregnenolone and its metabolites. *Steroids* **2016**, *111*, 54–59. [CrossRef]
109. Flood, J.F.; Morley, J.E.; Roberts, E. Memory-enhancing effects in male mice of pregnenolone and steroids metabolically derived from it. *Proc. Natl. Acad. Sci. USA* **1992**, *89*, 1567–1571. [CrossRef] [PubMed]
110. Brown, E.S.; Park, J.; Marx, C.E.; Hynan, L.S.; Gardner, C.; Davila, D.; Nakamura, A.; Sunderajan, P.; Lo, A.; Holmes, T. A randomized, double-blind, placebo-controlled trial of pregnenolone for bipolar depression. *Neuropsychopharmacology* **2014**, *39*, 2867–2873. [CrossRef]
111. Osuji, I.J.; Vera-Bolaños, E.; Carmody, T.J.; Brown, E.S. Pregnenolone for cognition and mood in dual diagnosis patients. *Psychiatry Res.* **2010**, *178*, 309–312. [CrossRef]
112. Bianchi, M.; Baulieu, E.-E. 3β-Methoxy-pregnenolone (MAP4343) as an innovative therapeutic approach for depressive disorders. *Proc. Natl. Acad. Sci. USA* **2012**, *109*, 1713–1718. [CrossRef] [PubMed]
113. Parésys, L.; Hoffmann, K.; Froger, N.; Bianchi, M.; Villey, I.; Baulieu, E.-E.; Fuchs, E. Effects of the Synthetic Neurosteroid: 3β-Methoxypregnenolone (MAP4343) on Behavioral and Physiological Alterations Provoked by Chronic Psychosocial Stress in Tree Shrews. *Int. J. Neuropsychopharmacol.* **2016**, *19*, pyv119. [CrossRef] [PubMed]

Appendix II

Neuropharmacology 164 (2020) 107897

Contents lists available at ScienceDirect

Neuropharmacology

journal homepage: www.elsevier.com/locate/neuropharm

Pregnenolone and pregnenolone-methyl-ether rescue neuronal defects caused by dysfunctional CLIP170 in a neuronal model of CDKL5 Deficiency Disorder

I. Barbiero[a,1], D. Peroni[a,1], P. Siniscalchi[a], L. Rusconi[a], M. Tramarin[a], R. De Rosa[a], P. Motta[a,2], M. Bianchi[b,c], C. Kilstrup-Nielsen[a,*]

[a] Dept. of Biotechnology and Life Sciences, (DBSV), Center of Neuroscience, University of Insubria, Varese, Italy
[b] Ulysses Neuroscience Ltd., Trinity College Dublin, Dublin, Ireland
[c] Institute of Neuroscience, Trinity College Dublin, Dublin, Ireland

HIGHLIGHTS

- CLIP170 has reduced affinity for microtubule plus-ends in Cdkl5-deficient cells.
- Pregnenolone and pregnenolone-methyl-ether can restore CLIP170 microtubule binding.
- Pregnenolone and pregnenolone-methyl-ether can restore CDKL5-dependent neuronal defects.

ARTICLE INFO

Keywords:
CDKL5
CLIP170
Microtubule dynamics
Pregnenolone
Primary neurons

ABSTRACT

Mutations in the X-linked cyclin-dependent kinase-like 5 (*CDKL5*) gene are responsible for the onset of CDKL5 Deficiency Disorder (CDD), a neurological pathology characterised by severe infantile seizures, intellectual disability, impairment of gross motor skills, sleep and gastrointestinal disturbances. CDKL5 is a serine/threonine kinase the molecular network of which is not yet fully understood. Loss of CDKL5 both *in vitro* and *in vivo* leads to altered neuronal morphology including axon specification and outgrowth, dendritic arborisation and spine morphology suggesting a link between CDKL5 and the regulation of proper cytoskeleton functioning.

Recently, we found that CDKL5 regulates the binding of CLIP170 to microtubules (MT). CLIP170 is a MT-plus end tracking protein (+TIP) that associates with MTs when present in its open, active conformation. Here we present evidence suggesting CLIP170 contributes to neuronal CDKL5-dependent defects and that it represents an important novel druggable target for CDD; indeed, CLIP170 is directly targeted by the neuroactive steroid pregnenolone (PREG), which induces the active conformation of the protein thus promoting MT-dynamics. We here show that PREG and a synthetic derivative pregnenolone-methyl-ether (PME) can restore the MT association of CLIP170 and revert morphological and molecular defects in *Cdkl5*-KO neurons at different stages of maturation. All together, these findings identify CLIP170 as possible novel druggable target for CDKL5 related disorders providing an intriguing prospective for future disease-modifying drug-based therapies.

1. Introduction

CDKL5 Deficiency Disorder (CDD) is an X-linked epileptic encephalopathy caused by mutations in the cyclin-dependent kinase-like 5 (*CDKL5*) gene (Fehr et al., 2013). The onset of treatment-resistant epilepsy in the first three months after birth together with severe motor and cognitive developmental delays, are considered the minimal diagnostic criteria to identify CDD patients. Other common features characterising CDD patients include dyskinesia, gastrointestinal symptoms, and sleep and breathing disturbances. Albeit the epidemiology of CDD is not fully studied, the estimated incidence is one in 40,000 to 60,000 live births, of which 4:1 are females (Olson et al., 2019).

* Corresponding author. DBSV, University of Insubria, Italy.
E-mail address: c.kilstrup-nielsen@uninsubria.it (C. Kilstrup-Nielsen).
[1] These authors corresponded equally to the work.
[2] Present address: Department of Food, Environmental and Nutritional Sciences, University of Milan, Milan, Italy.

https://doi.org/10.1016/j.neuropharm.2019.107897
Received 20 June 2019; Received in revised form 20 November 2019; Accepted 30 November 2019
Available online 30 November 2019
0028-3908/

CDKL5 is a serine/threonine kinase the expression of which is developmentally regulated in the rodent brain. The expression of the protein increases sensibly after birth and reaches highest levels around postnatal day 14, where after it remains relatively constant during the adult stages (Rusconi et al., 2008). These data are mirrored also in primary neuronal cultures where CDKL5 levels correlate with neuronal maturation (Rusconi et al., 2008; Chen et al., 2010). At the cellular level, CDKL5 is present in both the nuclear and cytoplasmic compartments. *In vitro* and *in vivo*, CDKL5 controls neuronal morphology; indeed, its down-regulation impairs axon elongation and neuronal polarisation in primary neurons (Nawaz et al., 2016). Furthermore, CDKL5 cooperates with Rac1 in dendritic arborisation (Chen et al., 2010): cultures of *Cdkl5*-silenced or knock-out (KO) primary neurons reveal a reduction in the extension of the dendritic tree, a phenotype that is also present *in vivo* both in cortical and hippocampal CA1 pyramidal neurons of *Cdkl5*-KO mice (Amendola et al., 2014). Finally, CDKL5 deficiency impacts the stability of mature spines and their functionality, defects that are consistent with a reduced number of $PSD95^{+}$ puncta and expression of the AMPA-R GluA2 subunit (Della Sala et al., 2016; Pizzo et al., 2016; Tramarin et al., 2018; Yennawar et al., 2019).

Current therapies for CDD patients are aimed at relieving certain aspects of the complex symptomatology associated with CDKL5 deficiency such as seizures, but no disease-modifying treatments have been identified so far and the incomplete knowledge of CDKL5 functions still challenges the development of disease-modifying interventions. In such regard, the close relationship between CDKL5 and the regulation of neuronal morphology at different stages of neuronal development suggests a possible novel role of the kinase in the regulation of cytoskeleton dynamics. This hypothesis has recently been supported by independent findings from our and two other laboratories that demonstrated for the first time the participation of CDKL5 in the regulation of microtubule (MT) dynamics through its interaction with MT-associated proteins such as IQGAP1, MAP1S, and EB2 (Baltussen et al., 2018; Barbiero et al., 2017; Muñoz et al., 2018). MT dynamics is the property exhibited by the plus-end of the MTs to alternate periods of prolonged assembly to rapid disassembly and is fundamental for neurodevelopmental processes including formation, maintenance and remodelling of synaptic connections (Conde and Cáceres, 2009). IQGAP1 bridges MTs with the actin meshwork through the formation of a ternary complex with activated Rac1 and the MT plus-end tracking protein (+TIP) CLIP170. The latter regulates MT dynamics acting as a rescue factor, thus facilitating MT growth (Komarova et al., 2002). We previously showed that CDKL5 deficiency interferes with the formation of the IQGAP1/CLIP170/Rac1 ternary complex and negatively influences the MT binding of CLIP170 (Barbiero et al., 2017). These findings allowed us to recognise the neuroactive steroid pregnenolone (PREG) as an innovative candidate drug for CDKL5-related defects. Indeed, CLIP170 acts as an intracellular receptor for PREG that promotes MT dynamics by inducing the active conformation of CLIP170 (Weng et al., 2013). Accordingly, we found that PREG is capable of restoring the MT association of CLIP170 and defects in axonal outgrowth and neuronal polarisation of primary neurons silenced for CDKL5 expression (Barbiero et al., 2017). Although these data suggest the benefit of targeting CLIP170, its precise contribution to neuronal CDKL5-dependent defects still remain unknown. Further, the clinical use of PREG raises some concern due to its further metabolism into other steroids with various effects on neuronal functions (Vallée, 2016). The synthetic PREG derivative, pregnenolone-methyl-ether (PME; also known as 3β-Methoxy-Pregnenolone) has been found capable of improving depressive-like behaviour in animal models and in parallel increasing MT dynamics in specific brain regions (Baulieu, 2018; Bianchi and Baulieu, 2012; Parésys et al., 2016). PME cannot be converted into metabolites with hormonal activities and therefore represents an invaluable alternative to the clinical use of PREG for brain disorders linked to synaptic pathology (Bianchi et al., 2017).

In the current study we analysed the effect of PREG and PME on neuroanatomical defects in primary neuronal *Cdkl5*-KO cultures. Our novel data show that both compounds cause a robust rescue of axon outgrowth, dendritic arborisation and excitatory spine maturation. As PREG, PME promotes the MT-binding of CLIP170 in CDKL5 depleted cells, suggesting that both compounds act by activating CLIP170. MT dynamics in the axonal growth cone are tightly controlled by CLIP170 (Neukirchen and Bradke, 2011). Interestingly, we found that growth cones in *Cdkl5*-KO neurons were characterised by a deranged MT organisation, which was accompanied by an altered distribution of CLIP170. The concomitant reversion of growth cone morphology and the distribution of CLIP170 support the contribution of deranged CLIP170 functions to neuronal CDKL5-dependent defects.

Altogether, the positive effect of PREG and PME on morphological defects in *Cdkl5*-KO neurons and their capacity to ameliorate CLIP170 functions, suggest that CLIP170 constitutes a new druggable target for CDD and that PREG derivatives may possess an important therapeutic potential for this severe pathology.

2. Materials and methods

2.1. Ethical statement

We used the *Cdkl5*-knockout (KO) mice described in Amendola et al. (2014) on the genetic background CD1. Protocols and use of animals were approved by the Animal Ethics Committee of the University of Insubria and in accordance with the guidelines released by the Italian Ministry of Health (D.L. 2014/26) and the European Community directives regulating animal research (2010/63/EU). Adult mice were euthanised by cervical dislocation, while neonates were sacrificed by exposure to CO_2 followed by decapitation.

2.2. Antibodies, reagents and plasmid

The following primary antibodies were used for immunofluorescence and western blotting experiments: anti-CDKL5 (Sigma-Aldrich, HPA002847; Santa Cruz, sc-376314), anti-CLIP170 (Genetex, GTX117504; Santa Cruz H-300, sc-25613), anti-Tau1 (Millipore, MAB3420), rabbit anti-MAP2 (ab32454, Abcam), anti-PSD95 (Thermo Fischer Scientific, MA1045), anti-GluA2 (Millipore, MAB397), anti-α-tubulin (Sigma-Aldrich, T6074), anti-GAPDH (Sigma-Aldrich, G9545), anti-GFP (Roche, 1814460). Phalloidin-TRITC Conjugates (Sigma-Aldrich P1951). HRP-conjugated goat anti-mouse or anti-rabbit secondary antibodies for immunoblotting, DAPI, and secondary Alexa Fluor anti-rabbit and anti-mouse antibodies for immunofluorescence (IF) were purchased from Thermo Scientific. Pregnenolone (PREG) was from Sigma. Pregnenolone-Methyl-Ether (PME) was obtained from Steraloids, Newport, USA. mEmerald-CLIP170-N-18 (plasmid #54044; Addgene).

2.3. Cell cultures, RNA interference (RNAi) and transfections

COS7 cells were maintained in DMEM (Dulbecco's modified Eagle's medium; Sigma-Aldrich) supplemented with 10% FBS (EuroClone), L-glutamine (2 mM, EuroClone), penicillin/streptomycin (100 units/mL and 100 μg/mL respectively, EuroClone) at 37 °C with 5% CO2. For siRNA transfection, cells were cultured in 24-well dishes and 20 nM siRNA oligonucleotides targeting CDKL5, or a control siRNA (siCDKL5 5′GCAGAGTCGGCACAGCTAT3′, siCtrl 5′CGUACGCGGAAUACU UCGATT3′) were transfected using LipofectamineTM RNAiMAX (Life Technologies Incorporated). For plasmid transfection, LipofectamineTM 3000 (Life Technologies Incorporated) was used.

Primary hippocampal cultures were prepared from mouse embryos at embryonic day 17 (E17) considering the day of the vaginal plug as E0. Wild-type (WT) and *Cdkl5*-KO embryos were obtained from pregnant heterozygous females ($Cdkl5^{-/+}$, CD1 background) crossed with

wild-type males. Hippocampi from E17 embryos were dissected and maintained in HBSS (Hank's Balanced Salt Solution, Gibco) on ice till the definition of genotype, obtained with Rapid Extract PCR Kit (PCRBIO, PB10.24–40). The hippocampi were dissected as previously described (Rusconi et al., 2011) and neurons were plated on coverslips coated with poly-L-lysine (1 mg/mL, Sigma-Aldrich) or poly-D-lysine (Neuvitro) in 24-well plates (low-densitiy: 7500 cells/well; high-density: 60000 cells/well). Low-density cultures were used for growth cone morphology, axon length and dendritic arborisation analysis, whereas high-density cultures were used for the quantification of PSD95 puncta and GluA2 expression level). After 3 days *in vitro* (DIV3), cytosine-1-β-D-arabinofuranoside (Sigma-Aldrich) was added to cultured neurons at final concentration of 2 μM to prevent astroglial proliferation.

2.4. Pharmacological treatments

Primary hippocampal neurons were treated at DIV1 for 48 h for growth cone analysis, at DIV1, DIV7 or DIV11 for 72 h for axon, dendritic and spine analysis, respectively. PME was dissolved in DMSO and used at a final concentration of 1 μM (Duchossoy et al., 2011). PREG was dissolved in EtOH and used at a final concentration of 1 μM (Barbiero et al., 2017). DMSO and EtOH were used at a final concentration of 0.1% and 0.0032% respectively. Two different vehicles were used for PREG and PME in order to be in line with previous studies and to avoid inclusion of an important additional variable in the current study.

2.5. Western blotting

Primary neurons were lysed directly in Laemmli buffer (120 mM Tris-HCl pH 6.8, 4% SDS, 20% Glycerol (Sigma-Aldrich), 0.02% Bromophenol blue) and a volume corresponding to approximately 10 μg of proteins was separated by 8–10% SDS-PAGE.

COS7 cells were lysed with lysis buffer (50 mM Tris-HCl pH 7.5, 150 mM NaCl, 1% Triton X-100, 1 mM EDTA, protease inhibitor cocktail (Sigma Aldrich) and PhosSTOP (Roche)). After 30 min on ice, the lysates were clarified by centrifugation and the supernatants collected. Protein concentrations were quantified by Bradford assay; 1 μg (for α-tubulin and GAPDH) or 30 μg of proteins (for CDKL5 and CLIP170) were separated by 10% SDS-PAGE, transferred to nitrocellulose membranes, and blocked in 5% non-fat milk in TBS (20 mM Tris-HCl, pH 7.5, 150 mM NaCl) with 0.2% Tween-20 (T-TBS). Blots were incubated with primary antibodies overnight at 4 °C, washed in T-TBS, and incubated with appropriate secondary antibody for 1 h at room temperature. After extensive washes blots were developed with Protein Detection System-ECL (Genespin).

2.6. Immunofluorescence

After fixation in 4% paraformaldehyde (Thermo Fischer) with 4% sucrose (Sigma-Aldrich) neurons were blocked in PBS (EuroClone) containing 5% horse serum and 0.2% Triton X-100 (Sigma-Aldrich) before incubation with the appropriate primary antibody overnight at 4 °C and subsequently with the secondary antibody for 1 h at room temperature. Slides were mounted with ProLong Gold antifade reagent (Life Technologies).

2.7. Measurement of comet length and lifetime

For time-lapse imaging COS7 cells were transfected with the indicated siRNAs (siCDKL5 and siCTRL) and 60 h later with pGFP-CLIP170; microscopy analysis was performed after another 24 h. Pharmacological treatment was performed incubating cells with 1 μM PME or with 0.1% DMSO (Sigma-Aldrich) as vehicle control for three days (starting treatment 24 h after siRNA transfection). Fluorescence in the specimens was imaged every 3 s for 3 min with a confocal laser-scanning microscope (model TCS SP8; Leica) with a 63X NA 1.2 oil immersion objective (Leica). Comet length and life-time were analysed using the tracking function of the MTrackJ plug-in of ImageJ software.

2.8. Neuronal analyses

2.8.1. Growth cone analyses

To calculate the growth cone area, a fixed area of 18 × 18 μm^2 starting from the most distal MT tip towards the axon shaft was outlined manually. The MT area was then quantified using the α-tubulin stained region within the selected area. To analyse the localisation of CLIP170 at the growth cone site, a fixed area of 25 × 25 μm^2 starting from the edge of actin cytoskeleton towards the axon shaft was outlined manually. The ratio of CLIP170 versus α-tubulin was determined from fluorescence areas of both channels; the fold change value was used as measure of CLIP170 distribution. Growth cone morphology was analysed by staining with α-tubulin. Growth cones were classified as "extending" or "paused": growing growth cones characterised by straight bundles of MTs projecting outward into actin lamellipodium were considered as "extending"; whereas, large growth cones with MTs organised in the central region as a prominent loop were considered as "paused" (Dent and Kalil, 2001).

2.8.2. Analysis of neuronal polarisation and axon length

Neuronal polarisation was analysed at DIV4 by staining with the axonal marker Tau1. Neurites with a significant intensity of Tau1 staining increasing along the proximal to distal axis were counted as axons. Neurons were classified as polarised (one axon) or non-polarised (either lacking an axon or with multiple axons). Axon length was analysed with ImageJ using the NeuronJ plugin to compute the path from the beginning to the end of the axon.

2.8.3. Analysis of dendritic arborisation (Sholl analysis)

Acquired images of MAP2 stained neurons, specifically identifying dendrites, were analysed thanks to the "Sholl Analysis" plugin of the FiJi software (htpp://Fiji.sc). The number of processes intersecting each ring was provided by the software. The elaboration of these data allowed generating a cumulative curve of the number of intersections per cell, indicative of the branching complexity.

2.8.4. Analysis of PSD95 puncta

PSD95 puncta were analysed at DIV14 by staining with antibody against the postsynaptic density protein 95 (PSD95) and MAP2 to visualise spines along neuronal dendrites. The number of PSD95 puncta was measured along 30 μm long dendrite segments (proximal part of secondary branches) and analysed using the software ImageJ (function: Analyse particles).

2.9. Data analyses

Data quantification were analysed with Prism software (GraphPad) and were expressed as mean ± SEM. The significance of results was evaluated by Student's t-test, ANOVA (one or two-way) followed by Tuckey's or Dunnet's multiple comparison test when appropriate. The level of statistical significance was set at $p < 0.05$.

3. Results

3.1. Effect of PREG and PME on axonal defects and dendritic arborisation in Cdkl5-KO neurons

We recently showed that PREG was capable of restoring axonal defects caused by the silencing of CDKL5 in primary cultures of murine hippocampal neurons (Barbiero et al., 2017). Considering the properties of the synthetic PREG derivative PME described above we found it challenging to analyse whether it might possess an analogous effect on

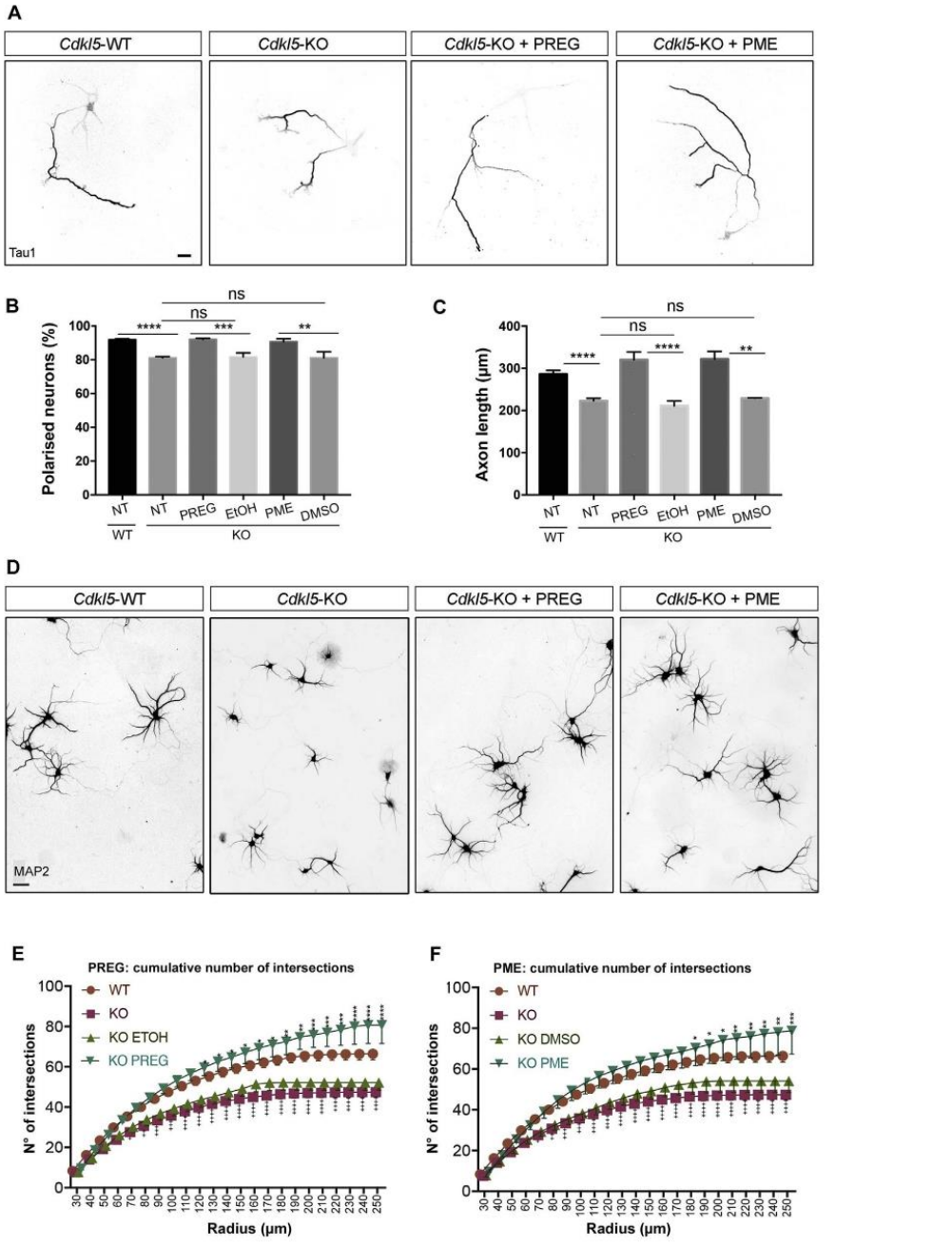

(caption on next page)

axonal defects in primary hippocampal neurons obtained from *Cdkl5*-KO embryos. Thus, in line with Barbiero et al. (2017), we treated *Cdkl5*-WT and KO primary hippocampal neurons at DIV1 with 1 µM PREG or PME (or the respective vehicles 0.0032% EtOH and 0.1% DMSO) for 72 h and then analysed axon outgrowth and polarisation by staining neurons at DIV4 with the axonal marker Tau1 (Fig. 1A). Correctly polarised neurons were recognised as those bearing a single axon with a strong distal staining for Tau1, whereas neurons with no axon or multiple axons were classified as non-polarised. *Cdkl5*-KO neurons, like those silenced for CDKL5, display defective neuronal polarisation.

Fig. 1. Effect of treatment with PREG or PME on axonal and dendritic defects in *Cdkl5*-KO neurons. (A) Representative images of WT and *Cdkl5*-KO hippocampal neurons (DIV4) stained with the axonal marker Tau1. Neurons were left untreated or were treated with 1 μM PREG or PME for 72 h. EtOH (0.0032%) was used as vehicle for PREG and DMSO (0.1%) for PME. Scale bar: 20 μm. (B,C) Graphs showing the mean percentage of polarised primary hippocampal neurons (B) and the mean axonal length (C) of neurons treated as in A. Data are presented as mean ± SEM. ****P < 0.0001; ***P < 0.001; **P < 0.01, OneWay-ANOVA followed by Tukey's *post-hoc* analysis. At least 15 neurons/mouse (n ≥ 3 mice/group) were analysed for each condition from n ≥ 3 independent neuronal preparations. (D) Representative images of WT and *Cdkl5*-KO hippocampal neurons (DIV10) stained with the dendritic marker MAP2. Neurons were treated with 1 μM PREG or PME for 72 h using the respective vehicles as control. Scale bar: 50 μm. (E) Graphs showing the cumulative number of intersections of neurons treated with PREG. (F) Graphs showing the cumulative number of intersections of neurons treated with PME. Significant differences between the drug and the respective vehicle control are indicated (*). Significant differences between untreated WT and KO neurons are shown in both E and F (+). Data are presented as mean ± SEM. ****P < 0.0001; ***P < 0.001; **P < 0.01; *P < 0.05, TwoWay-ANOVA followed by Tukey's *post-hoc* analysis. At least 10 neurons/mouse (n ≥ 3 mice/group) were analysed for each condition from n ≥ 3 independent neuronal preparations.

Interestingly, this defect was fully restored upon treatment with PREG or PME for 72 h (Fig. 1A and B). Indeed, the percentage of polarised *Cdkl5*-KO neurons treated with PREG or PME was similar to WT neurons (WT NT: 91.98% ± 0.47; KO NT: 81.24% ± 0.66; KO PREG: 92.12% ± 0.7; KO EtOH: 81.75% ± 2.39; KO PME: 90.67% ± 1.83; KO DMSO: 81.21% ± 3.55). Similarly, both PREG and PME were capable of normalising axon length (Fig. 1C; WT NT: 286.2 μm ± 9.13; KO NT: 222.9 μm ± 6.03, KO PREG: 320.2 μm ± 18.56; KO EtOH: 210.9 μm ± 11.58; KO PME: 321.9 μm ± 18.23; KO DMSO: 228.7 μm ± 0.95). All together, these results highlight the positive effect of PREG and PME on axonal defects caused by CDKL5 deficiency.

We proceeded testing the effect of PREG and PME on dendritic arborisation that is controlled by CDKL5 both *in vitro* and *in vivo* (Amendola et al., 2014; Chen et al., 2010). *Cdkl5*-WT and KO hippocampal neurons were, therefore, treated with PREG and PME for 72 h starting from DIV7 and dendritic branching was analysed at DIV10. Neurons were stained with the dendritic marker MAP2 and, as shown in Fig. 1D, MAP2-stained *Cdkl5*-KO neurons had a severely stunted appearance displaying a less complex dendritic arbour than WT neurons. The Sholl analysis confirmed this and revealed that the cumulative number of intersections, which is a measure of dendritic tree complexity, was significantly reduced in *Cdkl5*-KO neurons (Fig. 1E and F; Cumulative number of intersections at 250 μm: WT 66,42 ± 2,97; KO 47,45 ± 2,47). Furthermore, also the cumulative dendritic length was reduced in *Cdkl5*-KO neurons (Supplementary Fig. 1). Interestingly, the treatment with PREG (Fig. 1E) or PME (Fig. 1F) was capable of increasing the overall number of intersections and dendritic length of *Cdkl5*-KO neurons with respect to the vehicle controls, indicating a significant improvement of dendritic arborisation (Fig. 1E and F and Supplementary Fig. 1; Cumulative number of intersections at 250 μm: KO EtOH 52.2 ± 3.87; KO PREG 80.73 ± 9.19; KO DMSO 54.1 ± 5.67; KO PME 78.8 ± 11.479).

3.2. Treatment with PREG or PME normalises the density of PSD95+ clusters in Cdkl5-KO neurons

Loss of CDKL5 is widely accepted to impair the stability of excitatory spines *in vivo* and *in vitro,* which is reflected in a reduced number of PSD95+ puncta (Della Sala et al., 2016; Ricciardi et al., 2012; Tramarin et al., 2018). Considering that the invasion of MTs into dendritic spines is known to facilitate the delivery of postsynaptic proteins and promote spine maturation (Franker and Hoogenraad, 2013), we speculated whether PREG and PME might be capable of rescuing CDKL5-related excitatory synapse defects. We thus treated *Cdkl5*-WT and KO hippocampal neurons with PREG and PME at DIV11 and stained them at DIV14 with antibodies against PSD95 and MAP2 to identify excitatory spines and the dendritic shafts, respectively (Fig. 2A). As shown in Fig. 2B, the quantification of PSD95+ clusters along dendritic segments revealed a clear effect of PREG and PME on dendritic spine maturation in *Cdkl5*-KO neurons. Indeed, with both drugs we observed a significant increase of PSD95+ puncta compared to vehicle-treated KO neurons (Fig. 2B: WT NT: 1 ± 0.04; KO NT: 0.73 ± 0.03; KO PREG: 0.94 ± 0.04; KO EtOH: 0.74 ± 0.04; KO PME: 0.92 ± 0.03; KO DMSO: 0.73 ± 0.03). In concomitance with the normalisation of PSD95+ puncta we also observed restoration of AMPA-R subunit GluA2 levels (Fig. 2C–F) upon treatment with PME (WT DMSO: 1 ± 0; KO DMSO: 0.5 ± 0.00; KO PREG: 0.78 ± 0.14) and PREG (WT EtOH: 1 ± 0; KO EtOH: 0.75 ± 0.04; KO PREG: 0.93 ± 0.08).

3.3. PME enhances the binding of GFP–CLIP170 to microtubules in CDKL5-deficient cells

In accordance with the known capacity of PREG to induce the open active conformation of CLIP170 (Weng et al., 2013), we recently demonstrated that PREG normalises the binding of exogenous CLIP170 to MTs in CDKL5-depleted COS7 cells (Barbiero et al., 2017). Indeed, time-lapse microscopy of GFP-tagged CLIP170 allows visualising the accumulation of the +TIP at the plus-ends as comet-like structures, the dynamics of which is indicative of the association of the protein with the MTs (Dragestein et al., 2008; Perez et al., 1999). To test whether PME might exert an analogous effect on CLIP170 functioning we treated CDKL5-silenced COS7 cells expressing GFP–CLIP170 with 1 μM PME and analysed the fluorescent signal of the exogenously expressed protein through time-lapse microscopy (Fig. 3A and B). As shown in Fig. 3B, GFP-CLIP170 accumulates at the plus-end of growing MTs forming comet-like structures. As expected, the absence of CDKL5 had a negative effect on the length and lifetime of GFP-CLIP170 comets (Fig. 3B–D), which is indicative of the dissociation of the protein from MTs (Perez et al., 1999). Intriguingly, we found that the treatment of siCDKL5 cells with PME produced an increase in the length (Fig. 3C siCtr: 3.7 μm ± 0.12; siCDKL5: 1.2 μm ± 0.09; siCDKL5 DMSO: 1.9 μm ± 0.12; siCDKL5 PME: 3.3 μm ± 0.17) and the lifetime (Fig. 3C siCtr: 24.3 s ± 1.0; siCDKL5: 10.3 s ± 0.7; siCDKL5 DMSO: 12.5 s ± 0.73; siCDKL5 PME: 22.84 s ± 1.2) of GFP–CLIP170 positive comets. This result indicates that PME, like PREG, is capable of promoting MT-dynamics by acting directly on CLIP170.

3.4. CDKL5 regulates CLIP170 localisation and microtubule organisation in axonal growth cones

In the light of the above data, some CDKL5-dependent neuronal defects may at least in part be caused by an impairment of the activity of CLIP170. Neuronal CLIP170 functions have mainly been addressed in axonal growth cones where the expression of a hypo-functional CLIP170 derivative, which is deficient in MT-binding, was reported to alter MT-dynamics and impair axon formation (Neukirchen and Bradke, 2011). Thus, to elucidate how CDKL5 deficiency impacts CLIP170 functioning in neurons, we decided to use the axonal growth cone of young neurons (DIV3) as model. We therefore compared the localisation of CLIP170 in the axonal growth cone of *Cdkl5*-WT and KO hippocampal neurons that were stained with antibodies against CLIP170 together with α-tubulin and phalloidin to visualise the entire growth cone area (Fig. 4A). Interestingly, whereas the area occupied by CLIP170 in the majority of *Cdkl5*-WT neurons corresponded largely to that of α-tubulin, in *Cdkl5*-KO neurons CLIP170 covered a significantly larger area than that of tubulin and could be detected in the entire growth cone area including the peripheral phalloidin-positive region.

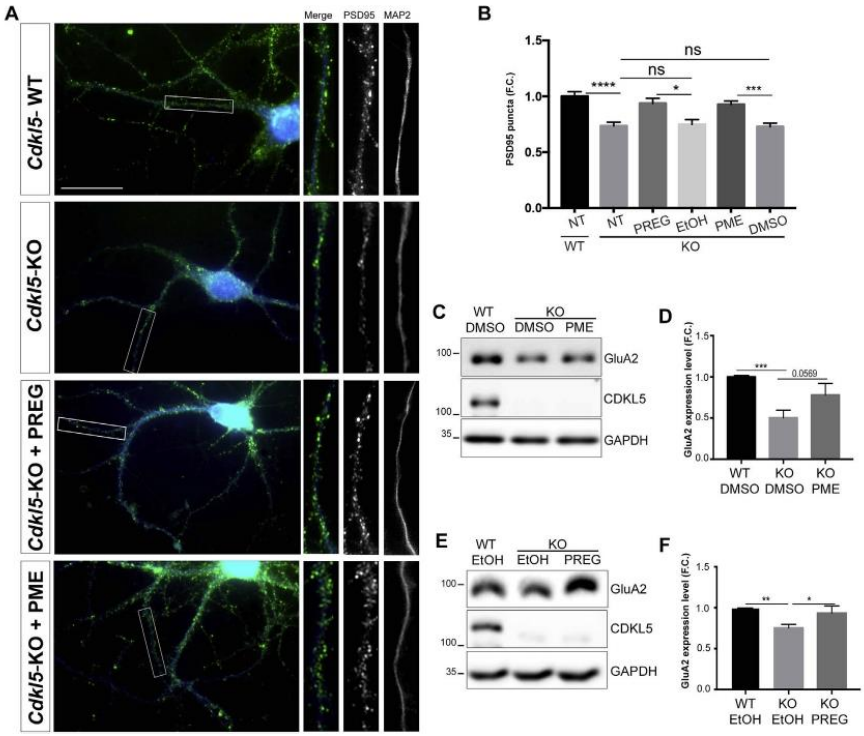

Fig. 2. Effect of treatment with PREG or PME on the density of PSD95$^+$ clusters in *Cdkl5*-KO neurons. (A) Representative images of WT and *Cdkl5*-KO hippocampal neurons stained at DIV15 for the postsynaptic density protein 95 (PSD95) and MAP2 to visualise spines and neuronal dendrites, respectively. Neurons were left untreated or were treated with 1 μM PREG or PME for 72 h. EtOH (0.0032%) and DMSO (0.1%) were used as vehicle for PREG and PME, respectively. Scale bar: 30 μm. (B) The graph shows the number of PSD95$^+$ puncta (expressed as fold change with respect to untreated WT neurons) per 30 μm (proximal part of secondary branches). Data are presented as mean ± SEM. ****P < 0.0001; ***P < 0.001; *P < 0.05), OneWay-ANOVA followed by Tukey's *post-hoc* analysis. At least 10 neurons/mouse (n ≥ 3 mice/group) were analysed for each condition from n ≥ 3 independent neuronal preparations. (C, E) Representative WBs showing GluA2 levels in *Cdkl5*-WT and KO neurons (DIV14) treated as indicated with 1 μM PME (C) or PREG (E) for 72 h using as control the respective vehicle controls. (D, F) Graphs showing the quantification of GluA2 levels in neurons treated as in C and E, expressed as fold change (F.C.) with respect to WT neurons. Data are presented as mean ± SEM. OneWay-ANOVA followed by Dunnet's *post-hoc* analysis. n ≥ 5 from at least 3 independent neuronal preparations.

Accordingly, the ratio of the areas occupied by CLIP170 and actin was significantly increased in growth cones of *Cdkl5*-KO neurons (Fig. 4B; CLIP170/tubulin ratio: WT: 1.1 ± 0.09; KO: 1.65 ± 0.15). Loss of CDKL5 thus leads to an altered distribution of CLIP170 within the axonal growth cones. As indicated in the WB and the graph in Fig. 4C and D, overall CLIP170 levels were unaltered between WT and KO neurons, indicating that the delocalisation is due to intrinsic properties of the protein. In line with the above data, showing that PREG and PME promote the association of GFP-tagged CLIP170 with MTs, the CLIP170/α-tubulin ratio was restored in *Cdkl5*-KO neurons treated with either of the two drugs (Fig. 4A and B). Indeed, the CLIP170/α-tubulin ratio decreased from 1.51 ± 0.07 and 1.4 ± 0.11 in vehicle treated *Cdkl5*-KO control neurons (EtOH and DMSO, respectively) to 1.04 ± 0.05 in PREG-treated and to 0,98 ± 0.04 in PME-treated *Cdkl5*-KO neurons.

A closer examination of the distribution of MTs in the axonal growth cones in *Cdkl5*-WT and KO neurons revealed, as shown in the representative image in Fig. 4E, that MTs in the absence of CDKL5 were characterised by markedly looped structures that occupied a significantly larger area. When calculating the area occupied by α-tubulin within a fixed area of the growth cones we found that the α-tubulin positive area of *Cdkl5*-KO neurons was significantly increased from 41.75 μm^2 ± 2.15, in control cells, to 71.26 μm^2 ± 1.91, corresponding to a 1.71-fold increase (Fig. 4F). Growth cone size inversely correlates with axonal growth rate and the looped MT organisation can typically be observed in paused growth cones (Dent and Kalil, 2001; Ren and Suter, 2016). The increased number of *Cdkl5*-KO neurons presenting the paused growth cones (WT: 8% ± 4.9; KO: 37.33% ± 6.36) is thus in accordance with the reduced axonal length described above. Both PREG and PME had a positive effect on growth cone phenotypes. PREG reduced the area occupied by MTs at the tip of the axon from 67.53 μm^2 ± 5.52 in vehicle (EtOH) treated *Cdkl5*-KO neurons to 38.92 μm^2 ± 2.28 and decreased the number of paused growth cones (KO EtOH: 36% ± 7.48; KO PREG 13.6% ± 2.6). A similar effect was observed with PME (α-tubulin area: KO DMSO: 65.24 μm^2 ± 3.65; KO PME: 37.31 μm^2 ± 2.38; paused growth cones: KO DMSO: 40.0% ± 5.77; KO PME: 12.28% ± 4.83).

All together, these results suggest that PREG and PME, acting on MT dynamics possibly via CLIP170, ameliorate the organisation of MTs and restore morphological defects associated with the loss of CDKL5.

4. Discussion

Several reports have recently suggested an important link between CDKL5 and the control of MT dynamics (Barbiero et al., 2019). In this regard, we recently showed that the +TIP CLIP170 participates in a

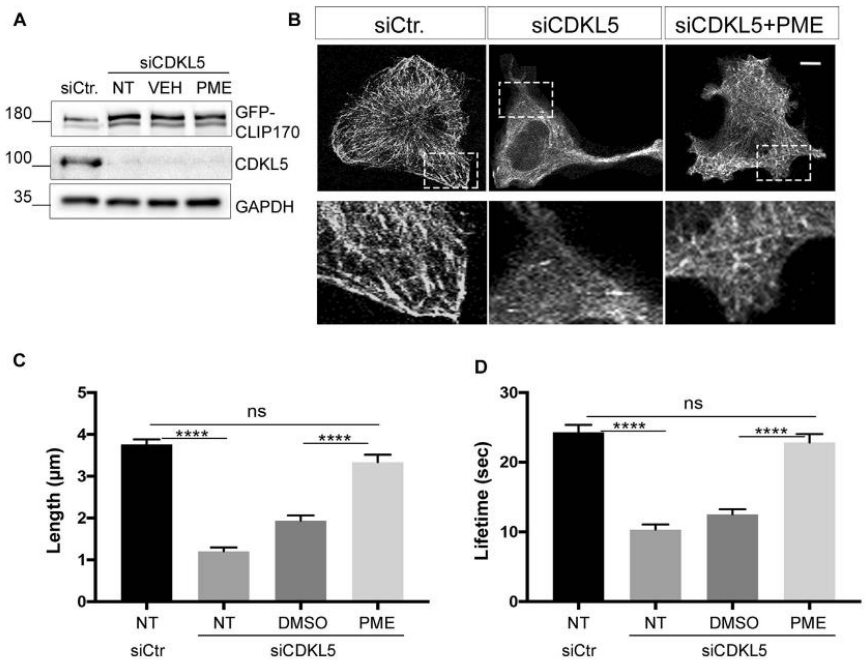

Fig. 3. PME enhances the binding of GFP–CLIP170 to microtubules in CDKL5-deficient cells. (A) COS7 cells were silenced with siCDKL5 or siCtr and transfected with an EGFP-CLIP170 expression vector. PME (1 µM) or its vehicle (0.1% DMSO) was added for 72 h. CDKL5 silencing was verified by WB analysis using GAPDH as loading control. (B) Representative images of COS7 cells treated as in A. Boxed areas are magnified underneath. Scale bar: 10 µm. (C–D) Graphs showing the length and the lifetime of EGFP-CLIP170 comet-like structures in cells treated as in A. EGFP-CLIP170 comets were recorded by time-lapse imaging; at least $n \geq 37$ comets from $n \geq 5$ cells were analysed for each condition. Data are presented as mean ± SEM. ****$P < 0.0001$, OneWay-ANOVA followed by Tukey's *post-hoc* analysis.

protein complex with CDKL5 (Barbiero et al., 2017) and that its affinity for MTs is reduced in the absence of CDKL5. The capacity of CLIP170 to bind MTs depends on its specific conformation: the interaction between the N-terminal CAP-Gly domains with the C-terminal zinc-knuckle motifs generates a closed conformation that reduces the affinity of CLIP170 for MTs (Lansbergen et al., 2004; Mishima et al., 2007). The neuroactive steroid PREG has been shown to activate CLIP170 by directly binding the protein and inducing its open active conformation (Weng et al., 2013). We previously demonstrated that the sub-chronic treatment with PREG was capable of enhancing defective MT-binding of CLIP170 in COS7 cells and to correct axonal alterations in primary mouse hippocampal neurons silenced for CDKL5 (Barbiero et al., 2017). Here, we expand these studies showing that: i) PREG is capable of causing a significant rescue of neuroanatomical and molecular defects in *Cdkl5*-KO neurons; ii) the synthetic PREG-derivative PME produces identical effects; and that iii) PREG and PME promotes CLIP170 functioning altogether, highlighting this + TIP as a putative target for drug-based therapies for CDD.

4.1. Possible contribution of CLIP170 to neuronal CDKL5-dependent defects

Loss of CDKL5 leads to altered neuronal morphology including reduced axon growth, dendritic arborisation and altered dendritic spine morphology. Here we show that the treatment of primary cultures of *Cdkl5*-KO neurons with PREG or PME normalises these defects. Considering that both drugs also restore the binding of CLIP170 to MTs we speculate that some CDKL5-dependent neuronal defects may be caused by the presence of a hypofunctional CLIP170.

Down-regulation of CLIP170 as well as its hypofunctionality has already been associated with aberrant axon formation and dendritic arborisation (Neukirchen and Bradke, 2011; Swiech et al., 2011). CLIP170 is enriched in axonal growth cones, where it promotes a moderate stabilisation of MTs that protrude into the actin-rich leading edge and creates a pushing force, which enables axon outgrowth (Neukirchen and Bradke, 2011; Van De Willige et al., 2016). Interference with the binding of endogenous CLIP170 to MTs through the expression of a dominant negative derivative in neurons led to impairment of axon outgrowth and an altered growth cone morphology (Weng et al., 2013). Here we demonstrate that *Cdkl5*-KO neurons display an altered growth cone morphology characterised by looped MTs and an overall increase in the growth cone area occupied by tubulin, usually coincident with reduced MT dynamics and paused growth cones (Dent and Kalil, 2001; Ren and Suter, 2016). All those axonal defects are similar to the ones caused by impaired binding of CLIP170 to MTs (Neukirchen and Bradke, 2011). Consistently, we also demonstrated that the relative distribution of CLIP170 with respect to tubulin is altered in growth cones of *Cdkl5*-KO neurons, supporting the data from COS7 cells where silencing of CDKL5 clearly reduces the affinity of CLIP170 for MTs. We therefore hypothesise that CDKL5 deficiency impacts the binding of CLIP170 to MTs, thus weakening their stabilisation and preventing their engorgement into the area protruded by actin filaments at the tip of the axon (Neukirchen and Bradke, 2011). We previously showed that CDKL5 modulates axon outgrowth and polarisation through its interaction with Shootin1 (Nawaz et al., 2016). Considering our present data, CDKL5 is thus likely to influence axon formation both through a CLIP170-dependent effect on MT-dynamics and through Shootin1, which acts as a clutch molecule that produces a traction force for axon outgrowth by coupling the retrograde flow of F-actin and cell adhesions (Kubo et al., 2015).

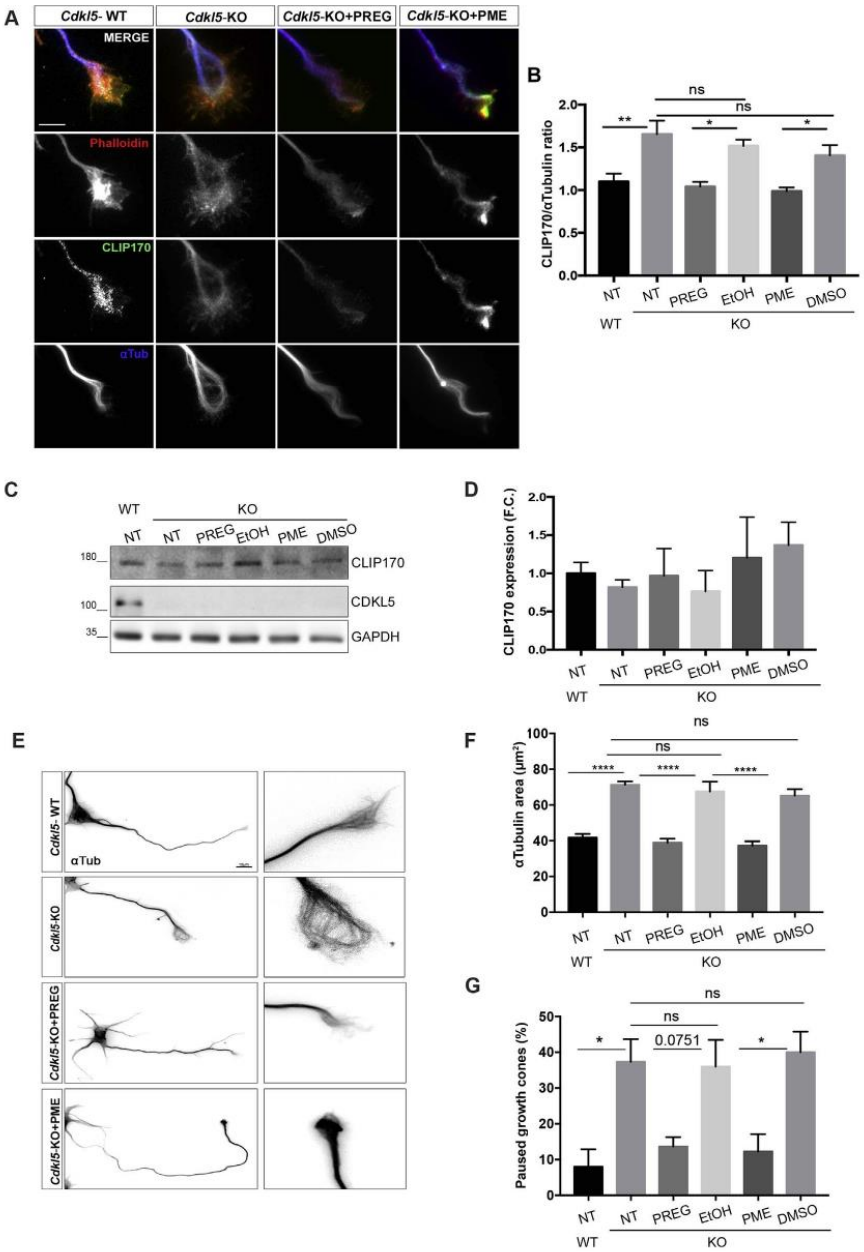

Fig. 4. CDKL5 regulates CLIP170 localisation and microtubule organisation in axonal growth cones. (A) Representative images of growth cones of WT and *Cdkl5*-KO hippocampal neurons (DIV3) stained for phalloidin (red), α-tubulin (blue) and CLIP170 (green) to visualise actin, MTs and CLIP170, respectively. Neurons were treated with 1 μM PREG or PME or with the respective vehicles EtOH (0.0032%) and DMSO (0.1%) for 48 h. Scale bar: 5 μm. (B) Graph showing the mean CLIP170/α-tubulin ratio in growth cones quantified as described in Materials and Methods. Data are presented as mean ± SEM. **P < 0.01, *P < 0.05, Student's t-test. At least 40 neurons/mouse (n ≥ 3 mice/group) were analysed for each genotype from n ≥ 3 independent neuronal preparations. (C) Representative WB showing CLIP170 levels in WT and *Cdkl5*-KO neurons (DIV4) treated as in A. (D) Graph showing the quantification CLIP170 levels in *Cdkl5*-KO neurons expressed as fold change (F.C.) of WT neurons. Data are presented as mean ± SEM, OneWay-ANOVA followed by Tukey's *post-hoc* analysis. (E) Representative images of WT and *Cdkl5*-KO hippocampal neurons (DIV3) treated as in A and stained for α-tubulin. The panels to the right show the magnified growth cones. Scale bar: 5 μm. (F) Graph showing the mean area occupied by α-tubulin in growth cones quantified as described in Materials and Methods. (G) Graph showing the mean percentage of paused growth cones. Data in F and G are presented as mean ± SEM. ****P < 0.0001; *P < 0.05, OneWay-ANOVA followed by Tukey's *post-hoc* analysis. At least 10 neurons/mouse (n ≥ 3 mice/group) were analysed for each condition from n ≥ 3 independent neuronal preparations.

Concerning dendritic arborisation, CLIP170 depletion causes a reduction in the complexity of the dendritic arbour. Interestingly, CLIP170 was shown to regulate dendritic arborisation through its interaction with IQGAP1 (Swiech et al., 2011). We recently showed that the interaction between CLIP170 and IQGAP1 is compromised in cells silenced for CDKL5 suggesting that CDKL5 may regulate dendritic arborisation through its effect on this complex.

In regard to dendritic spine maturation, both PREG and PME were capable of restoring the number of $PSD95^+$ puncta of *Cdkl5*-KO neurons implying that CLIP170 may contribute to this process under normal conditions. A role of CLIP170 in dendritic spine maturation has never been reported but the entry of dynamic MTs into dendritic spines during plasticity has been shown to rely on + TIPs (Dent, 2017). Indeed, the invasion of EB3-bound MTs into dendritic spines was found to contribute to activity-dependent spine enlargement (Gu et al., 2008; Jaworski et al., 2009). Of relevance, a truncating mutation in *CLIP1*, the human CLIP170 ortholog, was found to segregate with a mild form of intellectual disability (Larti et al., 2015), supporting the possible role of this + TIP in regulating spine functioning and synaptic activity. In this study we found that the two neuroactive steroids had a positive effect not only on the number of $PSD95^+$ puncta but also on overall GluA2 levels in *Cdkl5*-KO neurons. AMPA-Rs undergo constitutive recycling to and from the postsynaptic sites depending on endosomal trafficking; MT-dependent trafficking is involved in the delivery of AMPA-Rs into the dendrites and their further transport to the postsynaptic sites whereas internalised AMPA-Rs may undergo lysosomal degradation (Anggono and Huganir, 2012). PREG and PME may thus affect GluA2 levels by promoting their MT-based transport towards the postsynaptic sites.

Even if our data support a contribution of CLIP170 to some CDKL5-dependent neuronal defects, it is worth recalling that both PREG (Murakami et al., 2000) and PME (Fontaine-Lenoir et al., 2006) have been demonstrated to interact *in vitro* with the MT-associated protein 2 (MAP2). *In vitro* PME stimulates MT polymerisation and enhances neurite outgrowth in PC12 cells an effect, which is prevented if MAP2 expression is decreased by RNA interference (Fontaine-Lenoir et al., 2006). In neurons, MAP2 is mainly expressed in the cell bodies and dendrites where it modulates MT assembly and dynamics (Fontaine-Lenoir et al., 2006). It can, therefore, not be excluded that the modulation of neuronal morphology by PREG and PME observed in the present study can also be attributed to their interaction with MAP2.

As mentioned, the capacity of CLIP170 to bind MTs depends on its open conformation (Lansbergen et al., 2004; Mishima et al., 2007). Of note, the switching between the open and closed conformations of CLIP170 has been reported to depend on specific phosphorylation events. Indeed, the phosphorylation of several residues within a serine rich region in the N-terminus of CLIP170 was found to promote the intramolecular interaction inducing the closed conformation (Lee et al., 2010; Nirschl et al., 2016). On the other hand, phosphorylation mediated by FKBP12-rapamycin-associated protein was found to promote MT-binding (Choi et al., 2002). Altogether it appears that the phosphorylation of CLIP170 controls its binding to MTs in a complex and not yet fully understood manner. Thus, we cannot exclude that specific phosphorylation events of CLIP170 may be regulated directly or indirectly by CDKL5, thus promoting, the open active conformation of CLIP170. Through ongoing studies that will be published in the near future we are currently analysing how loss CDKL5 impacts the conformational status of CLIP170.

4.2. Therapeutic potential of PREG and PME for targeting of MT-defects in CDD

PREG is generated from cholesterol in the peripheral glands and in the brain and can be further metabolised into various other neuroactive steroids (Vallée, 2016). While PREG for long was considered just the precursor of other steroids, it is now believed to be involved in the regulation of neuronal activity. Indeed, diminished brain levels of PREG have been associated with aging of the brain and with different brain disorders associated with synaptic pathology such as psychiatric and neurodegenerative disorders (Luchetti et al., 2011; Schverer et al., 2018; Vallée et al., 2001). Moreover, administration of PREG was found to enhance memory and cognition in rodents (Flood et al., 1992).

In humans, clinical testing of PREG indicates potential antidepressive and antipsychotic effects and the drug has been well tolerated in these trials (Brown et al., 2014; Osuji et al., 2010). However, the possible side effects of the downstream metabolites raise some concern of the pharmacological use of PREG. Available data demonstrate that when injected once into rats PME is not converted back to PREG or metabolised to progesterone in either plasma or hippocampus (Bianchi and Baulieu, 2012). However, it cannot be excluded that alterations in endogenous neurosteroid biosynthesis and concentration might occur following single or repeated administration of PME.

PME is lipophilic so it easily and rapidly crosses the blood-brain-barrier; a pharmaco-kinetics study detected PME in the brain following a single injection at 12 mg/kg, s.c (Bianchi and Baulieu, 2012). and behavioural testing showed a clear antidepressant efficacy of single and repeated administration of PME in rats (Bianchi and Baulieu, 2012) and tree shrews (Parésys et al., 2016). In these studies, the behavioural efficacy of PME was paralleled to a modulatory activity on MT dynamics in specific brain regions.

In contrast to its metabolite PREG-sulfate, which is a positive allosteric modulator of the NMDA-R (Wu et al., 1991) and a negative allosteric modulator of the GABAA-R (Majewska et al., 1988), PREG and PME possess no such pharmacological activities. PREG does not bind to any neurotransmitter receptor but binds as an agonist to the nuclear pregnane X receptor (Kliewer et al., 1999) and interacts, as mentioned above, like PME with MAP2 (Murakami et al., 2000). PME was screened for *in vitro* affinity to 80 different neurotransmitter receptors (including NMDA and GABAA) or transporters and no significant affinity was found for any of them (Bianchi M, Villey I, Baulieu E-E, n.d.). It is therefore possible to hypothesise that the effects induced by both PREG and PME observed in the current study may result from a combined activity on both CLIP170 and MAP2, which eventually leads to rescue of altered microtubule dynamics and promotion of neuronal plasticity.

Taken all together, our findings support the possibility that PREG and PME may have potential therapeutic efficacy for CCD by a disease-modifying mechanism of action based on the modulation of microtubule dynamics.

Author contributions

Conceptualization: DP, IB, CKN.
Methodology: DP, PS, RDR, PM, IB.
Resources: LR, MT, RDR.
Validation: IB.
Data analysis: IB, CKN.
Funding acquisition: CKN.
Visualization: IB, RDR, CKN.
Supervision: CKN.
Original draft writing: IB, CKN;
Review and Editing: MB, CKN.

Declaration of competing interest

None declared.

Acknowledgements

This work was supported by funding to CKN from Telethon (GGP15098), from the University of Pennsylvania Orphan Disease Center on behalf of Loulou foundation (CDKL5-17-104-01) and from the

Italian parents' association l'Albero di Greta. Part of this work was carried out in ALEMBIC, an advanced microscopy laboratory established by the San Raffaele Scientific Institute. We thank Cesare Covino for the precious advice during these studies.

Abbreviations

+TIP	microtubule plus-end trafficking protein
CDD	CDKL5 Deficiency Disorder
CDKL5	cyclin-dependent kinase-like 5
CLIP170	CAP-Gly domain containing linker protein 170
DMSO	dimethyl sulfoxide
EB2	microtubule associated protein RP/EB family member 2
EtOH	ethanol
GluA2	glutamate ionotropic receptor AMPA type subunit 2
GFP	green fluorescent protein
IQGAP1	IQ motif containing GTPase activating protein 1
KO	knock-out
MAP1S	microtubule-associated protein 1S
MAP2	microtubule-associated protein 2
MT	microtubule
PME	pregnenolone-methyl-ether
PREG	pregnenolone
PSD95	post-synaptic density protein 95
Rac1	Rac family small GTPase 1
siCDKL5	short interfering CDKL5 RNA
siCTRL	short interfering control RNA
WT	wild-type

Appendix A. Supplementary data

Supplementary data to this article can be found online at https://doi.org/10.1016/j.neuropharm.2019.107897.

References

Amendola, E., Zhan, Y., Mattucci, C., et al., 2014. Mapping pathological phenotypes in a mouse model of CDKL5 disorder. PLoS One 9 (5), 5–16. https://doi.org/10.1371/journal.pone.0091613.

Anggono, V., Huganir, R.L., 2012. Regulation of AMPA receptor trafficking and synaptic plasticity. Curr. Opin. Neurobiol. https://doi.org/10.1016/j.conb.2011.12.006.

Baltussen, L.L., Negraes, P.D., Silvestre, M., et al., 2018. Chemical genetic identification of CDKL5 substrates reveals its role in neuronal microtubule dynamics. EMBO J. 37 (24), e99763. https://doi.org/10.15252/embj.201899763.

Barbiero, I., Peroni, D., Tramarin, M., et al., 2017. The neurosteroid pregnenolone reverts microtubule derangement induced by the loss of a functional CDKL5-IQGAP1 complex. Hum. Mol. Genet. 26 (18), 3520–3530. https://doi.org/10.1093/HMG/DDX237.

Barbiero, I., De Rosa, R., Kilstrup-Nielsen, C., 2019. Microtubules: a key to understand and correct neuronal defects in CDKL5 deficiency disorder? Int. J. Mol. Sci. https://doi.org/10.3390/ijms20174075.

Baulieu, E.E., 2018. Steroids and brain, a rising bio-medical domain: a perspective. Front. Endocrinol. https://doi.org/10.3389/fendo.2018.00316.

Bianchi, M., Baulieu, E.E., 2012. 3β-Methoxy-pregnenolone (MAP4343) as an innovative therapeutic approach for depressive disorders. In: Proceedings of the National Academy of Sciences of the United States of America, https://doi.org/10.1073/pnas.1121485109.

Bianchi M., Villey I., Baulieu E.-E. (2017) No Title Non-Bioconvertible C3-Substituted Pregnenolone Derivatives for Use in the Treatment of Treatment-Resistant Depression. US patent No US2017/0252358 A1.

Brown, E.S., Park, J., Marx, C.E., et al., 2014. A randomized , double-blind , placebo-controlled trial of pregnenolone for bipolar depression. Neuropsychopharmacology 39 (12), 2867–2873. https://doi.org/10.1038/npp.2014.138. Nature Publishing Group.

Chen, Q., Zhu, Y.-C., Yu, J., et al., 2010. CDKL5, a protein associated with rett syndrome, regulates neuronal morphogenesis via Rac1 signaling. J. Neurosci. 30 (38), 12777–12786. https://doi.org/10.1523/jneurosci.1102-10.2010.

Choi, C., Li, J.H., Vaal, M., et al., 2002. Use of parallel-synthesis combinatorial libraries for rapid identification of potent FKBP12 inhibitors. Bioorg. Med. Chem. Lett. https://doi.org/10.1016/S0960-894X(02)00147-6.

Conde, C., Cáceres, A., 2009. Microtubule assembly, organization and dynamics in axons and dendrites. Nat. Rev. Neurosci. https://doi.org/10.1038/nrn2631.

Della Sala, G., Putignano, E., Chelini, G., et al., 2016. Dendritic spine instability in a mouse model of CDKL5 disorder is rescued by insulin-like growth factor 1. Biol. Psychiatry 80 (4), 302–311. https://doi.org/10.1016/j.biopsych.2015.08.028.

Dent, E.W., 2017. Of microtubules and memory: implications for microtubule dynamics in dendrites and spines. Mol. Biol. Cell. https://doi.org/10.1091/mbc.e15-11-0769.

Dent, E.W., Kalil, K., 2001. Axon branching requires interactions between dynamic microtubules and actin filaments. J. Neurosci. 21 (24), 9757–9769.

Dragestein, K.A., Van Cappellen, W.A., Van Haren, J., et al., 2008. Dynamic behavior of GFP-CLIP-170 reveals fast protein turnover on microtubule plus ends. JCB (J. Cell Biol.). https://doi.org/10.1083/jcb.200707203.

Duchossoy, Y., David, S., Baulieu, E.E., et al., 2011. Treatment of experimental spinal cord injury with 3β-methoxy- pregnenolone. Brain Res. https://doi.org/10.1016/j.brainres.2011.05.065.

Fehr, S., Wilson, M., Downs, J., et al., 2013. The CDKL5 disorder is an independent clinical entity associated with early-onset encephalopathy. Eur. J. Hum. Genet. 21 (3), 266–273. https://doi.org/10.1038/ejhg.2012.156. Nature Publishing Group.

Flood, J.F., Morley, J.E., Robertst, E., 1992. Memory-enhancing effects in male mice of pregnenolone. Neurobiology 89 (March), 1567–1571.

Fontaine-Lenoir, V., Chambraud, B., Fellous, A., et al., 2006. Microtubule-associated protein 2 (MAP2) is a neurosteroid receptor. In: Proceedings of the National Academy of Sciences of the United States of America, https://doi.org/10.1073/pnas.0600113103.

Franker, M.A.M., Hoogenraad, C.C., 2013. Microtubule-based transport - basic mechanisms, traffic rules and role in neurological pathogenesis. J. Cell Sci. https://doi.org/10.1242/jcs.115030.

Gu, J., Firestein, B.L., Zheng, J.Q., 2008. Microtubules in dendritic spine development. J. Neurosci. https://doi.org/10.1523/jneurosci.2509-08.2008.

Jaworski, J., Kapitein, L.C., Gouveia, S.M., et al., 2009. Dynamic microtubules regulate dendritic spine morphology and synaptic plasticity. Neuron. https://doi.org/10.1016/j.neuron.2008.11.013.

Kliewer, S.A., Lehmann, J.M., Milburn, M.V., et al., 1999. The PPARs and PXRs: nuclear xenobiotic receptors that define novel hormone signaling pathways. In: Recent Progress in Hormone Research, 1999.

Komarova, Y.A., Akhmanova, A.S., Kojima, S.I., et al., 2002. Cytoplasmic linker proteins promote microtubule rescue in vivo. JCB (J. Cell Biol.). https://doi.org/10.1083/jcb.200208058.

Kubo, Y., Baba, K., Toriyama, M., et al., 2015. Shootin1-cortactin interaction mediates signal-force transduction for axon outgrowth. JCB (J. Cell Biol.). https://doi.org/10.1083/jcb.201505011.

Lansbergen, G., Komarova, Y., Modesti, M., et al., 2004. Conformational changes in CLIP-170 regulate its binding to microtubules and dynactin localization. JCB (J. Cell Biol.). https://doi.org/10.1083/jcb.200402082.

Larti, F., Kahrizi, K., Musante, L., et al., 2015. A defect in the CLIP1 gene (CLIP-170) can cause autosomal recessive intellectual disability. Eur. J. Hum. Genet. https://doi.org/10.1038/ejhg.2014.13.

Lee, H.-S., Komarova, Y.A., Nadezhdina, E.S., et al., 2010. Phosphorylation controls autoinhibition of cytoplasmic linker protein-170. Mol. Biol. Cell. https://doi.org/10.1091/mbc.e09-12-1036.

Luchetti, S., Bossers, K., Van de Bilt, S., et al., 2011. Neurosteroid biosynthetic pathways changes in prefrontal cortex in Alzheimer's disease. Neurobiol. Aging. https://doi.org/10.1016/j.neurobiolaging.2009.12.014.

Majewska, M.D., Mienville, J.M., Vicini, S., 1988. Neurosteroid pregnenolone sulfate antagonizes electrophysiological responses to GABA in neurons. Neurosci. Lett. https://doi.org/10.1016/0304-3940(88)90202-9.

Mishima, M., Maesaki, R., Kasa, M., et al., 2007. Structural basis for tubulin recognition by cytoplasmic linker protein 170 and its autoinhibition. Proc. Natl. Acad. Sci. https://doi.org/10.1073/pnas.0703876104.

Muñoz, I.M., Morgan, M.E., Peltier, J., et al., 2018. Phosphoproteomic screening identifies physiological substrates of the CDKL5 kinase. EMBO J. 37 (24), e99559. https://doi.org/10.15252/embj.201899559.

Murakami, K., Fellous, A., Baulieu, E.E., et al., 2000. Pregnenolone binds to microtubule-associated protein 2 and stimulates microtubule assembly. In: Proceedings of the National Academy of Sciences of the United States of America, https://doi.org/10.1073/pnas.97.7.3579.

Nawaz, M.S., Giarda, E., Bedogni, F., et al., 2016. CDKL5 and shootin1 interact and concur in regulating neuronal polarization. PLoS One 11 (2). https://doi.org/10.1371/journal.pone.0148634.

Neukirchen, D., Bradke, F., 2011. Cytoplasmic linker proteins regulate neuronal polarization through microtubule and growth cone dynamics. J. Neurosci. https://doi.org/10.1523/JNEUROSCI.3983-10.2011.

Nirschl, J.J., Magiera, M.M., Lazarus, J.E., et al., 2016. α-Tubulin tyrosination and CLIP-170 phosphorylation regulate the initiation of dynein-driven transport in neurons. Cell Rep. https://doi.org/10.1016/j.celrep.2016.02.046.

Olson, H.E., Demarest, S.T., Pestana-knight, E.M., et al., 2019. Pediatric Neurology Cyclin-dependent Kinase-like 5 De Fi Ciency Disorder : Clinical Review.

Osuji, I.J., Vera-bolaños, E., Carmody, T.J., et al., 2010. Pregnenolone for cognition and mood in dual diagnosis patients. Psychiatry Res. 178 (2), 309–312. https://doi.org/10.1016/j.psychres.2009.09.006. Elsevier Ltd.

Parésys, L., Hoffmann, K., Froger, N., et al., 2016. Effects of the synthetic neurosteroid 3β-methoxypregnenolone (MAP4343) on behavioral and physiological alterations provoked by chronic psychosocial stress in tree shrews. Int. J. Neuropsychopharmacol. https://doi.org/10.1093/ijnp/pyv119.

Perez, F., Diamantopoulos, G.S., Stalder, R., et al., 1999. CLIP-170 highlights growing microtubule ends in vivo. Cell. https://doi.org/10.1016/S0092-8674(00)80656-X.

Pizzo, R., Gurgone, A., Castroflorio, E., et al., 2016. Lack of Cdkl5 disrupts the organization of excitatory and inhibitory synapses and parvalbumin interneurons in the primary visual cortex. Front. Cell. Neurosci. https://doi.org/10.3389/fncel.2016.00261.

Ren, Y., Suter, D.M., 2016. Increase in growth cone size correlates with decrease in

neurite growth rate. Neural Plast. 20–22 2016.
Ricciardi, S., Ungaro, F., Hambrock, M., et al., 2012. CDKL5 ensures excitatory synapse stability by reinforcing NGL-1-PSD95 interaction in the postsynaptic compartment and is impaired in patient iPSC-derived neurons. Nat. Cell Biol. 14 (9), 911–923. https://doi.org/10.1038/ncb2566.
Rusconi, L., Salvatoni, L., Giudici, L., et al., 2008. CDKL5 expression is modulated during neuronal development and its subcellular distribution is tightly regulated by the C-terminal tail. J. Biol. Chem. 283 (44), 30101–30111. https://doi.org/10.1074/jbc.M804613200.
Rusconi, L., Kilstrup-Nielsen, C., Landsbergers, N., 2011. Extrasynaptic N-Methyl-D-aspartate (NMDA) receptor stimulation induces cytoplasmic translocation of the CDKL5 kinase and its proteasomal degradation. J. Biol. Chem. 286 (42), 36550–36558. https://doi.org/10.1074/jbc.M111.235630.
Schverer, M., Lanfumey, L., Baulieu, E.E., et al., 2018. Neurosteroids: non-genomic pathways in neuroplasticity and involvement in neurological diseases. Pharmacol. Ther. https://doi.org/10.1016/j.pharmthera.2018.06.011.
Swiech, L., Blazejczyk, M., Urbanska, M., et al., 2011. CLIP-170 and IQGAP1 cooperatively regulate dendrite morphology. J. Neurosci. https://doi.org/10.1523/jneurosci.6582-10.2011.
Tramarin, M., Rusconi, L., Pizzamiglio, L., et al., 2018. The antidepressant tianeptine reverts synaptic AMPA receptor defects caused by deficiency of CDKL5. Hum. Mol. Genet. 27 (12), 2052–2063. https://doi.org/10.1093/hmg/ddy108.
Vallée, M., 2016. Neurosteroids and potential therapeutics: focus on pregnenolone. J. Steroid Biochem. Mol. Biol. 160, 78–87. https://doi.org/10.1016/j.jsbmb.2015.09.030. Elsevier Ltd.
Vallée, M., Mayo, W., Le Moal, M., 2001. Role of pregnenolone, dehydroepiandrosterone and their sulfate esters on learning and memory in cognitive aging. Brain Res. Rev. https://doi.org/10.1016/S0165-0173(01)00135-7. 2001.
Van De Willige, D., Hoogenraad, C.C., Akhmanova, A., 2016. Microtubule plus-end tracking proteins in neuronal development. Cell. Mol. Life Sci. https://doi.org/10.1007/s00018-016-2168-3.
Weng, J.-H., Liang, M.-R., Chen, C.-T.C.-H., et al., 2013. Pregnenolone activates CLIP-170 to promote microtubule growth and cell migration. Nat. Chem. Biol. 9 (10), 636–642. https://doi.org/10.1038/nchembio.1321.
Wu, F.S., Gibbs, T.T., Farb, D.H., 1991. Pregnenolone sulfate: a positive allosteric modulator at the N-methyl-D-aspartate receptor. Mol. Pharmacol. 40, 333–336.
Yennawar, M., White, R.S., Jensen, F.E., 2019. AMPA Receptor Dysregulation and Therapeutic Interventions in a Mouse Model of CDKL5 Deficiency Disorder Department of Systems Pharmacology and Translational Therapeutics and 2. Department of Pennsylvania 19104 Correspondence should be sent to : Frances E . (215).

Appendix III

Neuropsychopharmacology [under revision]

Pregnenolone-methyl-ether (PME) activates CLIP170 and improves hippocampal-dependent deficits and spine maturation in a mouse model of CDKL5 deficiency disorder

Isabella Barbiero[1§], Erica Zamberletti[1], Marco Tramarin[1], Marina Gabaglio[1], Diana Peroni[1], Roberta De Rosa[1], Serena Baldin[1], Massimiliano Bianchi[2,3], Tiziana Rubino[1], Charlotte Kilstrup-Nielsen[1].

[1]Dept. of Biotechnology and Life Sciences, (DBSV), Centre of NeuroScience, University of Insubria, Varese, Italy;

[2] Ulysses Neuroscience Ltd., Trinity College Dublin, Dublin, Ireland.

[3] Institute of Neuroscience, Trinity College Dublin, Dublin, Ireland.

[§] Co-corresponding author

Corresponding author:

Charlotte Kilstrup-Nielsen

DBSV, University of Insubria

Tel. +39-0331339430

Fax. +39-0331339459

Email: c.kilstrup-nielsen@uninsubria.it

ABSTRACT (250 WORDS)

BACKGROUND: mutations in cyclin-dependent kinase-like 5 (*CDKL5*) cause CDKL5 deficiency disorder (CDD), a neurological pathology characterised by severe infantile seizure and intellectual disability. The absence of CDKL5 in mice causes defective spine maturation that can at least partly explain the cognitive impairment in CDKL5 patients and CDD mouse models. The molecular basis for such defect might partly depend on the capacity of CDKL5 to regulate microtubule (MT) dynamics through its association with the MT-plus end binding protein CLIP170.

METHODS: live-imaging studies in *Cdkl5*-silenced cells and knock-out neurons were performed to analyse CLIP170 functioning and the invasion of MTs into dendritic spines. Biochemical, neuroanatomical and behavioural tests were performed to evaluate the amount of MT-related proteins in the synaptosomal fraction and the effect of pregnenolone-methyl-ether (PME, a synthetic derivative of the neuroactive steroid pregnenolone that promotes MT dynamics) on spine maturation and hippocampal-dependent deficits in knock-out mice.

RESULTS: the absence of CDKL5 causes CLIP170 to be mainly in a closed inactive conformation. Treatment with PME induces the open active conformation of CLIP170 and the entry of MTs into dendritic spines *in vitro*. The administration of PME to symptomatic knock-out mice improved hippocampal-dependent behaviour and restored spine maturation and the localisation of MT-related proteins in the synaptic compartment. The positive effect on cognitive defects was maintained also one week after treatment withdrawal.

CONCLUSIONS: our results suggest that CDKL5 affects spine maturation and cognitive processes through its control of CLIP170 and MT dynamics that we highlight as apparently valid candidates for target-based therapies.

Introduction

Mutations in the X-linked cyclin-dependent kinase-like 5 (*CDKL5;* OMIM 300672, 300203) gene cause the neurodevelopmental CDKL5 deficiency disorder (CDD), characterised by a complex symptomatology including intellectual disability, early-onset epilepsy, developmental delay, and autistic-like features (1). The prevalence of CDD is ~1:40.000 live births of which 4:1 are females (2). No cure exists for CDD and the development of disease-modifying interventions is still challenged by the incomplete knowledge of CDKL5 functions.

CDKL5 is a serine-threonine kinase that is highly abundant in the mammalian forebrain where it is present in all neuronal subcompartments including dendritic spines (3–5). Loss of CDKL5 *in vitro* and *in vivo* is associated with neuroanatomical defects resulting in a global neuronal atrophy ranging from reduced axon length, dendritic complexity and spine maturation (6,7). Such alterations are likely to underlie the cognitive impairment that is a hallmark of *Cdkl5*-KO mice and of the human pathology. The emerging role of CDKL5 in regulating microtubule (MT) dynamics may, at least in part, explain these defects (6,8). MTs are long polarised polymers that regulate numerous morphological and functional processes during brain development including spine maturation and activity (9). Such functions depend on the capacity of MTs to switch from growth to disassembly enabling their exploration of the cellular environment and capture at specific sites. MT plus-ends are in particular involved in regulating MT dynamics through the accumulation of plus-end tracking proteins (+TIPs) including the end-binding proteins (EBs) and the cytoplasmic linker proteins (CLIPs), which catalyse rapid changes in MT organisation upon upstream signalling events.

We identified CLIP170 as an important downstream CDKL5 effector in the regulation of MT dynamics and as an interesting druggable target (6,8). CLIP170 is a key +TIP involved in the regulation of neuronal morphology through its control of MT dynamics (10,11). MT-binding of CLIP170 depends on its open conformation that can be induced by the direct binding of the neuroactive steroid pregnenolone (PREG) (12,13). PREG and its synthetic derivative pregnenolone-methyl-ether (PME) can restore the impaired MT-binding of CLIP170 in CDKL5 deficient cells together with morphological defects in primary cultures of *Cdkl5*-KO neurons (6,8). PME is a lipophilic compound that easily crosses the blood-brain-barrier; behavioural studies have proven its anti-depressant and pro-cognitive efficacy in animal models, which was accompanied by a modulatory activity on MT dynamics in specific brain regions (14,15).

Here we used *in vitro* and *in vivo* models of CDD to investigate the effect of PME on CLIP170 activity, MT functioning and cognitive processes associated with the absence of CDKL5. Our results indicate that altered MT dynamics contribute to neuronal defects underlying hippocampal-dependent deficits in *Cdkl5*-KO mice

and that the pharmacological modulation of MT dynamics represents a disease-modifying therapeutic strategy for CDD.

Results

1. PME induces the open active conformation of CLIP170 in the absence of CDKL5.

CLIP170 has reduced affinity for MTs in CDKL5 deficient cells that can be restored by both PREG and PME (6,8). We speculated that the absence of CDKL5 might cause CLIP170 to be mostly in a closed inactive conformation and that PME, as PREG, could induce its active state. We therefore analysed the intra-molecular state of CLIP170 through the fluorescence resonance energy transfer (FRET) assay expressing a YFP-CLIP170-CFP chimera in COS7 cells silenced for CDKL5 expression (siCdkl5) (Figure 1). Upon excitation of the CFP donor we observed a higher FRET efficiency (FRET/donor fluorescence intensity) in siCdkl5 cells compared to controls (siCtr; Figure 1D) indicating a closed conformation of CLIP170 in the absence of CDKL5. In accordance with the capacity of PREG to induce the open conformation of CLIP170, FRET efficiency was reduced in PREG-treated siCdkl5 cells. The same effect was obtained upon treatment of CDKL5-silenced cells with PME. The effect of the two drugs on FRET efficiency is compatible with a capacity to specifically target CLIP170, inducing its open conformation and thus its MT-binding in accordance with our previous data (6,8).

2. PME treatment improves spatial memory acquisition and long-term retention in *Cdkl5*-KO mice.

To analyse the effect of treatment with PME *in vivo* in *Cdkl5*-KO mice we focused on hippocampus-associated circuits that are strongly compromised in this animal model (16,17).

Cdkl5-KO and -WT mice received subcutaneous injections with PME (10 mg/kg) or vehicle for 7 consecutive days starting from post-natal day 60 when they are fully symptomatic. After ended treatment, the Barnes maze test was used to evaluate hippocampal dependent spatial learning and memory. During the training phase, lasting three days with two trials/day, the mice were tested for their ability to learn the location of the escape hole. On day 4 they were subjected to the probe test.

Over the 6 training trials both vehicle- and PME-treated WT mice showed a reduction in the primary latency to reach the correct hole. A similar reduction was not observed in vehicle-treated *Cdkl5*-KO mice, indicating an impaired spatial reference memory that was partially improved upon PME-treatment (Figure 2A). No difference was observed between the groups in the total distance travelled, indicating a comparable motor capacity (Figure 2B). On day 4 the escape box was removed and the probe test was performed. Spatial

memory was assessed measuring the latency to reach the escape hole and counting the number of nose pokes into the target hole (Figure 2C,D). Vehicle-treated *Cdkl5*-KO mice showed a significant increase in the latency to reach the target hole, which was reduced upon treatment with PME. Consistently, vehicle-treated WT mice showed a preference for the target hole as compared to *Cdkl5*-KO mice, as indicated by the higher number of nose pokes. Importantly, the number of nose pokes was increased in *Cdkl5*-KO mice treated with PME.

To assess the effect of PME on long-term retention, a second probe test was applied 7 days after treatment discontinuation (Figure 2E,F). Whereas the retention of spatial memory was clearly impaired in vehicle-treated *Cdkl5*-KO mice, the positive effect of PME was still present 7 days after treatment withdrawal. We observed no significant difference in the number of nose pokes between groups. This may be due to an overall loss of interest for the familiar hole; indeed, the number of nose pokes in WT and in PME-treated KO mice is almost halved compared to 7 days before. In contrast, the number of nose pokes for *Cdkl5*-KO vehicle-treated mice was comparable with that of the previous test.

Spatial short-term memory was also assessed using the object location task (Figure 2G). During the test phase, vehicle-treated *Cdkl5*-KO mice showed a significantly smaller discrimination index than that of *Cdkl5*-WT mice, confirming a significant impairment of short-term spatial memory. PME treatment significantly improved the performance of *Cdkl5*-KO mice: indeed, the discrimination index was similar between PME-treated *Cdkl5*-KO mice and vehicle-treated WT mice. In line with the results of the Barnes maze test, this effect was maintained 7 days after discontinuation of PME treatment (Figure 2H).

Altogether these results confirmed a cognitive deficit in short-term memory and long-term retention in *Cdkl5*-KO mice and showed a beneficial effect of PME treatment on hippocampal-dependent spatial memory that persisted for seven days after treatment discontinuation.

3. Treatment with PME normalises spine maturation in *Cdkl5*-KO mice.

We next investigated whether the positive effect of PME treatment on hippocampal-dependent memory in *Cdkl5*-KO mice might be accompanied by an effect on dendritic spine maturation *in vivo*. Spine morphology was examined in Golgi-stained granule neurons of the dentate gyrus; the spines were classified as immature or mature according to their shape (Figure 3A-C). In accordance with previous reports (18,19), dendritic spines in vehicle-treated *Cdkl5*-KO mice appeared longer and thinner and the quantification showed a significant reduction of mature spines and a concomitant increase in the number of in immature spines. This defect was fully restored upon treatment with PME. As expected, no difference in total spine density was

observed between vehicle-treated WT and *Cdkl5*-KO mice (18,19) but PME produced a slight but significant increase in spine density in *Cdkl5*-KO mice (Figure 3D).

Spine maturation was further examined evaluating the expression of PSD95, a major scaffolding factor of post-synaptic excitatory synapses that is deregulated in the absence of CDKL5 (18,20). Hippocampal sections of mice treated as above were subjected to immunofluorescent staining against PSD95 (Figure 3E,F). The number of $PSD95^+$ puncta, corresponding to mature spines, was visibly and significantly reduced in the dentate gyrus of vehicle-treated *Cdkl5*-KO hippocampi but was normalised upon PME treatment. These results demonstrate that the positive effect of PME on hippocampal-dependent spatial memory in *Cdkl5*-KO mice is paralleled by an increased maturation of excitatory synapses.

4. PME treatment restores the deranged localisation of MT-related proteins in the post-synaptic compartment of *Cdkl5*-KO hippocampi.

The dynamic entry of MTs into spines is involved in the regulation of spine morphology and synaptic plasticity (21). We therefore proceeded analysing the content of MT-binding proteins together with other excitatory post-synaptic proteins in dendritic spines of *Cdkl5*-KO hippocampi; to this aim we isolated the synaptosomal fraction, highly enriched in synaptic proteins, and analysed the amount of CLIP170 and EB3, a +TIP that invades spines and is essential for the maintenance of spine morphology and mature synapses (21). First, the quality of the synaptosomal fractionation was confirmed through western blotting showing the expected enrichment of PSD95, the AMPA-receptor subunit GluA2, and CDKL5 in the synaptosomal fraction while nuclear histone H1 was totally absent (Figure 4A). As expected, we also detected EB3 in the synaptosomal fraction (21) together with CLIP170 and its interaction partner, the scaffolding protein IQGAP1. Western blot of synaptosomes isolated from treated *Cdkl5*-WT and -KO mice was then performed to evaluate how the absence of CDKL5 and PME treatment affects levels of synaptic proteins.

We loaded the same amount of lysates in order to evaluate synaptic protein composition in a comparable number of synaptosomes, as verified by the comparable levels of PSD95 (in accordance with a previous report, 22), and used GAPDH as internal standard (Figure 4B-C). As already demonstrated (23,24) GluA2 levels were reduced in vehicle-treated *Cdkl5*-KO mice in (Figure 4C, D). Interestingly, a significant decrease in the amounts of EB3 and IQGAP1 and a strong reduction of CLIP170 were observed in synaptosomes of vehicle-treated *Cdkl5*-KO mice compared to the controls. Consistent with the above-described effect of PME, levels of GluA2, EB3, IQGAP1 and CLIP170 in *Cdkl5*-KO synaptosomes were restored upon PME treatment to those in WT mice (Figure 4 D-G). We observed no difference in total levels of CLIP170, EB3, IQGAP1,

and GluA2 between the four experimental groups (supplementary figure S1). The reduction of these proteins in the synaptosomes thus cannot be explained by CDKL5 loss affecting total protein levels but may rather be due to impaired localisation events, possibly caused by defective MT dynamics.

5. MT invasion is impaired in dendritic spines of *Cdkl5*-KO neurons but is restored upon treatment with PME.

In light of the above, we hypothesised that loss of CDKL5 might impact spine formation and maintenance at least in part by affecting the entry of MTs into dendritic spines. To address this, we live-imaged *Cdkl5*-WT and -KO neurons expressing GFP-tagged EB3 (EB3-GFP) that binds growing MT plus-ends and represents a valid marker to visualise MT dynamics (25) (Figure 5). We quantified MT dynamics as described in Kapitein et al. (25). Briefly, using the ImageJ software we generated for each movie the average projection and the maximum projection of stacks serving respectively as marker for neuron morphology and to identify MT-bound EB3-GFP comets. The appearance of EB3-GFP comets was enhanced by subtracting the average projection from the maximum projection reducing the background caused by diffuse EB3-GFP and permits producing a colour merge of background and comets.

The quantification of dendritic protrusions that were invaded by EB3-GFP positive comets during the time of imaging showed that, while 68% of protrusions in *Cdkl5*-WT neurons were invaded by EB3-GFP labelled MTs, this event could be detected in only 40% of protrusions in *Cdkl5*-KO neurons. The prior treatment with PME promoted MT invasion in *Cdkl5*-KO neurons, increasing the EB3-GFP positive protrusions to almost 62%. This indicates that loss of CDKL5 impacts the invasion of MTs into dendritic spines and that PME is capable of rescuing such defect by promoting MT dynamicity.

Discussion

In this study we investigated the effect of the synthetic neurosteroid PME on cognitive and neuroanatomical deficits linked to the absence of CDKL5. Since CDKL5 was previously found to control CLIP170 functioning and MT dynamics, we focused our attention on analysing these aspects (6,26,27). We demonstrate that PME treatment is capable of bypassing the absence of CDKL5 and promotes MT dynamics and cognitive processes probably through a direct effect on CLIP170.

CDKL5 deficiency causes CLIP170 inactivation that can be reverted by PME

The +TIP CLIP170 regulates MT dynamics by binding to the plus-ends of growing MTs, serving as a rescue factor that supports the growth and elongation of MTs towards the cell cortex. CLIP170 alternates between an autoinhibited closed conformation and the active linear conformation that allows its binding to MTs (12). The *in vivo* FRET assay in COS7 cells demonstrated that CLIP170 is mainly present in its closed conformation upon CDKL5 silencing. This is in line with our recent publications showing that CDKL5 deficiency renders CLIP170 hypo-functional reducing its MT-binding (6,8). The association of CLIP170 with MTs ensures their capture at the cell cortex; this occurs in part through the interaction of CLIP170 with IQGAP1, a scaffolding factor regulating cytoskeleton dynamics (28). CDKL5 deficiency destabilises the CLIP170-IQGAP1 complex (8); this may be a consequence of the closed conformation of CLIP170 that impacts the binding not only to MTs but also with its effector proteins. Interestingly, a binding partner of CLIP170 is dynactin that mediates dynein-based transport of vesicles and organelles along MTs. The CLIP170-dynactin interaction is involved in the initiation of retrograde transport (29). Notably, the absence of CDKL5 was shown to affect the velocity of retrograde transport in neuronal dendrites (26). We speculate that such defect can in part be explained by a compromised CLIP170-dynactin interaction.

In neurons, the hypo-functionality of CLIP170 impacts the engorgement of MTs into the actin-rich area at the axonal tip, causing an increase in the growth cone area (10). *Cdkl5*-KO neurons are characterised by enlarged growth cones in which CLIP170 is delocalised from tubulin (6); such phenotype is in line with an impaired MT-binding of CLIP170 as consequence of its closed conformation.

As mentioned, the neuroactive steroid PREG activates CLIP170 by directly binding the protein and forcing its open conformation (13). Our FRET analysis revealed an analogous effect of PME; indeed, both compounds induced the unfolded conformation of CLIP170. This is in line with our previous studies demonstrating that both PREG and PME restored the MT-association of CLIP170 in CDKL5 deficient cells and re-localised CLIP170 to MTs in the axonal growth cone (6,8).

Our data thus provide important information regarding the mechanism of action of PME adding CLIP170 as a novel target of the compound. PME was previously shown to enhance MT polymerisation by interacting with MAP2 (30), the expression and functioning of which has not yet been studied in *Cdkl5*-KO models. We cannot therefore at present exclude that the effect of PME may be due to a dual action involving not only CLIP170 but also MAP2. Future experiments will investigate this subject.

Possible involvement of MTs in CDKL5-dependent cognitive deficits

PME has been demonstrated to have anti-depressive and pro-cognitive properties in animals (14,15), and was tested in humans against psychiatric symptoms with no apparent adverse effects (31). We here showed that chronic treatment with PME completely restored hippocampal-dependent spatial memory in fully symptomatic *Cdkl5*-KO mice. Importantly, we found that the positive effect of PME persists one week after treatment discontinuation. The pharmacokinetics of PME was studied in rats using gas chromatography / mass spectrometry upon a single administration of the compound (12 mg/kg); one hour after treatment, PME had crossed the blood-brain barrier and accumulated in the brain; this accumulation persisted at lower levels also 24h later (32). The long-lasting effect of PME that we observed in *Cdkl5*-KO mice may thus be due to its continued presence in the brain. Conversely, we cannot exclude a persistent activation of signalling cascades as reported for other neuroplasticity-enhancing molecules (33,34).

The cognitive improvement generated by PME in *Cdkl5*-KO mice was accompanied by a positive effect on spine maturation. Indeed, whereas *Cdkl5*-KO mice are characterised by an increased number of immature spines and a decreased number of mushroom/cup-shaped spines (18), the treatment with PME restored this imbalance as well as the number of PSD95 puncta in hippocampal slices. Interestingly, PME treatment promoted spine maturation also in WT mice. The pro-cognitive effect is also reflected by the increased performance of PME-treated WT mice during the training phase of the Barnes maze test. It is worth remembering that most CDD patients are heterozygous females who, due to random X-chromosome inactivation, are chimeras with cells expressing either mutated or WT CDKL5. Thus, it is possible to hypothesise that the positive effect of PME on mutated neurons could synergistically add to that obtained on WT neurons in a non-autonomous manner.

At the molecular level, the effect of PME on spine maturation is mirrored by the restored levels of MT-associated proteins in the synaptic compartment of *Cdkl5*-KO brains. Through the recruitment of the +TIPs EB3, MTs polymerise into dendritic spines and regulate spine-formation and synaptic activity (35); it is therefore not surprising that mutations in genes that modulate MT dynamics have been found in many neurodevelopmental disorders (36). Here we demonstrated that the synaptosomal fraction of *Cdkl5*-KO hippocampi displayed a depauperation of CLIP170, IQGAP1 and EB3. Noteworthy, the ablation of IQGAP1 and EB3 was previously associated with defects in spine morphology and synaptic activity (21,37). The presence of CLIP170 in dendritic spines has, for all we know, not been reported previously. However, our results, suggesting a role of CLIP170 in dendritic spine maturation, may provide an explanation for the cognitive impairment associated with a loss-of-function mutation in *CLIP1* (human CLIP170 ortholog) (38).

Together with an effect on MT-associated proteins, PME treatment also restored GluA2 levels in hippocampal synaptosomes. The absence of CDKL5 did not affect total levels of either of these proteins; their reduction in the synaptosomal fractions is therefore likely a consequence of altered transport or recycling. Of relevance, we previously demonstrated that CDKL5 silencing delocalises IQGAP1 from the leading edge of polarised cells (8). Since dendritic spines, like the leading edge of proliferating cells, represent a highly active area where MT dynamicity contributes to cellular plasticity (35) we speculate that IQGAP1 via its binding to CLIP170 could serve as a docking site for MTs in spines. By causing both the delocalisation of IQGAP1 and the reduced MT-binding of CLIP170, CDKL5 deficiency may therefore impact the entry and capture of MTs in dendritic spines. In line with this hypothesis, we found that the percentage of dendritic protrusions invaded by EB3-bound MTs is reduced in *Cdkl5*-KO neurons. Importantly, MT invasions have been found to be temporally and spatially associated with increased PSD95 levels in mature spines (39). Similarly, AMPARs are transported along MTs in Rab11-positive recycling endosomes and use both the MT and actin cytoskeleton to enter dendritic spines (40); thus, the reduction of PSD95 and GluA2 in *Cdkl5*-KO hippocampi may be a consequence of defective MT dynamics, which partially depends on the abrogated binding of CLIP170.

Altogether we demonstrate for the first time that learning and memory impairment caused by loss of CDKL5 can be associated with defective MT dynamics, the pharmacological targeting of which appears as an intriguing disease-modifying therapeutic approach for the improvement of cognitive functions in CDD patients.

Methods

Antibodies and reagents

Details can be found in the Supplemental Methods and Materials in Supplement 2.

Animal maintenance, *in vivo* treatment, behavioral studies and neuroanatomical procedures

Protocols and use of animals were approved by the Animal Ethics Committee of the University of Insubria and in accordance with the guidelines released by the Italian Ministry of Health (D.L. 2014/26) and the European Community directives regulating animal research (2010/63/EU). Adult mice were euthanised by cervical dislocation, while neonates were sacrificed by decapitation.

For the *in vivo* treatment mice received daily subcutaneous injections from PND60-PND67 of 10 mg/kg PME or vehicle between 9:00-11:00 a.m. based on previous studies (Bianchi et al., 2012) and pilot tests

performed in our laboratory. PME was suspended in sesame oil and freshly prepared each day of treatment. Details of mice strains, behavioral studies and *ex vivo* procedures (analysis of PSD95 puncta and Golgi-staining) can be found in the Supplemental Methods and Materials in Supplement 2.

Cell cultures, RNA interference (RNAi) and transfections

Details can be found in the Supplemental Methods and Materials in Supplement 2.

Synaptosomal preparation

A single hippocampus (left) was used for each synaptosomal fractionation performed as in Heo 2018 (41). The homogenate and the P1, S2 and synaptosomal fractions were incubated in RIPA buffer (50 mM Tris-HCl pH 7.5, 150 mM NaCl, 1% NP40, 0.5% SDC, 0.1% SDS, 1 mM EDTA, 1 mM EGTA, PIC (Sigma Aldrich) and PhosSTOP (Roche)) for 20 min on ice, quantified with BCA Protein Assay Kit (Pierce) and analysed by Western blotting. *Synaptosomes*: 25-30 µg were loaded to analyse IQGAP1 and CLIP170 levels; 5 µg were loaded to analyse PSD95, GluA2, EB3 and GAPDH levels. *Total homogenate:* the amount of lysate was determined for each protein through linear range analysis procedures. 10-15 µg were loaded to analyse PSD95, GluA2, IQGAP1, CLIP170, EB3 protein expression levels. 2,5 µg were loaded to detect GAPDH used as loading control.

FRET measurements

COS7 cells were seeded in a 6-well plate with glass coverslips (20000 cells/well), transfected with the indicated siRNAs and 48 h later with YFP-CLIP170-CFP; 48 h post-silencing, cells were left untreated or treated daily with 1µM PREG, 0,3 µM PME or the respective vehicles (0.0032% EtOH and 0.1% DMSO, Sigma-Aldrich). Live microscopy images were obtained by an inverted point scanning confocal Leica SMD SP8 (Leica Microsystems) with a 63X objective with the LASX software and the module of FRET Sensitized Emission (excitations at 458 nm) at 37°C. FRET efficiency (ratio of FRET/donor signals) was calculated using the LASX software and considering the entire cell as region of interest (ROI).

Analysis of MT dynamics

MT entry in dendritic protrusions was analysed as described in Kapitein et al. (25). Details can be found in the Supplemental Methods and Materials in Supplement 2.

Data analyses

Statistical analyses of the data were performed using Graph-Pad Prism (GraphPad Software, San Diego, CA). All data are presented as mean ± SEM. p values <0.05 represent statistical significance.

Legends

Figure 1. PME induces the open conformation of CLIP170 in CDKL5 deficient cells. A) Representative images of COS7 cells expressing YFP–CLIP170–CFP upon silencing with siCdkl5 or siCtr and treated with PREG (0.1 μM) or PME (0.3 μM) and their respective vehicles (EtOH 0.0032% or 0.1% DMSO) for 48 h. The rows show CFP and YFP images. The third row shows a false colour rendering of the FRET signal, the intensity of which is indicated with the calibration bar. Scale bar 10 μm. B) Schematic representation of YFP–CLIP170–CFP in the closed and open conformations. C) Western blot showing CDKL5 levels in COS7 cells treated as described in A. D-F) Graphs showing the FRET efficiency in siCdkl5 and siCtr cells left untreated (D) or treated with PREG (E) or PME (F) as described above. siCtr/siCdkl5 untreated, n=39/33 cells; siCtr EtOH, n=31; siCdkl5 EtOH/PREG, n=97/72 cells; siCtr DMSO, n=32; siCdkl5 DMSO/PME, n=66/74 cells. Mean±SEM. **p<0.01; ***p<0.001; ****p<0.0001. One Way ANOVA, Dunnet's posthoc.

Figure 2. PME treatment positively affects defective spatial memory acquisition and long-term retention in *Cdkl5*-KO mice. WT and KO mice were treated with PME (10 mg/kg/day s.c.) or vehicle (sesame oil) for 7 days and then submitted to the Barnes maze (BM, B-D) and the object location task (OLT, G) to test spatial memory. A) Training phase of BM: 2 trials in 3 consecutive days were performed. The asterisks indicate the learning improvement between trials 1 and 6. B) Total distance travelled during the training phase. C) Latency to reach the escape hole. D) Number of nose pokes in the escape hole. E-F) Latency to reach the escape hole and number of nose pokes following one week of treatment discontinuation. G) Discrimination index (DI) during the test phase of OLT calculated as: [(Er-Ef)/(Er+Ef)]x100; *Ef* and *Er,* time spent exploring the familiar and relocated objects, respectively. H) DI following one week of treatment discontinuation. Mean±SEM. *p<0.05; **p<0.01; ****p<0.0001. Two Way ANOVA, Tukey's posthoc test.

Figure 3. PME treatment reverts defective spine maturation in *Cdkl5*-KO mice. A) Classification of dendritic spine maturation according to morphology. B) Representative images of Golgi-stained dentate gyrus neurons from hippocampi of treated WT/KO mice. C,D) Graphs showing the percentage of mature and immature spines (C) and spine density of dentate gyrus neurons. N=50 spines from 5 mice/group. E) PSD95 staining of hippocampal slices (dentate gyrus) from treated WT/KO mice. Scale bar 5 μM. F) Graph showing

the number of PSD95 puncta. N=4/5 mice/group. Mean±SEM *p<0.05; **p<0.01; ****p<0.0001. Two Way ANOVA, Tukey's posthoc test.

Figure 4. PME treatment restores the deranged localisation of MT-related proteins in the post-synaptic compartment of *Cdkl5*-KO mice. A) Subcellular fractionation of mouse hippocampi was monitored by western blot analyses of synaptic and non-synaptic proteins. Whole lysate (homogenate), nuclei/debris (P1), cytosol (S1), and synaptosomal fractions (Syn) were analysed. B) Representative WB of synaptosomes from hippocampi of treated WT/KO mice. C-G) Graphs showing PSD95, GluA2, IQGAP1, CLIP170 and EB3 levels normalised to GAPDH. N>8 animals group. Mean ±SEM *p<0.05;**p<0.01. Two Way ANOVA, Fischer's LSD test.

Figure 5. Impaired MT invasion in dendritic spines of primary hippocampal *Cdkl5*-KO neurons is restored upon treatment with PME. A) Stills of live imaged EB3-GFP bound MTs in primary WT/KO neurons (confocal laser-scanning microscope, 3 min time lapse/neuron). The ImageJ software was used to generate the average projection (diffuse pool of EB3-GFP as marker of neuronal morphology) and the maximum projection (EB3-GFP comets bound to MT plus-ends) of stacks. B) Graph showing the percentage of protrusions invaded or not by EB3-GFP during the time of imaging. N>70 spines in 4 neurons/condition. Mean ±SEM *p<0.05. One Way ANOVA, Dunnet's posthoc test.

Supplementary Figure 1

A) Representative WB of hippocampal total lysate from WT/KO mice treated with PME or vehicle as described. B-F) Graphs showing PSD95, GluA2, IQGAP1, CLIP170 and EB3 levels normalised to GAPDH. N>8 animals group. Mean ±SEM. Two Way ANOVA, Fischer's LSD test.

Acknowledgement and disclosures

This work was supported by funding to CKN from the University of Pennsylvania Orphan Disease Center on behalf of the Loulou foundation (CDKL5-17-104-01) and from the Italian parents' association l'Albero di Greta. MG has a postdoctoral fellowship from Zardi-Gori Foundation (Milan, Italy).

Part of this work was carried out in ALEMBIC, an advanced microscopy laboratory established by the San Raffaele Scientific Institute; we thank Cesare Covino and Valeria Berno for the previous advice during these studies.

IB and CKN planned and designed the research and wrote the manuscript. EZ and MG performed the behavioral tests supervised by TR. IB and DP performed the FRET analyses. IB, MT and RDR performed the synaptosomal fractionation and immunostaining of hippocampal slices. IB and SB analysed spine maturation of Golgi stained hippocampi. MB provided PME.

The authors report no biomedical financial interests or potential conflicts of interests.

Supplement 2 Methods and Materials

Mouse colony

Cdkl5-knockout (KO) mice described in (7) on the genetic background CD1 were used. The day of birth was designated as post-natal day (PND) zero. After weaning, three to five animals were housed in enriched cages on a 12 h light/dark cycle in a temperature and humidity-controlled room with food and water provided *ad libitum*, and checked daily for general health conditions.

Genotyping

Genotyping was performed through PCR on genomic DNA from tail biopsies. Forward PCR primers: 5'-ACGATAGAAATAGAGGATCAACCC for the identification of the null allele, 5'-CCCAAGTATACCCCTTTCCA for the WT allele. Common reverse primer: 5'-CTGTGACTAGGGGCTAGAGA. The obtained PCR products were a single band of 340 base pairs (bp) for *Cdkl5*-KO mice, a single band of 240 bp for the WT animals and both bands for heterozygous females.

Behavioural studies

Behavioural testing was carried out by two observers, blind to the treatment conditions. Tests started on PND67 (after 7 days of treatment) and PND74 (one week after withdrawal).

A total of 97 male mice from different cohorts, obtained crossing heterozygous females with WT males, were used in the study. Littermate *Cdkl5*-WT and -KO male mice were randomly divided into 4 treatment groups. For the object location task at PND67 were used 13 mice (from ≥7 cohorts) in each experimental group whereas 5 mice (from ≥2 cohorts) per group were used at PND74. For the Barnes maze test at PND67 and PND74 were used 11 WT-vehicle, 12 KO-vehicle, 8 WT-PME, 10 KO-PME (from ≥4 cohorts).

Object location task (OLT). The experimental apparatus used for the test was an open-field box, 43x43x32 cm (Ugo Basile, Varese, Italy) made of Plexiglas, placed in a dimly illuminated room. Animals performed each test individually. Briefly, each animal was placed in the arena and allowed to explore two identical, unknown objects for 10 min (familiarisation phase). The chambers were cleaned with 70% ethanol between testing of individual mice. Thirty minutes after the familiarisation phase, mice were placed again in the same arena in which one of the two objects was relocated. During the test phase, the time spent exploring the familiar object (object 1) and the relocated object (object 2) was recorded and the discrimination index was calculated: [(Er-Ef)/(Er+Ef)]x100 with Er and Ef indicating the time spent exploring the relocated and familiar objects, respectively.

Barnes maze test (BM). The maze apparatus consisted of a white circular disk 1.0 m in diameter with 20 holes. A black escape box was located under one of the holes representing the target. The BM apparatus was placed in the centre of a dedicated room with two 120 W lights oriented towards the maze. Three simple black and white shapes were mounted around the maze as visual cues, in addition to the asymmetry of the room itself. In the training phase, mice were placed inside an opaque cardboard cylinder in the centre of the BM for 15 seconds allowing the mouse to be facing a random direction when the cylinder was lifted and the trial began. When the cylinder was removed, the mouse was allowed to explore the maze for 3 min during which the primary latency to reach the escape hole was measured. Six such trials were distributed over 3 consecutive days (until the WT mice were able to remember the position of the target hole). On the probe day, 24h after the last training day, the escape cage was removed; mice were placed inside the central opaque cylinder for 15 seconds where after each mouse was given 90 seconds to explore the maze and the mouse was returned to its holding cage. The latency to reach the escape hole and the number of nose pokes in the escape hole were recorded with the ANY-maze Video Tracking Software.

Antibodies, plasmids and reagents

Anti-CDKL5 (Sigma-Aldrich, HPA002847; Santa Cruz, sc-376314), anti-IQGAP1 (Santa Cruz, sc-10792) anti-CLIP170 (Genetex, GTX117504; Santa Cruz H-300, sc-25613), anti-EB3 (Santa Cruz, sc136405), anti-PSD95 (Thermo Fischer Scientific, MA1045), anti-GluA2 (Millipore, MAB397), anti-α-tubulin (Sigma-Aldrich, T6074), anti-GAPDH (Sigma-Aldrich, G9545), anti-GFP (Roche, 1814460). HRP-conjugated goat anti-mouse or anti-rabbit secondary antibodies for immunoblotting, DAPI, and secondary Alexa Fluor anti-rabbit and anti-mouse antibodies for immunofluorescence were purchased from Thermo Scientific. mEmerald-CLIP170-N-

18 (plasmid #54044; Addgene). pEGFPN2-EB3 and YFP-CLIP170-CFP were kindly provided by the Casper Hoogenraad and Anna Akhmanova, respectively. Pregnenolone (PREG) was from Sigma. Pregnenolone-Methyl-Ether (PME) was obtained from Steraloids, Newport, USA.

Histochemical procedures and analysis of PSD95 puncta

Upon dislocation, mice were decapitated and brains were rapidly excised and frozen in liquid nitrogen. 40 µm cryosections were cut and mounted onto coated slides (SuperFrost® Plus, Thermo Scientific) and stored at -80°C. The slides were fixed in 2% paraformaldehyde (4°C) for 90 seconds, then rinsed 3 times with PBS 1X and blocked in 5% horse serum and 0.2% Triton X-100/PBS for 60 min. Upon overnight incubation with anti-PSD95 antibody (1:1000), the slides were incubated for 60 min at RT with a TRITC-conjugated goat anti-mouse IgG (1:1000) in blocking solution, rinsed 3 times with PBS and covered with ProLong Gold Antifade reagent (Invitrogen). As negative control a slide was incubated with only the secondary antibody.

PSD95 immuonreactive puncta were quantified using images from the molecular layer of the DG acquired with a LEICA TCS SL confocal microscope (LEITZ; Leica Mycrosystems, Wetzlar, Germany) with objective 63X (NA 1.32; zoom factor = 8) and the pinhole set at 1 Airy unit. Three to four slides per animal were analysed using Imagej software ("analyse particles" plugin). Optimised threshold values and size filters were applied for all the images to identify PSD95 puncta. The number of PSD95 puncta was calculated in 4 identical sections for each slides (in order to have a mean of 4 separate zones of the DG per single slide) and expressed per μm^2.

Golgi-staining

Golgi-staining was carried out following the FD Rapid GolgiStain™ kit instructions (fdNeuroTechnologies, inc). Brains were kept at −80°C until cryosectioning that was performed at −22°C. Coronal sections (100 µm) were cut and transferred to Superfrost Plus (Thermo Scientific J1800AMNZ) onto small drops of FD Solution C. Sections were dried at RT in the dark for 24h where after slides were stained as described in the FD Rapid GolgiStain instructions.

In Golgi-stained sections, spines of granule neurons were counted using a 100X oil immersion objective coupled with an Olympus BX51 Fluorescence microscope equipped with Retiga R1 (QImaging) CCD camera. Spine density was measured by manually counting the number of spines on 30 µm long dendritic segments. Spine morphology was evaluated classifying spines according to criteria described in Risher 2014

(42): filopodia, long thin, thin- and stubby-shaped as immature spines and mushroom- and cup-shaped as mature spines.

Cell cultures, RNA interference (RNAi) and transfections

COS7 cells were maintained in DMEM (Dulbecco's modified Eagle's medium; Sigma-Aldrich) supplemented with 10% FBS (EuroClone), L-glutamine (2mM, EuroClone), penicillin/streptomycin (100 units/mL and 100 µg/mL respectively, EuroClone) at 37°C with 5% CO_2.Primary hippocampal cultures were prepared from *Cdkl5* WT and KO embryos at embryonic day 17 (E17) considering the day of the vaginal plug as E0 as previously described (Trovò 2020). siRNA transfection was performed with 20 nM siRNA oligonucleotides targeting CDKL5, or a control siRNA (siCdkl5 5'GCAGAGTCGGCACAGCTAT3', siCtrl 5'CGUACGCGGAAUACU UCGATT3') using Lipofectamine™ RNAiMAX (Life Technologies Incorporated). Plasmid transfection of cells and primary hippocampal neurons was performed with respectively Lipofectamine™ 3000 and Lipofectamine™ 2000 (Life Technologies Incorporated).

Analysis of MT dynamics

For the analysis of MT entry in dendritic protrusions, neurons were plated in a 6-well plate with glass coverslips (225000 neurons/well) and transfected at DIV11 with pEGFPN2-EB3. The same day neurons were treated with 1µM PME or vehicle (0.1% DMSO). Live microscopy was performed at DIV14. Fluorescence in the specimens was imaged every 3 second for 3 min with a confocal laser-scanning microscope (Leica SMD SP8) with a 63X oil immersion objective (Leica) at 37°C. The percentage of dendritic protrusions invaded by MTs was quantified as described in Kapitein et al. (25). Briefly, using the ImageJ software we generated for each movie the average projection and the maximum projection of stacks in order to identify the mask of neuronal morphology (exploiting the diffuse pool of EB3-GFP) and EB3-GFP comets bound to MTs respectively. The average projection was subtracted from the maximum projection for reducing the background caused by diffuse EB3-GFP and enhancing the appearance of EB3-GFP comets.

Bibliography

1. Kilstrup-Nielsen C, Rusconi L, La Montanara P, Ciceri D, Bergo A, Bedogni F, et al. (2012): What We Know and Would Like to Know about CDKL5 and Its Involvement in Epileptic Encephalopathy. Neural Plast; 2012:728267.
2. Olson HE, Demarest ST, Pestana-knight EM, Swanson LC, Iqbal S, Lal D, et al. (2019): Cyclin-Dependent Kinase-Like 5 Deficiency Disorder : Clinical Review. Pediatr Neurol. 97:18-25.
3. Rusconi L, Salvatoni L, Giudici L, Bertani I, Kilstrup-Nielsen C, Broccoli V, et al. (2008); CDKL5 expression is modulated during neuronal development and its subcellular distribution is tightly regulated by the C-terminal tail. J Biol Chem. 283:30101-11.
4. Ricciardi S, Ungaro F, Hambrock M, Rademacher N, Stefanelli G, Brambilla D, et al. (2012); CDKL5 ensures excitatory synapse stability by reinforcing NGL-1-PSD95 interaction in the postsynaptic compartment and is impaired in patient iPSC-derived neurons. Nat Cell Biol. 14:911–23.
5. Nawaz MS, Giarda E, Bedogni F, Montanara P La, Ricciardi S, Ciceri D, et al. (2016); CDKL5 and shootin1 interact and concur in regulating neuronal polarization. PLoS One. 11:e0148634.
6. Barbiero I, Peroni D, Siniscalchi P, Rusconi L, Tramarin M, Rosa R De, et al. (2020); Pregnenolone and pregnenolone-methyl-ether rescue neuronal defects caused by dysfunctional CLIP170 in a neuronal model of CDKL5 Deficiency Disorder. Neuropharmacology. 164:107897.
7. Amendola E, Zhan Y, Mattucci C, Castroflorio E, Calcagno E, Fuchs C, et al. (2014); Mapping pathological phenotypes in a mouse model of CDKL5 disorder. PLoS One. 9:e91613.
8. Barbiero I, Peroni D, Tramarin M, Chandola C, Rusconi L, Landsberger N, et al. (2017); The neurosteroid pregnenolone reverts microtubule derangement induced by the loss of a functional CDKL5-IQGAP1 complex. Hum Mol Genet. 26:3520–30.
9. Kapitein LC, Hoogenraad CC. (2015); Building the Neuronal Microtubule Cytoskeleton. Neuron. 87:492–506.
10. Neukirchen D, Bradke F. (2011); Cytoplasmic Linker Proteins Regulate Neuronal Polarization through Microtubule and Growth Cone Dynamics. J Neurosci. 31:1528-38.
11. Swiech L, Blazejczyk M, Urbanska M, Pietruszka P, Dortland BR, Malik AR, et al. (2011); CLIP-170 and IQGAP1 Cooperatively Regulate Dendrite Morphology. J Neurosci. 31:4555-68.
12. Lansbergen G, Komarova Y, Modesti M, Wyman C, Hoogenraad CC, Goodson H V., et al. (2004); Conformational changes in CLIP-170 regulate its binding to microtubules and dynactin localization. J Cell Biol. 166:1003-14.
13. Weng J-H, Liang M-R, Chen C-TC-H, Tong S-K, Huang T-C, Lee S-P, et al. (2013); Pregnenolone activates CLIP-170 to promote microtubule growth and cell migration. Nat Chem Biol. 9:636–42.
14. Bianchi M, Baulieu E-E. (2012); 3 -Methoxy-pregnenolone (MAP4343) as an innovative therapeutic approach for depressive disorders. Proc Natl Acad Sci. 109:1713-8.
15. Parésys L, Hoffmann K, Froger N, Bianchi M, Villey I, Baulieu EE, et al. (2016); Effects of the Synthetic Neurosteroid 3β-Methoxypregnenolone (MAP4343) on Behavioral and Physiological Alterations Provoked by Chronic Psychosocial Stress in Tree Shrews. Int J Neuropsychopharmacol. 19:pyv119.
16. Fuchs C, Rimondini R, Viggiano R, Trazzi S, De Franceschi M, Bartesaghi R, et al. (2015); Inhibition

of GSK3β rescues hippocampal development and learning in a mouse model of CDKL5 disorder. Neurobiology of Disease. 82:298-310.

17. Okuda K, Takao K, Watanabe A, Miyakawa T, Mizuguchi M, Tanaka T. (2018); Comprehensive behavioral analysis of the Cdkl5 knockout mice revealed significant enhancement in anxiety- and fear-related behaviors and impairment in both acquisition and long-term retention of spatial reference memory. PLoS One. 13:e0196587.
18. Fuchs C, Fustini N, Trazzi S, Gennaccaro L, Rimondini R, Ciani E. (2018); Treatment with the GSK3-beta inhibitor Tideglusib improves hippocampal development and memory performance in juvenile, but not adult, Cdkl5 knockout mice. Eur J Neurosci. 47:1054–66.
19. Trovò L, Fuchs C, Rosa R De, Barbiero I, Tramarin M, Ciani E, et al. (2020); The green tea polyphenol epigallocatechin-3-gallate (EGCG) restores CDKL5-dependent synaptic defects in vitro and in vivo. Neurobiology of Disease.138:104791.
20. Pizzo R, Gurgone A, Castroflorio E, Amendola E, Gross C, Sassoè-Pognetto M, et al. (2016); Lack of Cdkl5 Disrupts the Organization of Excitatory and Inhibitory Synapses and Parvalbumin Interneurons in the Primary Visual Cortex. Front Cell Neurosci. 10:261.
21. Jaworski J, Kapitein LC, Gouveia SM, Dortland BR, Wulf PS, Grigoriev I, et al. (2009); Dynamic Microtubules Regulate Dendritic Spine Morphology and Synaptic Plasticity. Neuron. 61:85-100.
22. Okuda K, Kobayashi S, Fukaya M, Watanabe A, Murakami T, Hagiwara M, et al. (2017); CDKL5 controls postsynaptic localization of GluN2B-containing NMDA receptors in the hippocampus and regulates seizure susceptibility. Neurobiol Dis.106:158-170.
23. Tramarin M, Rusconi L, Pizzamiglio L, Barbiero I, Peroni D, Scaramuzza L, et al. (2018); The antidepressant tianeptine reverts synaptic AMPA receptor defects caused by deficiency of CDKL5. Hum Mol Genet. 27:2052-2063
24. Yennawar M, White RS, Jensen FE. (2019); AMPA receptor dysregulation and therapeutic interventions in a mouse model of CDKL5 Deficiency Disorder. J Neurosci. 39:4814-4828.
25. Kapitein LC, Yau KW, Hoogenraad CC. (2010); Microtubule Dynamics in Dendritic Spines. Methods Cell Biol 97:111-32.
26. Baltussen LL, Negraes PD, Silvestre M, Claxton S, Moeskops M, Christodoulou E, et al. (2018); Chemical genetic identification of CDKL5 substrates reveals its role in neuronal microtubule dynamics. EMBO J. 37:e99763.
27. Muñoz IM, Morgan ME, Peltier J, Weiland F, Gregorczyk M, Brown FC, et al. (2018); Phosphoproteomic screening identifies physiological substrates of the CDKL5 kinase. EMBO J. 37:e99559.
28. Fukata M, Watanabe T, Noritake J, Nakagawa M, Yamaga M, Kuroda S, et al. (2002); Rac1 and Cdc42 Capture Microtubules through IQGAP1 and CLIP-170. Cell. 109:873-85
29. Nirschl JJ, Magiera MM, Lazarus JE, Janke C, Holzbaur ELF (2016); α-Tubulin Tyrosination and CLIP-170 Phosphorylation Regulate the Initiation of Dynein-Driven Transport in Neurons. Cell Rep. 14:2637-52
30. Murakami K, Fellous A, Baulieu E, Robel P, (2000); Pregnenolone binds to microtubule-associated protein 2 and stimulates microtubule assembly. Proc Natl Acad Sci USA . 97:3579-84.
31. Sleeper HG, (1955); Experimental use of pregnenolone methyl ether in treating psychiatric

symptoms. Dis Nerv Syst. 16:93-4.

32. Baulieu E. E, Seine N, Fellous E., Robel P., Bianchi M., (2012). Use of 3-methoxy-pregnenolone for the preparation of a drug for treating depressive disorders and long-term neurological diseases. US patent No US 8,334,278 B2.
33. Alshammari TK (2020). The Ketamine Antidepressant Story : New Insights. Molecules. 25:5777.
34. Kryst J, Kawalec P, Mikrut A, Andrzej M, Lasoń W, Brzostek T, (2020); Efficacy of single and repeated administration of ketamine in unipolar and bipolar depression: a meta - analysis of randomized clinical trials. Pharmacol Reports. 72:543–62.
35. Dent EW, (2017); Of microtubules and memory: implications for microtubule dynamics in dendrites and spines. Mol Biol Cell. 28:1-8
36. Lasser M, Tiber J, Lowery LA, (2018); The Role of the Microtubule Cytoskeleton in Neurodevelopmental Disorders. 12:165
37. Gao C, Frausto SF, Guedea AL, Tronson NC, Jovasevic V, Leaderbrand K, et al. (2011); IQGAP1 Regulates NR2A Signaling , Spine Density , and Cognitive Processes. J Neurosci. 31:8533-42.
38. Larti F, Kahrizi K, Musante L, Hu H, Papari E, Fattahi Z, et al. (2015); A defect in the CLIP1 gene (CLIP-170) can cause autosomal recessive intellectual disability. Eur J Hum Genet. 23:416
39. Hu X, Ballo L, Pietila L, Viesselmann C, Ballweg J, Lumbard D, et al. (2011); BDNF-Induced Increase of PSD-95 in Dendritic Spines Requires Dynamic Microtubule Invasions. J Neurosci. 31:15597-603.
40. Da Silva ME, Adrian M, Schätzle P, Lipka J, Watanabe T , Cho S, et al. (2015); Positioning of AMPA Receptor-Containing Endosomes Regulates Synapse Architecture. Cell Rep. 13:933-43.
41. Heo S, Diering GH, Hyun C, Sekhar R, Bachman JL, (2018); Identification of long-lived synaptic proteins by proteomic analysis of synaptosome protein turnover. Proc Natl Acad Sci USA. 115:E3827-E3836.
42. Risher WC, Ustunkaya T, Alvarado JS, Eroglu C, (2014); Rapid Golgi Analysis Method for Efficient and Unbiased Classification of Dendritic Spines. PLoS One. 9:e107591.

FIGURE 1

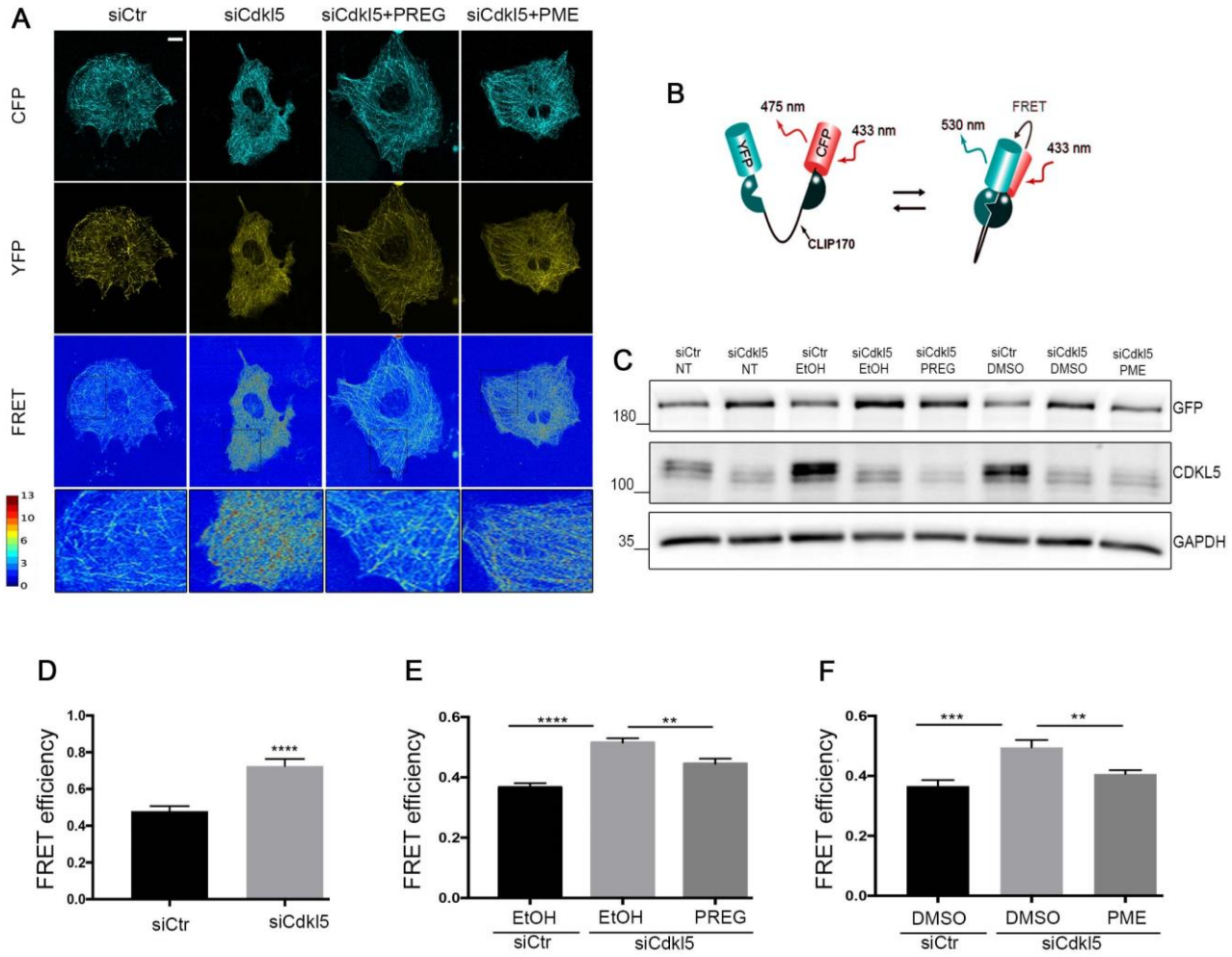
A
siCtr
siCdkl5
siCdkl5+PREG
siCdkl5+PME
CFP
YFP
FRET
13
10
6
3
0
B
475 nm
433 nm
YFP
CFP
CLIP170
FRET
530 nm
433 nm
C
siCtr NT
siCdkl5 NT
siCtr EtOH
siCdkl5 EtOH
siCdkl5 PREG
siCtr DMSO
siCdkl5 DMSO
siCdkl5 PME
180
100
35
GFP
CDKL5
GAPDH
D
FRET efficiency
1.0
0.8
0.6
0.4
0.2
0.0
****
siCtr
siCdkl5
E
FRET efficiency
0.6
0.4
0.2
0.0
****
**
EtOH
EtOH
PREG
siCtr
siCdkl5
F
FRET efficiency
0.6
0.4
0.2
0.0
***
**
DMSO
DMSO
PME
siCtr
siCdkl5

FIGURE 2

Barnes Maze (BM)

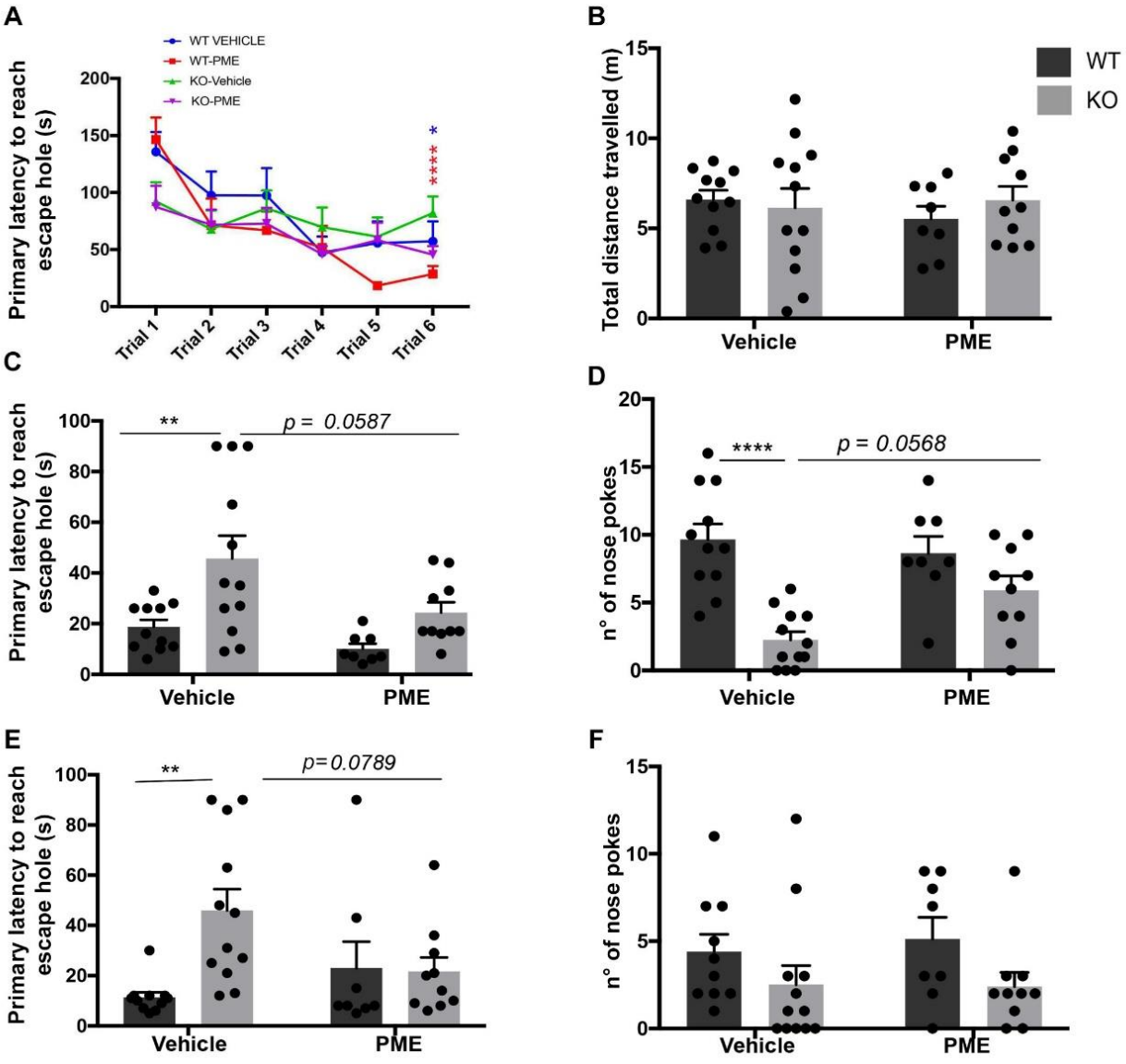

Object location task (OLT)

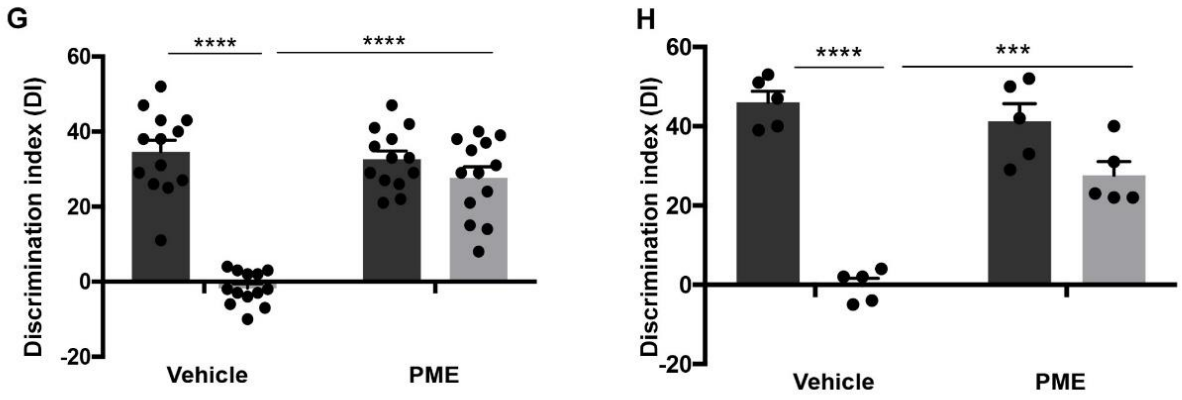

FIGURE 3

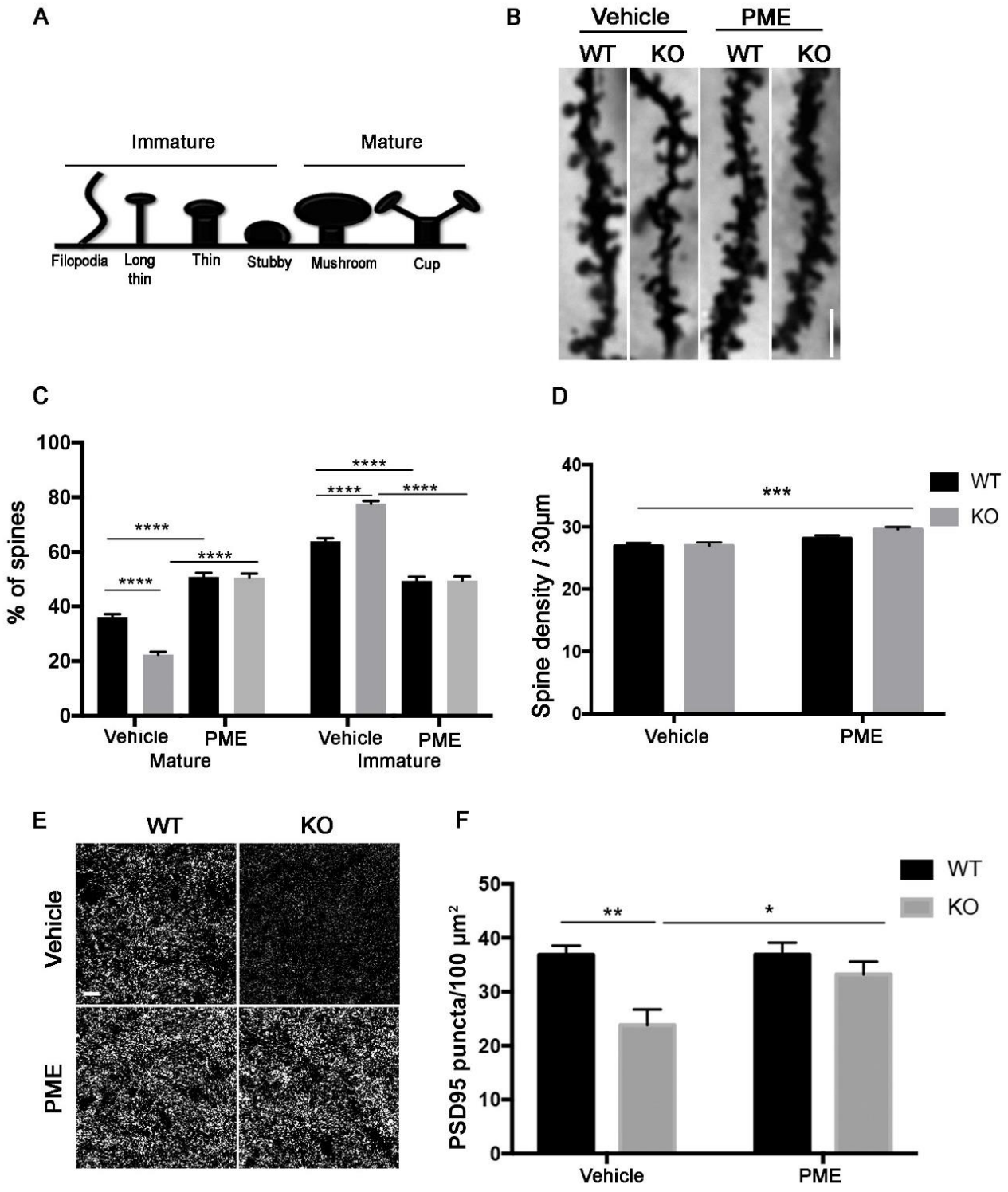
A
Immature
Mature
Filopodia
Long thin
Thin
Stubby
Mushroom
Cup
B
Vehicle
PME
WT
KO
WT
KO
C
% of spines
100
80
60
40
20
0
****
****
****
****
****
Vehicle
PME
Mature
Vehicle
PME
Immature
D
Spine density / 30µm
40
30
20
10
0
***
WT
KO
Vehicle
PME
E
WT
KO
Vehicle
PME
F
PSD95 puncta/100 µm²
50
40
30
20
10
0
**
*
WT
KO
Vehicle
PME

FIGURE 4

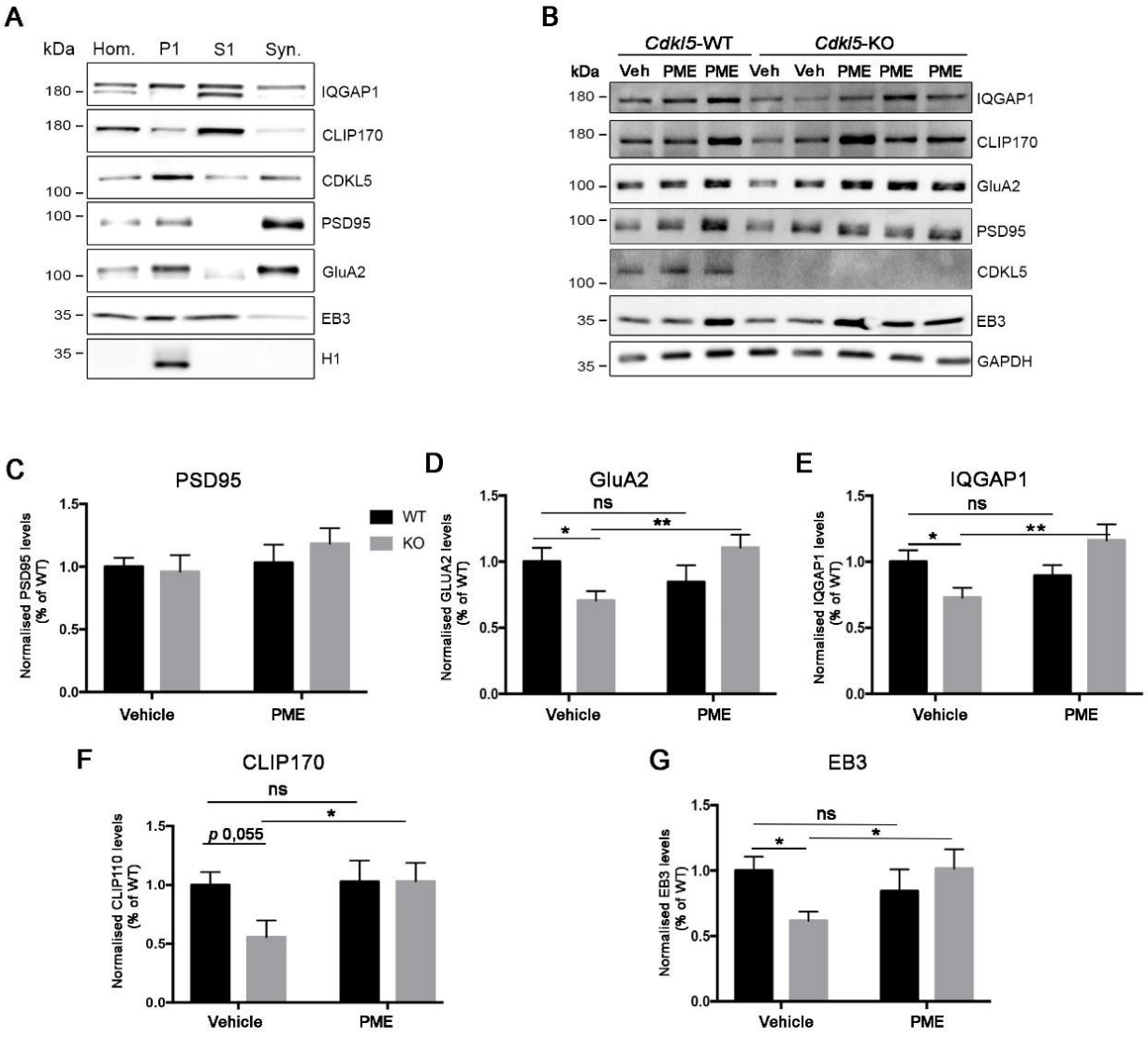
A
kDa
Hom.
P1
S1
Syn.
180
IQGAP1
CLIP170
CDKL5
PSD95
GluA2
EB3
H1
B
Cdkl5-WT
Cdkl5-KO
Veh
PME
GAPDH
C
PSD95
Normalised PSD95 levels (% of WT)
WT
KO
Vehicle
D
GluA2
Normalised GLUA2 levels (% of WT)
ns
E
IQGAP1
Normalised IQGAP1 levels (% of WT)
F
CLIP170
Normalised CLIP110 levels (% of WT)
p 0,055
G
EB3
Normalised EB3 levels (% of WT)

FIGURE 5

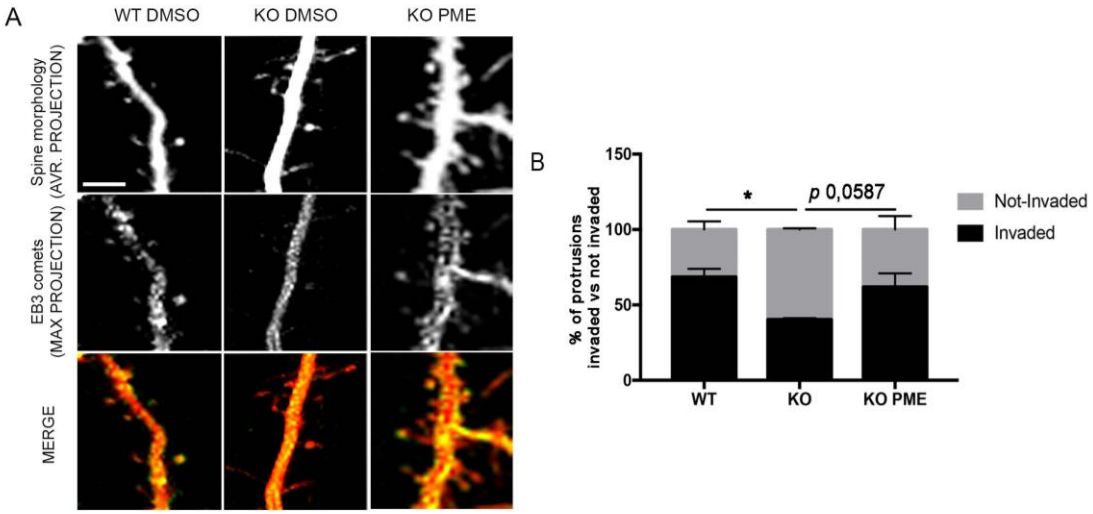
A
WT DMSO
KO DMSO
KO PME
Spine morphology (AVR. PROJECTION)
EB3 comets (MAX PROJECTION)
MERGE
B
% of protrusions invaded vs not invaded
150
100
50
0
*
p 0,0587
Not-Invaded
Invaded
WT
KO
KO PME

Supplementary 1